Fundamental Studies of Early Transition Metal-Ligand Multiple Bonds: Structure, Electronics, and Catalysis

Thesis by
Ian Albert Tonks

In Partial Fulfillment of the Requirements for the Degree of

Doctor of Philosophy

CALIFORNIA INSTITUTE OF TECHNOLOGY
Pasadena, California
2012
Defended December 6th 2011

© 2012
Ian A Tonks
All Rights Reserved

ACKNOWLEDGEMENTS

I am extremely fortunate to have been surrounded by enthusiastic, dedicated, and caring mentors, colleagues, and friends throughout my academic career. A Ph.D. thesis is by no means a singular achievement; I wish to extend my wholehearted thanks to everyone who has made this journey possible.

First and foremost, I must thank my Ph.D. advisor, Prof. John Bercaw. I think more so than anything else, I respect John for his character, sense of fairness, and integrity. I also benefitted greatly from John's laissez-faire approach to guiding our research group; I've always learned best when left alone to screw things up, although John also has an uncanny ability for sensing when I need direction or for something to work properly on the high-vac line. John also introduced me to hiking and climbing in the Eastern Sierras and Owens Valley, which remain amongst my favorite places on Earth. Thanks for always being willing to go to the Pizza Factory in Lone Pine before and after all the group hikes!

While I never worked on any of the BP projects that were spearheaded by our co-PI Dr. Jay Labinger, I must also thank Jay for coming to all of my group meetings, teaching me an incredible amount while I was TAing Ch154, and for always being willing to talk chemistry and answer tough questions.

Much thanks also go to my committee: my chairman, Prof. Harry Gray, who played a large part in the intellectual development of the 2nd half of this thesis and treated me as one of his own group; Prof. Bob Grubbs, who is a major reason why I ended up at Caltech and who never fails to embarrass me in front of new people by recounting how Katie tricked me at a bar in Hawaii when we first met; and Prof. Brian Stoltz, who threw me into

the flames my first term at Caltech in Ch 242, and made me enjoy many aspects of organic chemistry a lot more than I thought I would.

In the lab, I've had the pleasure of working with over 30 wonderful colleagues and friends. The office dynamic has greatly changed over the years, but one truth remains constant: the Bercaw lab is a strange but wonderful group of people, and I wouldn't have it any other way. We've all gone on adventures in the wilderness on the group hike, spend countless hours in meetings and lab together, travelled the country for conferences, and eaten countless meals together. Everyone in the group has my sincerest gratitude, and since there is no page limit for my thesis I would like to acknowledge everyone individually.

First, I would like to thank Prof. Nilay Hazari and Dr. Aaron "ARod" Wilson. When I was on the fence about joining the group, they took me out to Barn Burner, bought me some Shiner, and made me feel incredibly welcome in the group. Throughout my first two years in the group, Nilay served as a mentor for me: he helped me start up the hydrazide project, showed me where the stockrooms were, helped me get my DFT learner's permit, and was always available for some blunt and realistic advice. Nilay was also the brave soul who shared a tent with Jay on the group hike to the Grand Canyon. ARod was, and still is, one of the nicest, most down to earth people I've met in our field. ARod was always down for an adventure—whether it was doing some crazy off-piste skiing or rock climbing, ARod was always willing and able.

Prof. Jeff Byers was one of the people that initially—much to his shock, I think—convinced me to join the group. Jeff is an incredibly thoughtful and talented chemist, and I appreciate the time that he took to teach me how to vac transfer and save a box (and

swivel frit, boy) while he was writing his thesis. I'm happy that our friendship has grown since he left the group.

Prof. Theo Agapie initiated the non-metallocene project within our group, so I have much to thank him for on the research front. We've been extremely fortunate to have such a vibrant and creative young professor join the department as the Bercaw group winds down. Dr. Paul Elowe was my first baymate in 213 North, and I appreciate all the help he gave me as I started to work with the high vac line. Paul was also an excellent teammate on the soccer pitch; our team was never the same once he left for Dow. Also part of the 2006/2007 edition of 213 was Prof. Travis "T-Rav" Williams. Travis was our talented organic postdoc—an endless font of synthetic knowledge and progenitor of the ever-useful "Travis Williams Theory that All Organic Compounds are Colorless." Travis was a constant source of wry humor, and his group meeting "Travisties" remain legendary.

Prof. Dave Weinberg remains a sideburn inspiration to me. Not much else needs to be said about Dave—dude's just a great guy. The other half of Dave's "Shaq and Kobe" duo was Dr. George Chen. George always manages to put a positive spin on chemistry when your research is going down the tubes, and was always happy to talk chemistry and Star Wars. Dr. Bolin Lin was a wonderful TA for organometallics, and also full of surprises—after one vacation, he came back married! Dr. Suzanne "Bulldog" Golisz was always a social hub of the group; thanks for being such a gracious host and inviting us all to football parties, Halloween parties, and the like. Good luck up at Brookhaven! Dr. Valerie Scott always had one of the best attitudes in the group, and you can always count on Val for a good laugh or a great story (or bizarre pictures of cartoon bunnies!). Luckily, we still get Val dropping by every now and then from her postdoc at JPL.

An extra special thanks goes to Dr. Sze-Man Yu for a special delivery of the 10 g of $HgMe_2$ and 10 g $CdMe_2$ that we recently received. Dr. Melanie Zimmerman, a visiting scholar in the group, was a great source of knowledge for all things Group 3, and helped me get involved in a few scandium and yttrium projects.

Prof. Ned West, Prof. Alex Miller, and Dr. Steve Baldwin could always be counted on to get a soda sometime between 2:00-3:00 every day. On top of being great break folks, these three all contributed greatly to my scientific and personal growth. Alex was my office neighbor for 4 years and was great to bat ideas around with; Steve was an early transition metal co-conspirator and late night lab partner, and Ned was a wonderful labmate in 213 North who seemed to pretty well tolerate my messes and the general "lameness" of the lab. Thanks guys.

During my stay we've had 6 solid undergraduates working in the lab. Koyel Bhattacharyya, who worked with Bolin, was a ball of energy in the lab, and continues to work hard up at Stanford in grad school. Daniel Tofan, who started the NNN project, is currently working with Kit Cummins at MIT; thanks for giving us a great start on that project! "Little" Alex Velian, who worked with Big Alex and Theo, is one of the happiest undergrads I've ever met from Caltech, and is also now part of the Caltech-MIT undergrad-grad exchange. She is also deathly afraid of snakes. Yuxiao Sun worked with Matt Winston, and will be starting grad school now-ish. Good luck!

I had the great fortune of having 2 wonderful young scientists as my mentees. First, Josef Meier, from TU-Munich, worked with me on the ONO hydroamination project. On top of being an enthusiastic (and successful!) chemist, Josef was a great friend to the whole group. His love of a good burger drove us to some excellent restaurants. Tonia

Ahmed from WVU worked with me on the indene C-H activation project, and was likewise extremely excited about doing research and getting into the Caltech life. Working with these students has been extremely rewarding, and I hope they learned half as much as I did working with them. Good luck to you both going forward.

My two classmates, Dr. Paul Oblad and Dr. Ted Weintrob, were with me all the way. We were lucky to get the both of you from Jonas' group before he left! Paul is a certified scout, and was super clutch to have along on all the group hikes. He also has some absolutely crazy stories about blowing up 3 liter bottles filled with chemicals in the middle of lakes! Ted and I started undergrad at Columbia together, worked for Ged Parkin together, and then came to Caltech together and (circuitously) ended up in the Bercaw group together. Ted was my go-to guy early on for all the stupid questions that I was too afraid to ask anyone else, a constant night-shift lab presence, and an all around good guy. I'm happy to count him amongst my friends. We've learned together, struggled together, played sports together, and now it's time to strike out on our own. Good luck to both of you out in Oklahoma at ConocoPhillips—let's hope the research arm stays intact!!

As John prepares to retire, the lab is slowly being taken over by postdocs and visiting scholars. Dr. Amaruka Hazari is a synthetic force in the lab, and a friendly and charismatic person out of it. Dr. Loi Do has been a welcome friendly face in the office. Thanks for taking over the BMW Box Czar duties! Dr. Carl Laskowski has been my officemate for the past year, and a worthy successor to my longtime officemate Alex. Carl tells it like it is, and is always happy to unwind a bit with an adult beverage after a hard/easy/long/short day in the lab. Dr. TJ Kim, our newest addition from Korea, is an awesome hiker, fellow Ernie's aficionado, and is always up for trying something new. It's

been nice to get to know you the past few months. Dr. Emmanuelle Despagnet-Ayoub, our visiting scholar from the Laboratoire de Chimie de Coordination at CNRS Toulouse, has been a wonderful coworker on the early transition metal projects. It has been really nice to have an additional senior scientist develop new directions for our chemistry as the lab begins to shift focus.

After me, there are only 5 students left in the Bercaw Group. I could always count on Rachel "Phoebe" Klet for an honest opinion when I really needed one, or a death stare when I called her Phoebe. Matt Winston joined us late from the Stoltz group, and was an excellent resource on all things organic, as well as a great Thanksgiving host. Ross Fu will forever be known for asking some of the most ludicrous and hilarious questions in the history of Bercaw Group meetings—"How many arsonists *are* there in Southern California, John?" or "Steve… I didn't know you had a Mexican brother?!" Taylor Lenton always made me feel included in social events; it's often hard being single when virtually everyone else is paired up, and Taylor made sure that I wouldn't be left out all the time. Taylor also had the misfortune of becoming our latest safety officer. Sorry about exploding 1 kg of bromine in your hood. Finally, Yan Choi Lam has been my baymate for the past two years. Thank you for not exploding/killing me, although we had a few too many close calls for my taste! For all 5 of you, may you be able to easily assemble your committees, publish papers in a timely manner, and continue to draw on the fun spirit of Bercaw traditions until the end. Best of luck.

Outside of the Bercaw group, I need to thank my longtime roommates, Justin Chartron and Dave Montgomery, for putting up with me for an extended period of time

and hanging in there through rough periods of insane landladies, random French roommates, impromptu after parties, and all the rest of the chaos.

A few other research groups have been really important to me during my tenure at Caltech. The Gray group has been a constant source of science, parties, and craziness over the years. Special thanks go to Gretchen Keller for being a great friend, Jillian Dempsey for helping to convince me to come to Caltech, and Alec Durrell for collaborating and tolerating my ignorance of photophysics. Postdocs Dr. Jeff Warren and Dr. Paul Bracher were extremely helpful in guiding me through the postdoctoral fellowship application process. Thanks guys! The Agapie group has been a growing presence in the department—it's been a real pleasure to watch the first crop of students mature into leaders in the lab. The Peters group has been a wonderful addition the past couple of years—thanks for all the trips to Hot Wings and the power hours and other craziness at John's place. Special thanks to Sam MacMillan for being such a great friend and confidante during my last year. Finally, the guys in the Dervan group—Dave Montgomery, Ben Li, Thomas Martinez, and Jordan Meier—were great to go on adventures with. I'll never forget our trip out to Coachella or the ticket "malfunction" at the Clippers game!

In addition to being great labmates and friends, many of the folks listed above also made enormous contributions to our success on the sports field. Thanks to everyone that played with the Cp All Stars in softball and Bearcaw Bulls in basketball. Our successes are a testament that being inclusive and playing for fun will ultimately bring championships. At least in the Caltech D Leagues. I think some my most treasured memories of Caltech will be from our sports adventures.

None of this work could have been completed without the expert assistance of the Chemistry Department staff. Thanks to Pat Anderson for being able to get pretty much anything done; Anne Penney, Agnes Tong, Laura Howe, and Diane Buchness for running a tight ship in the front office; Tom Dunn for fixing *everything* electronic; Rick Gerhart for masterfully creating and fixing glassware; and Dave Vandervelde for creating a fantastic NMR facility. Extra thanks go to Larry Henling and Mike Day, who have taught me much about crystallography, allowed me to run a ridiculous number of crystals, and worked up all the data for me.

Thanks to all the professors, grad students, and postdocs who mentored/tolerated me as an undergraduate: Dr. Jon Melnick in Ged Parkin's group at Columbia; Dr. Zhaohui Wang in Craig Jensen's group at UHawaii, Dr. Qiaobing Xu in George Whitesides' group at Harvard, and everyone in John Margrave's group at Rice. Thanks to Prof. Ged Parkin for being a true advocate for me over the past 5+ years. These are the people that truly made me want to end up in grad school, and fostered within me a love of teaching. Thanks also go to all of my high school teachers at the Academy of Science and Technology. You all provided a really special environment to grow and foster my interest in science, and gave me a chance to succeed during a really difficult period in my life. I would like to specifically acknowledge Scott Rippetoe, who convinced me to apply for a summer fellowship that ultimately earned me a position with Prof. John Margrave in the Chemistry Department at Rice—and the rest, they say, is history.

Finally, I must thank my family—Dad Colin Tonks, Mom Beverly Asher, and Sister Lauren. None of this would have been possible without your support.

Of course, special thanks go to Ernie Mercado for catering much of my PhD affair.

ABSTRACT

Two major topics are covered: the first section is focused on the structure, electronics, stoichiometric reactivity and catalysis of nonmetallocene early transition metal complexes that often contain metal-ligand multiple bonds (Chapters 2-4); the second section is dedicated to the development of hydrazide(2-) ligands for group 5 elements, which were heretofore unexplored as ligands for group 5 (Chapters 5-6).

A series of tantalum imido and amido complexes supported by a pyridine-linked *bis*(phenolate) (ONO) ligand has been synthesized. Characterization of these complexes *via* X-ray crystallography reveals both C_s and C_2 binding modes of the *bis*(phenolate)pyridine ligand. DFT calculations and molecular orbital analyses of the complexes have revealed that the preference for C_s-symmetric ligand binding is a result of Ta-O π-bonding: in cases where Ta-O π-bonding is overridden by stronger Ta-N π-bonding, C_2-symmetric ligand binding is preferred because this is the lowest-energy geometric conformation.

Titanium and zirconium complexes supported by a related pyridine *bis*(anilide) ligand (NNN = pyridine-2,6-*bis*(N-mesitylanilide)) have been synthesized. The ligand geometry of these complexes is dictated solely by chelate ring strain rather than metal-ligand π-bonding. These complexes were tested as propylene polymerization precatalysts, with most complexes giving low to moderate activities (10^2-10^4 g/mol*h) for the formation of polypropylene.

(ONO)TiX_2 complexes are highly active precatalysts for the intermolecular hydroamination of internal alkynes with primary arylamines and some alkylamines. (ONO)$TiBn_2$ also cyclotrimerizes dimethylacetylene. During the cyclotrimerization reaction

the Ti^{IV} precatalyst is reduced to Ti^{II}, which is the active species for catalysis. The mechanism of formation of Ti^{II} has been investigated and an (ONO)Ti^{II} species has been trapped by ethylene and crystallographically characterized.

Hydrazide complexes (dme)$TaCl_3(NNPh_2)$ and (dme)$NbCl_3(NNPh_2)$ (dme = 1,2-dimethoxyethane) were synthesized. Unlike the corresponding imido derivatives, (dme)$TaCl_3(NNPh_2)$ is dark blue due to an LMCT that has been lowered in energy as a result of an N_α-N_β antibonding interaction that raises the HOMO. Reaction of (dme)$TaCl_3(NNPh_2)$ with a variety of neutral, mono- and dianionic ligands generates the corresponding ligated complexes retaining the k^1-bound [Ta-$NNPh_2$] moiety.

Furthermore, a series of colorful terminal hydrazide complexes of the type (dme)$MCl_3(NNR_2)$ (M = Nb, Ta; R = alkyl or aryl) or (MeCN)$WCl_4(NNR_2)$ have been synthesized. Perturbing the electronic environment of the β nitrogen significantly impacts the lowest-energy charge transition in these complexes, and in the W complexes leads to metal based reduction. The photophysics of these complexes highlights the importance of the difference in reduction potential between metal centers, and could lead to differences in ligand- and/or metal-based redox chemistry in early transition metal hydrazidos, especially in the context of N_2 fixation.

Finally, the hydroxy-bridged dimer $[(COD)IrOH]_2$ (COD = 1,5-cyclooctadiene) cleanly C-H activates indene and cyclopentadiene to form (COD)Ir(η^3-indenyl) and (COD)Ir(η^5-C_5H_5), respectively. The kinetics of the formation of (COD)Ir(η^3-indenyl) has been investigated, and the mechanism involves coordination of indene to the dimeric $[(COD)IrOH]_2$ followed by rate determining C-H activation from the dimer-indene unit.

TABLE OF CONTENTS

LIST OF FIGURES

Chapter 2

Chapter 3

LIST OF TABLES

Chapter 6

Chapter 7

Appendix A

Appendix C

CHAPTER 1

General Introduction

This dissertation is focused on the study of metal-ligand multiple bonding and its implications in the structure and reactivity of early transition metals. In overall approach, the present work can be divided into two general sections. Research in the first section was driven by attempts to rationally design propylene polymerization catalysts based on a new class of "non-metallocene" ligands. This section is focused on the structure, electronics, stoichiometric reactivity and catalysis of nonmetallocene early transition metal complexes that often contain metal-ligand multiple bonds. The second section is dedicated to the development of hydrazide(2-) ligands for group 5 elements, which were heretofore unexplored as ligands for group 5. Within each chapter, there are specific introductory sections and references relevant for the work; this introduction will rather attempt to explain the author's rationale and give context and narrative for the two general research topics.

The development of homogeneous metallocene-based catalysts for polyolefin production represents one of the most successful and pervasive achievements of organometallic chemistry on an industrial scale. Recently, research on these highly active catalysts has focused on stereocontrol of the insertion of an incoming olefin monomer into the polymer chain. In many cases, high degrees of stereospecificity and regiospecificity can be obtained by following simple steric control models, in which the enantioface of the olefin is selected based on the ligand environment of the metallocene catalyst. This mechanistic model is called enantiomorphic site control. In search of higher selectivities and new applications (such as the kinetic resolution of chiral olefin

precursors), many research groups have sought to synthesize more and more elaborate metallocene ligand sets.

In recent years, concurrent with the development of more advanced metallocene catalysts there has been a resurgence in the development of "non-metallocene" ligand sets for early transition metal catalyzed polymerization—this (unfortunately) broad term typically encompasses a large class of polydentate ligands such as tripodal ligands, pincer ligands and others. The advantages of these ligands compared to the more traditional metallocene class are myriad: (sometimes) simpler syntheses, easily tuned steric and electronic environments and fewer intellectual property minefields. In many cases, the lessons learned from metallocene chemistry can be directly applied to these new nonmetallocene catalysts, and the rate of advancement in nonmetallocene-based catalysis is comparably fast.

Our interest in nonmetallocene ligands grew from a metallocene-based project to kinetically resolve chiral α-olefins. In this project, enantiopure, C_1-symmetric metallocene catalysts were found to kinetically resolve some α-olefins with reasonable selectivity. These catalysts operated under enantiomorphic site control, and it was presumed that increasing the steric bulk of the metallocene would increase selectivity. However, these catalysts proved incredibly difficult to synthesize and the selectivity advancements were limited. As a result, a former graduate student in the Bercaw group, Theodor Agapie, began investigating a variety of different nonmetallocene ligand sets in the hopes that catalysts comparable to the C_1-symmetric metallocenes could be easily accessed. After some trial and error, a class of 1,3-arene linked *bis*(phenolate)-ligated early transition

metal complexes was found to be highly active catalysts for propylene polymerization. In many cases, the activity of these catalysts were comparable to some of the better metallocene-based systems. However, the polypropylene generated using these nonmetallocene catalysts was atactic. The solid-state structures of these catalysts were either C_2 or C_S-symmetric, and following the enantiomorphic site control model it was unclear why polymerization using these catalysts would give no selectivity.

As a first year, I inherited a large part of the nonmetallocene project from Theo. In some early attempts to make tantalum alkylidenes based on the pyridine-linked *bis*(phenolate) ligand (ONO ligand), we serendipitously noted a relationship between the electronic parameters of the complexes and their solid state structure (Chapter 2). One of the key findings was that these nonmetallocene ligands adopted either sterically preferred C_2 geometries or electronically preferred C_S geometries, and the degree of metal-ligand π bonding determined which control factor dominated. This led to the elaboration of the ONO system to incorporate different types of X-type donors with varying electronic and steric demands: anilides (Daniel Tofan, Chapter 3), thiophenoxides (Taylor Lenton) and phosphides (Matthew Winston), as well as some asymmetric, mixed phenoxide/amide ligands (Rachel Klet and Emmanuelle Despagnet-Ayoub). The majority of this work has confirmed our initial structural hypotheses from Chapter 2, but has not yet led to significant improvements in tacticity control or activity in propylene polymerization. Despite these setbacks, significant progress has been made from a fundamental chemistry standpoint—particularly in understanding weak π bonds in early transition metal complexes.

Since we discovered that our *bis*(phenolate) pyridine framework was particularly good at stabilizing metal-ligand multiple bonds, we began incorporating (ONO)-based complexes in other catalytic cycles that feature metal-ligand multiply-bonded species as intermediates. One reaction that immediately appealed to us was titanium-catalyzed intermolecular alkyne hydroamination. Ti imido species are key intermediates in the hydroamination cycle, which then undergo [2+2] reactions with alkynes to generate a C-N bond. When we initially started investigating this reaction, we had a diplome student from TU-Munich, Josef Meier, join the group, and he and I went on to discover that (ONO)Ti-based catalysts are amongst the fastest group 4 hydroamination catalysts known, and also undergo interesting reactivity to generate Ti^{II} species that are capable of alkyne trimerizations (Chapter 4).

Our interest in group 5 hydrazide complexes grew out of some preliminary results that were obtained during our research into group 4 and 5 imido complexes. Nilay Hazari, a postdoc in the group, suggested that I try to synthesize the dimethylhydrazide complex (ONO)TaCl(py)($NNMe_2$) in an analogous fashion to our synthesis of (ONO)TaCl(py)(NPh). This reaction worked well, and we were surprised to find that there was virtually no precedent for tantalum or niobium hydrazide(2^-) complexes.

Over the past decade, group 4 and group 6 hydrazido complexes have become increasingly important complexes in both organic catalysis and N_2 reduction chemistry. Mountford and Odom have shown that Ti hydrazides can catalyze the diamination or hydrohydrazination of alkynes with hydrazines. These are powerful transformations from an organic chemistry perspective, although they are severely limited in scope. Gade and

Bergman have demonstrated similar stoichiometric reactions with Zr hydrazides. Additionally, group 6 hydrazides have been recognized as key intermediates in a Chatt-type N_2 reduction cycle, and many groups have demonstrated the stoichiometric and catalytic reduction of group 6 hydrazides to nitrides and amines. Owing to this rich chemistry, we embarked on a project to develop the reaction chemistry of analogous group 5 complexes (Chapters 5 and 6). In addition to synthesizing a diverse array of group 5 hydrazides, we have found that these complexes exhibit rich photophysical properties that may open up the possibility for utilizing the ligands in redox noninnocent manifolds. Interestingly, the group 5 hydrazido complexes resist metal-based reduction by the hydrazido ligand, unlike some analogous tungsten and molybdenum complexes. Unfortunately reactivity at the hydrazido(2-) ligand with group 5 metals remains elusive, although our preliminary reactivity studies have been limited in scope.

Finally, the Bercaw group has been investigating the C-H activation of a variety of substrates with platinum and palladium diimine hydroxydimers, $[(\text{diimine})\text{MOH}]_2^{2+}$. These complexes share a few of advantages over many other C-H activation model systems: they are air- and water-tolerant and do not require breaking an M-C bond before or during C-H activation. Nilay Hazari investigated a similar neutral system, $[(\text{COD})\text{RhOH}]_2$, and found that it C-H activated indene *via* a different mechanism than the group 10 congeners, although the exact mechanism of the C-H activation step remained unclear. As a result, a SURF student from West Virginia University, Tonia Ahmed, and I investigated the kinetics and activation parameters of the iridium congener, and found that the C-H activation step was likely a deprotonation rather than oxidative addition to the metal center.

CHAPTER 2

Amine, Amido, and Imido Tantalum Complexes Supported by a Pyridine-Linked *Bis*(phenolate) Pincer Ligand. Ta-N π Bonding Influences Pincer Ligand Geometry.

Published in part as:
Tonks, I. A.; Henling, L. M.; Day, M. W.; Bercaw, J. E. *Inorg. Chem.* **2009**, *48*, 5096.

ABSTRACT

A series of tantalum imido and amido complexes supported by a pyridine-linked *bis*(phenolate) ligand has been synthesized. Characterization of these complexes *via* X-ray crystallography reveals both C_s and C_2 binding modes of the *bis*(phenolate)pyridine ligand, with complexes containing two or fewer strong π-donor interactions from ancillary ligands giving C_s symmetry, while three strong π-donor interactions (e.g. three amido ligands or one amido ligand and one imido ligand) give C_2-symmetric binding of the *bis*(phenolate)pyridine ligand. DFT calculations and molecular orbital analyses of the complexes have revealed that the preference for C_s-symmetric ligand binding is a result of tantalum-phenolate π-bonding; whereas in cases where tantalum-phenolate π-bonding is overridden by stronger Ta-N π-bonding, C_2-symmetric ligand binding is preferred, likely because this is the lowest-energy conformation. This electronically driven change in geometry indicates that, unlike analogous metallocene systems, the *bis*(phenolate)pyridine pincer ligand is not a strong enough π-donor to exert dominant control over the electronic and geometric properties of the complex.

INTRODUCTION

The chemistry of the early transition metals has, to a large extent, been advanced by the use of bent metallocene frameworks. However, there has been increased interest in using well-defined, mono- and polydentate "non-metallocene" ligand sets to support a diverse range of organometallic complexes, transformations, catalysis, and small molecule activation studies.[1-13] Non-metallocene ligand sets offer a wide variety of symmetries and donor groups; these traits are particularly desirable for developing catalysts capable of mediating new stereocontrolled reactions. These multidentate ligands have been used in olefin polymerization catalysis and as scaffolds to study basic organometallic transformations.[14-33]

Recently, our group[34] and others[35,36] have been investigating arene- and heterocycle-linked *bis*(phenolate)donor ligand sets (heterocycle = pyridine, furan, thiophene) as supports for titanium and zirconium polymerization catalysts[34] and as ancillary ligands for tantalum to explore other organometallic transformations.[37,38] These non-metallocene ligand sets are connected through sp^2-sp^2 aryl-aryl or aryl-heterocycle linkages[39] instead of more flexible sp^3-sp^3 linkages, imparting increased rigidity of the backbone, which could result in more thermally robust catalysts that are less prone to undergo ligand C-H activation.[36] One advantage of these LX_2-type ligand systems is that they easily accommodate higher oxidation states commonly found for compounds of the early transition metals. Metal complexes with *bis*(phenolate)donor ligands are also attractive because they have frontier orbitals similar to metallocenes,[38] and can adopt a

range of symmetries (C_1, C_2 C_{2v}, C_s) similar to metallocene propylene polymerization catalysts that can generate atactic, isotactic, or syndiotactic polypropylene (Scheme 2.1).

Scheme 2.1

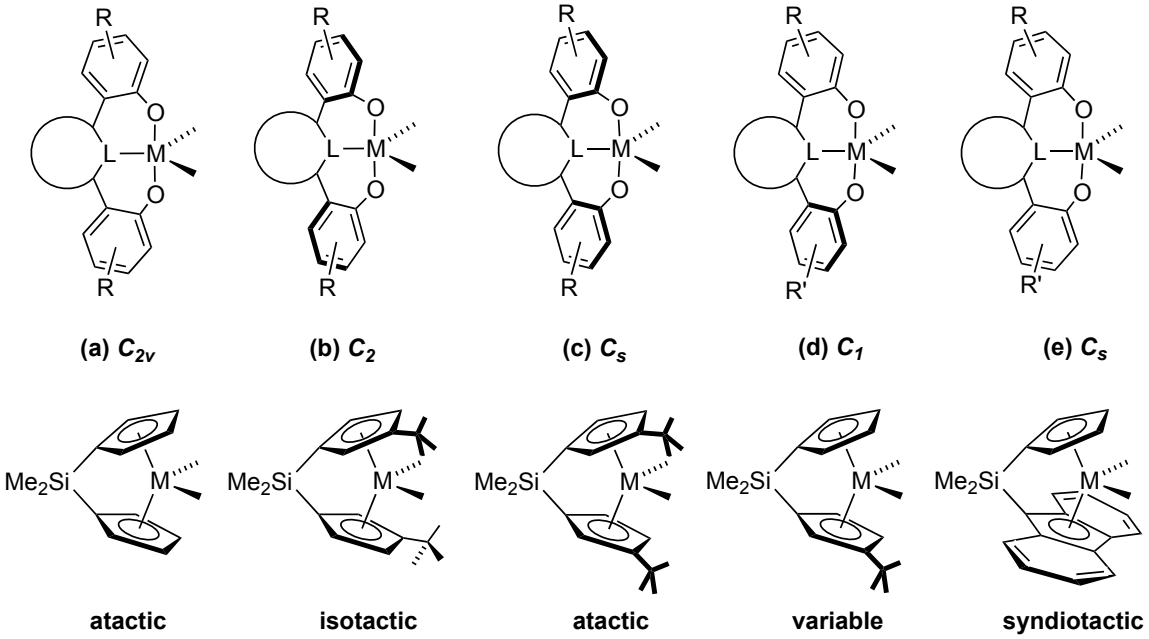

R, R' = alkyl, aryl; Linker = pyridine, phenyl, pyrrole, furan, thiophene, or NHC; L = C (neutral or anionic), N, O, or S

With the intent to further develop the organometallic chemistry of early transition metals supported by these pincer ligands, a series of tantalum amine, amido, and imido complexes has been synthesized. These complexes have been particularly instructive for furthering our understanding of the importance of phenolate–metal π–bonding on the preferred [(ONO)Ta] symmetry and have provided insights into the differences between the [(ONO)Ta] and [Cp_2Ta] platforms (ONO = pyridine-2,6-*bis*(4,6-^{t}Bu$_2$-phenolate)). Herein we describe the synthesis of an unusual amino–amido–imido tantalum species supported by a pyridine-linked *bis*(phenolate) ligand, and discuss its structural preferences in relation to other new dimethylamido and phenylimido tantalum complexes having the *bis*(phenolate)pyridine [(ONO)Ta] ligand platform.

RESULTS

Reaction of (ONO)TaMe$_3$ (ONO = pyridine-2,6-*bis*(4,6-^{t}Bu$_2$-phenolate)) with three equivalents of aniline at 90 °C over the course of 12 hours yields the imido-amido-amino tantalum complex, (ONO)Ta(NPh)(NHPh)(NH$_2$Ph) (**2.1**) (eq 2.1)[40]. **2.1** crystallizes from a concentrated solution of benzene upon cooling from 90 °C to room temperature and was characterized by X-ray crystallography.

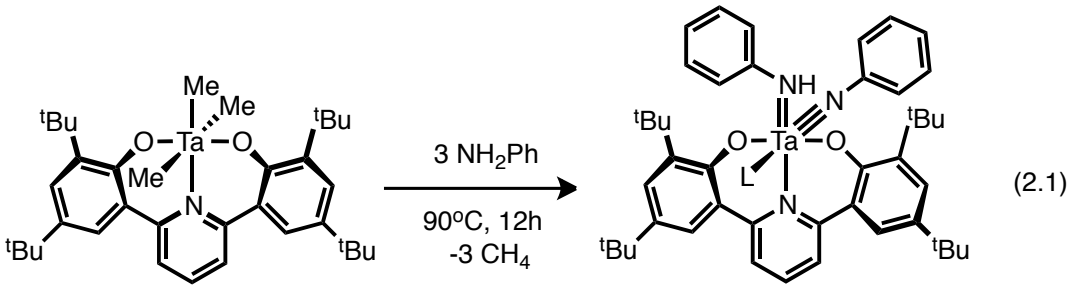

(2.1)

The Ta-N bond lengths for **2.1** (Figure 2.1) are indicative of three types of Ta-N bonding: 2.480(1) Å for the L-type aniline; 2.027(1) Å for the LX-type anilide; and 1.786(1) Å for the LX$_2$-type phenylimide. The *bis*(phenolate)pyridine ligand binds in a meridional fashion, with the anilide ligand *trans* to the pyridine linker and aligned perpendicular to the O-Ta-O plane—opposite alignment to what was observed in the benzylidene complex (ONO)Ta(CHPh)(Bn)(PR$_3$).[38] This meridional binding mode is typical for early metal complexes of the *bis*(phenolate)pyridine ligand; however, it is the first six-coordinate tantalum complex to exhibit a C_2-symmetric binding of the ligand instead of the typically observed C_s-symmetric binding (for example for the (ONO)TaMe$_3$ starting material in equation 2.1 is C_s). The dihedral angle of 58.7° between the two phenolate groups indicates a significant C_2 twist of the ligand. Additionally, the pyridine linker of

2.1 binds in a much more linear fashion: the Ta1–N4–C11 angle is 170.8°, whereas in the C_s-symmetric cases the angle is typically 150–160°. Interestingly, the NH protons on the L-type aniline appear as a broad singlet in the ^{1}H NMR despite being diastereotopic. We believe this is a result of equilibration due to rapid interconversion of enantiomers of the C_2 geometry in solution, probably progressing through a C_{2v}-symmetric intermediate. The average Ta–O bond distance in **2.1** is 2.002(1) Å, which is significantly (~ 0.1 Å) longer than the distances observed earlier.[38] These structural features prompted further investigation of the underlying reasons for a preference for C_2 versus C_s ligand geometry and the preferences for the ligand *trans* to the pyridine in these complexes.

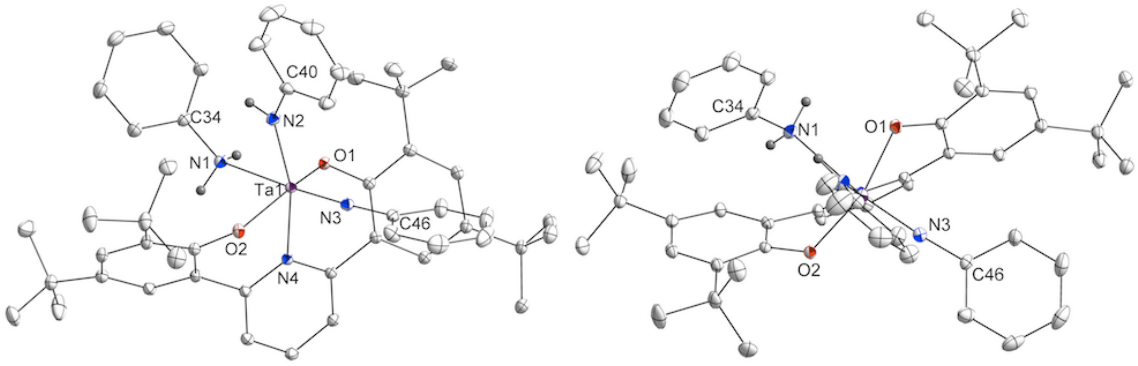

Figure 2.1. Thermal ellipsoid drawing of **2.1**. Side view and top-down view showing C_2-symmetric bisphenolate ligand. Selected bond lengths (Å) and angles (°): Ta–O1 2.0045(10); Ta–O2 1.9999(11); Ta–N1 2.4796(13); Ta–N2 2.0271(11); Ta–N3 1.7865(13); Ta–N4 2.3126(10); Ta–N4–C34 127.21(9); Ta–N2–C40 139.07(10); Ta–N3–C46 176.07(11). N-bound hydrogens in calculated positions, all others omitted for clarity. Solvent omitted for clarity.

A distinctive feature of **2.1** (an (ONO)Ta(L)(LX)(LX_2)-type complex), as opposed to all previously studied (ONO)TaX_3 complexes, is presence of three strong Ta–X π bonds—one for the amido and two for the imido ligand. We therefore hypothesized that these Ta–N π bonds were responsible for the observed C_2 rather than C_s ligand geometry. A

series of [(ONO)Ta] amides and imides with varying X-type, LX-type, and LX_2-type ligands, and hence differing numbers Ta-N of π-bonds, were synthesized (Scheme 2.2).

Scheme 2.2

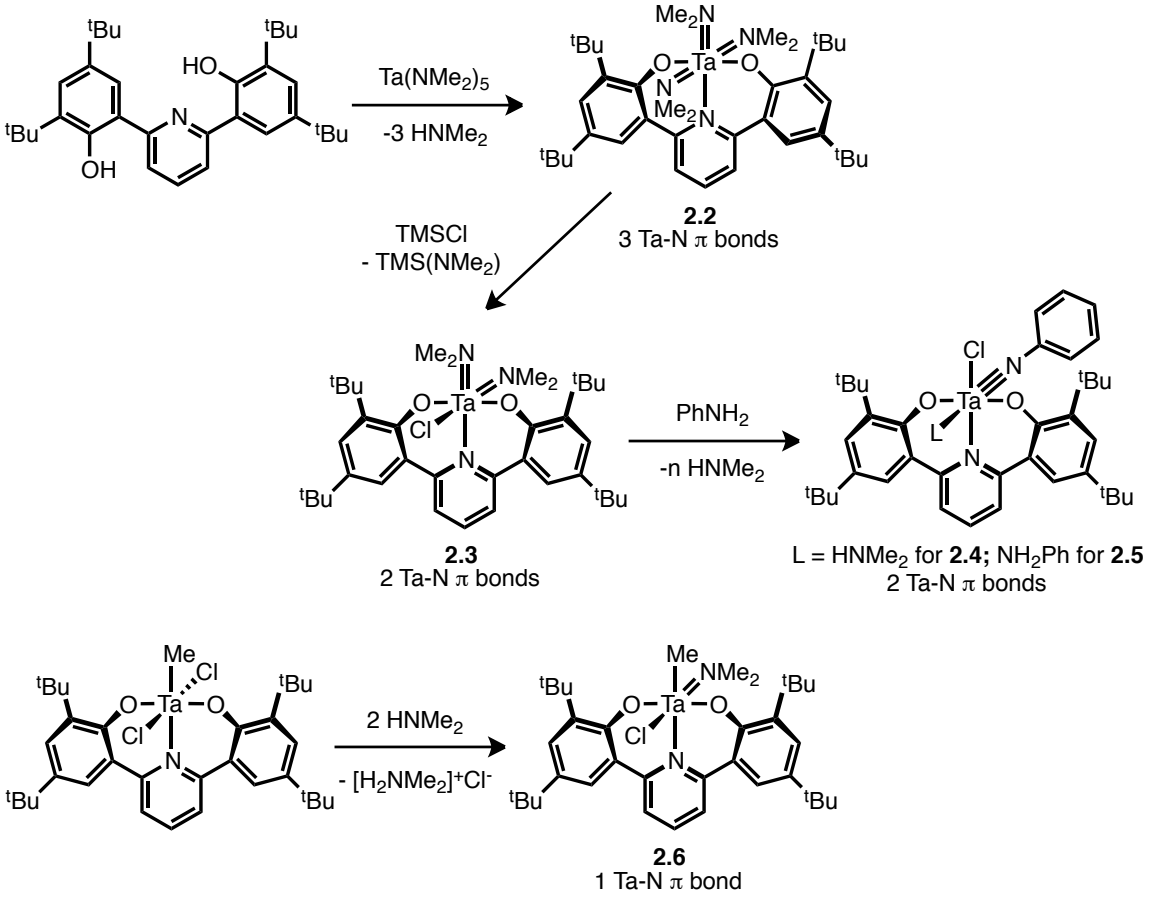

$(ONO)H_2$ reacts cleanly with $Ta(NMe_2)_5$ at room temperature in benzene to yield the *tris*(amide) complex $(ONO)Ta(NMe_2)_3$ (**2.2**). The ^1H NMR spectrum of **2.2** shows two sharp singlets at 2.98 and 3.74 ppm in a 12:6 ratio, indicative of two distinctive types of dimethylamido groups—one type *cis* to NC_6H_3 and the other *trans*. In contrast to $(ONO)TaMe_3$,[38] **2.2** shows no fluxional exchange between the dimethylamido groups even at elevated temperatures; likely a result of the increased preference for octahedral, rather than trigonal prismatic geometry (the proposed intermediate for ligand site exchange),[38]

resulting from strong Ta=N π-bonding. X-ray quality crystals of **2.2** were grown from a saturated diethyl ether solution cooled to -30 °C. The crystal structure (Figure 2.2) of **2.2** reveals the *bis*(phenolate)pyridine ligand binds to tantalum meridionally in a C_2-symmetric fashion as expected for a complex similar to complex **2.1** with three strong Ta-N π bonds. In fact, the *bis*(phenolate)pyridine ligand in **2.2** shares all of the new characteristic properties observed for **2.1**. The dihedral angle between the two phenyl rings of the *bis*(phenoxide) ligand is 59.7°, again indicating a significant C_2 twist of the ligand. The Ta1-N1-C11 angle is 178°, indicating an almost linear binding of the pyridine linker; and finally, the average Ta-O bond distances are long at 1.985(2) Å. The Ta-N bond lengths of the amides *cis* to pyridine are slightly longer than that for the amide *trans* to pyridine: 2.029(2) and 2.032(2) versus 1.994(2)Å, respectively, indicative of a slightly larger amide *trans* influence, but well within the range of Ta-N double bonds.

When complex **2.2** is treated with 1 equivalent of TMSCl in benzene, the monochlorinated product (ONO)Ta$(NMe_2)_2$Cl (**2.3**) is generated quantitatively over two hours at 90 °C. Complex **2.3** exhibits sharp singlets at 3.03 and 3.92 ppm corresponding to the dimethylamido groups *cis* and *trans* to pyridine, respectively, and similar to complex **2.2**, no fluxionality is observed even at elevated temperatures. X-ray quality crystals of **2.3** were grown by slow evaporation from a saturated diethyl ether solution (Figure 2.3). The *bis*(phenolate)pyridine ligand in complex **2.3** binds meridionally, as for **2.1** and **2.2**, but in a C_s-symmetric fashion where the mirror plane in the molecule bisects the phenolate-tantalum-phenolate angle. Consistent with the ^{1}H NMR spectrum, one of the dimethylamides lies *cis* to the pyridine while the other is *trans* and their bond

lengths are 1.979(2) Å and 1.982(2) Å, respectively—again, consistent with Ta=N double bonds. The average Ta-O phenolate bond distances in **2.3** are 1.924(3) Å, significantly shorter than seen in **2.1** and **2.2** (2.002(1) and 1.985(2) Å, respectively), implicating a greater degree of phenolate π-bonding in this complex. Indeed, this would be expected, as one phenolate π bond is required to complete an 18 electron count at tantalum.

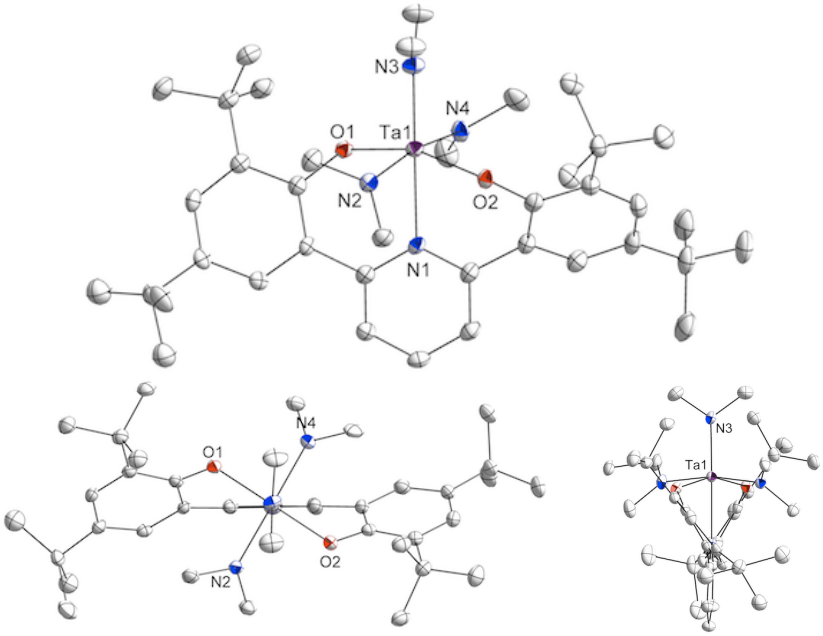

Figure 2.2. Thermal ellipsoid drawing of **2.2**, front view, top-down view showing C_2 symmetry, and side-on view showing the *bis*(phenolate)pyridine dihedral angle. Selected bond lengths (Å) and angles (º): Ta1-O1 1.9908(18); Ta1-O2 1.9788(18); Ta-N1 2.3111(23); Ta1-N2 2.0325(18); Ta1-N3 1.9941(24); Ta1-N4 2.0289(18); Ta1-N1-C9 178. H atoms admitted for clarity.

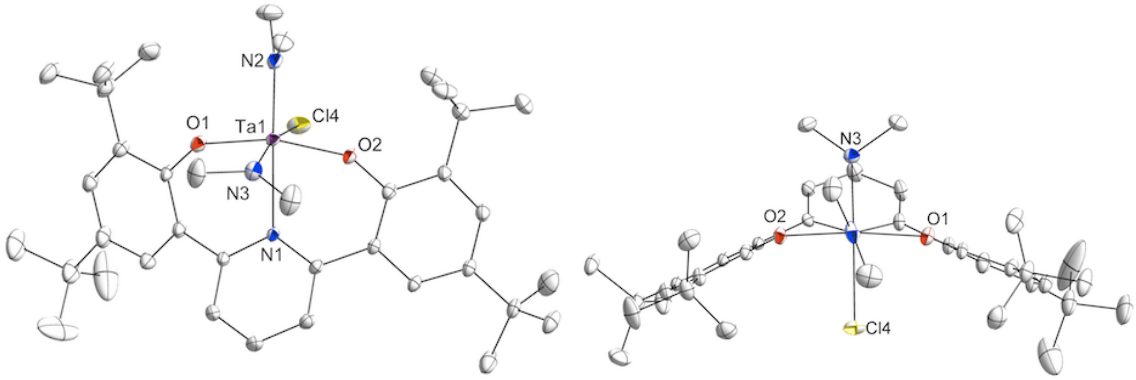

Figure 2.3. Thermal ellipsoid drawing of **2.3**. Front view (left) and top-down view (right) showing the C_s symmetry of *bis*(phenolate)pyridine ligand. Selected bond lengths (Å) and angles (°): Ta1-O1 1.9282(15); Ta1-O2 1.9207(17); Ta-N1 2.3922(18); Ta1-N2 1.9708(22); Ta1-N3 1.9848(21); Ta1-Cl1 2.4686(6); Ta-N1-C9 147.78(2). H atoms and solvent omitted for clarity.

Reaction of one equivalent of aniline with **2.3** in benzene at 90 °C for one week quantitatively yields the phenylimide chloride, (ONO)Ta(NPh)($HNMe_2$)Cl (**2.4**). A similar reaction with excess aniline yields (ONO)Ta(NPh)(H_2NPh)Cl (**2.5**), although only limited crystallographic identification of **2.5** has been obtained due to twinned, thermally unstable crystals. X-ray quality crystals of **2.4** were grown by slow evaporation of a saturated benzene solution. Complex **2.4**, as for **2.3**, has a C_s-symmetric, meridionally-bound (ONO) ligand (Figure 2.4). It is interesting to note that one of the phenolate arms is twisted 13.3° away from perfect C_s symmetry, possibly due to crystal packing forces. The pyridine linker is canted out of the O-Ta-O plane by 23.3°, which is typical in the C_s-symmetric binding mode. The Ta-N3 distance of 1.791(3) Å is typical for tantalum imides and the Ta1-N2-C26 angle of 174.1° indicates that it is an LX_2-type donor. The average Ta-O bond distance of 1.954(2) Å is shorter than observed in

complexes **2.1** and **2.2**, and more comparable to those in complex **2.3**, indicating some degree of Ta–O multiple bond character.

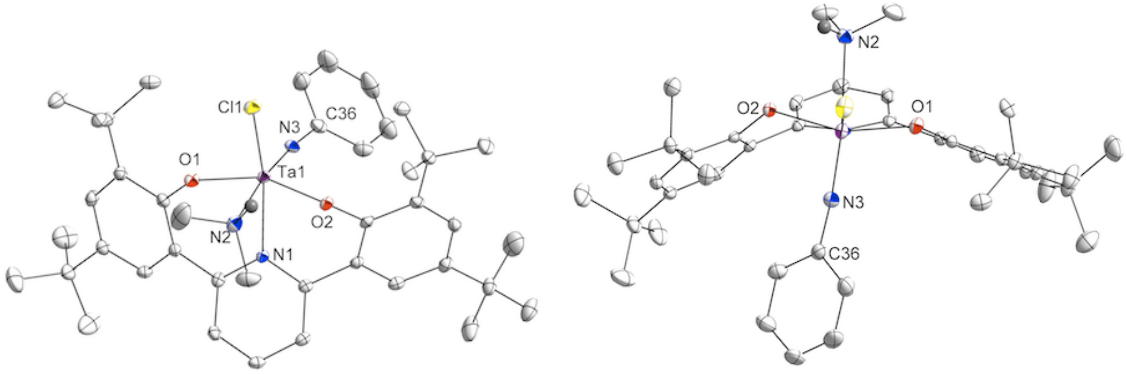

Figure 2.4. Thermal ellipsoid drawing of **2.4**. Front view (left) and top-down view (right) showing the C_s-geometry of *bis*(phenolate)pyridine ligand. Selected bond lengths (Å) and angles (°): Ta1–O1 1.9437(14); Ta1–O2 1.9643(13); Ta–N1 2.2918(17); Ta1–N2 2.4568(17); Ta1–N3 1.7841(14); Ta1–Cl1 2.3920(5); Ta–N1–C9 156.82(8); Ta–N3–C36 174.2(2). H atoms removed for clarity.

Reaction of an excess of $HNMe_2$ with $(ONO)TaCl_2Me$ in benzene rapidly forms the mono(dimethylamido) complex, $(ONO)Ta(NMe_2)MeCl$ (**2.6**), with concomitant precipitation of H_2NMe_2Cl. X-ray quality crystals were obtained by cooling a saturated solution of **2.6** in diethyl ether to -30 °C overnight. Complex **2.6** (Figure 2.5) displays the usual meridional binding of the *bis*(phenolate)pyridine ligand, and like complexes **2.3**–**2.5**, is C_s symmetric. The average Ta–O bond length is 1.887(2), and the dimethylamido Ta–N distance of 1.975(2) is typical of a Ta=N double bond. Interestingly, the π-bonding amide in **2.6** lies *cis* to the pyridine linker, whereas in the previously reported benzylidene[38] the π-bond lies *trans* to pyridine. The ^{1}H NMR spectrum is consistent with a *cis* amide, as the dimethylamide singlet resonates at 3.21 ppm, in the range of the *cis* dimethylamide peaks seen in complexes **2.2** and **2.3**. Because a tantalum dπ orbital is

available in both the *cis* and *trans* positions (*vide infra*), there does not appear to be a strong electronic preference for either coordination site. Thus, we attribute this *cis* preference of the amide to steric interactions for the alternate geometry; the bulkiest ligand (NMe_2) would be best accommodated in one of the *cis* positions. In the benzylidene example, the π-bonding benzylidene is the *least* bulky substituent. This could also be a result of the strongest *trans*-influencing ligand (Me or Bn) preferring to be *trans* to weak NC_6H_3 ligand.

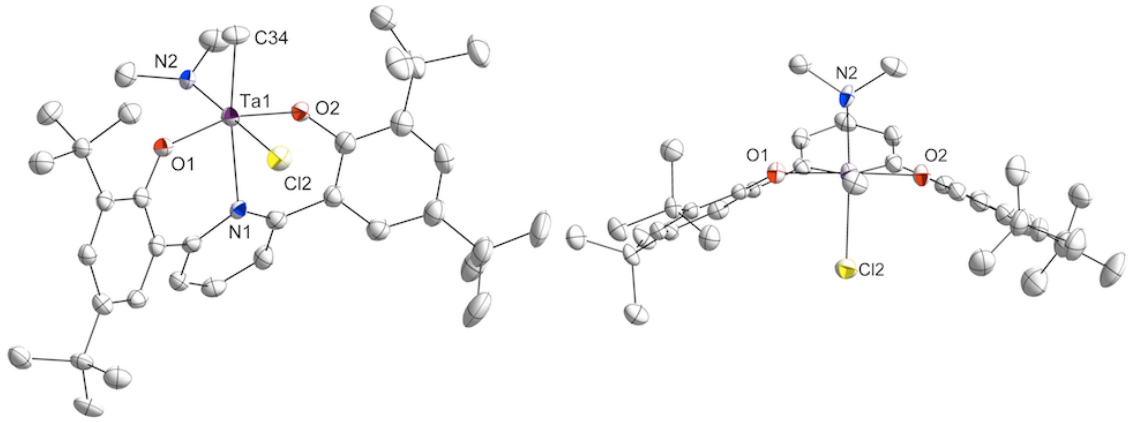

Figure 2.5. Thermal ellipsoid drawing of **2.6**. Front view (left) and top-down view (right) showing C_s-symmetric binding of the *bis*(phenolate)pyridine ligand. Selected bond lengths (Å) and angles (°): Ta1-O1 1.8936(25); Ta1-O2 1.8810(26); Ta-N1 2.3916(31); Ta1-N2 1.9746(37); Ta1-C34 2.1908(51); Ta1-Cl1 2.4683(11); Ta-N1-C9 149.6(2). H atoms removed for clarity.

DISCUSSION

From the structural data for complexes **2.1–2.6**, as well as for other previously reported tantalum complexes containing the *bis*(phenolate)pyridine ancillary ligand, it is apparent that the number of strong tantalum–nitrogen π bonds for the remaining three ligands significantly affects the degree of Ta–O π bonding for the two phenolate arms. The amount of Ta–O π bonding can be quantified by examining the distances in the solid state structures (Table 2.1). In complexes where there is no π bonding, i.e., the remaining three ligands are X-type, the average Ta–O bond length is roughly 1.9 Å. As the number of π-bonding ligands is increased, a corresponding increase in Ta–O bond length is also observed, reaching as high as 2.0 Å in cases where there are three strong π-donating ancillary ligands, as is the case with **2.1** (L, LX, and LX_2 ligands) and **2.2** (three LX ligands). Thus, it is apparent that the Ta–O bond order decreases as additional strong π bonders are introduced into the system—going from a Ta–O bond order of 2 in the case of zero π donating ligands down to an order of 1 when there are three strong π donating ligands. The rather small change in the Ta–O bond length over all of the compounds (~ 0.1 Å) is likely due to generally poor π donating ability of electronegative oxygen and the inherent rigidity of the system, which should limit the overall change in bond lengths.

From a molecular orbital perspective, a C_s-symmetric *bis*(phenolate)pyridine ligand should be able to form π bonding interactions with d_{xz} and d_{xy} orbitals of Ta using lone pairs on each oxygen (the bonding linear combination of oxygen p_z's (and p_y's) and tantalum d_{xz} (and d_{xy}) are shown at the top of Scheme 2.3). In the case of the

mono(amide) **2.6** and the previously reported benzylidene complex,[38] where a single ancillary ligand engages in π bonding, these Ta–O π interactions force the amide (or benzylidene) ligand to π bond with d_{yz}, despite the steric consequence of forcing the amide methyls or phenyl of the benzylidene toward a phenolate *tert*–butyl group(s).

Table 2.1. Solid–state ligand symmetries and Ta–O bond length in selected (ONO)Ta complexes.

L_3 for (ONO)TaL_3	Symmetry	# of Ta=L π bonds	Avg. Ta–O bond order[a]	d(Ta–O)$_{avg}$ (Å)
(NPh)(NHPh)(NH_2Ph) (**2.1**)	C_2	3	1	2.002(1)
(NMe_2)$_3$ (**2.2**)	C_2	3	1	1.985(2)
(NMe_2)$_2$Cl (**2.3**)	C_s	2	1.5	1.924(3)
(NPh)($HNMe_2$)Cl (**2.4**)	C_s	2	1.5	1.954(2)
(NPh)(NH_2Ph)Cl (**2.5**)	C_s	2	1.5	1.948(3)[b]
(NMe_2)(CH_3)Cl (**2.6**)	C_s	1	2	1.887(2)
(=CHPh)(CH_2Ph)(PR_3)[c]	C_s	1	2	1.922(1)
(CH_3)$_3$[d]	C_s	0	2[d]	1.906(1)

[a]To complete the 18 electron count at Ta. [b]Complex not anisotropically refined. [c]Taken from ref. 38. [d]16 electron maximum.

However, in the case where there are two ligand π bonds such as the *bis*(amide) **2.3** or the phenylimide–chlorides **2.4** and **2.5**, one of the two Ta–O π bonds must be sacrificed to make the second amido/imido π bond. For **2.4** and **2.5** (shown in Scheme 2.3) the remaining Ta–O π interaction occurs through d_{xz}; for **2.3** (not shown) it interacts with d_{xy}.[41] Finally, in the case where there are three strong ancillary ligand π bonds, all Ta–O π bonding is precluded to accommodate the other ligands. In these cases, the *bis*(phenolate) ligand twists from C_s–symmetry to C_2–symmetry. This alternate geometry is likely due to two factors. First, twisting to C_2 symmetry reduces overlap between the

oxygen p orbitals and the filled N–to–Ta π bonds, reducing energetically unfavorable filled–filled repulsions. Second, this twist could be a geometric relaxation effect; the C_2–symmetry can better accommodate the large tantalum atom because twisting lengthens the Ta–O bonds. As evidenced by the canted pyridine rings, C_s symmetry, while increasing Ta–O bonding, also forces an unnatural Ta–pyridine bond length. The implication of either explanation is that any oxygen π–bonding encourages C_s–symmetric binding, since the overlap between the tantalum d orbitals and occupied oxygen p orbitals is essentially lost in the C_2 geometry.

Scheme 2.3

0 or 1 (shown) strong Ta-N π bonds

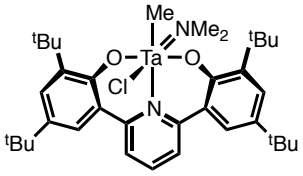

2.6
(similarly for (ONO)Ta(=CHPh)(CH$_2$Ph)(PR$_3$))

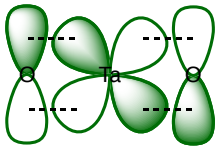

phenolate p_z-d_{xz}

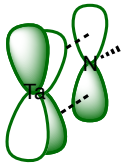

amide p_z-d_{yz}

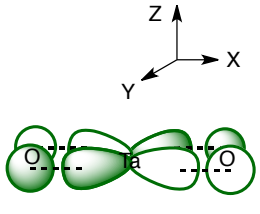

phenolate p_y-d_{xy}

2 strong Ta-N π bonds

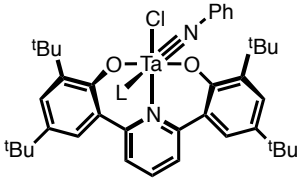

2.4, **2.5**
(similarly for **2.3**)

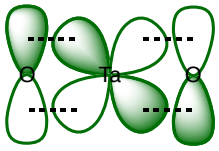

phenolate p_z-d_{xz}

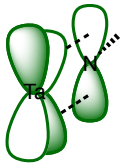

imide p_z-d_{yz}

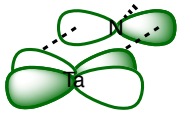

imide p_y-d_{xy}

3 strong Ta-N π bonds

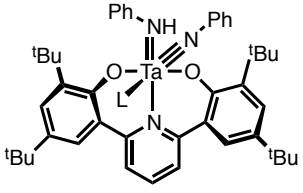

2.1 and **2.2**

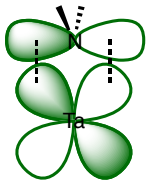

amide p_z-d_{xz}

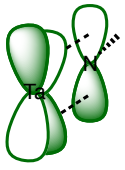

imide p_z-d_{yz}

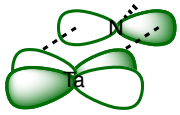

imide p_y-d_{xy}

DFT calculations (B3LYP, 6-31G**, LANL2DZ Ta pseudopotential) were performed on complex **2.1** in order to affirm the bonding description described above. A structural optimization starting from the crystal structure coordinates was performed and produced a structure very similar to the experimentally observed one. The calculated HOMO, HOMO-1, and HOMO-2 distinctly show the anilide-d_{xz}, imide-d_{yz}, and imide-d_{xy} π bonding interactions, consistent with the bond distances observed in the crystal structure (Figure 2.6). Notably absent in the calculated results are any phenolate-tantalum 3-center-4-electron π bonding, which is observed in other calculations performed on complexes supported by this ligand set.[38] The absence of phenolate π bonding is, however, not entirely surprising; assuming that the phenylimide and anilide are stronger π donors than the phenolate, no phenolate π bonding would be necessary to complete the 18-electron count at tantalum. This bonding picture, however, is very different from its earlier-reported metallocene counterpart $Cp^*_2Ta(=NPh)(H)$.[42] In the metallocene case, rather than displace the strong Cp*-Ta bonds, the nitrogen lone pair remains nonbonding—demonstrating one key difference between the *bis*(phenolate)pyridine and metallocene ligand systems: unlike metallocenes, phenolates are not strong enough π donors to effectively compete with strong π donating amido and imido ancillary ligands.

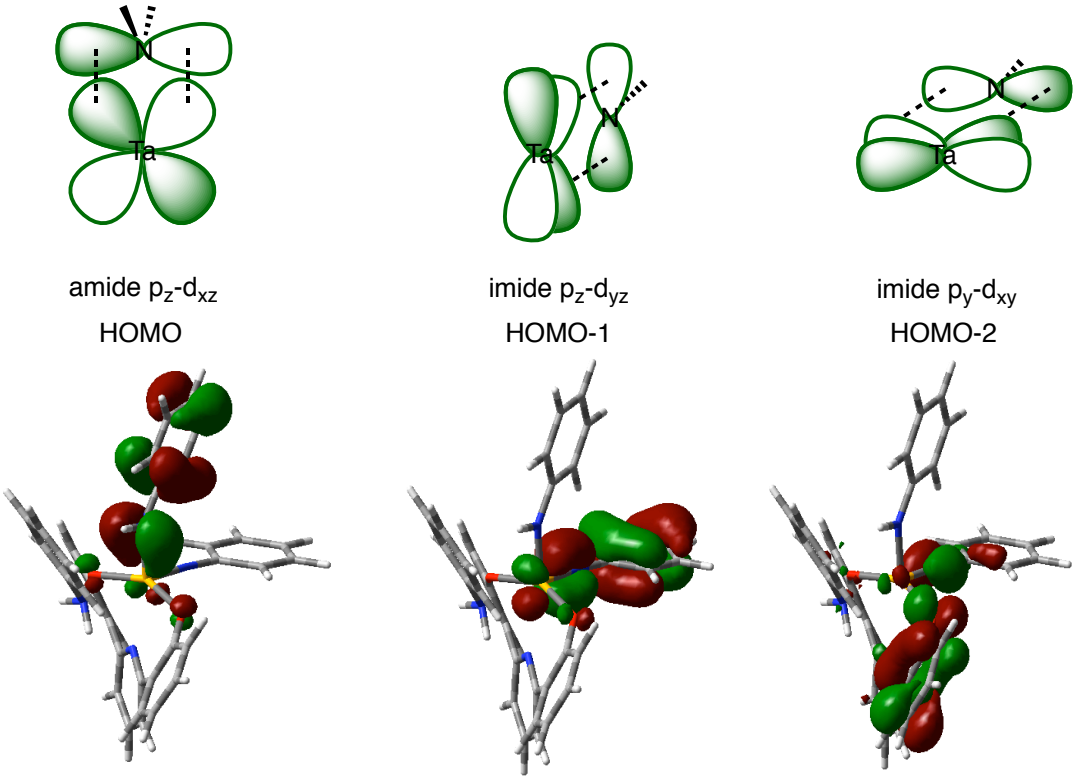

Figure 2.6. DFT calculations of **2.1** (B3LYP, 6-31G**, LANL2DZ Ta pseudopotential) showing HOMO, HOMO-1, and HOMO-2 (L-R), representing the three Ta-N π bonds.

In order to address the possibility of steric repulsion driving the C_s-to-C_2 geometry switch, DFT calculations (B3LYP, 6-31G**, LANL2DZ Ta pseudopotential) were also carried out on simpler complexes with significantly less steric bulk than the synthesized complexes. In all of these cases, the *ortho* and *para tert*-butyl groups in the ligand backbone were removed. Calculations were performed on (ONO)Ta(NH_3)(NH_2)(NH) and (ONO)Ta(NMe_2)$_3$ which are expected to be C_2-symmetric according to the bonding arguments above. The expected C_2-symmetry is obtained upon optimization of either C_{2v} or C_2 unoptimized starting structures. Similarly, calculations on (ONO)Ta(NH_2)$_2$Cl, (ONO)Ta(NH_3)(NH)Cl, and (ONO)Ta(NMe_2)$_2$Cl, expected to display C_s-symmetry, also yield

this symmetry upon optimization from either C_{2v} or C_s unoptimized starting structures. The optimized structures from these calculations are shown in Figure 2.7. It is noteworthy that in (ONO)Ta(NMe_2)$_3$ and (ONO)Ta(NMe_2)$_2$Cl, which differ from their synthesized analogues only by removal of the *tert*-butyl bulk, the optimized structures do not significantly differ from the structures obtained from X-ray diffraction (< 0.01 Å Ta-O bond length and < 0.7° phenolate torsion angle). Additionally, small steric effects can be seen by comparing the optimized structures of (ONO)Ta(NH_2)$_2$Cl and (ONO)Ta(NMe_2)$_2$Cl. In the case of (ONO)Ta(NH_2)$_2$Cl the NH_2 *trans* to pyridine lies perpendicular to the O-Ta-O plane, while in (ONO)Ta(NMe_2)$_2$Cl the dimethylamide is twisted away from perpendicular. We attribute this twist to a small steric effect that is also seen in complexes **2.2** and **2.3**; it is notable that while the amide ligands rotate to reduce steric repulsion, no perturbation of the (ONO) framework is observed. These results, as well as earlier observations that other quite bulky complexes based on this ligand set such as (ONO)Ta(Bn)(CHPh)(PMe_2Ph) still exhibit C_s-symmetry,[38] lead us to believe that the steric demands of the ligands are not a major cause of geometric rearrangement.

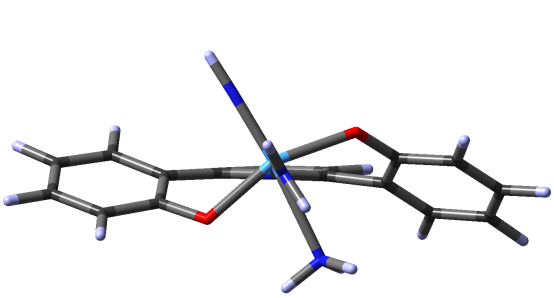

(ONO)Ta(NH)(NH_2)(NH_3) – C_2

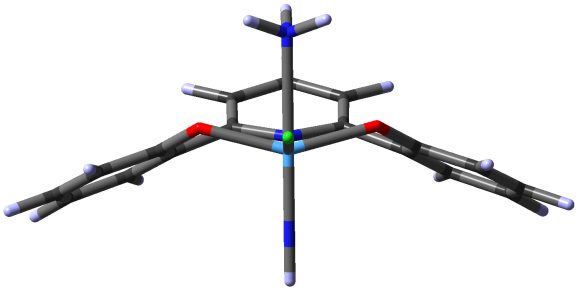

(ONO)Ta(NH)(NH_3)Cl – C_s

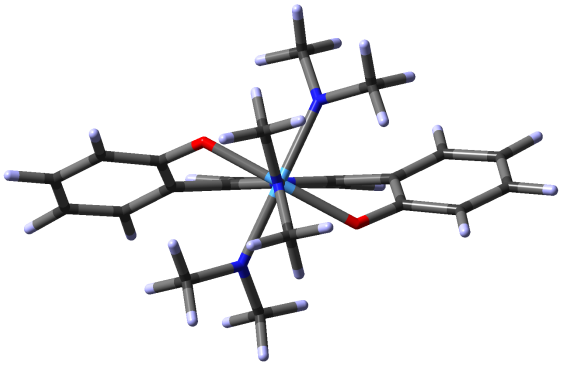

(ONO)Ta(NMe_2)$_3$ – C_2

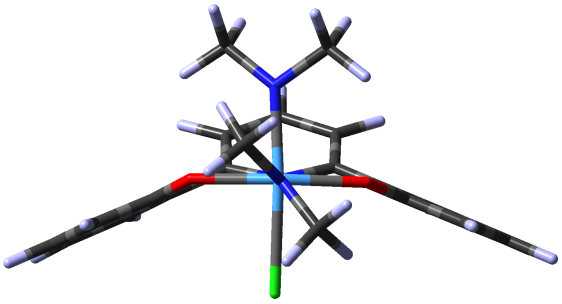

(ONO)Ta(NMe_2)$_2$Cl – C_s

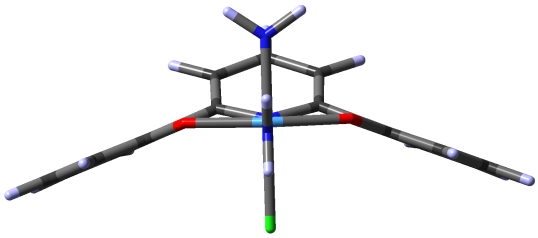

(ONO)Ta(NH_2)$_2$Cl – C_s

Figure 2.7. DFT (B3LYP, 6–31G**, LANL2DZ Ta pseudopotential) optimized structures (see text) of calculated complexes displaying C_2 and C_s–symmetric structures with significantly smaller ligands.

Attempts to make the analogous tantalum oxo series of compounds have been unsuccessful to date. Instead, the reaction of (ONO)$TaMe_3$ with degassed H_2O yields oxo–bridged dimer products (eq 2.2). The *bis*–μ–oxo complex **2.7** represents the first

crystallographically characterized tantalum *bis*(phenolate)pyridine complex that exhibits facial binding of the ligand (Figure 2.8). This complex, along with a related titanium complex[43] supports the proposed intermediacy of a facially bound isomer in the exchange of methyl groups in (ONO)$TaMe_3$ as proposed earlier.[38]

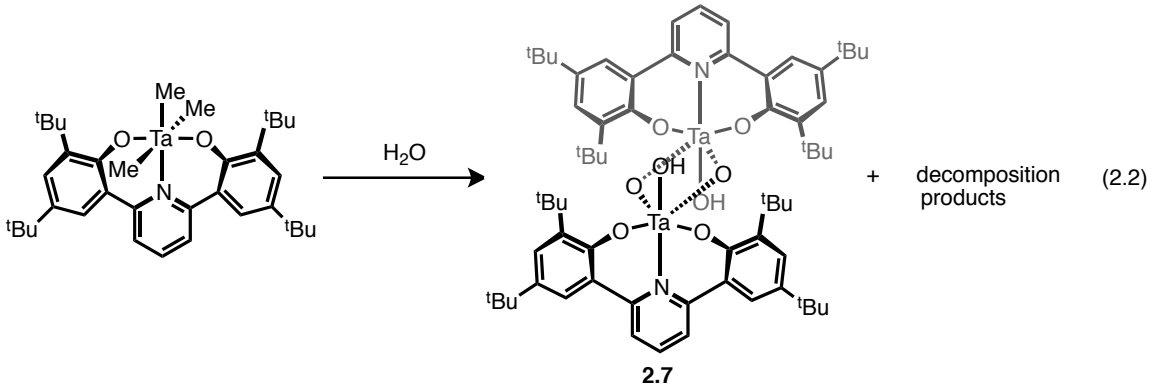

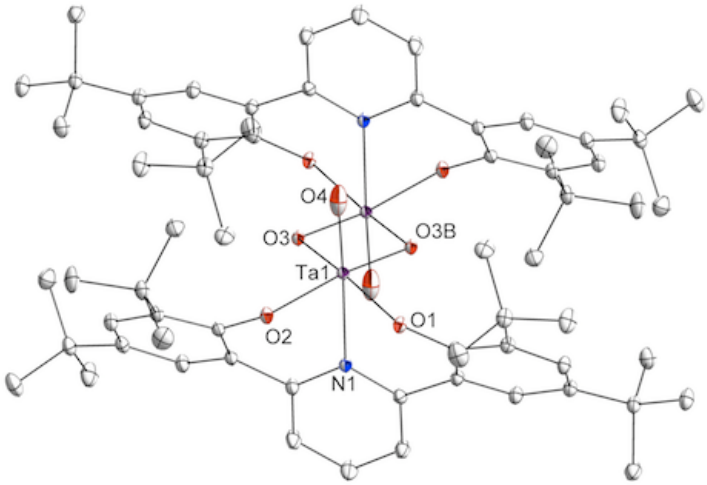

Figure 2.8. Thermal ellipsoid drawing of **2.7**. Front view showing *fac*- binding of the *bis*(phenolate)pyridine ligand. Selected bond lengths (Å): Ta1-O1 1.9502(5); Ta1-O2 1.9622(5); Ta-O3 1.9431(5); Ta1-O3b 1.9328(5); Ta1-O4 2.0733(8); Ta1-N1 2.3120(5); Ta1-Ta1b 2.9917(1). H atoms and solvent removed for clarity.

CONCLUSIONS

A series of imido and amido complexes supported by a pyridine-linked *bis*(phenolate) ligand have been synthesized and structurally characterized *via* NMR and X-ray crystallography. These complexes exhibit either a C_s- or C_2-symmetric meridional binding of the *bis*(phenolate) ligand. The preferred geometry appears to be determined by the degree of Ta-O π bonding with the phenolate ligands. When Ta-O π bonds are required to complete the 18 electron count of the Ta center, the *bis*(phenolate)pyridine ligand binds in a C_s-symmetric fashion. In cases where strong π donation from ancillary ligands precludes Ta-O π bonding (i.e., when there are three strong π donor interactions from the other ligands), the *bis*(phenolate) ligand twists in a C_2 fashion to reduce filled-filled repulsions between the Ta-X π bonds and the oxygen lone pairs and to a less strained (ONO) geometry. This electronically driven change in geometry indicates that, unlike analogous metallocene systems, the *bis*(phenolate) pincer ligand is not a strong enough π-donor to exert total control over the electronic and geometric properties of the complex.

EXPERIMENTAL SECTION

General Considerations and Instrumentation. All air- and moisture-sensitive compounds were manipulated using standard high vacuum and Schlenk techniques or manipulated in a glovebox under a nitrogen atmosphere. Solvents for air- and moisture-sensitive reactions were dried over sodium benzophenone ketyl and stored over titanocene, where compatible or dried by the method of Grubbs.[44] Benzene-d_6 and toluene-d_8 were purchased from Cambridge Isotopes and dried over sodium benzophenone ketyl, while methylene chloride-d_2, also purchased from Cambridge Isotopes, was dried over CaH_2 and filtered through a plug of activated alumina. $TaCl_5$ was purchased from Strem Chemicals was sublimed prior to use. Amines were purchased from Sigma-Aldrich, and were distilled from CaH_2 and degassed prior to use. 2,6-$(HOC_6H_2$-^{t}Bu$_2)_2C_5H_3N$, (2,6-$(OC_6H_2$-^{t}Bu$_2)_2C_5H_3N)TaMe$_3$, and (2,6-$(OC_6H_2$-^{t}Bu$_2)_2C_5H_3N)TaCl$_2$Me were prepared as previously reported.[38] All other materials were used as received. ^{1}H, and ^{13}C spectra were recorded on Varian Mercury 300 or Varian INOVA 500 spectrometers and chemical shifts are reported with respect to residual protio-solvent impurity for ^{1}H (*s*, 7.16 ppm for C_6D_5H; *t*, 5.32 ppm for $CDHCl_2$) and solvent carbons for ^{13}C (*t*, 128.39 for C_6H_6; *s*, 20.40 for CD_2Cl_2). Despite repeated attempts acceptable elemental analyses for complexes **2.1**, **2.4**, and **2.5** were not obtained, likely a result of the labile L-donors or the loss of some solvent from the crystal lattices.

Computational Details. Density functional calculations were carried out using Gaussian 03 Revision D.01.[45] Calculations on the model systems (with minimal steric bulk)

were performed using the nonlocal exchange correction by Becke[46,47] and nonlocal correlation corrections by Perdew,[48] as implemented using the b3lyp[49,50] keyword in Gaussian. The following basis sets were used: LANL2DZ[51-53] for Ta atoms and 6-31G** basis set for all other atoms. Pseudopotentials were utilized for Ta atoms using the LANL2DZ ECP. All optimized structures were verified using frequency calculations and did not contain any imaginary frequencies. Iso-surface plots were made using the Gaussian 03 Revision D.01 program.[45]

X-ray Crystal Data: General Procedure. Crystals were removed quickly from a scintillation vial to a microscope slide coated with Paratone N oil. Samples were selected and mounted on a glass fiber with Paratone N oil. Data collection was carried out on a Bruker KAPPA APEX II diffractometer with a 0.71073 Å MoKα source. The structures were solved by direct methods. All non-hydrogen atoms were refined anisotropically. Some details regarding refined data and cell parameters are available in Tables 2.2 and 2.3. Selected bond distances and angles are supplied in the corresponding figures.

Synthesis of (2,6-(OC$_6$H$_2$-^{t}Bu$_2$)$_2$C$_5$H$_3$N)Ta(NPh)(NHPh)(NH$_2$Ph) (2.1). In an inert atmosphere glovebox, a 25 mL glass tube fitted with a teflon screwcap valve was charged with (2,6-(OC$_6$H$_2$-^{t}Bu$_2$)$_2$C$_5$H$_3$N)TaMe$_3$ (100 mg, .141 mmol, 1 equiv) and 10 mL C$_6$H$_6$. PhNH$_2$ (38.5 μL, .4225 mmol, 3 equiv) was syringed in, and the vessel was sealed and placed in a 90 °C bath for 14 hours. After 14 hours, solvent was removed *in vacuo*, and the resulting yellow solid was washed with petroleum ether and collected on a sintered glass funnel as 68 mg (51% yield) of a white powder. ^{1}H NMR (300 MHz, CD$_2$Cl$_2$) δ, ppm: 1.065 (*s*, 1H, Ta-N*H*Ph); 1.394 (*s*, 18H, C(C*H*$_3$)$_3$); 1.428 (*s*, 18H, C(C*H*$_3$)$_3$); 4.106 (*s*,

2H, Ta-NH_2Ph); 5.96 (*d* + *t*, 3H, aryl-*H*); 6.358 (*d*, 2H, aryl-*H*); 6.505 (*t*, 1H, aryl-*H*); 6.575 (*d*, 2H, aryl-*H*); 6.853 (*t*, 2H, aryl-*H*); 6.893 (*t*, 2H, aryl-*H*); 7.035 (*t*, 1H, aryl-*H*); 7.213 (*t*, 2H, aryl-*H*); 7.596 (*s*, 1H, aryl-*H*); 7.635 (*s*, 1H, aryl-*H*); 7.892 (*d*, 2H, 3,5-C_5NH_3); 8.038 (*t*, 1H, p-C_5NH_3). ^{13}C NMR (125 MHz, CD_2Cl_2) δ, ppm: 29.87 (C(*C*H_3)$_3$); 31.71 (C(*C*H_3)$_3$); 34.62 (*C*$(CH_3)_3$); 35.38 (*C*$(CH_3)_3$); 118.47, 119.26, 119.43, 122.07, 123.51, 124.07, 124.31, 125.50, 126.68, 127.17, 127.47, 128.15, 129.59, 138.71, 139.29, 141.16, 141.34, 153.50, 115.83, 156.30, 159.73 (aryl). Calcd for $C_{51}H_{61}N_4O_2Ta$: C 64.96, H 6.52, N 5.94; Found: C 66.26, H 6.44, N 5.96 %.

Synthesis of (2,6-(OC$_6$H$_2$-^{t}Bu$_2$)$_2$C$_5$H$_3$N)Ta(NMe$_2$)$_3$ (2.2). In an inert atmosphere glovebox, 2,6-(HOC$_6$H$_2$-^{t}Bu$_2$)$_2$C$_5$H$_3$N (200 mg, .4115 mmol, 1 equiv) and Ta(NMe$_2$)$_5$ (165 mg, .4115 mmol, 1 equiv) were mixed in a 20 mL vial with 2 mL Et_2O. The reaction was stirred for 4 hours, resulting in a mustard-colored precipitate and a darker yellow solution. After 4 hours, the solvent and $HNMe_2$ were removed *in vacuo*, yielding 311 mg (95% yield) **2.2** as a yellow solid. X-ray quality crystals were obtained by the cooling of a saturated Et_2O solution of **2.2** to -30 °C overnight. ^{1}H NMR (300 MHz, C_6D_6) δ, ppm: 1.429 (*s*, 18H, C(C*H*$_3$)$_3$); 1.749 (*s*, 18H, C(C*H*$_3$)$_3$); 2.975 (*s*, 12H, Ta-(N(C*H*$_3$)$_2$)$_2$); 3.741 (*s*, 6H, Ta-N(C*H*$_3$)$_2$); 7.078 (*t*, 1H, 4-C_5NH_3); 7.227 (*d*, 2H, 3,5-C_5NH_3); 7.520 (*d*, 2H, aryl-*H*); 7.637 (*d*, 2H, aryl-*H*). ^{13}C NMR (125 MHz, C_6D_6) δ, ppm: 30.67 (C(*C*H_3)$_3$); 32.48 (C(*C*H_3)$_3$); 34.88 (*C*$(CH_3)_3$); 36.09 (*C*$(CH_3)_3$); 45.28 (N(*C*H_3)$_2$); 47.57 (N(*C*H_3)$_2$); 123.26, 123.99, 124.99, 127.52, 137.76, 138.57, 140.76, 155.14, 159.96 (aryl). Calcd for $C_{39}H_{61}N_4O_2Ta$: C 58.63, H 7.70, N 7.01; Found: C 58.40, H 7.10; N 6.79 %.

Synthesis of (2,6-(OC_6H_2-^{t}Bu_2)$_2$$C_5H_3N$)Ta($NMe_2$)$_2$Cl (2.3). In an inert atmosphere glovebox, **2.2** (69 mg, .087 mmol, 1 equiv) was dissolved in 4 mL C_6H_6 and 11 μL TMSCl (.087 mmol, 1 equiv) was syringed in. The reaction was sealed and stirred for 48 hours. After the reaction was complete, volatile coproducts were removed *in vacuo* quantitatively yielding **2.3** as a yellow solid. X-ray quality crystals were grown from the slow evaporation of a saturated Et_2O solution of **2.3**. ^{1}H NMR (300 MHz, $C_6D_5CD_3$) δ, ppm: 1.325 (*s*, 18H, C(C*H*$_3$)$_3$); 1.763 (*s*, 18H, C(C*H*$_3$)$_3$); 3.029 (*s*, 6H, N(C*H*$_3$)$_2$); 3.919 (*s*, 6H, N(C*H*$_3$)$_2$); 7.121 (*t*, 1H, 4-C_5N*H*$_3$); 7.338 (*d*, 2H, aryl-*H*); 7.477 (*d*, 2H, 3,5-C_5N*H*$_3$); 7.704 (*d*, 2H, aryl-*H*). ^{13}C NMR (125 MHz, C_6D_6) δ, ppm: 31.06 (C(*C*H$_3$)$_3$); 32.19 (C(*C*H$_3$)$_3$); 34.99 (*C*(CH$_3$)$_3$); 36.09 (*C*(CH$_3$)$_3$); 47.59 (N(*C*H$_3$)$_2$); 49.45 (N(*C*H$_3$)$_2$); 123.65, 126.57, 128.95, 138.69, 139.29, 143.37, 154.62, 157.88 (aryl). Calcd for $C_{37}H_{55}ClN_3O_2Ta$: C 56.23, H 7.02; N 5.32; Found: C 57.09, H 6.33, N 4.74 %.

Synthesis of (2,6-(OC_6H_2-^{t}Bu_2)$_2$$C_5H_3N$)Ta(NPh)($HNMe_2$)Cl (2.4). 2.3 (11 mg, .014 mmol, 1 equiv) and aniline (1.3 μL, .014 mmol, 1 equiv) were mixed together in a J-Young NMR tube with .7 mL C_6D_6. The vessel was sealed and heated to 90 ℃ in an oil bath. The reaction was monitored by ^{1}H NMR, and after 3 days at 90 ℃ the reaction was complete as confirmed by the disappearance of the Ta-NMe_2 peaks. The solvent and $HNMe_2$ were removed *in vacuo*, yielding **2.4** quantitatively. X-ray quality crystals were grown from slow evaporation of a saturated solution of **2.4** in benzene. ^{1}H NMR (300 MHz, C_6D_6) δ, ppm: 1.37 (*s*, 18H, C(C*H*$_3$)$_3$); 1.71 (*s*, 6H, N(C*H*$_3$)$_2$); 1.78 (*s*, 18H, C(C*H*$_3$)$_3$); 6.33 (*d*, 2H, aryl-*H*); 6.46 (*t*, 1H, aryl-*H*); 6.88 (*t*, 2H, aryl-*H*); 6.94 (*t*, 1H, 4-C_5N*H*$_3$); 7.25 (*d*, 2H, 3,5-C_5N*H*$_3$); 7.30 (*d*, 2H, aryl-*H*); 7.74 (*d*, 2H, aryl-*H*). ^{13}C NMR (125 MHz, C_6D_6) δ,

ppm: 30.8 (C(*C*H$_3$)$_3$); 32.3 (C(*C*H$_3$)$_3$); 34.9 (*C*(CH$_3$)$_3$); 36.0 (*C*(CH$_3$)$_3$); 38.5 (N(*C*H$_3$)$_2$); 123.3, 123.9, 125.2, 126.3, 127.2, 127.3, 127.8, 138.6, 139.3, 142.2, 156.4, 158.2, 159.5 (aryl).

Synthesis of (2,6-(OC$_6$H$_2$-^{t}Bu$_2$)$_2$C$_5$H$_3$N)Ta(NPh)(NH$_2$Ph)Cl (2.5). 2.3 (12 mg, .0152 mmol, 1 equiv) and aniline (2.8 μL, .031 mmol, 2.1 equiv) were mixed together in a J-Young NMR tube with .7 mL of C_6D_6. The vessel was sealed and heated to 90 °C in an oil bath. The reaction was monitored by ^{1}H NMR, and after 3 days at 90 °C the reaction was complete as confirmed by the disappearance of the Ta-NMe$_2$ peaks. The solvent, excess aniline and HNMe$_2$ were removed *in vacuo*, yielding **2.5** quantitatively. X-ray quality crystals were grown from slow evaporation of a saturated solution of **2.5** in toluene. ^{1}H NMR (300 MHz, C_6D_6) δ, ppm: 1.37 (*s*, 18H, C(C*H*$_3$)$_3$); 1.77 (*s*, 18H, C(C*H*$_3$)$_3$); 2.92 (*br s*, 2H, N*H*$_2$); 6.31 (*dd*, 4H, aryl-*H*); 6.46 (*t*, 1H, aryl-*H*); 6.69 (*t*, 1H, aryl-*H*); 6.88 (*t*, 2H, aryl-*H*); 6.98 (*m*, 3H, 4-C$_5$N*H*$_3$ + aryl-*H*); 7.25 (*d*, 2H, 3,5-C$_5$N*H*$_3$); 7.29 (*d*, 2H, aryl-*H*); 7.73 (*d*, 2H, aryl-*H*). ^{13}C NMR (125 MHz, C_6D_6) δ, ppm: 30.9 (C(*C*H$_3$)$_3$); 32.2 (C(*C*H$_3$)$_3$); 34.9 (*C*(CH$_3$)$_3$); 36.1 (*C*(CH$_3$)$_3$); 123.3, 123.5, 125.2, 125.4, 126.3, 127.1, 127.2, 127.8, 129.6, 138.6, 139.1, 139.3, 142.2, 157.3, 158.2, 159.4 (aryl).

Synthesis of (2,6-(OC$_6$H$_2$-^{t}Bu$_2$)$_2$C$_5$H$_3$N)Ta(NMe$_2$)MeCl (2.6). (2,6-(OC$_6$H$_2$-^{t}Bu$_2$)$_2$C$_5$H$_3$N)TaCl$_2$Me (159 mg, .212 mmol, 1 equiv) was dissolved in 10 mL C_6H_6 in an inert atmosphere glovebox, transferred to a 50 mL round-bottom flask equipped with a teflon needle valve, sealed, and degassed on a high-vacuum line. 4.7 mmol of degassed HNMe$_2$ was then vac transferred into the round bottomed flask, and the reaction was thawed and stirred for 1 hour at room temperature. The orange solution

turned dark yellow with a white precipitate (H_2NMe_2Cl). After the reaction was complete, the reaction was filtered through a sintered glass funnel in an inert atmosphere glovebox, and the filtrate dried *in vacuo* yielding 148 mg (89.5%) of **2.6** as a yellow powder. ^{1}H NMR (300 MHz, $C_6D_5CD_3$) δ, ppm: 1.319 (*s*, 18H, C(C*H*$_3$)$_3$); 1.659 (*s*, 3H, Ta–*CH*$_3$); 1.808 (*s*, 18H, C(C*H*$_3$)$_3$); 3.214 (*s*, 6H, N(C*H*$_3$)$_2$); 7.031 (*t*, 1H, 4–C$_5$N*H*$_3$); 7.290 (*d*, 2H, aryl–*H*); 7.375 (*d*, 2H, 3,5–C$_5$N*H*$_3$); 7.767 (*d*, 2H, aryl–*H*). ^{13}C NMR (125 MHz, $C_6D_5CD_3$) δ, ppm: 31.10 (C(*C*H$_3$)$_3$); 32.10 (C(*C*H$_3$)$_3$); 35.05 (*C*(CH$_3$)$_3$); 36.03 (*C*(CH$_3$)$_3$); 48.69 (N(*C*H$_3$)$_2$); 48.90 (Ta–*C*H$_3$); 123.77, 126.86, 126.96, 128.95, 139.14, 139.27, 144.86, 152.77, 157.98 (aryl). Calcd for $C_{36}H_{52}ClN_2O_2Ta$: C 56.80, H 6.89, N 3.68; Found: C 55.58, H 6.08, N 3.36%.

Synthesis of [(2,6-(OC$_6$H$_2$-^{t}Bu$_2$)$_2$C$_5$H$_3$N)Ta(OH)]$_2$(μ-O)$_2$ (2.7). In an NMR tube (2,6-(OC$_6$H$_2$-^{t}Bu$_2$)$_2$C$_5$H$_3$N)TaMe$_3$ (7.7 mg, .011 mmol, 1 equiv) was dissolved in 1 mL C_6D_6 and 4 equivalents of H_2O were quantitatively gas transferred onto the solution on a high vacuum line. The yellow solution immediately turned clear with a significant amount of white precipitate. The solvent was decanted off in an inert atmosphere glove box and the product dried *in vacuo*; crystals were obtained from a saturated solution of the mixture of products in CH_2Cl_2.

Table 2.2. Crystal and refinement data for complexes **2.1**, **2.2**, and **2.3**.

	2.1	**2.2**	**2.3**
CCDC Number	680573	693510	693797
Empirical formula	$C_{51}H_{61}N_4O_2Ta \cdot 1½(C_6H_6)$	$C_{39}H_{61}N_4O_2Ta$	$C_{37}H_{55}N_3O_2ClTa \cdot 0.75(C_4H_{10}O)$
Formula weight	1060.15	798.87	845.83
T (K)	100(2)	100(2)	100(2)
a, Å	25.7250(8)	9.8149(5)	14.7164(6)
b, Å	17.8546(5)	29.0840(14)	18.3370(7)
c, Å	23.6141(7)	14.0826(6)	31.2188(13)
α, deg			
β, deg	105.9790(10)	104.357(3)	101.802(2)
γ, deg			
Volume, Å^3	10427.1(5)	3894.4(3)	8246.4(6)
Z	8	4	8
Crystal system	Monoclinic	Monoclinic	Monoclinic
Space group	C2/c	$P2_1/c$	$P2_1/n$
d_{calc}, g/cm^3	1.351	1.363	1.363
θ range, deg	2.07 to 43.26	1.65 to 33.20	1.68 to 47.98
μ, mm^{-1}	2.154	2.858	2.767
Abs. Correction	None	Semi Emp.	Semi Emp.
GOF	1.117	1.426	2.760
R_1 ,[a] wR_2 [b] [I>2σ(I)]	0.0299, 0.0520	0.0350, 0.0448	0.0731, 0.1059

[a] $R_1 = \Sigma||F_o| - |F_c||/\Sigma|F_o|$. [b] $wR_2 = [\Sigma[w(F_o^2-F_c^2)^2]/\Sigma[w(F_o^2)^2]]^{1/2}$.

Table 2.3. Crystal and refinement data for complexes **2.4**, **2.6**, and **2.7**.

	2.4	**2.6**	**2.7**
CCDC Number	694413	698486	683409
Empirical formula	$C_{41}H_{55}N_3O_2ClTa$	$C_{36}H_{52}N_2O_2ClTa \cdot C_4H_{10}O$	$C_{66}H_{86}N_2O_8Ta_2 \cdot 4(CH_2Cl_2)$
Formula weight	838.28	835.32	1736.97
T (K)	100(2)	100(2)	100(2)
a, Å	9.9628(5)	47.432(2)	16.0570(7)
b, Å	10.6118(5)	13.7447(7)	12.8407(6)
c, Å	18.9240(9)	12.4876(6)	18.4561(9)
α, deg	80.804(3)		
β, deg	89.355(3)	100.510(3)	103.542(3)
γ, deg	81.578(3)		
Volume, Å^3	1953.54(16)	8004.5(7)	3699.5(3)
Z	2	8	2
Crystal system	Triclinic	Monoclinic	Monoclinic
Space group	P–1	C2/c	$P2_1/c$
d_{calc}, g/cm^3	1.425	1.386	1.559
θ range, deg	1.97 to 35.14	1.54 to 27.85	1.95 to 51.56
μ, mm^{-1}	2.919	2.850	3.297
Abs. Correction	None	None	Semi Emp.
GOF	1.281	1.678	1.629
R_1 ,[a] wR_2 [b] [I>2σ(I)]	0.0326, 0.0452	0.0358, 0.0563	0.0250, 0.0388

[a] $R_1 = \Sigma||F_o| - |F_c||/\Sigma|F_o|$. [b] $wR_2 = [\Sigma[w(F_o^2-F_c^2)^2]/\Sigma[w(F_o^2)^2]^{1/2}$.

REFERENCES

1. a.) Britovsek, G. J. P.; Gibson, V. C.; Wass, D. F. *Angew. Chem., Int. Ed. Engl.* **1999**, *38*, 428–447. b.) Gibson, V. C.; Spitzmesser, S. K. *Chem. Rev.* **2003**, *103*, 283–315.
2. Wolczanski, P. T.; *Polyhedron,* **1995**, *14*, 3335.
3. Coates, G. W.; Hustad, P. D.; Reinartz, S. *Angew. Chem. Int. Ed. Engl.* **2002**, *41*, 2236–2257.
4. Watson, D. A.; Chiu, M.; Bergman, R. G.; *Organometallics* **2006**, *25*, 4731–4733.
5. Anderson, L. L.; Arnold, J.; Bergman, R. G. *J. Am. Chem. Soc.* **2005**, *127*, 14542–14543.
6. Ackermann, L.; Bergman, R. G.; Loy, R. N. *J. Am. Chem. Soc.* **2003**, *125*, 11956–11963.
7. Rothwell, I. P. *Chem. Commun.* **1997**, 1331–1338.
8. Wallace, K. C.; Liu, A. H.; Dewan, J. C.; Schrock, R. R. *J. Am. Chem. Soc.* **1988**, *110*, 4964–4977.
9. Schrock, R. R. *Angew. Chem., Int. Ed. Engl.* **2006**, *45*, 3748–3759.
10. Schrock, R. R.; Hoveyda, A. H. *Angew. Chem., Int. Ed. Engl.* **2003**, *42*, 4592–4633.
11. Tsang, W. C. P.; Hultzsch, K. C.; Alexander, J. B.; Bonitatebus, P. J.; Schrock, R. R.; Hoveyda, A. H. *J. Am. Chem. Soc.* **2003**, *125*, 2652–2666.
12. Schrock, R. R. *Chem. Rev.* **2002**, *102*, 145–179.
13. Spencer, L. P.; Beddie, C.; Hall, M. B.; Fryzuk, M. D. *J. Am. Chem. Soc.* **2006**, *128*, 12531–12543.
14. Mason, A. F.; Coates, G. W. *J. Am. Chem. Soc.* **2004**, *126*, 16326–16327.
15. Tian, J.; Hustad, P. D.; Coates, G. W. *J. Am. Chem. Soc.* **2001**, *123*, 5134–5135.
16. Tshuva, E. Y.; Goldberg, I.; Kol, M. *J. Am. Chem. Soc.* **2000**, *122*, 10706–10707.
17. Tshuva, E. Y.; Goldberg, I.; Kol, M.; Goldschmidt, Z. *Organometallics* **2001**, *20*, 3017–3028.
18. Tshuva, E. Y.; Groysman, S.; Goldberg, I.; Kol, M.; Goldschmidt, Z. *Organometallics* **2002**, *21*, 662–670.
19. Groysman, S.; Goldberg, I.; Kol, M.; Genizi, E.; Goldschmidt, Z. *Adv. Synth. Catal.* **2005**, *347*, 409–415.

20. Groysman, S.; Segal, S.; Goldberg, I.; Kol, M.; Goldschmidt, Z. *Inorg. Chem. Commun.* **2004**, *7*, 938-941.
21. Groysman, S.; Goldberg, I.; Kol, M.; Genizi, E.; Goldschmidt, Z. *Organometallics* **2004**, *23*, 1880-1890.
22. Groysman, S.; Goldberg, I.; Kol, M.; Goldschmidt, Z. *Organometallics* **2003**, *22*, 3793-3795.
23. Groysman, S.; Segal, S.; Shamis, M.; Goldberg, I.; Kol, M.; Goldschmidt, Z.; Hayut-Salant, E. *J. Chem. Soc.-Dalton Trans.* **2002**, 3425-3426.
24. Freundlich, J. S.; Schrock, R. R.; Davis, W. M. *Organometallics* **1996**, *15*, 2777-2783.
25. Freundlich, J. S.; Schrock, R. R.; Davis, W. M. *J. Am. Chem. Soc.* **1996**, *118*, 3643-3655.
26. Baumann, R.; Davis, W. M.; Schrock, R. R. *J. Am. Chem. Soc.* **1997**, *119*, 3830-3831.
27. Baumann, R.; Stumpf, R.; Davis, W. M.; Liang, L. C.; Schrock, R. R. *J. Am. Chem. Soc.* **1999**, *121*, 7822-7836.
28. Liang, L. C.; Schrock, R. R.; Davis, W. M.; McConville, D. H. *J. Am. Chem. Soc.* **1999**, *121*, 5797-5798.
29. Mehrkhodavandi, P.; Bonitatebus, P. J.; Schrock, R. R. *J. Am. Chem. Soc.* **2000**, *122*, 7841-7842.
30. Mehrkhodavandi, P.; Schrock, R. R. *J. Am. Chem. Soc.* **2001**, *123*, 10746-10747.
31. Mehrkhodavandi, P.; Schrock, R. R.; Pryor, L. L. *Organometallics* **2003**, *22*, 4569-4583.
32. Nakayama, Y.; Saito, H.; Ueyama, N.; Nakamura, A. *Organometallics,* **1999**, *18*, 3149-3158.
33. Sernetz, F. G.; Mulhaupt, R.; Fokken, S.; Okuda, J. *Macromolecules* **1997**, *30*, 1562-1569.
34. Agapie, T.; Henling, L. H.; DiPasquale, A. G.; Rheingold, A. L.; Bercaw, J. E. *Organometallics* **2008**. *27*, 6245-6246.
35. a.) Chan, M. C. W.; Tam, K. H.; Zhu, N. Y.; Chiu, P.; Matsui, S. *Organometallics*, **2006**, *25*, 785. b.) Chan, M. C. W.; Tam, K. H.; Pui, Y. L.; Zhu, N. Y. *J. Chem. Soc., Dalton Trans.* **2002**, 3085-3087.

36. a.) Sarkar, S.; Abboud, K. A.; Veige, A. S. *J. Am. Chem. Soc.* **2008**, *130*, 16128-16129. b.) Sarkar, S.; Carlson, A. R.; Veige, M. K.; Falkowski, J. M.; Abboud, K. A.; Veige, A. S. *J. Am. Chem. Soc.* **2008**, *130*, 1116-1117.
37. Agapie, T.; Bercaw, J. E. *Organometallics* **2007**, *26*, 2957-2959.
38. Agapie, T.; Day, M. W.; Bercaw, J. E. *Organometallics* **2008**, *27*, 6123-6142.
39. Steinhauser, S.; Heinz, U.; Sander, J.; Hegetschweiler, K. Z. *Anorg. Allg.Chem.,* **2004**, *630*, 1829-1838.
40. In all of the schemes in this section, amido (LX) ligands will be represented as double bonds and imido ligands (LX_2) as triple bonds since these representations most accurately describe the bonding within these systems (as evidenced by simple electron counting and DFT calculations), despite this notation not being the normal convention. Additionally, all Ta-O bonds will be drawn as single bonds, although some of the Ta-O bonds in these complexes are best described as having 3-center-4-electron bonds and bond orders greater than 1. See Table 2.1 for a full description of the Ta-O bond order in all of these complexes.
41. One might question why the imido ligand of complexes **2.4** and **2.5** does not occupy the site trans to pyridine in order to preserve the phenolate-to-d_{xy} p bonding. We do not fully understand the preference for a cis imido, but the weakest trans influencing L-type amine ligand may direct the imido.
42. Parkin, G.; van Asselt, A.; Leahy, D. J.; Whinnery, L.; Hua, N. G.; Quan, R. W.; Henling, L. M.; Schaefer, W. P.; Santarsiero, B. D.; Bercaw, J. E.; *Inorg. Chem.* **1992**, *31*, 82-85.
43. S. Golisz, Thesis, Caltech.
44. Pangborn, A. B.; Giardello, M. A.; Grubbs, R. H.; Rosen, R. K.; Timmers, F. J.; *Organometallics*, **1996**, *15*, 1518.
45. Frisch, M. J.; Trucks, G. W.; Schlegel, H. B.; Scuseria, G. E.; Robb, M. A.; Cheeseman, J. R.; Montgomery, Jr., J. A.; Vreven, T.; Kudin, K. N.; Burant, J. C.; Millam, J. M.; Iyengar, S. S.; Tomasi, J.; Barone, V.; Mennucci, B.; Cossi, M.; Scalmani, G.; Rega, N.; Petersson, G. A.; Nakatsuji, H.; Hada, M.; Ehara, M.; Toyota, K.; Fukuda, R.; Hasegawa, J.; Ishida, M.; Nakajima, T.; Honda, Y.; Kitao, O.; Nakai, H.; Klene, M.; Li, X.; Knox, J. E.; Hratchian, H. P.; Cross, J. B.; Bakken, V.; Adamo, C.; Jaramillo, J.; Gomperts, R.; Stratmann, R. E.; Yazyev, O.; Austin, A. J.; Cammi, R.; Pomelli, C.; Ochterski, J. W.; Ayala, P. Y.; Morokuma, K.; Voth, G. A.; Salvador, P.; Dannenberg, J. J.; Zakrzewski, V. G.; Dapprich, S.; Daniels, A. D.;

Strain, M. C.; Farkas, O.; Malick, D. K.; Rabuck, A. D.; Raghavachari, K.; Foresman, J. B.; Ortiz, J. V.; Cui, Q.; Baboul, A. G.; Clifford, S.; Cioslowski, J.; Stefanov, B. B.; Liu, G.; Liashenko, A.; Piskorz, P.; Komaromi, I.; Martin, R. L.; Fox, D. J.; Keith, T.; Al-Laham, M. A.; Peng, C. Y.; Nanayakkara, A.; Challacombe, M.; Gill, P. M. W.; Johnson, B.; Chen, W.; Wong, M. W.; Gonzalez, C.; Pople, J. A.; *Gaussian 03*, revision C.02,Gaussian, Inc., Wallingford CT, **2004**.

46. Becke, A. D. *Phys. Rev. A: At., Mol., Opt. Phys.* **1988**, *38*, 3098-3100.
47. Becke, A. D. *J. Chem. Phys.* **1988**, *88*, 1053-1062.
48. Perdew, J. P. *Phys. Rev. B* **1986**, *33*, 8800-8802.
49. C. Lee, W. Yang, and R. G. Parr, *Phys. Rev. B* **1988**, *37*, 785.
50. B. Miehlich, A. Savin, H. Stoll, and H. Preuss, *Chem. Phys. Lett.* **1989** *157*, 200.
51. Hay, P. J.; Wadt, W. R. *J. Chem. Phys.* **1985**, *82*, 270-283.
52. Wadt, W. R.; Hay, P. J. *J. Chem. Phys.* **1985**, *82*, 284-298.
53. Hay, P. J.; Wadt, W. R. *J. Chem. Phys.* **1985**, *82*, 299-310.

CHAPTER 3

Zirconium and Titanium Propylene Polymerization Precatalysts Supported by a Fluxional C_2-Symmetric Pyridine *Bis*(anilide) Ligand

ABSTRACT

Titanium and zirconium complexes supported by a pyridine *bis*(anilide) ligand (NNN = pyridine-2,6-*bis*(N-mesitylanilide)) have been synthesized and crystallographically characterized. The crystal structures of the 5-coordinate dihalide complexes (NNN)MCl_2 (M = Ti, Zr) display a stabilizing *ipso* interaction between the metal and the anilide ligand, creating C_1-symmetric complexes. The coordination of THF to (NNN)$ZrCl_2$ generates a 6-coordinate C_2-symmetric complex. C_2-symmetric *bis*(dimethylamido) complexes were generated from aminolysis of $M(NMe_2)_4$ or salt metathesis from $M(NMe_2)_2Cl_2$. In contrast to previously reported pyridine *bis*(phenoxide) complexes, the ligand geometry of these complexes is dictated by chelate ring strain rather than metal-ligand π-bonding. The antipode interconversion of the C_2 complexes has been investigated by variable temperature ^1H NMR spectroscopy and is facile at room temperature. These complexes were tested as propylene polymerization precatalysts, with most complexes giving low to moderate activities (10^2-10^4 g/mol*h) for the formation of polypropylene.

INTRODUCTION

The chemistry of the early transition metals has, to a large extent, been advanced by the use of bent metallocene frameworks. However, there has been increased interest in using well defined, mono- and polydentate "non-metallocene" ligand sets to support a diverse range of organometallic complexes and transformations, catalysis, and small molecule activation studies.[1-33]

Recently, our group[34,35] and others[36-38] have been investigating the use of arene- and heterocycle-linked *bis*(phenolate)donor ligand sets (heterocycle = pyridine, furan, thiophene) to support titanium, zirconium, and vanadium polymerization catalysts[34] and as ancillary ligands for other early transition metals[35] to explore other organometallic transformations. These non-metallocene ligand sets are connected through rigid sp^2-sp^2 aryl-aryl linkages instead of more flexible sp^3-sp^3 linkages, imparting increased rigidity of the backbone, which could result in more thermally robust catalysts that are less prone to undergo ligand C-H activation.

We have found that transition metal complexes based on this class of ligand are capable of adopting C_1, C_S, C_{2v} or C_2 symmetry.[34,35] Despite observing these symmetries in the solid state, propylene polymerization using C_2-symmetric *bis*(phenolate) early transition metal precatalysts yields atactic polypropylene or mixtures of atactic and isotactic.[34] An investigation into the electronics of 6-coordinate tantalum complexes supported by an ONO (ONO = pyridine-*bis*(phenolate)) ligand has revealed that the preference for certain ligand symmetries (either C_S or C_2) is controlled by a delicate competition between ONO ligand-metal π-bonding and ring strain within the (ONO)M

chelate fragment,[35c] and that the barrier for interconversion between geometries is low (< 5 kcal/mol in (ONO)Ir complexes).[39] As a result of our observations into this competition, we have begun investigating related ligand frameworks where either electronics or ring strain/steric components might completely dominate rather than compete for symmetry control. This should allow for the development of catalysts with very well-defined and well-understood geometry preferences that could be used in enantiomorphic site-controlled propylene polymerization catalysis. Herein we report the synthesis and structural characterization of group 4 complexes supported by a pyridine-*bis*(anilide) ligand and results into their use as propylene polymerization precatalysts.

RESULTS AND DISCUSSION

Synthesis and Characterization of Precatalysts

The pyridine *bis*(anilide) ligand **3.1**-H_2 was synthesized following a previously-reported[40] two-step reaction sequence. Both titanium and zirconium *bis*(dimethylamide) complexes of **3.1** can be generated through salt metathesis of the potassium salt **3.1**-K_2, with $MCl_2(NMe_2)_2(THF)_n$ (M = Ti, n = 0; M = Zr, n = 2) (eq 3.1). X-ray quality orange/red crystals of (NNN)Ti(NMe_2)$_2$ **3.2** and (NNN)Zr(NMe_2)$_2$ **3.3** were obtained from layering pentane over a concentrated THF solution of **3.2** or **3.3** and cooling to −30 °C overnight.

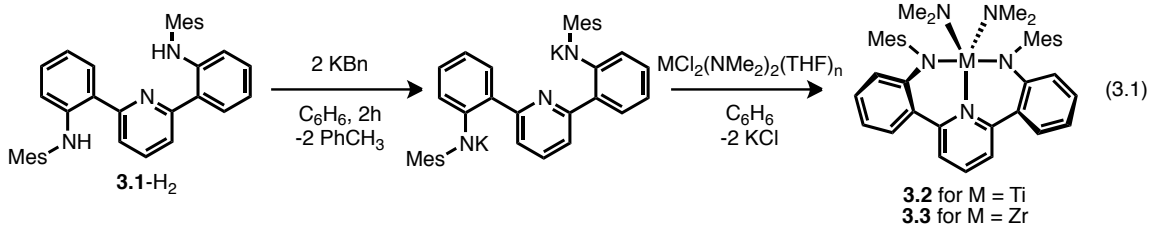

(3.1)

The *bis*(anilide) ligand in **3.2** is bound in a highly C_2-symmetric fashion, with the two anilide arms occupying the axial positions of a distorted trigonal bipyramid (Figure 3.1). The dihedral angle between the two phenyl rings connected to the pyridine is 81.8°, which is substantially larger (by 30-40°) than those observed in C_2-symmetric complexes of the related ONO ligand system (ONO = pyridine-2,6-*bis*(4,6-^{t}Bu$_2$-phenoxide)).[35c] Although the anilide nitrogens are essentially planar, the titanium-anilide distances (2.078(2) and 2.080(2) Å) are substantially longer than a typical titanium amide double bond (for comparison, the Ti-N distances for the doubly-bonded dimethylamido ligands in **3.2** are much shorter—1.881(2) and 1.892(2)Å). As a result, there is likely little to no Ti-N double bond character in the titanium-anilide bond and the nitrogen planarity is due

to the sterics of the bulky diarylamine and/or resonance of the nitrogen lone pair into the aryl rings. DFT calculations performed on **3.2** and **3.3** agree with this assessment—there was no obvious M-N π bonding in any of the molecular orbitals that we investigated, and in both the Ti and Zr cases we could identify orbitals containing the nitrogen lone pair delocalized across the aryl rings rather than into the metal center (Figure 3.2).

Interestingly the complex (ONO)Ti(NMe_2)$_2$, the *bis*(phenoxide) analogue of **3.2**, exhibits a C_S symmetry in its crystal structure.[41] We attribute this difference to the smaller binding pocket of the NNN ligand and to the steric bulk of the N-mesityl groups, which likely forces **3.2** to adopt the more sterically accommodating C_2 symmetry. The overall structural features of the Zr analog **3.3** are very similar to those described above for **3.2**.

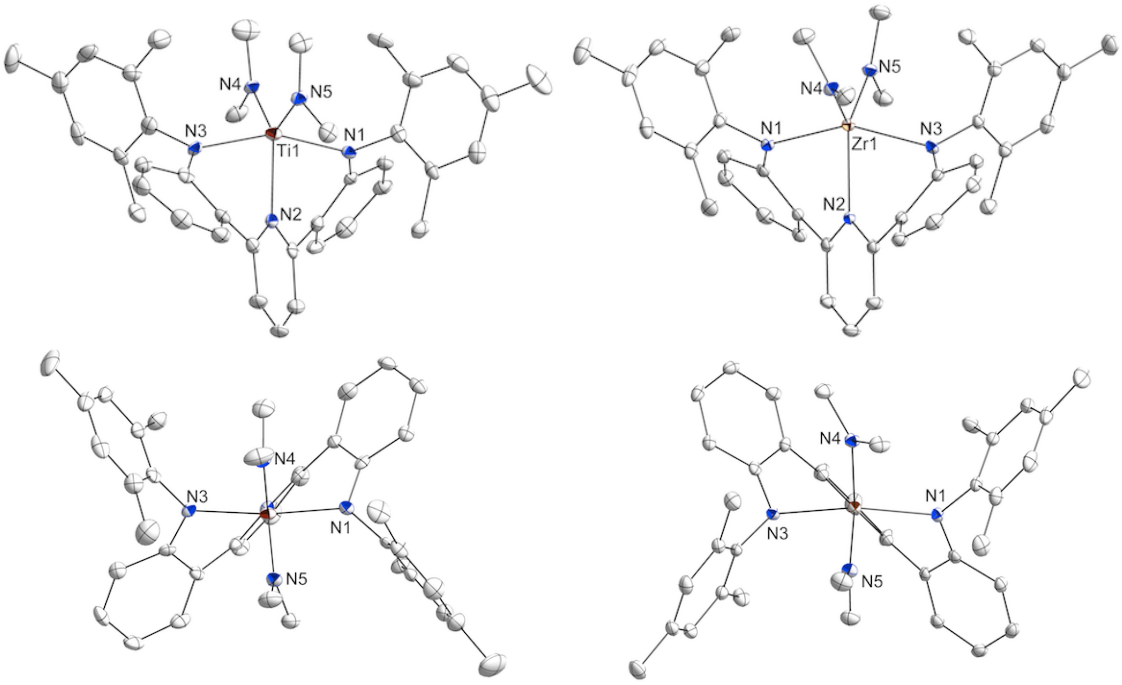

Figure 3.1. 50% Thermal ellipsoid drawings of **3.2** (left) and **3.3** (right). Selected bond lengths (Å): Complex **3.2**: Ti1-N1 2.0781(23); Ti1-N2 2.1170(19); Ti1-N3 2.0803(24); Ti1-N4 1.8807(19); Ti1-N5 1.8922(20). Complex **3.3**: Zr1-N1 2.2096(10); Zr1-N2 2.3140(10); Zr1-N3 2.1799(10); Zr1-N4 2.0264(10); Zr1-N5 2.0281(10). Solvents of crystallization and H atoms removed for clarity.

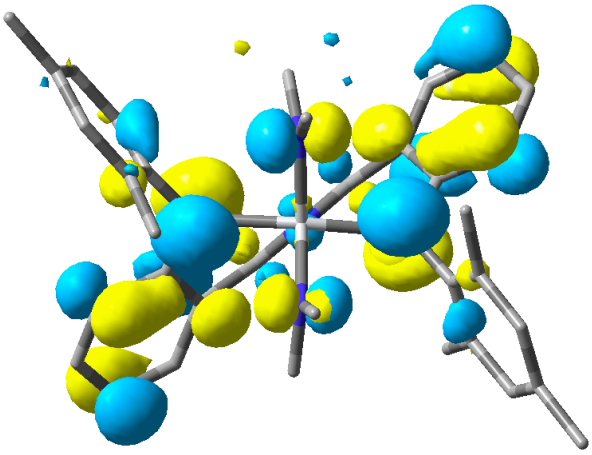

Figure 3.2. DFT calculated HOMO of (NNN)Ti(NMe_2)$_2$ **3.2** (top-down view) showing nitrogen lone pair delocalization into the aryl backbone.

The Zr complex (NNN)Zr(NMe_2)$_2$ **3.3** could alternately be generated *via* aminolysis between the protonated ligand, **3.1**-H_2, and Zr(NMe_2)$_4$; however, (NNN)Ti(NMe_2)$_2$ could not be synthesized *via* this pathway even under significant heating and extended reaction times (eq 3.2). By switching to a less bulky ligand ($^{t\text{Bu}}$NNN)H_2, where the mesitylene groups are replaced by 3,5-di-^{t}Bu-phenyl groups, the aminolysis is successful for both Ti and Zr and proceeds at much lower (55 °C) temperatures.

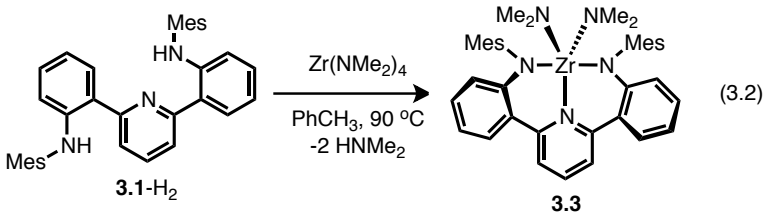

(3.2)

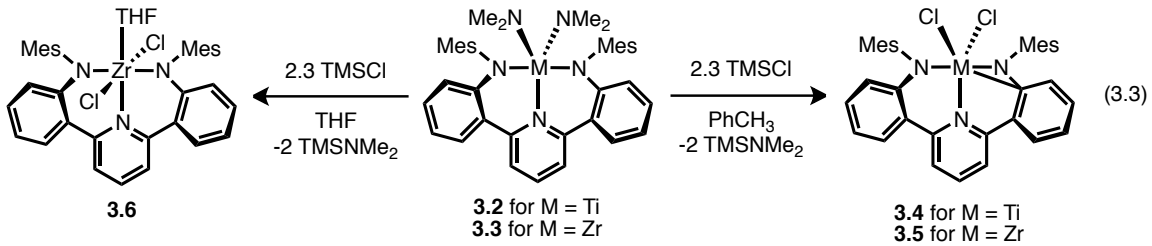

(3.3)

Reaction of **3.2** or **3.3** with 2.3 equivalents of Me_3SiCl in toluene quantitatively generates the dichloride complexes (NNN)$TiCl_2$ **3.4** and (NNN)$ZrCl_2$ **3.5** (eq 3.3). Both **3.4** and **3.5** are very insoluble and crystallize out of the reaction mixture. **3.4** and **3.5** have been characterized by X-ray crystallography (Figure 3.3). **3.4** has the NNN ligand bound unsymmetrically. In addition to the typical tridentate LX_2 binding of the NNN ligand, there is a stabilizing *ipso* interaction between one of the anilide arms and the metal center. The Ti1-C17 bond length is 2.584(1) Å, more than 0.4 Å shorter than the distance to the *ipso* carbon on the other anilide arm (Ti1-C1 3.009 Å). This *ipso* interaction is likely necessary to stabilize the highly electrophilic 14 electron Ti center. The Zr analogue **3.5** is structurally very similar to **3.4** and also contains an unsymmetrically bound NNN ligand with an *ipso* interaction. Complexes **3.2** and **3.3**, on the other hand, are significantly more electron-rich due to the π-donating dimethylamido ligands and do not need the *ipso* interaction to stabilize the metal center. Since both **3.4** and **3.5** appear symmetric by ^1H NMR spectroscopy, it is likely that in solution the *ipso* interaction is either nonexistent or fluxional between the two anilide arms.

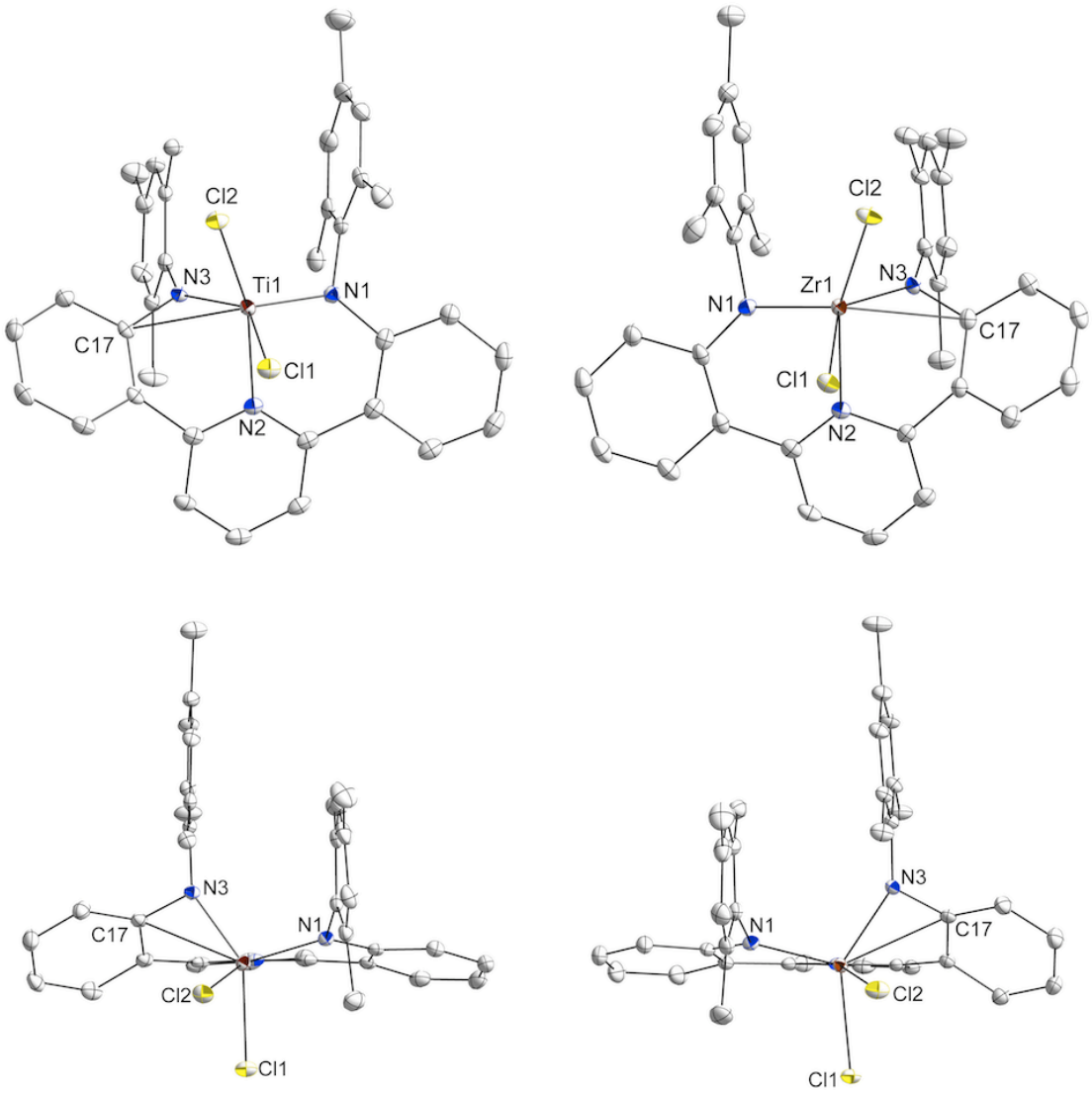

Figure 3.3. 50% Thermal ellipsoid drawings of **3.4** (left) and **3.5** (right). Selected bond lengths (Å): Complex **3.4**: Ti1–N1 1.891(1); Ti1–N2 2.129(1); Ti1–N3 1.9263(9); Ti1–Cl1 2.3717(1); Ti1–Cl2 2.3323(1); Ti1–C17 2.584(1). Complex **3.5**: Zr1–N1 2.033(1); Zr1–N2 2.262(1); Zr1–N3 2.066(1); Zr1–Cl1 2.4692(1); Zr1–Cl2 2.4638(1); Zr1–C17 2.654(1). Solvents of crystallization and H atoms removed for clarity.

If **3.3** is reacted with 2.3 equivalents of Me_3SiCl in THF rather than toluene, the THF adduct (NNN)$ZrCl_2$(THF) **3.6** crystallizes (eq 3.3). Unlike **3.4** and **3.5**, the solid-state

structure of **3.6** is C_2-symmetric and has no stabilizing *ipso* interaction with the NNN ligand aryl rings (Figure 3.4). The lack of an *ipso* interaction is a result of the increased electron count around the metal center; as a nominally 16 electron complex, the Zr metal center is significantly less electrophilic than in **3.5**. The C_2-symmetric structure of **3.6** is significant because in the related *bis*(phenoxide) complexes, the addition of a 6th ligand to the coordination sphere shifted the solid state geometry of the complexes from C_2 to C_S. In the *bis*(anilide) case, however, change in coordination number does not affect the solid state geometry; thus **3.6** further confirms our hypothesis that the new *bis*(anilide) ligand set imparts greater steric control over the molecule than *bis*(phenolate) ligands. Binding of THF in **3.6** is reversible, and successive washings of **3.6** with toluene removes the THF to generate **3.5**. The analogous Ti complex, (NNN)$TiCl_2$(THF), is not generated upon reaction of **3.2** with excess Me_3SiCl in THF. We attribute this difference in reactivity to the fact that the smaller titanium center can't accommodate a 6th ligand in its coordination sphere.

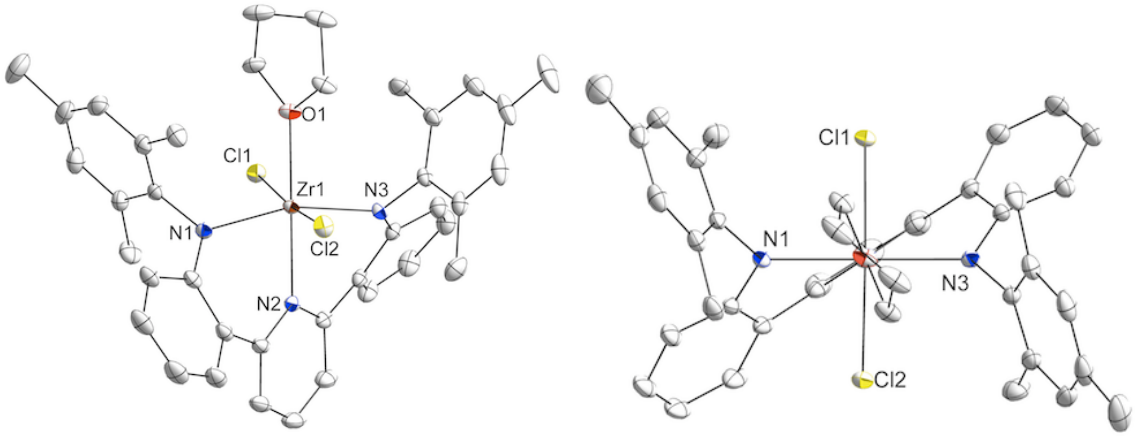

Figure 3.4. 50% Thermal ellipsoid drawing of **3.6** showing front (left) and top-down view (right). Selected bond lengths (Å): Zr-N1 2.133(1); Zr-N2 2.3103(8); Zr-N3 2.152(1); Zr-Cl1 2.4498(3); Zr-Cl2 2.4496(3); Zr-O1 2.2432(7). H atoms removed for clarity.

Reaction of **3.1**-H_2 with $ZrBn_4$ or $TiBn_4$ led only to decomposition products. Protonolysis of $ZrBn_4$ with the less bulky (^{tBu}NNN)H_2 proceeded very slowly (eq 3.4). The reaction to form (^{tBu}NNN)$ZrBn_2$ (**3.7**) requires reaction times of 24-48 hours at 90 °C. **3.7** is light sensitive and decomposes over the course of days when exposed to ambient light. **3.7** was crystallized from a saturated pentane solution and is roughly C_S-symmetric in the solid state (Figure 3.5). However, in solution the structure appears fluxional because in the ^{1}H NMR the benzylic protons of **3.7** show up as a singlet rather than a doublet. The related (ONO)$ZrBn_2$ complex is C_2 in solution and the solid state, and this unexpected discrepancy shows that the energy differences between the possible conformations of the (^{tBu}NNN) framework are likely very small when compared to the more bulky mesitylene substituted (NNN) framework.

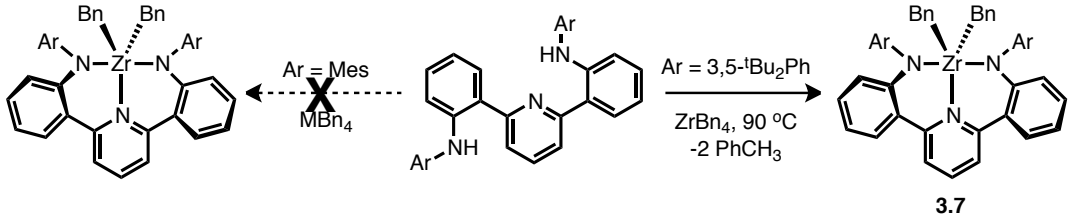

(3.4)

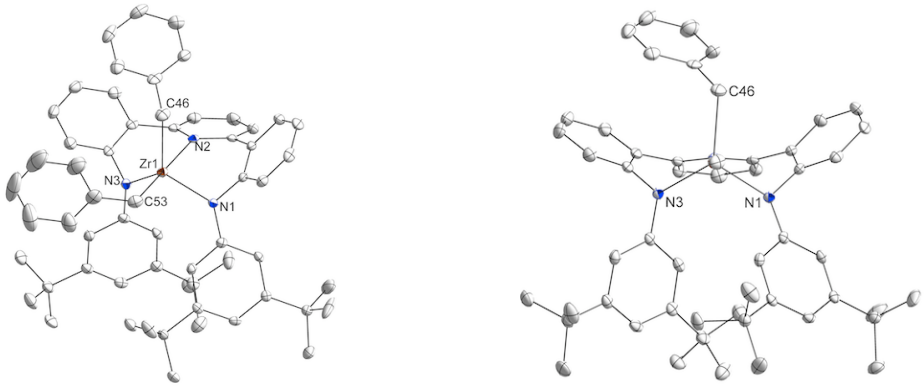

Figure 3.5. 50% Thermal ellipsoid drawings of **3.7.** Right drawing has C53 aryl group removed for clarity. Selected bond lengths (Å): Zr-N1 2.079(1); Zr-N2 2.385(1); Zr-N3 2.031(1); Zr-C46 2.261(2); Zr-C53 2.322(2). Solvent of crystallization and H atoms removed for clarity.

NMR Studies of Ligand Fluxionality

In complexes **3.2**-**3.6**, the *ortho* methyl groups of the N-mesityl functionality appear as a broad signal in the ^{1}H NMR at room temperature. In a C_2-symmetric molecule, the *ortho* methyl groups on each mesitylene ring should be inequivalent with one being in an *endo* position—pointing in toward the metal center—and one *exo* pointing away from the metal. The broadening could be a result of one of two factors (Scheme 3.1): First, interconversion between the two possible C_2 antipodes could exchange the *ortho* methyls. Alternately, if the molecule remains locked in a C_2 geometry, slow rotation about the N-mesityl bond would result in the interconversion of the two *ortho* methyl groups and cause the broadening.

Variable temperature ^{1}H NMR studies were carried out on complexes **3.2**-**3.7** to determine the nature of the *ortho*-methyl fluxionality and $\Delta G^{\ddagger}$ of interconversion. Figure 3.6 shows the VT ^{1}H NMR spectrum of **3.5** in d_8-toluene from 25 °C to -90 °C, which is typical of complexes **3.2**-**3.5**. At room temperature, the *ortho* methyls display as a singlet at 1.80 ppm. Upon cooling, this singlet broadens, disappears at -60 °C, and splits to two singlets at 2.59 ppm and 1.05 ppm at -90 °C. These singlets each integrate to a total of 6 protons (relative to the *para* methyl group on the mesitylene rings) and represent the *endo* and *exo ortho*-methyl positions in the C_2 symmetric complex. From the coalescence rate constant (k_C) and coalescence temperature (T_C), the free energy of activation, $\Delta G^{\ddagger}$, was determined to be 9.2 kcal/mol at the coalescence temperature for **3.5**. All four complexes measured (**3.2**, **3.3**, **3.4**, and **3.5**) gave free energies between 9

Scheme 3.1

Potential A-B Interconversion Mechanisms:

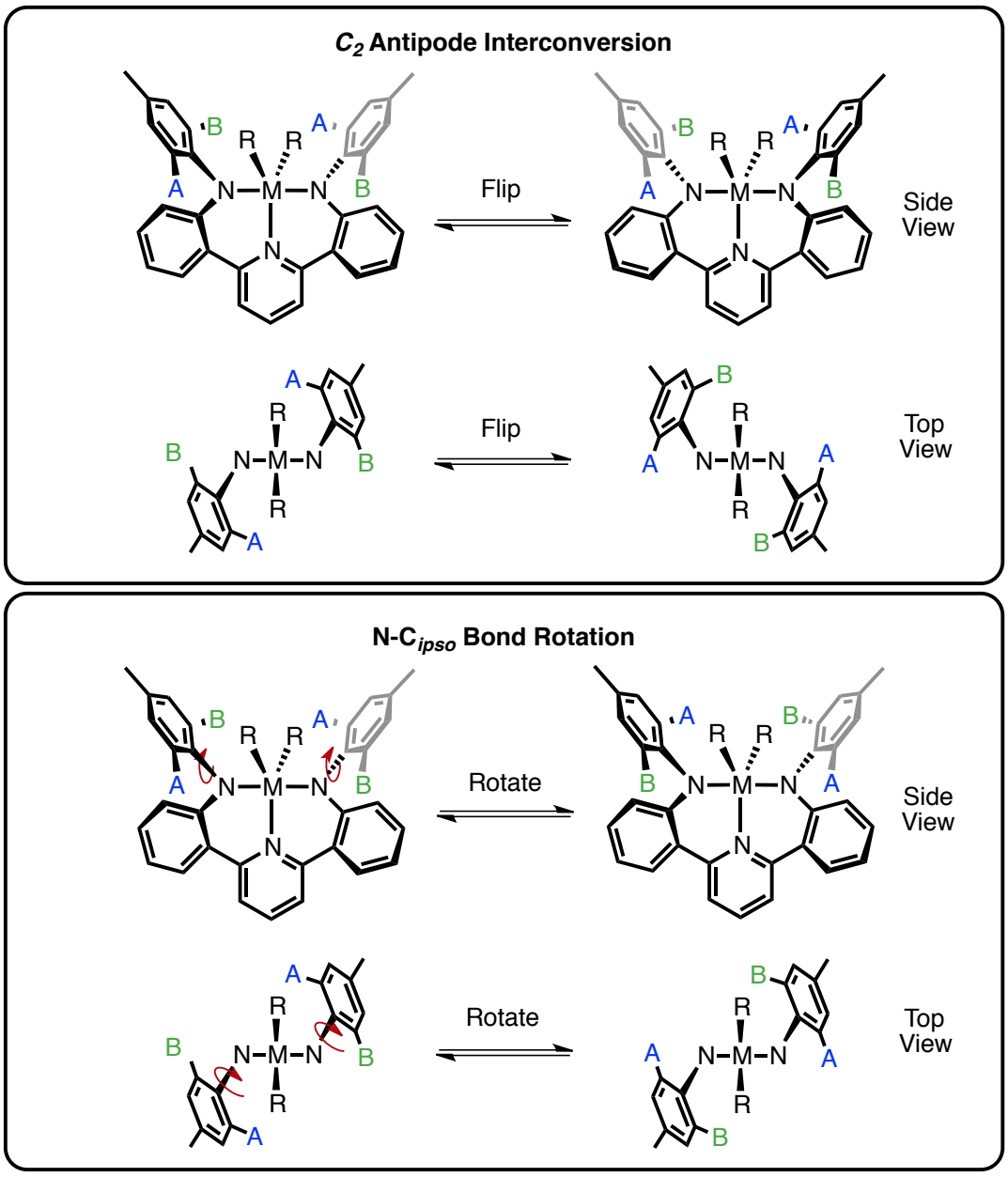

and 11 kcal/mol (Table 3.1). In complex **3.7**, which is ligated by (^{tBu}NNN), the room temperature ^{1}H NMR shows that the benzylic protons are coalesced (Figure 3.7). Upon cooling a toluene sample of **3.7** to −95 °C, the peak corresponding to the benzylic

protons broadens and disappears into the baseline. Unfortunately, $\Delta G^{\ddagger}$ cannot be calculated for **3.7** because of temperature limitations.

Table 3.1. Experimentally determined barriers of *o*-methyl interconversion in complexes **3.2**-**3.5**.

Complex	Coalescence Temperature (K)	$\Delta G^{\ddagger}_{T}$ (kcal/mol)	k_C (s^{-1})
(NNN)Ti(NMe_2)$_2$ (**3.2**)	243	10.8	899
(NNN)Zr(NMe_2)$_2$ (**3.3**)	233	10.4	899
(NNN)$TiCl_2$ (**3.4**)	253	10.9	1898
(NNN)$ZrCl_2$ (**3.5**)	213	9.2	1704

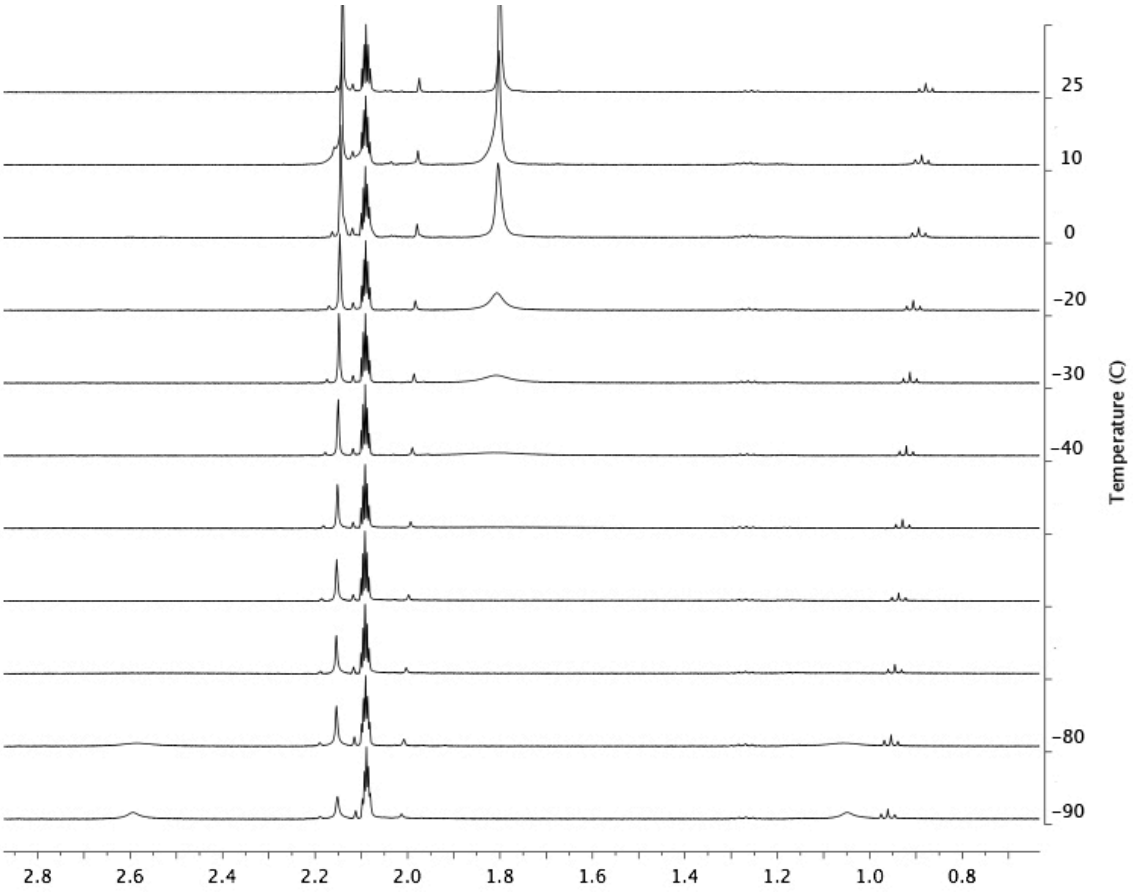

Figure 3.6. Variable temperature ^{1}H NMR spectrum of (NNN)$ZrCl_2$ (**3.5**) in d_8-toluene. The decoalesced *ortho* methyl peaks appear at 2.60 and 1.05 ppm at -90 °C.

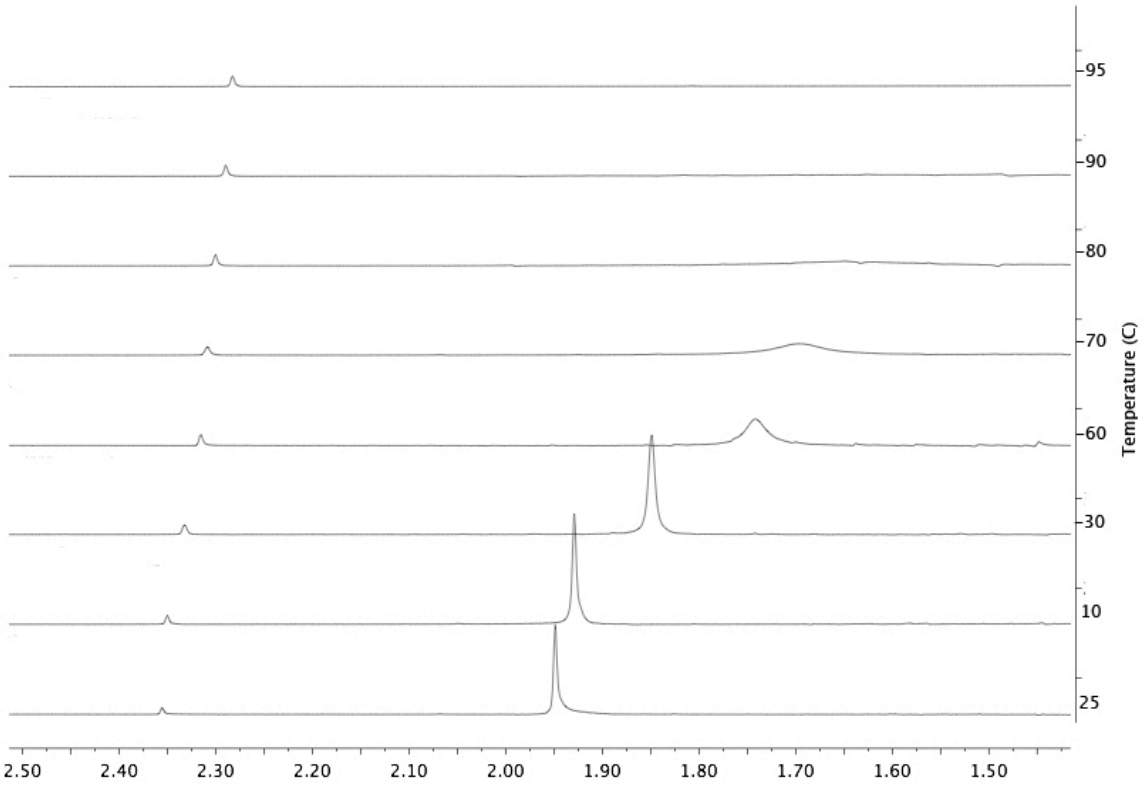

Figure 3.7. Variable temperature ^{1}H NMR spectrum of (^{tBu}NNN)ZrBn$_2$ (**3.7**) in d_8-toluene.

From the variable temperature data, we speculate that antipode interconversion accounts for the fluxionality seen by ^{1}H NMR. First, the calculated $\Delta G^{\ddagger}$ values are similar to barriers observed by Carpentier for fluxional processes in a related ligand set.[38b] Additionally, Mislow and coworkers[42] have shown that N–C$_{ipso}$ bond rotation barrier in Mes$_3$N and related complexes to be between 18–22 kcal/mol, which is substantially higher than our observed values. Furthermore, space-filling and DFT models of the N–C$_{ipso}$ bond rotation in **3.2** reveal that the mesitylene ring can't rotate through the plane of the (NNN) ligand framework since the *ortho* methyl's movement is blocked by an NMe$_2$ group.

While we have been unable entirely rule out N–C_{ipso} bond rotation in complexes **3.2–3.5**, the situation is less ambiguous in **3.7**. Assuming a C_2 geometry in solution, the two benzylic protons on the benzyl groups are diastereotopic. In this case, coalescence of these protons could only be a result of antipode interconversion (Scheme 3.2). Figure 3.7 shows that at room temperature the benzylic protons are equivalent, and when the sample is cooled the benzylic peak broadens out into the baseline. While the peaks decoalesce below the freezing point of toluene, this behavior demonstrates that the benzylic protons must be exchanging due to NNN ligand fluxionality.

Scheme 3.2

Diastereotopic Benzyl H Interconversion:

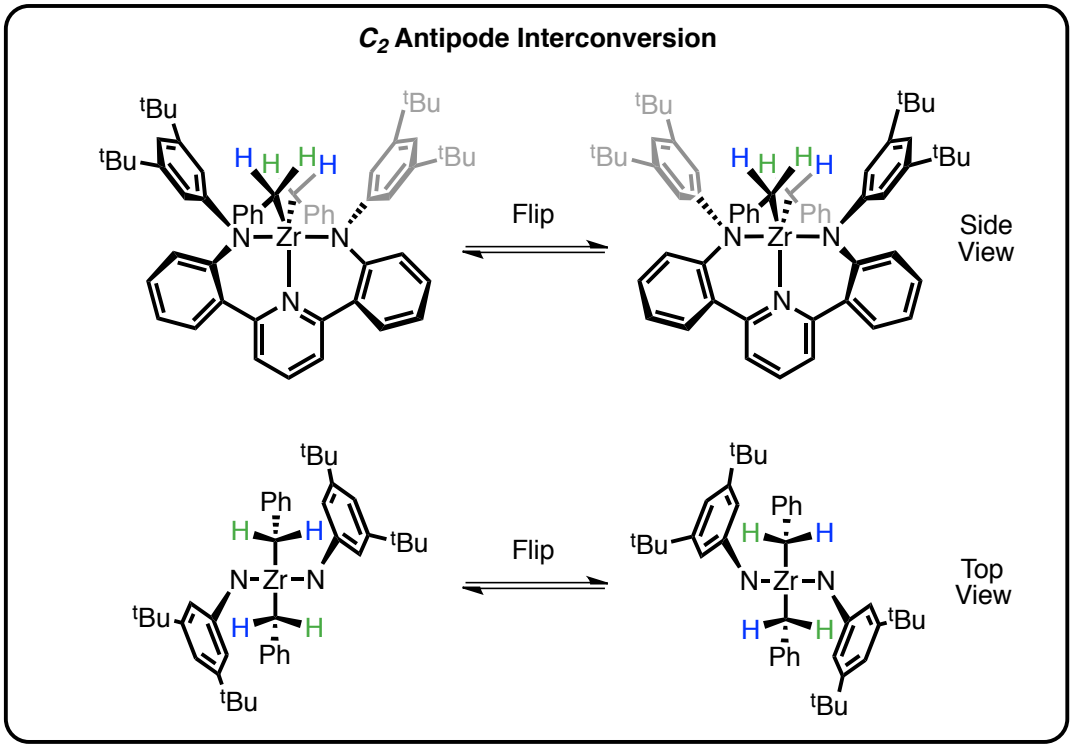

Consequently, the diastereotopic protons in **3.7** interconvert on the NMR timescale by flipping between antipodes and we believe that the same fluxional process

causes the interconversion of the *ortho* methyl protons in complexes **3.2-3.5.** It follows from the variable temperature ^{1}H NMR studies that the barrier for interconversion in **3.2-3.5** is higher than **3.7** since the full decoalescence pattern can be observed for these complexes. This can be reconciled by comparing the likely "C_{2v}-like" intermediates for the interconversions: **3.2-3.5** have more sterically encumbered *bis*(anilide) ligands, and as a result the C_{2v} intermediate should be higher in energy as more atoms are pushed into the N-M-N plane.

Propylene Polymerization

Complexes **3.2-3.6** were tested as propylene polymerization precatalysts. The test polymerizations were run in 35 mL propylene at 0 °C with 500-2000 equivalents of MAO used as an activator (Table 3.2). Under these conditions, most of the precatalysts yielded poor to moderate (10^{2}-10^{4} g/mol*h) activities for polymerization.

Surprisingly, the most active catalyst tested was the Ti *bis*(amide) complex, **3.2**, which yielded activities on the order of 10^{4} g/mol*h. This result is in contrast to the *bis*(phenolate)-based catalyst systems, in which the Zr precatalysts were typically 3 orders of magnitude more active than their Ti congeners.[34] As it was the most active precatalyst, the polymers generated from **3.2** were studied in depth to determine tacticity, molecular weight distribution, and activator effects. Activities for propylene polymerization using **3.2** appear to be slightly dependent of the amount of MAO used and maintain activity over the course of at least three hours. Increasing the catalyst loading does not lead to

increased activity, indicating that there is not an initial sacrifice of catalyst when these highly sensitive precatalysts are introduced to the reaction mixture.

Table 3.2. Propylene polymerization results obtained with precatalysts **3.2-3.6**. Conditions: 0 °C, 30-40 mL propylene, 2.7 mL toluene distilled from "Cp_2TiH."

Entry	$(NNN)MX_2$	Catalyst Loading (mmol)	MAO (equiv)	Time (h)	Polymer (mg)	Activity ($x10^4$ g/mol*h)	Mw ($x10^6$)	PDI
1	$Ti(NMe_2)_2$	.007	1000	0.5	34.9	.997		
2		.007	1000	3	242.2	1.15		
3		.007	2000	3	239.9	1.14		
4		.05	500	3	474	.316	1.037	31.21
5		.05	1000	2.5	1160	.928	.821	4.91
6		.05	2000	2	1780	1.78	1.151	5.58
7	$Zr(NMe_2)_2$	.007	1000	1	n.d.	n.d.		
8	$TiCl_2$	.007	1000	1	6	.0857		
9	$ZrCl_2$	.007	1000	1	17.7	.253		
10		.007	2000	1	28.9	.413		
11	$ZrCl_2THF$	.007	1000	1	1.7	.024		

Polymers generated by **3.2** activated with 500, 1000, or 2000 equivalents of MAO were examined by ^{13}C NMR (Figure 3.8). The polymers are mostly atactic with slight enrichment of the *mmmm* pentad. There are no isobutyl or olefinic peaks visible by NMR, and changing the concentration of MAO does not appreciably change the spectrum. The lack of visible end groups in the ^{13}C NMR spectrum is due to the extremely high molecular weights of the polymers—GPC analysis shows molecular weights of 10^6, albeit with very broad PDIs. Such high PDIs are atypical of single site catalysis, and as such precatalyst **3.2** may generate a multimetallic species or decompose into a mixture of different active species upon activation with MAO. We were optimistic that by employing precatalysts

which could fluctuate between C_2-symmetric enantiomers we could generate stereoblock isotactic polypropylene,[43] but it appears that the active species may be significantly changed from the precatalyst.

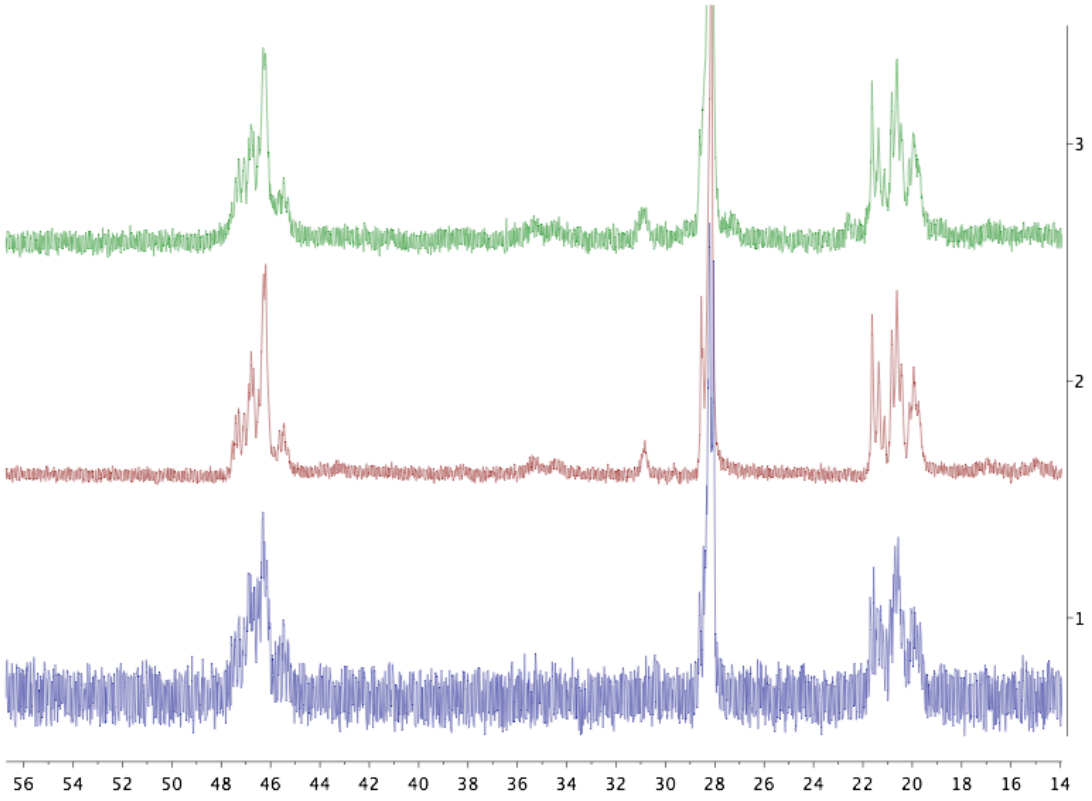

Figure 3.8. ^{13}C NMR of the alkyl region of polypropylene generated from **3.2** with 500, 1000, or 2000 equivalents MAO (bottom to top) used as an activator.

While the ^{13}C NMR of polypropylene generated by **3.2** appears atactic, the polymers are solids that exhibit thermoplastic elastomeric properties. These features are likely a result of a significant amount of misinsertions in the polymeryl chain, which are evident in the ^{13}C NMR between 30–46 ppm. Another contributing factor could be the high molecular weights of the polymers. Further investigation into these interesting

macroscopic polymer properties and their relationship to the polymer microstructure are ongoing using related ligand sets.

CONCLUSIONS

A series of group 4 complexes based on a pyridine *bis*(anilide) ligand set has been synthesized. These complexes fluctuate between C_2-symmetric antipodes in the solution state, with barriers of interconversion around 10 kcal/mol. Unlike the related *bis*(phenolate) complexes these complexes do not exhibit C_S symmetry upon coordination of a 6th ligand, which indicates that the *bis*(anilide) ligand imparts greater geometric control over the complex than the *bis*(phenolate) ligand. These complexes were tested as propylene polymerization precatalysts and yielded poor to moderate (10^2-10^4 g/mol*hr) polymerization activities. Disappointingly, the most active precatalyst (NNN)Ti(NMe_2)$_2$ yielded only slightly isotactically-enriched high molecular weight polypropylene with a very broad polydispersity index. Despite the limited success in using these complexes for propylene polymerization, understanding the solution state fluxional processes that these complexes undergo will allow for the development of new catalysts for stereoselective transformations with well-understood geometric preferences.

EXPERIMENTAL SECTION

General Considerations and Instrumentation. All air- and moisture-sensitive compounds were manipulated using standard high vacuum and Schlenk techniques or manipulated in a glovebox under a nitrogen atmosphere. Solvents for air- and moisture-sensitive reactions were dried over sodium benzophenone ketyl and stored over titanocene where compatible or dried by the method of Grubbs.[44] **3.1**-H_2,[40] $TiCl_2(NMe_2)_2$,[45] and $ZrCl_2(NMe_2)_2(THF)_2$[46] were prepared following literature procedures. Benzene-d_6, toluene-d_8, and THF-d_8 were purchased from Cambridge Isotopes and dried over sodium benzophenone ketyl. CD_2Cl_2 was distilled from CaH_2 and run through a plug of activated alumina prior to use. ^1H and ^{13}C spectra were recorded on Varian Mercury 300 or Varian INOVA 500 spectrometers and chemical shifts are reported with respect to residual protio-solvent impurity for ^1H (s, 7.16 ppm for C_6D_5H; t, 5.32 ppm for $CDHCl_2$) and solvent carbons for ^{13}C (t, 128.39 for C_6H_6; p, 53.84 for CD_2Cl_2).

Computational Details. Density functional calculations were carried out using Gaussian 03 Revision D.01.[47] Calculations were performed using the nonlocal exchange correction by Becke[48,49] and nonlocal correlation corrections by Perdew,[50] as implemented using the b3lyp[51,52] keyword in Gaussian. The following basis sets were used: LANL2DZ[53-55] for Ti and Zr atoms and 6-31G** basis set for all other atoms. Pseudopotentials were utilized for Ti and Zr atoms using the LANL2DZ ECP. All optimized structures were verified using frequency calculations and did not contain any imaginary frequencies. Iso-surface plots were made using the Gaussian 03 Revision D.01 program.[47]

X-ray Crystal Data: General Procedure. Crystals were removed quickly from a scintillation vial to a microscope slide coated with Paratone N oil. Samples were selected and mounted on a glass fiber with Paratone N oil. Data collection was carried out on a Bruker KAPPA APEX II diffractometer with a 0.71073 Å MoKα source. The structures were solved by direct methods. All non-hydrogen atoms were refined anisotropically. Details regarding refined data and cell parameters are available in Tables 3.3 and 3.4.

Synthesis of (NNN)Ti(NMe$_2$)$_2$ (3.2). A 10 mL toluene solution of bisaniline **3.1**-H$_2$ (602.5 mg, 1.210 mmol) was added to a 20 mL toluene suspension of KBn (314.6 mg, 2.420 mmol) and stirred for 2 hours. After two hours, a 10 mL toluene solution of TiCl$_2$(NMe$_2$)$_2$ (251 mg, 1.210 mmol) was added. The mixture was left to stir for twelve hours, and the resulting dark red solution was filtered through celite to remove salts. The toluene was then removed *in vacuo*, giving 687 mg (90%) of **3.2** as a red solid. Further purification and X-ray quality crystals were obtained by layering pentane over a saturated THF solution of **3.2** and cooling to -30 °C overnight. ^{1}H NMR (500 MHz, C$_6$D$_6$) δ, ppm: 1.97 (br s, 12H, NC*H*$_3$); 2.18 (s, 6H, p-C*H*$_3$); 2.50 (s, 12H, o-C*H*$_3$); 6.56 (dd, *J* = 8.5, 1.1 Hz, 2H); 6.70 (ddd, *J* = 8.0, 6.9, 1.2 Hz, 2H); 6.82 (s, 4H, *m*-mesityl); 7.08 (ddd, *J* = 8.5, 6.9, 1.7 Hz, 2H); 7.16, (t, *J* = 7.9 Hz, 1H, *p*-py); 7.26 (d, *J* = 7.9 Hz, 3,5-py, 2H); 7.60 (dd, *J* = 7.9, 1.6 Hz, 2H). ^{13}C NMR (125 MHz, C$_6$D$_6$) δ, ppm: 19.4 (*C*H$_3$); 21.3 (*C*H$_3$); 44.4 (N*C*H$_3$); 116.5, 116.6, 123.5, 123.6, 129.2, 129.4, 131.1, 132.7, 134.8, 136.4, 151.4, 151.4, 154.6 (aryl). Calcd for C$_{39}$H$_{45}$N$_5$Ti: C 74.15, H 7.18, N 11.09; Found: C 73.37, H 7.31, N 10.15%.

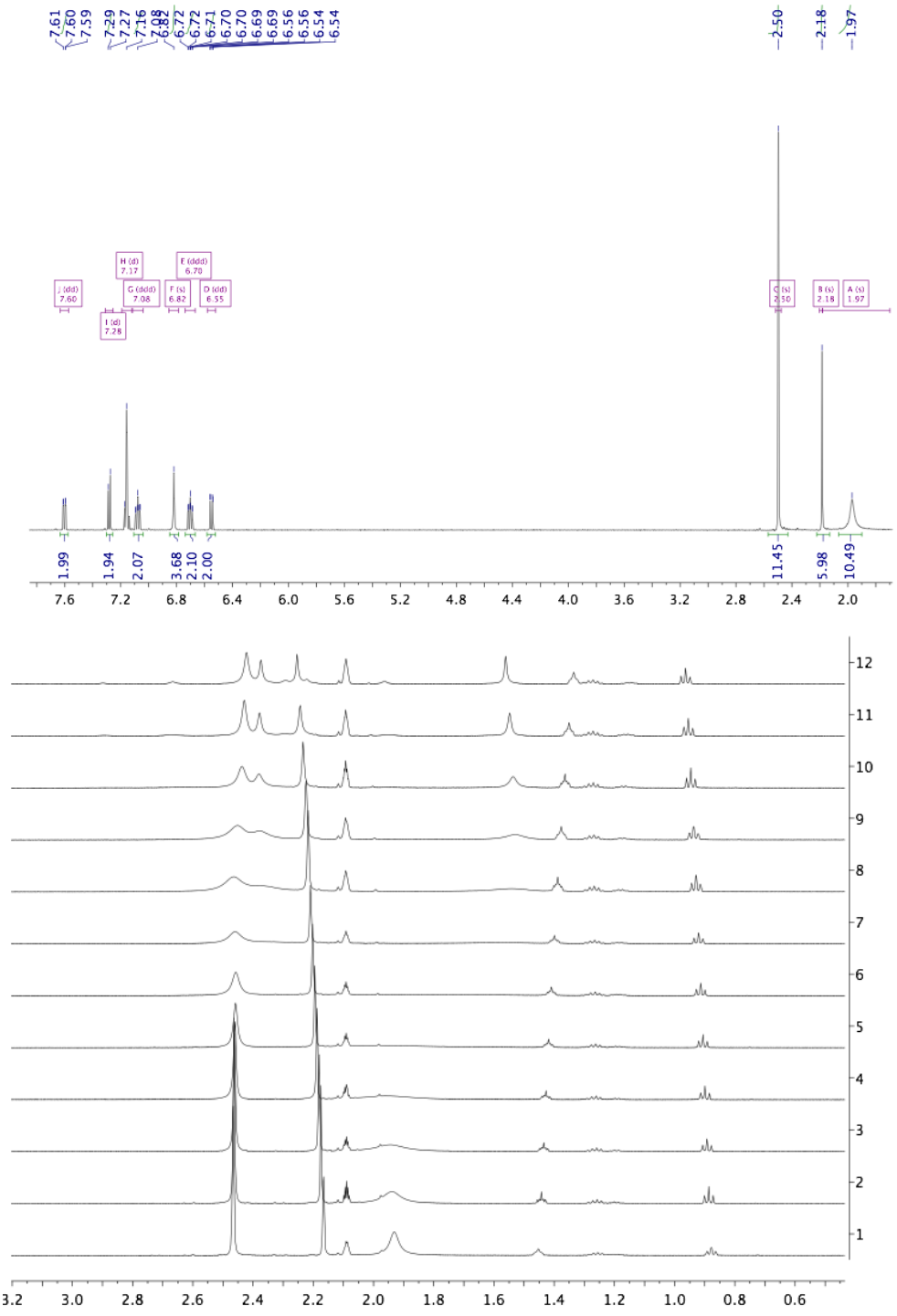

Figure 3.9. Room temperature (top) and variable temperature (bottom) ^{1}H NMR spectrum of (NNN)Ti(NMe_2)$_2$ (**3.2**) in CD_2Cl_2 and d_8–toluene, respectively. The VT range is 25 °C (spectrum 1) to –80 °C (spectrum 12). The decoalesced *ortho* methyl peaks appear at 2.40 and 1.50 ppm at –80 °C.

Synthesis of (NNN)Zr(NMe$_2$)$_2$ (3.3). *Route A: Salt Metathesis*. Using a procedure identical to the synthesis of **3.2** starting with Zr(NMe$_2$)$_2$Cl$_2$(THF)$_2$ yielded **3.3** as yellow crystals. *Route B: Aminolysis*. In a glovebox, a 100 mL bomb fitted with a Kontes valve was charged with a stirbar, 393 mg (0.79 mmol) **3.1**–H$_2$, and 211.6 mg (0.79 mmol) Zr(NMe$_2$)$_4$, and the vessel was then evacuated on a high vacuum line. 20 mL of benzene was vacuum transferred onto the solid mixture and then the vessel was heated to 90 °C and stirred overnight. The vessel was degassed and then heated at 90 °C for a further 12 hours. Solvent was then removed *in vacuo*, and the resulting yellow residue was recrystallized from a concentrated THF solution that was layered with pentane and cooled to –30 °C overnight. Yielded 346 mg **3.3** as yellow crystals (65%). ^{1}H NMR (300 MHz, CD_2Cl_2) δ, ppm: 1.82 (br s, 12H, *o*–CH_3); 2.09 (s, 12H, N(CH_3)$_2$); 2.18 (s, 6H, *p*–CH_3); 6.33 (dd, J = 8.5, 1.0 Hz, 2H); 6.70 (dd, J = 7.9, 1.0 Hz, 4H); 6.77 (s, 4H, *m*–mesityl); 7.13 (ddd, J = 8.5, 7.0, 1.6 Hz, 2H); 7.64 (d, J = 8 Hz, 2H, 3,5–py); 7.71 (dd, J = 7.9, 1.6 Hz, 2H); 7.96 (t, J = 7.9 Hz, 1H, *p*–py). ^{13}C NMR (125 MHz, C_6D_6) δ, ppm: 19.1 (CH_3); 21.3 (CH_3); 39.5 (NCH_3); 116.6, 118.0, 122.6, 124.2, 129.3, 130.3, 131.9, 132.6, 134.9, 137.4, 149.0, 150.7, 154.8 (aryl). Calcd for $C_{39}H_{45}N_5Zr$: C 69.39, H 6.72, N 10.37; Found: C 69.14, H 6.73 N 10.09%.

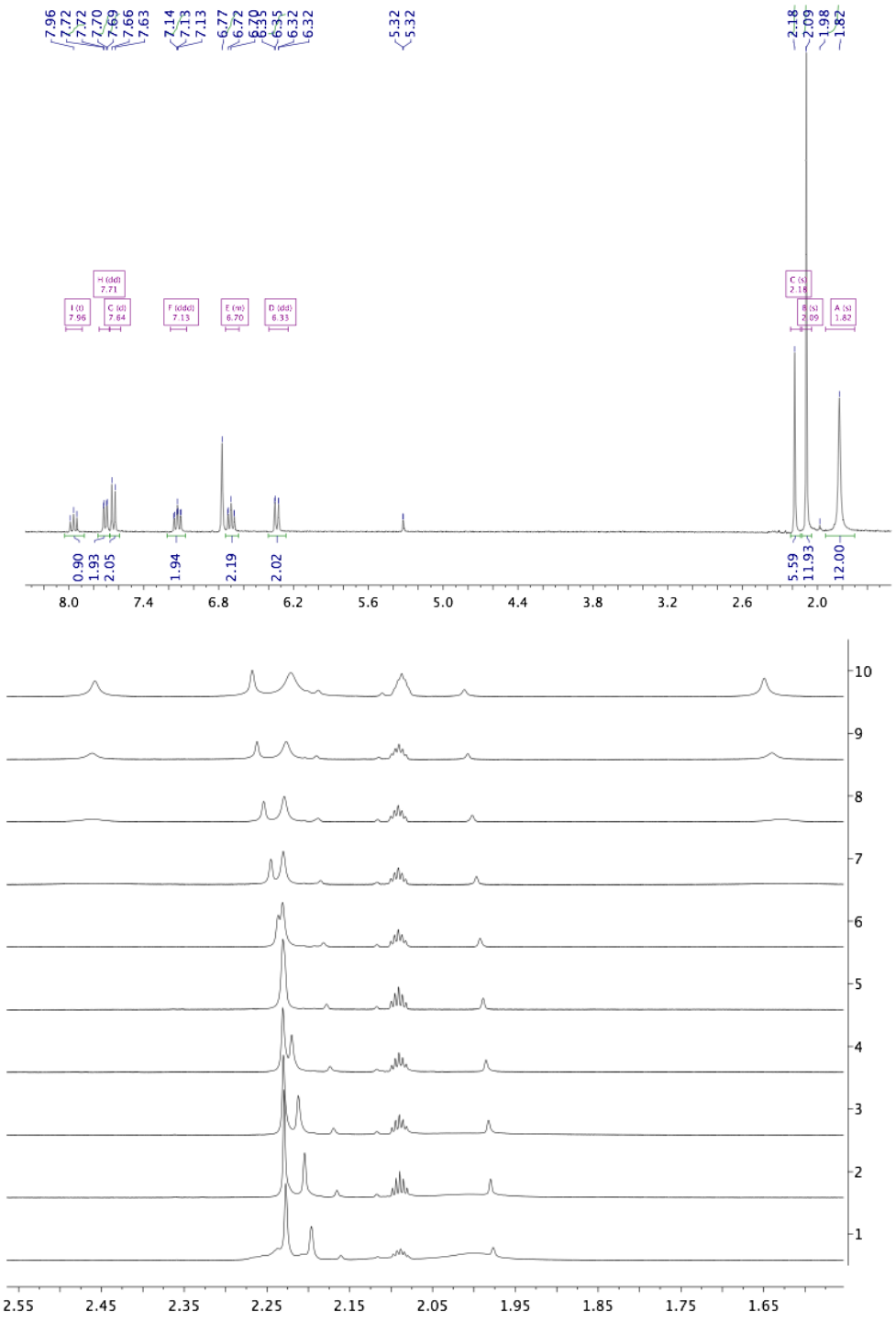

Figure 3.10. Room temperature (top) and variable temperature (bottom) ^{1}H NMR spectrum of (NNN)Zr(NMe$_2$)$_2$ (**3.3**) in CD_2Cl_2 and d_8–toluene, respectively. The VT range is 0 °C (spectrum 1) to –90 °C (spectrum 10). The decoalesced *ortho* methyl peaks appear at 2.45 and 1.65 ppm at –90 °C.

Synthesis of (NNN)$TiCl_2$ (3.4). Me_3SiCl (210 µL, 1.65 mmol) was added by syringe to a CH_2Cl_2 solution (20 mL) containing bisamide **3.2** (200 mg, .317 mmol). The reaction was stirred for three hours, then volatiles were removed *in vacuo*. The red residue was recrystallized from a concentrated toluene solution cooled to -30 °C, giving 175 mg (90%) of **3.4** as red crystals. ^1H NMR (300 MHz, CD_2Cl_2) δ, ppm: 1.49 (br s, 12H, *o*-CH_3); 2.29 (s, 6H, *p*-CH_3); 6.51 (d, J = 8.3 Hz, 2H); 6.71 (s, 4H, *m*-mesityl); 7.38 (t, J = 7.6 Hz, 2H); 7.51 (t, J = 7.7 Hz, 2H); 8.09 (d, J = 8.1 Hz, 2H); 8.15 (d, J = 7.9 Hz, 2H); 8.26 (t, J = 7.8 Hz, 1H, *p*-py). ^{13}C NMR (125 MHz, CD_2Cl_2) δ, ppm: 20.1 (*C*H_3); 26.0 (*C*H_3); 120.1, 123.3, 123.9, 126.5, 129.6, 130.1, 133.4, 136.9, 138.7, 139.8, 142.2, 143.6, 151.3 (aryl). Satisfactory combustion analysis could not be obtained for this compound.

Synthesis of (NNN)$ZrCl_2$ (3.5). Me_3SiCl (210 µL, 1.65 mmol) was added *via* syringe to a CH_2Cl_2 solution (20 mL) containing bisamide **3.3** (223 mg, .330 mmol). The reaction was stirred for 10 minutes, then volatiles were removed *in vacuo* to yield a yellow residue. Recrystallization from a toluene solution of **3.5** at -30 °C yielded yellow crystals of **3.5** (179 mg, 83% yield) over the course of two days. ^1H NMR (300 MHz, CD_2Cl_2) δ, ppm: 1.59 (s, 12H, *o*-CH_3); 2.30 (s, 6H, *p*-CH_3); 6.61 (d, J = 8.3 Hz, 2H); 6.78 (s, 4H, *m*-mesityl); 7.26 (t, J = 7.6 Hz, 2H); 7.46 (t, J = 7.7 Hz, 2H); 7.97 (d, J = 8.1 Hz, 2H); 8.06 (d, J = 8.1 Hz, 2H); 8.19 (t, J = 7.8 Hz, 1H, *p*-py). ^{13}C NMR (125 MHz, CD_2Cl_2) δ, ppm: 19.4 (*C*H_3); 21.1 (*C*H_3); 122.4, 122.7, 123.7, 124.3, 130.3, 131.1, 133.8, 138.4, 139.7, 140.2, 143.0, 152.4 (aryl). Satisfactory combustion analysis could not be obtained for this compound.

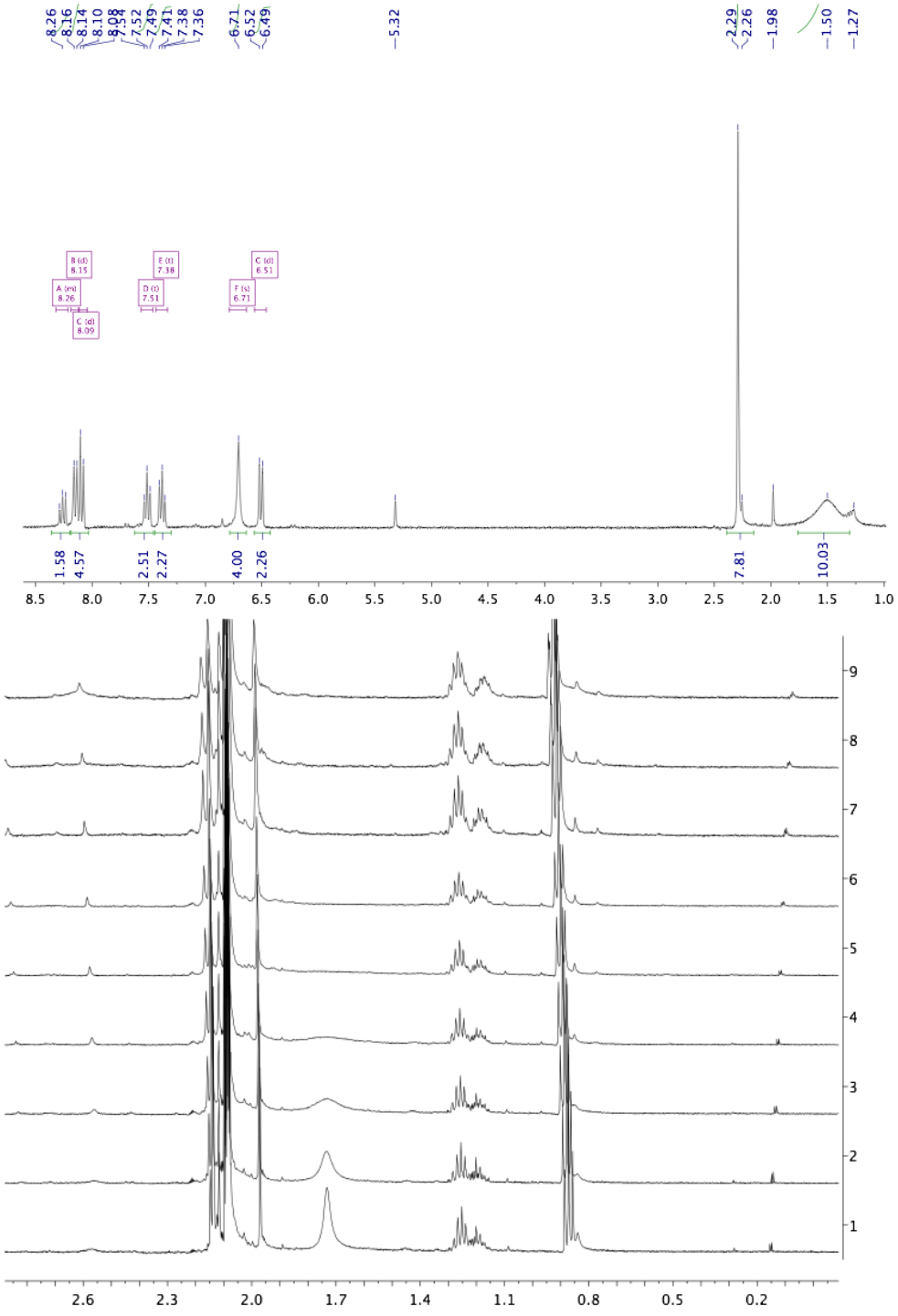

Figure 3.11. Room temperature (top) and variable temperature (bottom) ^{1}H NMR spectrum of (NNN)TiCl$_2$ (**3.4**) in CD_2Cl_2 and d_8–toluene, respectively. The VT range is 35 °C (spectrum 1) to −50 °C (spectrum 9). The decoalesced *ortho* methyl peaks appear at as broad peaks at 2.60 and 0.9 ppm at −90 °C.

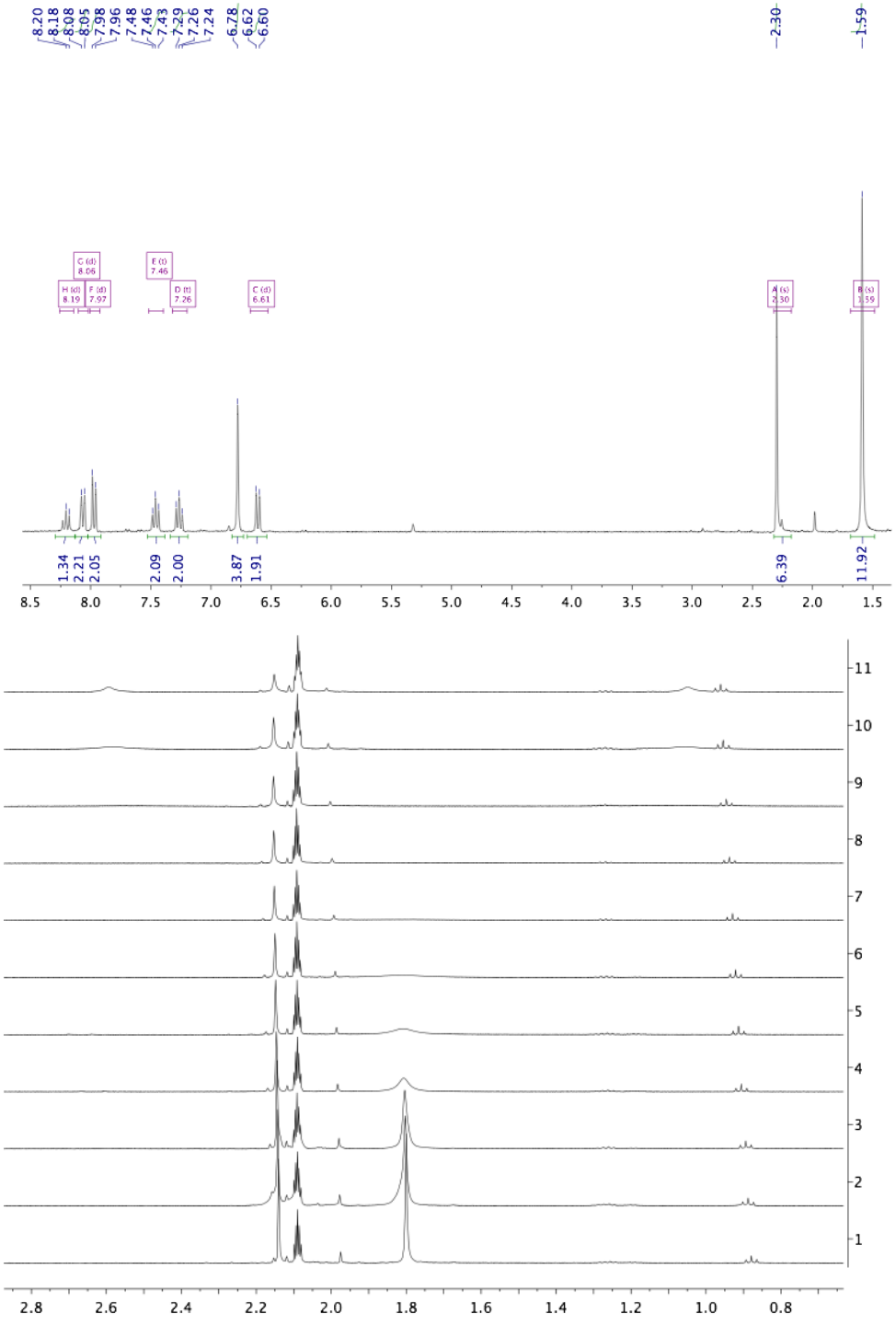

Figure 3.12. Room temperature (top) and variable temperature (bottom) ^{1}H NMR spectrum of (NNN)$ZrCl_2$ (**3.5**) in CD_2Cl_2 and d_8–toluene, respectively. The VT range is 25 °C (spectrum 1) to −90 °C (spectrum 11). The decoalesced *ortho* methyl peaks appear at 2.60 and 1.05ppm at −90 °C.

Synthesis of (^{tBu}NNN)ZrBn$_2$ (3.7). (^{tBu}NNN)H$_2$[56] (44.2 mg, 0.07 mmol) and ZrBn$_4$ (31.6 mg, 0.07 mmol) were dissolved in 0.7 mL C_6D_6 and sealed in a J-Young NMR tube. The tube was shielded from light using aluminum foil, and heated to 90 °C in an oil bath. Reaction progress was monitored *via* NMR, and after 24 h volatiles were removed *in vacuo* yielding a red/orange residue. This residue was dissolved in a minimal amount of pentane and cooled to -30 °C, yielding yellow crystals of **3.7** (45%). ^{1}H NMR (500 MHz, CD_2Cl_2) δ, ppm: 1.16 (s, 36H, C(C*H*$_3$)$_3$); 1.97 (s, 4H, PhC*H*$_2$); 6.34 (d, *J* = 7.1 Hz, 4H); 6.61 (t, *J* = 7.3 Hz, 2H); 6.73 (t, *J* = 2.3 Hz, 4H, *ortho* C$_6$*H*$_3$(*t*Bu)$_2$); 6.79 (t, *J* = 7.7 Hz, 4H); 7.01 (dd, *J* = 8.3, 1.1 Hz, 2H); 7.07 (t, *J* = 1.7 Hz, 2H, *para* C$_6$*H*$_3$(*t*Bu)$_2$); 7.15 (dt, *J* = 12.7, 2.9 Hz, 2H); 7.36 (m, 2H); 7.48 (dd, *J* = 7.9, 1.6 Hz, 2H); 7.59 (d, *J* = 8.0 Hz, 2H, *m*-py); 7.91 (t, *J* = 8.0 Hz, 1H, *p*-py). ^{13}C NMR (125 MHz, CD_2Cl_2) δ, ppm: 31.2 (C(*C*H$_3$)$_3$); 34.7 (*C*(CH$_3$)$_3$); 68.4 (Ph*C*H$_2$); 117.8, 119.4, 120.1, 123.0, 123.5, 125.7, 126.7, 127.7, 129.3, 131.0, 131.4, 139.2, 142.7, 148.0, 148.1, 151.6, 154.6 (aryl). Satisfactory combustion analysis could not be obtained for this compound.

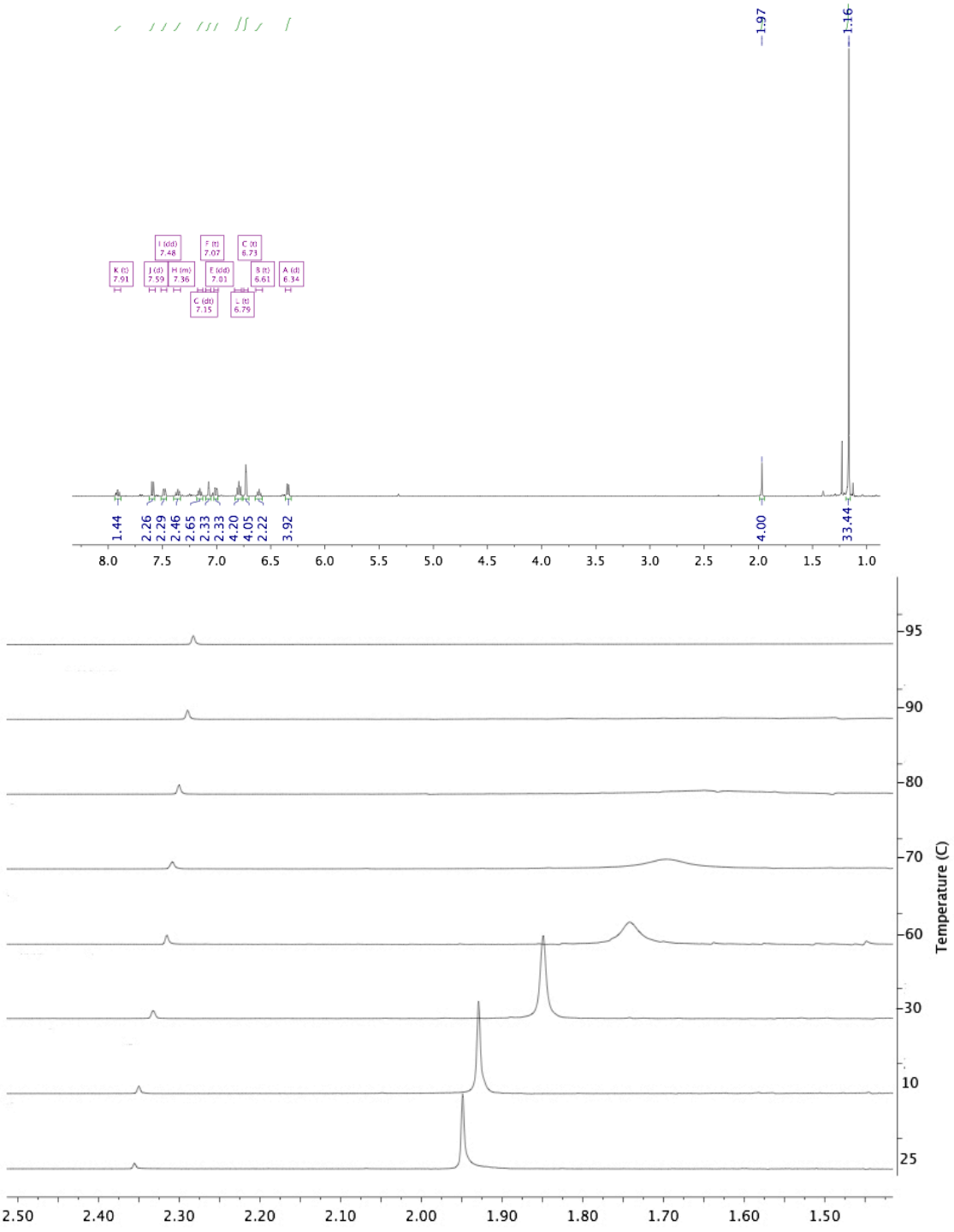

Figure 3.13. Room temperature (top) and variable temperature (bottom) ^{1}H NMR spectrum of (^{tBu}NNN)ZrBn$_2$ (**3.5**) in CD_2Cl_2 and d_8–toluene, respectively.

General Polymerization Protocol. A high-pressure glass reactor was charged with solid MAO (0.207 to 0.828 mg, 500 to 4000 equiv), and toluene (3 mL, distilled from "Cp_2TiH_2") was added. The vessel was sealed and attached to a propylene tank and purged. Upon cooling to 0 °C, propylene (35-39 mL) was condensed in. Zirconium or titanium precatalysts were added via syringe as a toluene solution (0.7 mL). The reaction mixture was stirred vigorously at 0 °C for the desired amount of time. Excess propylene was carefully vented. Then the cold bath was removed, and a MeOH/HCl solution (10:1, 50 mL) was added slowly. The resulting mixture was transferred to an Erlenmeyer flask, additional MeOH/HCl solution was added (50 mL), and the mixture was allowed to stir at room temperature overnight. The methanol solution was decanted and the polymer was rinsed with methanol. Upon decanting the methanol, the polymer was transferred to a vial, and volatile materials were removed by placing the vial under vacuum and heating to 80 °C overnight. The resulting materials were investigated by NMR spectroscopy and GPC. Polymer NMR spectroscopy data were acquired at 120 °C in tetrachloroethane. No polymer was formed without titanium or zirconium precatalyst addition or in just the presence of the (NNN) ligand.

Table 3.3. Crystal and refinement data for complexes **3.2–3.4**.

	3.2	**3.3**	**3.4**
CCDC Number	800979	800978	697201
Empirical formula	$C_{39}H_{45}N_5Ti \cdot C_4H_8O$	$C_{39}H_{45}N_5Zr$	$C_{35}H_{33}N_3Cl_2Ti \cdot C_4H_8O$
Formula weight	703.80	675.02	686.55
T (K)	100(2)	100(2)	100(2)
a, Å	32.3018(14)	16.6663(7)	36.2843(15)
b, Å	14.9286(7)	11.7383(5)	11.6553(5)
c, Å	16.9824(8)	18.2430(7)	16.9710(8)
a, deg			
b, deg	110.525(2)	104.524(2)	109.665(2)
g, deg			
Volume, Å^3	7669.4(6)	3454.9(2)	6758.5(5)
Z	8	4	8
Crystal system	Monoclinic	Monoclinic	Monoclinic
Space group	C 2/*c*	P 2_1/*c*	C2/*c*
d_{calc}, g/cm^3	1.219	1.298	1.349
q range, deg	1.83 to 30.50	2.08 to 33.50	1.85 to 33.19
μ, mm^{-1}	0.263	0.352	0.448
Abs. Correction	None	None	None
GOF	2.491	1.774	1.938
R_1 ,[a]	R1 = 0.0677,	R1 = 0.0325,	R1 = 0.0420,
wR_2 [b] [I>2s(I)]	*w*R2 = 0.1063	*w*R2 = 0.0505	*w*R2 = 0.0523

[a] $R_1 = \Sigma||F_o| - |F_c||/\Sigma|F_o|$. [b] $wR_2 = [\Sigma[w(F_o^2-F_c^2)^2]/\Sigma[w(F_o^2)^2]]^{1/2}$.

Table 3.4. Crystal and refinement data for complexes **3.5–3.7**.

	3.5	**3.6**	**3.7**
CCDC Number	697086	723743	800979
Empirical formula	$C_{35}H_{33}N_3Cl_2Zr \cdot 0.75(C_7H_8)$	$C_{39}H_{41}N_3OCl_2Zr$	$C_{59}H_{67}N_3Zr \cdot C_5H_{12}$
Formula weight	726.86	729.87	981.52
T (K)	100(2)	100(2)	100(2)
a, Å	17.1199(7)	11.7169(5)	10.5191(4)
b, Å	23.1437(10)	12.7754(6)	12.8102(5)
c, Å	34.8624(15)	13.0786(6)	20.6372(8)
a, deg		61.415(2)	96.952(2)
b, deg		85.745(3)	90.511(2)
g, deg		85.899(3)	98.726(2)
Volume, Å^3	13813.1(10)	1712.89(13)	2727.45(18)
Z	16	2	2
Crystal system	Orthorhombic	Triclinic	Triclinic
Space group	$P2_12_12_1$	P–1	P–1
d_{calc}, g/cm^3	1.398	1.415	1.195
q range, deg	1.48 to 36.20	1.74 to 39.30	1.79 to 27.45
μ, mm^{-1}	0.506	0.513	0.243
Abs. Correction	None	Empirical, Twinabs, Multi-scan	None
GOF	1.589	1.957	1.925
R_1 ,[a]	R1 = 0.0345,	R1 = 0.0381,	R1 = 0.0352,
wR_2 [b] [I>2s(I)]	wR2 = 0.0543	wR2 = 0.0678	wR2 = 0.0492

[a] $R_1 = \Sigma||F_o| - |F_c||/\Sigma|F_o|$. [b] $wR_2 = [\Sigma[w(F_o^2-F_c^2)^2]/\Sigma[w(F_o^2)^2]]^{1/2}$.

REFERENCES

1. a.) Britovsek, G. J. P.; Gibson, V. C.; Wass, D. F. *Angew. Chem., Int. Ed. Engl.* **1999**, *38*, 428–447. b.) Gibson, V. C.; Spitzmesser, S. K. *Chem. Rev.* **2003**, *103*, 283–315.
2. Wolczanski, P. T.; *Polyhedron,* **1995**, *14*, 3335.
3. Coates, G. W.; Hustad, P. D.; Reinartz, S. *Angew. Chem. Int. Ed. Engl.* **2002**, *41*, 2236–2257.
4. Watson, D. A.; Chiu, M.; Bergman, R. G.; *Organometallics* **2006**, *25*, 4731–4733.
5. Anderson, L. L.; Arnold, J.; Bergman, R. G. *J. Am. Chem. Soc.* **2005**, *127*, 14542–14543.
6. Ackermann, L.; Bergman, R. G.; Loy, R. N. *J. Am. Chem. Soc.* **2003**, *125*, 11956–11963.
7. Rothwell, I. P. *Chem. Commun.* **1997**, 1331–1338.
8. Wallace, K. C.; Liu, A. H.; Dewan, J. C.; Schrock, R. R. *J. Am. Chem. Soc.* **1988**, *110*, 4964–4977.
9. Schrock, R. R. *Angew. Chem., Int. Ed. Engl.* **2006**, *45*, 3748–3759.
10. Schrock, R. R.; Hoveyda, A. H. *Angew. Chem., Int. Ed. Engl.* **2003**, *42*, 4592–4633.
11. Tsang, W. C. P.; Hultzsch, K. C.; Alexander, J. B.; Bonitatebus, P. J.; Schrock, R. R.; Hoveyda, A. H. *J. Am. Chem. Soc.* **2003**, *125*, 2652–2666.
12. Schrock, R. R. *Chem. Rev.* **2002**, *102*, 145–179.
13. Spencer, L. P.; Beddie, C.; Hall, M. B.; Fryzuk, M. D. *J. Am. Chem. Soc.* **2006**, *128*, 12531–12543.
14. Mason, A. F.; Coates, G. W. *J. Am. Chem. Soc.* **2004**, *126*, 16326–16327.
15. Tian, J.; Hustad, P. D.; Coates, G. W. *J. Am. Chem. Soc.* **2001**, *123*, 5134–5135.
16. Tshuva, E. Y.; Goldberg, I.; Kol, M. *J. Am. Chem. Soc.* **2000**, *122*, 10706–10707.
17. Tshuva, E. Y.; Goldberg, I.; Kol, M.; Goldschmidt, Z. *Organometallics* **2001**, *20*, 3017–3028.
18. Tshuva, E. Y.; Groysman, S.; Goldberg, I.; Kol, M.; Goldschmidt, Z. *Organometallics* **2002**, *21*, 662–670.
19. Groysman, S.; Goldberg, I.; Kol, M.; Genizi, E.; Goldschmidt, Z. *Adv. Synth. Catal.* **2005**, *347*, 409–415.
20. Groysman, S.; Segal, S.; Goldberg, I.; Kol, M.; Goldschmidt, Z. *Inorg. Chem.*

Commun. **2004**, *7*, 938-941.

21. Groysman, S.; Goldberg, I.; Kol, M.; Genizi, E.; Goldschmidt, Z. *Organometallics* **2004**, *23*, 1880-1890.
22. Groysman, S.; Goldberg, I.; Kol, M.; Goldschmidt, Z. *Organometallics* **2003**, *22*, 3793-3795.
23. Groysman, S.; Segal, S.; Shamis, M.; Goldberg, I.; Kol, M.; Goldschmidt, Z.; Hayut-Salant, E. *J. Chem. Soc.-Dalton Trans.* **2002**, 3425-3426.
24. Freundlich, J. S.; Schrock, R. R.; Davis, W. M. *Organometallics* **1996**, *15*, 2777-2783.
25. Freundlich, J. S.; Schrock, R. R.; Davis, W. M. *J. Am. Chem. Soc.* **1996**, *118*, 3643-3655.
26. Baumann, R.; Davis, W. M.; Schrock, R. R. *J. Am. Chem. Soc.* **1997**, *119*, 3830-3831.
27. Baumann, R.; Stumpf, R.; Davis, W. M.; Liang, L. C.; Schrock, R. R. *J. Am. Chem. Soc.* **1999**, *121*, 7822-7836.
28. Liang, L. C.; Schrock, R. R.; Davis, W. M.; McConville, D. H. *J. Am. Chem. Soc.* **1999**, *121*, 5797-5798.
29. Mehrkhodavandi, P.; Bonitatebus, P. J.; Schrock, R. R. *J. Am. Chem. Soc.* **2000**, *122*, 7841-7842.
30. Mehrkhodavandi, P.; Schrock, R. R. *J. Am. Chem. Soc.* **2001**, *123*, 10746-10747.
31. Mehrkhodavandi, P.; Schrock, R. R.; Pryor, L. L. *Organometallics* **2003**, *22*, 4569-4583.
32. Nakayama, Y.; Saito, H.; Ueyama, N.; Nakamura, A. *Organometallics,* **1999**, *18*, 3149-3158.
33. Sernetz, F. G.; Mulhaupt, R.; Fokken, S.; Okuda, J. *Macromolecules* **1997,** *30*, 1562-1569.
34. a.) Agapie, T.; Henling, L. H.; DiPasquale, A. G.; Rheingold, A. L.; Bercaw, J. E. *Organometallics* **2008**, *27*, 6245-6246. b.) Golisz, S. R.; Bercaw, J. E. *Macromolecules* **2009**, *42*, 8751.
35. a.) Agapie, T.; Bercaw, J. E. *Organometallics* **2007**, *26*, 2957-2959. b.) Agapie, T.; Day, M. W.; Bercaw, J. E. *Organometallics* **2008**, *27*, 6123-6142. c.) Tonks, I. A.; Henling, L. M.; Day, M. W.; Bercaw, J. E. *Inorg. Chem.* **2009**, *48*, 5096. d.) Winston, M. S.; Bercaw, J. E. *Organometallics* **2010**, *29*, 6408.
36. a.) Chan, M. C. W.; Tam, K. H.; Zhu, N. Y.; Chiu, P.; Matsui, S. *Organometallics*

2006, *25*, 785. b.) Chan, M. C. W.; Tam, K. H.; Pui, Y. L.; Zhu, N. Y. *J. Chem. Soc., Dalton Trans.* **2002**, 3085–3087. c.) Tam, K. H.; Chan, M. C. W.; Kaneyoshi, H.; Makio, H.; Zhu, N. Y. *Organometallics* **2009**, *28*, 5877.

37. a.) Sarkar, S.; Abboud, K. A.; Veige, A. S. *J. Am. Chem. Soc.* **2008**, *130*, 16128–16129. b.) Sarkar, S.; Carlson, A. R.; Veige, M. K.; Falkowski, J. M.; Abboud, K. A.; Veige, A. S. *J. Am. Chem. Soc.* **2008**, *130*, 1116–1117. c.) O'Reilly, M.; Falkowski, J. M.; Ramachandran, V.; Pati, M.; Abboud, K. A.; Dalal, N. S.; Gray, T. G.; Veige, A. S. *Inorg. Chem.* **2009**, *48*, 10901. d.) Kuppuswamy, S.; Peloquin, A. J.; Ghiviriga, I.; Abboud, K. A.; Veige, A. S. *Organometallics*, **2010**, *29*, 4227.
38. a.) Grunova, E.; Kirillov, E.; Roisnel, T.; Carpentier, J. *J. Chem. Soc. Dalton Trans.* **2010**, *39*, 6739. b.) Kirillov, E.; Roisnel, T.; Razavi, A.; Carpentier, J. *Organometallics*, **2009**, *28*, 5036. c.) Steinhauser, S.; Heinz, U.; Sander, J.; Hegetschweiler, K. Z. *Anorg.Allg.Chem.,* **2004**, *630*, 1829–1838.
39. Weinberg, D. R.; Hazari, N.; Labinger, J. A.; Bercaw J. E. *Organometallics* **2010**, *29*, 89.
40. Weintrob, E. C.; Tofan, D.; Bercaw, J. E. *Inorg. Chem.* **2009**, *48*, 3808.
41. See Chapter 4 for synthesis and characterization of (ONO)Ti(NMe_2)$_2$.
42. Mislow, K. *Acc. Chem. Res.* **1976**, *9*, 26.
43. Coates, G. W.; Waymouth, R. M. *Science*, **1995**, *267*, 217.
44. Pangborn, A. B.; Giardello, M. A.; Grubbs, R. H.; Rosen, R. K.; Timmers, F. J. *Organometallics* **1996**, *15*, 1518.
45. Benzing, E.; Kornicker, W. *Chem. Ber.* **1961**, *94*, 2263.
46. Kempe, R. K.; Brenner, S.; Arndt, P. *Z. Anorg. Allg. Chem*. **1995**, *621*, 2021.
47. Frisch, M. J.; Trucks, G. W.; Schlegel, H. B.; Scuseria, G. E.; Robb, M. A.; Cheeseman, J. R.; Montgomery, Jr., J. A.; Vreven, T.; Kudin, K. N.; Burant, J. C.; Millam, J. M.; Iyengar, S. S.; Tomasi, J.; Barone, V.; Mennucci, B.; Cossi, M.; Scalmani, G.; Rega, N.; Petersson, G. A.; Nakatsuji, H.; Hada, M.; Ehara, M.; Toyota, K.; Fukuda, R.; Hasegawa, J.; Ishida, M.; Nakajima, T.; Honda, Y.; Kitao, O.; Nakai, H.; Klene, M.; Li, X.; Knox, J. E.; Hratchian, H. P.; Cross, J. B.; Bakken, V.; Adamo, C.; Jaramillo, J.; Gomperts, R.; Stratmann, R. E.; Yazyev, O.; Austin, A. J.; Cammi, R.; Pomelli, C.; Ochterski, J. W.; Ayala, P. Y.; Morokuma, K.; Voth, G. A.; Salvador, P.; Dannenberg, J. J.; Zakrzewski, V. G.; Dapprich, S.; Daniels, A. D.; Strain, M. C.; Farkas, O.; Malick, D. K.; Rabuck, A. D.; Raghavachari, K.; Foresman, J. B.; Ortiz, J. V.; Cui, Q.; Baboul, A. G.; Clifford, S.; Cioslowski, J.;

Stefanov, B. B.; Liu, G.; Liashenko, A.; Piskorz, P.; Komaromi, I.; Martin, R. L.; Fox, D. J.; Keith, T.; Al-Laham, M. A.; Peng, C. Y.; Nanayakkara, A.; Challacombe, M.; Gill, P. M. W.; Johnson, B.; Chen, W.; Wong, M. W.; Gonzalez, C.; Pople, J. A.; *Gaussian 03*, revision C.02,Gaussian, Inc., Wallingford CT, 2004.

48. Becke, A. D. *Phys. Rev. A: At., Mol., Opt. Phys.* **1988**, *38*, 3098-3100.
49. Becke, A. D. *J. Chem. Phys.* **1988**, *88*, 1053-1062.
50. Perdew, J. P. *Phys. Rev. B* **1986**, *33*, 8800-8802.
51. C. Lee, W. Yang, and R. G. Parr, *Phys. Rev. B* **37**, 785 (1988).
52. B. Miehlich, A. Savin, H. Stoll, and H. Preuss, *Chem. Phys. Lett.* **157**, 200 (1989).
53. Hay, P. J.; Wadt, W. R. *J. Chem. Phys.* **1985**, *82*, 270-283.
54. Wadt, W. R.; Hay, P. J. *J. Chem. Phys.* **1985**, *82*, 284-298.
55. Hay, P. J.; Wadt, W. R. *J. Chem. Phys.* **1985**, *82*, 299-310.
56. For synthesis of ($^{t\text{Bu}}$NNN)H_2 see: Weintrob, E. C. Caltech Thesis, **2011**.

CHAPTER 4

Titanium Complexes Supported by a Pyridine-*bis*(phenolate) Ligand: Active Precatalysts for the Intermolecular Hydroamination or Cyclotrimerization of Alkynes

ABSTRACT

A class of titanium precatalysts of the type (ONO)TiX_2 (ONO = pyridine-2,6-*bis*(4,6-^{t}Bu$_2$-phenolate); X = Bn, NMe_2) have been synthesized and crystallographically characterized. The (ONO)TiX_2 complexes are highly active precatalysts for the intermolecular hydroamination of internal alkynes with primary arylamines and some alkylamines. A class of titanium imido complexes, (ONO)Ti(L)(NR) (L = $HNMe_2$, py; R = Ph, ^{t}Bu) have also been synthesized and characterized and provide structural analogues to intermediates on the purported catalytic cycle. These imido complexes are also competent hydroamination precatalysts. When (ONO)$TiBn_2$ (**4.1**) is heated only in the presence of an electron-rich alkyne, alkyne cyclotrimerization is observed. During the cyclotrimerization reaction the Ti^{IV} precatalyst is reduced to Ti^{II}, which is the active species for catalysis. The mechanism of formation of Ti^{II} has been investigated and an (ONO)Ti^{II} species has been trapped by ethylene and crystallographically characterized. **4.1** represents a convenient and stable Ti^{IV} trimerization precatalyst and does not require an external reductant to initiate cyclotrimerization.

INTRODUCTION

The inter- and intramolecular hydroamination of alkenes and alkynes has been catalyzed by a large range of transition metals, lanthanides, and even main group elements.[1] Among this broad range of catalysts, group 4 complexes[2] have been found to be excellent catalysts for the intermolecular hydroamination of alkynes. Bergman and others have investigated the mechanism[2] of the group 4 catalyzed reaction and have found that it typically proceeds first by protonolysis by an amine and subsequent formation of a transient metal imido species, then [2+2] addition with an alkyne to generate an azametallacyclobutene which can be protonolyzed by another equivalent of amine to continue the catalytic cycle (Scheme 4.1). These reactions are often carried out at elevated temperature (often in excess of 100 °C) and can require long reaction times on the order of 12-24 hours. A common catalyst deactivation pathway involves dimerization of a low-coordinate Ti-imido intermediate. This decomposition is often overcome by utilizing bulky amines to limit dimerization or high temperatures to break the dimer. While the product of this reaction, either an imine or enamine, might often be more easily formed *via* amine condensation with a ketone, alkyne hydroamination remains a useful synthetic tool—particularly because of its atom economy.

Recently our group[3] and others[4] have been investigating pyridine-linked *bis*(phenoxide) pincer ligands as ancillary ligands for early transition metal catalyzed olefin polymerization catalysts. Early transition metal complexes of these ONO ligands are very thermally robust due to their rigid, all-aryl backbone. In light of reports that phenoxide-based[5] titanium complexes were precatalysts for intermolecular alkyne

hydroamination, we envisioned that ONO titanium complexes could also be competent catalysts and might be long-lived due to their thermal stability.

Scheme 4.1

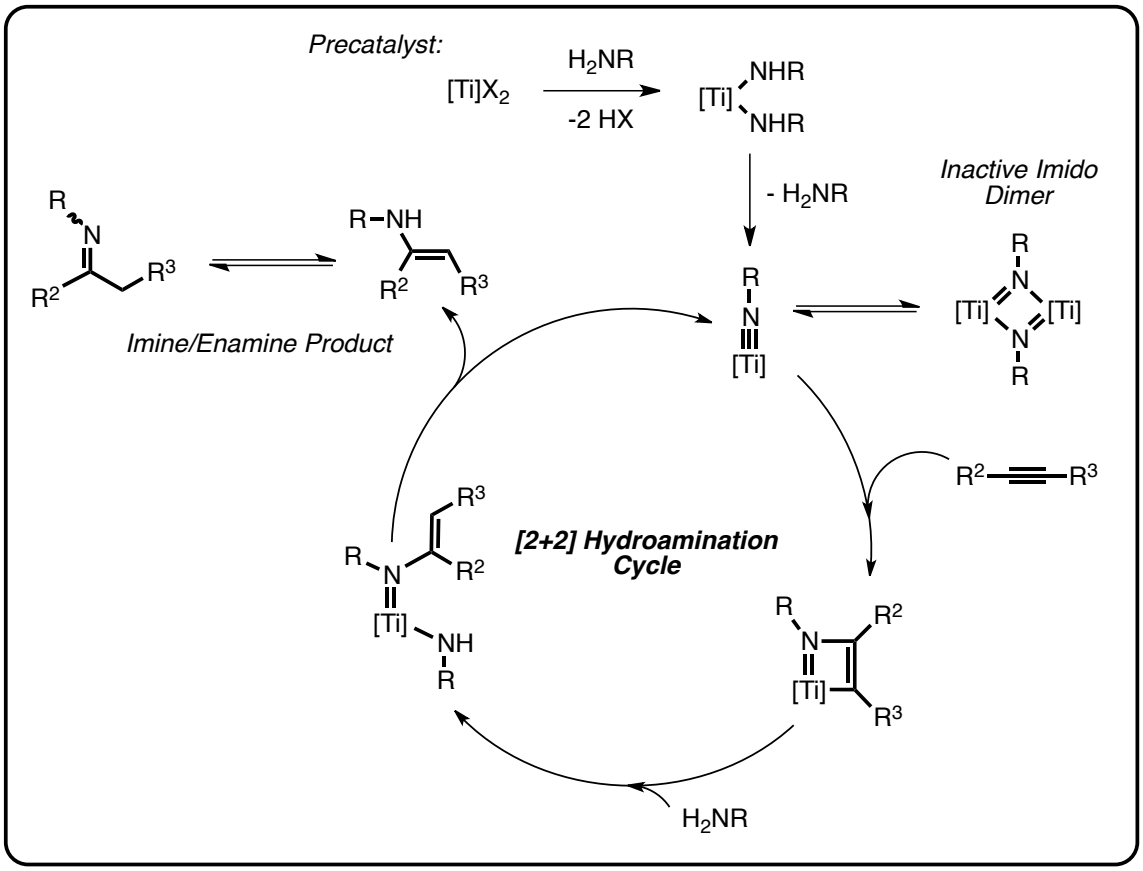

Results and Discussion

Synthesis and Characterization of Precatalysts

(ONO)TiBn$_2$ (**4.1**) (ONO = pyridine-2,6-*bis*(4,6-^{t}Bu$_2$-phenolate)) was synthesized *via* protonolysis of TiBn$_4$ with (ONO)H$_2$ following literature procedure[3c] (Scheme 4.2). Salt metathesis of TiCl$_2$(NMe$_2$)$_2$ and the deprotonated ligand (ONO)K$_2$ generated the *bis*(amide) (ONO)Ti(NMe$_2$)$_2$ (**4.2**). Similarly, salt metathesis of TiCl$_2$(HNMe$_2$)$_2$(NPh) with (ONO)K$_2$ yielded the phenylimido complex, (ONO)Ti(HNMe$_2$)(NPh) (**4.3**). A series of (ONO)Ti imido complexes can be synthesized by utilizing differently-substituted Ti-imido starting materials of the nature TiCl$_2$(L)$_2$(NR) (L = HNMe$_2$, py; R = alkyl, aryl. For **4.4**, R = ^{t}Bu, L = py). Finally, the base-stabilized dichloride complex (ONO)TiCl$_2$(py) (**4.6**) was synthesized through aminolysis of TiCl$_2$(NMe$_2$)$_2$ with (ONO)H$_2$ and treatment with excess pyridine. In the absence of pyridine, the HNMe$_2$ adduct (ONO)TiCl$_2$(HNMe$_2$) (**4.5**) is obtained, although this complex loses some HNMe$_2$ to form a mixture of (ONO)TiCl$_2$ and (ONO)TiCl$_2$(HNMe$_2$) upon workup. We were unable to synthesize (ONO)TiCl$_2$-type complexes through salt metathesis of TiCl$_4$ or TiCl$_4$(THF)$_2$ with (ONO)K$_2$, presumably because the deprotonated ligand reduces the titanium starting material.

The crystal structure of the C_2-symmetric **4.1** has been previously reported.[3c] Interestingly, in the solid state **4.2** shows a C_S-symmetric ONO ligand with the two phenolate arms occupying equatorial sites of a distorted trigonal bipyramid (Figure 4.1). This is likely the electronically preferred[3d] geometry for π-loaded 5-coordinate ONO complexes, whereas 5-coordinate ONO complexes without additional π donors prefer C_2 structures. Due to the small, electron-rich Ti metal center, neither **4.1** nor **4.2** can easily

accommodate a 6th ligand: THF, Et_2O, pyridine, and PMe_3 do not coordinate in these complexes, whereas the larger congener (ONO)$ZrBn_2$ easily coordinates a 6th ligand. The comparatively electron-poor complex **4.6**, unlike **4.1** and **4.2**, is a 6-coordinate, C_S-symmetric complex in the solid state.

Scheme 4.2

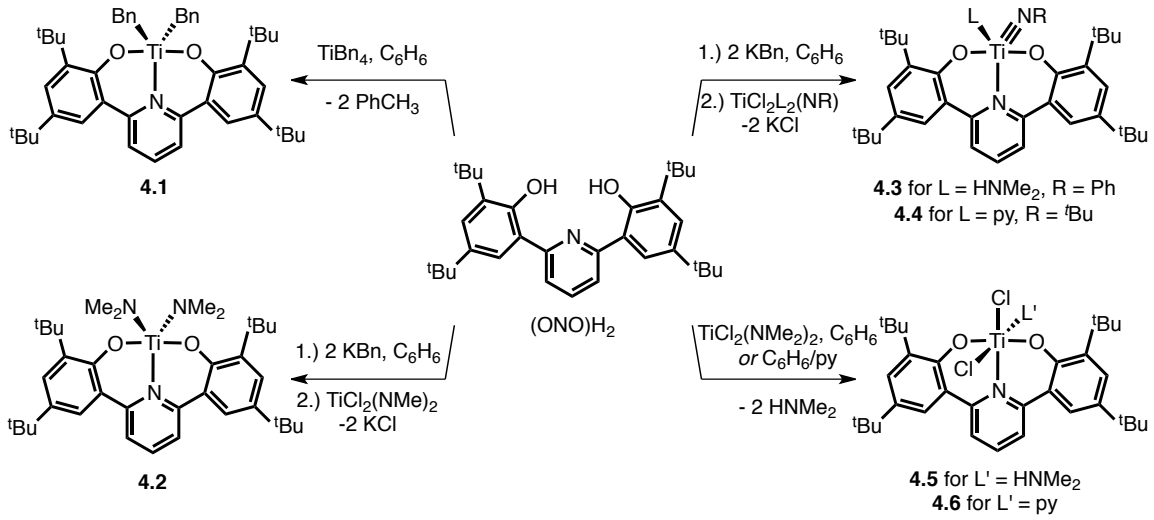

4.3 is not crystalline, but the related complex (ONO)Ti(py)(N*t*Bu) (**4.4**) can be crystallized from a 5:1 pentane:toluene solution at -30 °C. The C_S-symmetric ONO ligand in **4.4** occupies two equatorial sites as in **4.2**, and the linear imido functionality occupies the third equatorial site of the distorted trigonal bipyramid. In a [2+2] hydroamination mechanism, Ti imido species are key intermediates along the catalytic cycle. As a result, **4.4** could provide a structural analog to a catalytically relevant [(ONO)TiNR] intermediate. In this case, an incoming alkyne would likely occupy the same coordination site as pyridine in **4.4**.

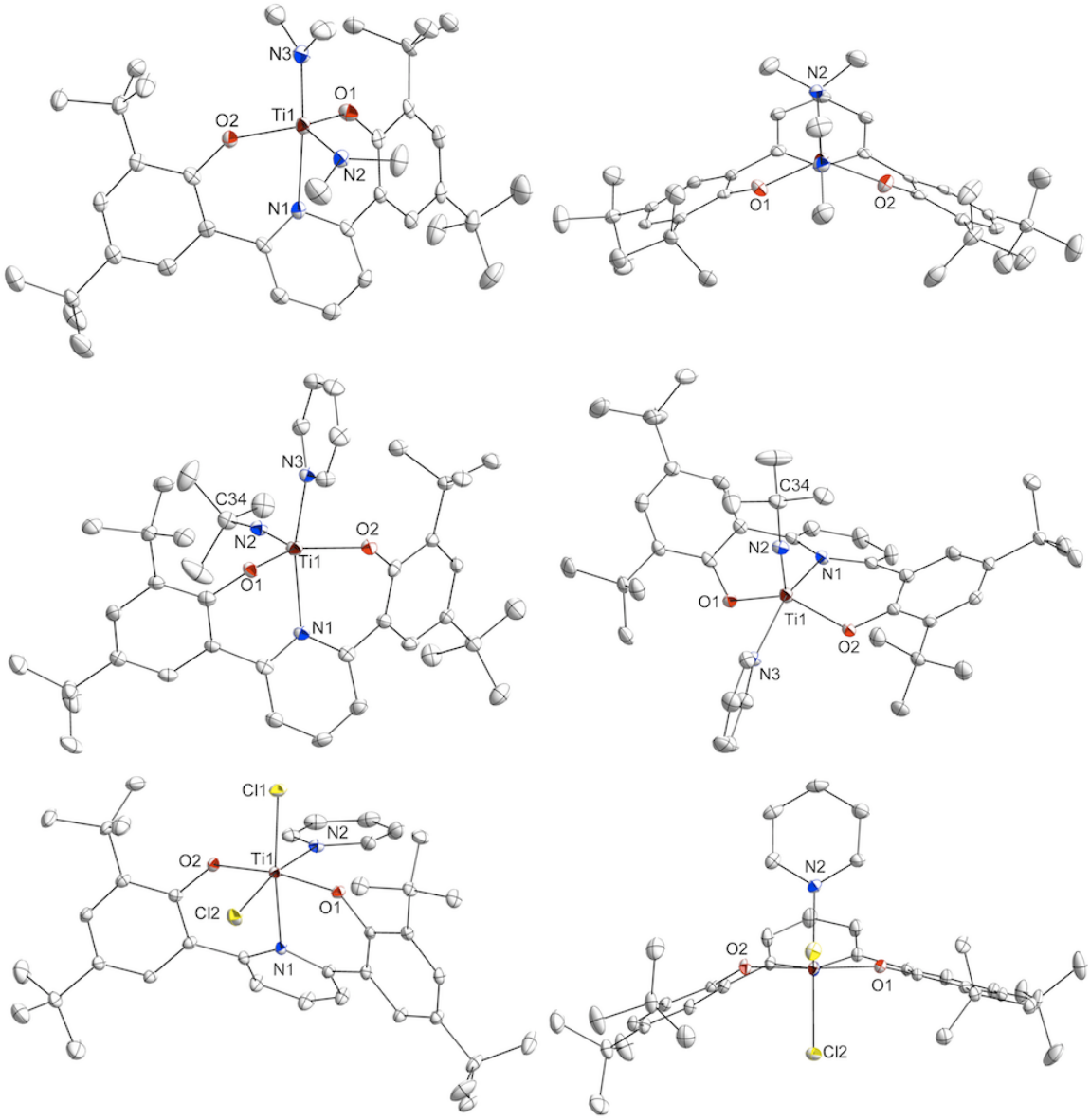

Figure 4.1. 50% Thermal ellipsoid drawings of **4.2** (top), **4.4** (middle), and **4.6** (bottom). Selected bond lengths (Å) and angles (°): Complex **4.2**: Ti1–N1 2.3982(3); Ti1–N2 1.9049(2); Ti1–N3 1.8707(2); Ti1–O1 1.8734(2); Ti1–O2 1.8756(2). Complex **4.4**: Ti1–N1 2.2192(1); Ti1–N2 1.6877(1); Ti1–N3 2.2116(1); Ti1–O1 1.9236(1); Ti1–O2 1.9320(1); Ti1–N2–C16 170.97. Complex **4.6**: Ti1–N1 2.2941(1); Ti1–N2 2.2542(1); Ti1–O1 1.8132(1); Ti1–O2 1.8487(1). Solvent molecules and H atoms removed for clarity.

Intermolecular Hydroamination with (ONO)TiBn$_2$

Table 4.1 summarizes the hydroamination of a variety of alkynes with primary amines catalyzed by **4.1**. Mixing **4.1** with amine and alkyne at room temperature results in no reaction. Upon heating the reaction mixtures to 90 °C, all of the precatalyst is consumed: ^{1}H NMR resonances corresponding to the precatalyst disappear, and 2 equivalents of toluene (per equivalent of Ti) are observed.

For reactions with 2-butyne or 1-phenyl-1-propyne, 20 turnovers (based on amine) are achieved in less than 1 hour, while reactions with the electron-poor diphenylacetylene are substantially slower. Mixtures of the E and Z imine isomers were obtained, with the enamine/imine tautomerization and resultant E:Z ratio being dictated after hydroamination catalysis. In the case of the hydroaminations of the unsymmetrically substituted 1-phenyl-1-propyne, the 1-phenylpropylidene isomer was exclusively obtained. Electron-rich, sterically unencumbered arylamines are particularly good substrates, and even some relatively bulky arylamines (such as *ortho*-toluidine) undergo reaction. Substrates with excessive steric bulk in the *ortho* position or with strong electron withdrawing groups are unreactive. Bulky alkylamines such as ^{i}PrNH$_2$ react, albeit extremely slowly when compared to the arylamines.

Table 4.1. Catalytic hydroamination of alkynes with (ONO)TiBn$_2$ (**4.1**).

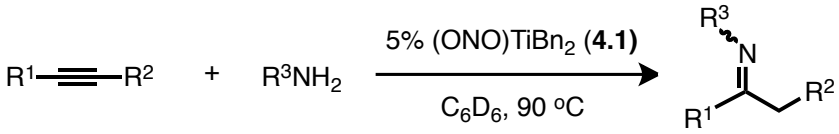

Entry	R^1	R^2	R^3	Time (h)	% Yield (E:Z)
1	Me	Me	Ph	1	100 (5:1)
2			*o*-CH_3Ph	1	100 (5.6:1)
3			*p*-CH_3Ph	1	100 (5:1)
4			2,6-Me_2Ph	1	0
5			*p*-MeOPh	1	100 (5.2:1)
6			*p*-CF_3Ph	1	0
7			3,5-^{t}Bu$_2$Ph	1	100 (4.9:1)
8			2,4-^{t}Bu$_2$Ph	1	0
9			CH_2Ph	1	0
10			^{i}Pr	140	95 (5:1)
11	Me	Ph	Ph	1	100 (3:1)
12			*o*-CH_3Ph	1	100 (3.6:1)
13			*p*-CH_3Ph	1	100 (3:1)
14			*p*-MeOPh	1	100 (3.6:1)
15			3,5-^{t}Bu$_2$Ph	1	100 (2.3:1)
16			CH_2Ph	1	0
17[a]	Ph	Ph	Ph	8	66 (1:0)
18[a]			*o*-CH_3Ph	8	83 (1:0)
19[a]			*p*-CH_3Ph	8	77 (1:0)
20[a]			*p*-MeOPh	8	76 (1:0)
21[a]			3,5-^{t}Bu$_2$Ph	1	100 (1:0)

Conditions: 0.5 mmol alkyne, 0.5 mmol amine, 0.025 mmol **4.1**, 0.75 mL C_6D_6, 0.25 mmol $SiMe_4$. Yield and E/Z ratio determined by ^{1}H NMR. [a]1 mL C_6D_6 was used instead.

Sterically demanding amines such as 2,6-Me_2-aniline are usually amongst the better substrates[6] for many Ti-based catalysts (such as Cp_2TiMe_2) because the increased steric bulk prevents catalyst deactivation through imido dimerization. For **4.1** though, the

bulky, tridentate ONO ligand likely precludes reaction with such bulkier substrates, although this may also inhibit some catalyst dimerization.[7] Substrates with no *ortho* or *meta* aryl substitution (entries 1–3, 5 for example) precipitate out an unknown Ti species (presumably an imido dimer) near the end of the reaction as the substrate concentrations decrease. These reactions do not proceed through a heterogeneous process upon precipitation, as filtering the reaction mixture still results in a catalytically competent solution. However, for reactions with bulkier amines (entries 2 and 7) the reaction solutions remain homogeneous throughout and presumably 100% of the Ti species is participating in catalysis.

In the case of reactions with diphenylacetylene, the reaction with 3,5-^{t}Bu$_2$-aniline (entry 21) was substantially faster and contained significantly less precipitate than less bulky arylamines (entries 17–20). In this case, the steric protection provided by the arylimido intermediate is important for effective catalysis. Since diphenylacetylene reacts significantly slower with a transient imido species compared to dimethyl- or methylphenylacetylene (*vide supra*), the arylimido species likely persists longer in solution and has a higher probability of deactivating through dimerization. As a result, reactions with sterically unencumbered amines, while efficient with electron-rich alkynes, suffer from significant catalyst deactivation and lower effective turnover numbers when paired with diphenylacetylene.

Comparison of Additional Precatalysts

Complexes **4.2** and **4.3** were also tested as catalysts for the hydroamination of diphenylacetylene and 3,5-^{t}Bu$_2$-aniline. Under the optimized reaction conditions in Table 4.1, most of the reactions are complete in under 1 hour. As a result, we carried out the hydroamination of 3,5-^{t}Bu$_2$-aniline and diphenylacetylene at 75 °C with a 10% catalyst loading of **4.1**, **4.2**, or **4.3** under more dilute conditions in order to monitor the rate of the reaction *via* ^{1}H NMR.

For the reaction catalyzed by **4.2**, 2 equivalents of HNMe$_2$ were generated per equivalent of Ti, indicating complete consumption of precatalyst **4.2** under the reaction conditions. For the reaction catalyzed by **4.3** a substoichiometric amount of the aniline-hydroaminated product, *N*-(1,2-diphenylethylidene)-aniline, was generated.

Figure 4.2 shows the time course of the hydroaminations catalyzed by **4.1**-**4.3**. Assuming reactions catalyzed by **4.1**-**4.3** proceed through the same mechanism, the active species (and as a result, reaction velocity) should be the same in for all three. While **4.1** and **4.2** do proceed at roughly the same rate, **4.3** catalyzes the reaction at roughly 50% of the rate of **4.1**. Since **4.2** proceeds at the same rate as **4.1** and also produces HNMe$_2$ over the course of the reaction, we do not believe that HNMe$_2$ inhibition is the cause for lower reaction rates with **4.3**. Instead, inefficient catalyst activation could affect the overall rate: in order to enter the catalytic cycle, **4.3** must lose HNMe$_2$ to form a sterically unencumbered, 4-coordinate phenylimido species that, as evidenced in earlier reactions, could easily dimerize and deactivate. Supporting this hypothesis, **4.3** generates

a substoichiometric amount of *N*-(1,2-diphenylethylidene)-aniline, indicating that some of the precatalyst never undergoes a [2+2] reaction with alkyne.

Although its activity is lower, the competency of **4.3** for hydroamination and the observation of the aniline-hydroaminated product, *N*-(1,2-diphenylethylidene)-aniline, is further evidence that these [(ONO)Ti]-catalyzed reactions proceed through a typical imido+alkyne [2+2] addition mechanism.

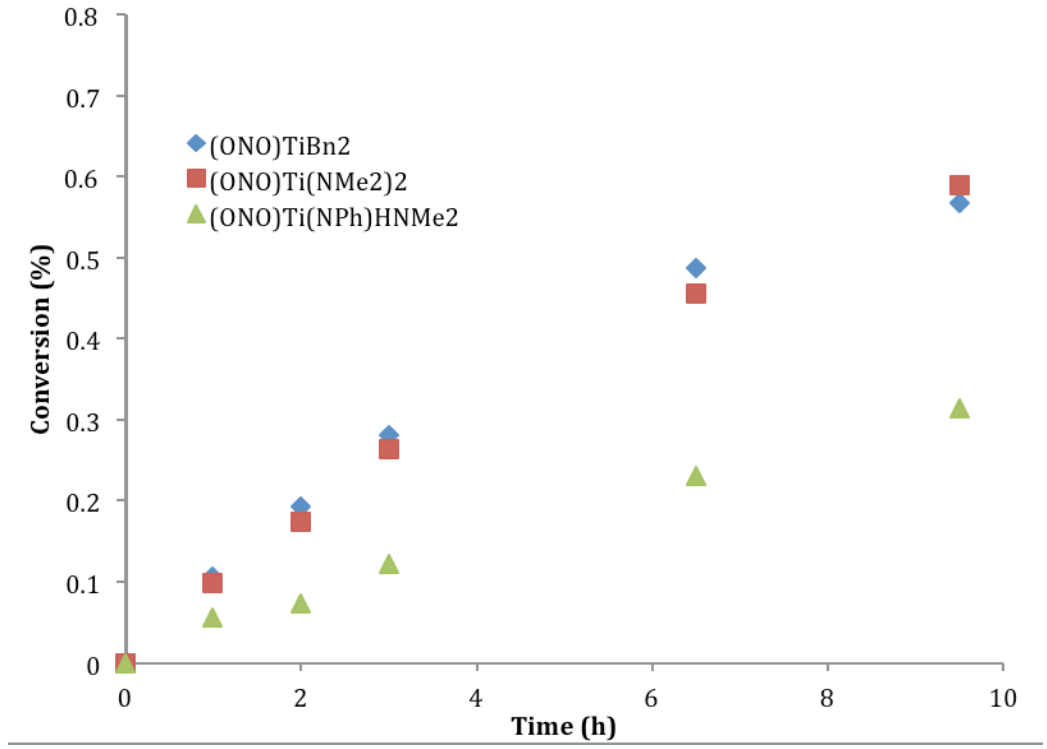

Figure 4.2. Reaction time course of diphenylactylene hydroamination with 3,5-^{t}Bu$_2$-aniline catalyzed by **4.1**, **4.2**, and **4.3** at 75 °C.

(ONO)Ti^{III}-Catalyzed Alkyne Cyclotrimerization

When (ONO)TiBn$_2$ (**4.1**) was reacted under catalytic conditions for 14 hours with 10 equivalents of 3,5-^{t}Bu$_2$-aniline and 30 equivalents of dimethylacetylene, two new

peaks corresponding to the M^+ for hexamethylbenzene and N-(3,5-di-*tert*-butylphenyl)-2,3,4,5-tetramethylpyrrole were observed by GC-MS in addition to the hydroaminated product (Scheme 4.3, Figure 4.3). The N-aryltetramethylpyrrole is likely generated by a second equivalent of dimethylacetylene inserting into an azatitanocyclobutene intermediate, which can then reductively eliminate the pyrrole and generate a Ti^{II} species. Ti^{II} complexes are well-known catalysts[8] for alkyne cyclotrimerization, and it is likely that the resultant Ti^{II} species generated from the pyrrole reductive elimination also carries out the cyclotrimerization.

Scheme 4.3

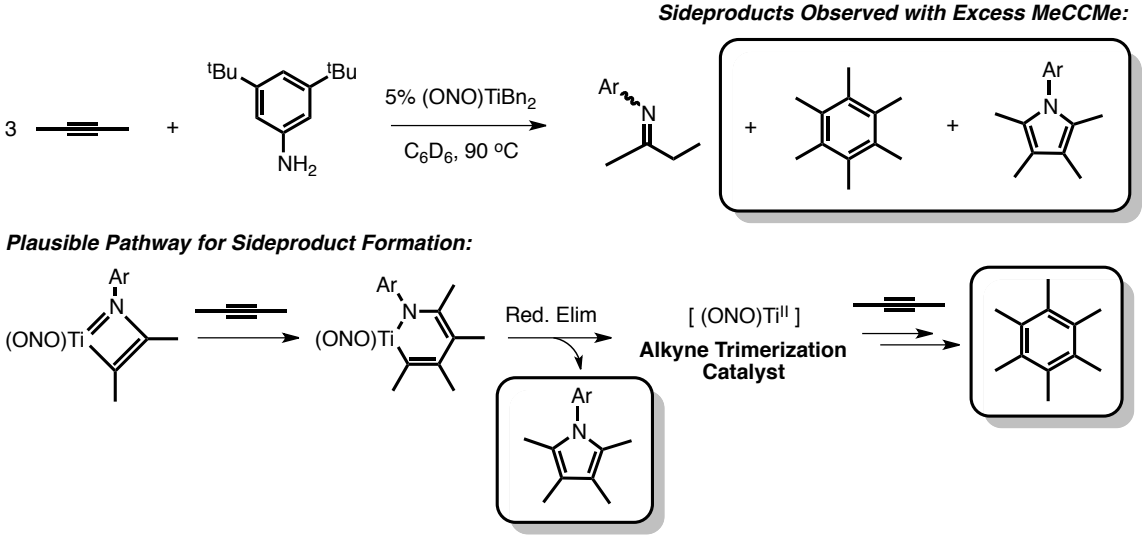

Perhaps more surprisingly, **4.1** is also a precatalyst for alkyne cyclotrimerization in the *absence* of any primary amines. When 20 equivalents of dimethylacetylene is reacted with **4.1** at 90 °C for 1 hour, 88% of the dimethylacetylene converted into hexamethylbenzene (eq 4.1). Unlike the hydroamination experiments, the precatalyst **4.1**

was *not* entirely consumed over the course of the reaction. Instead, roughly 50% of the precatalyst remained after the reaction was completed.

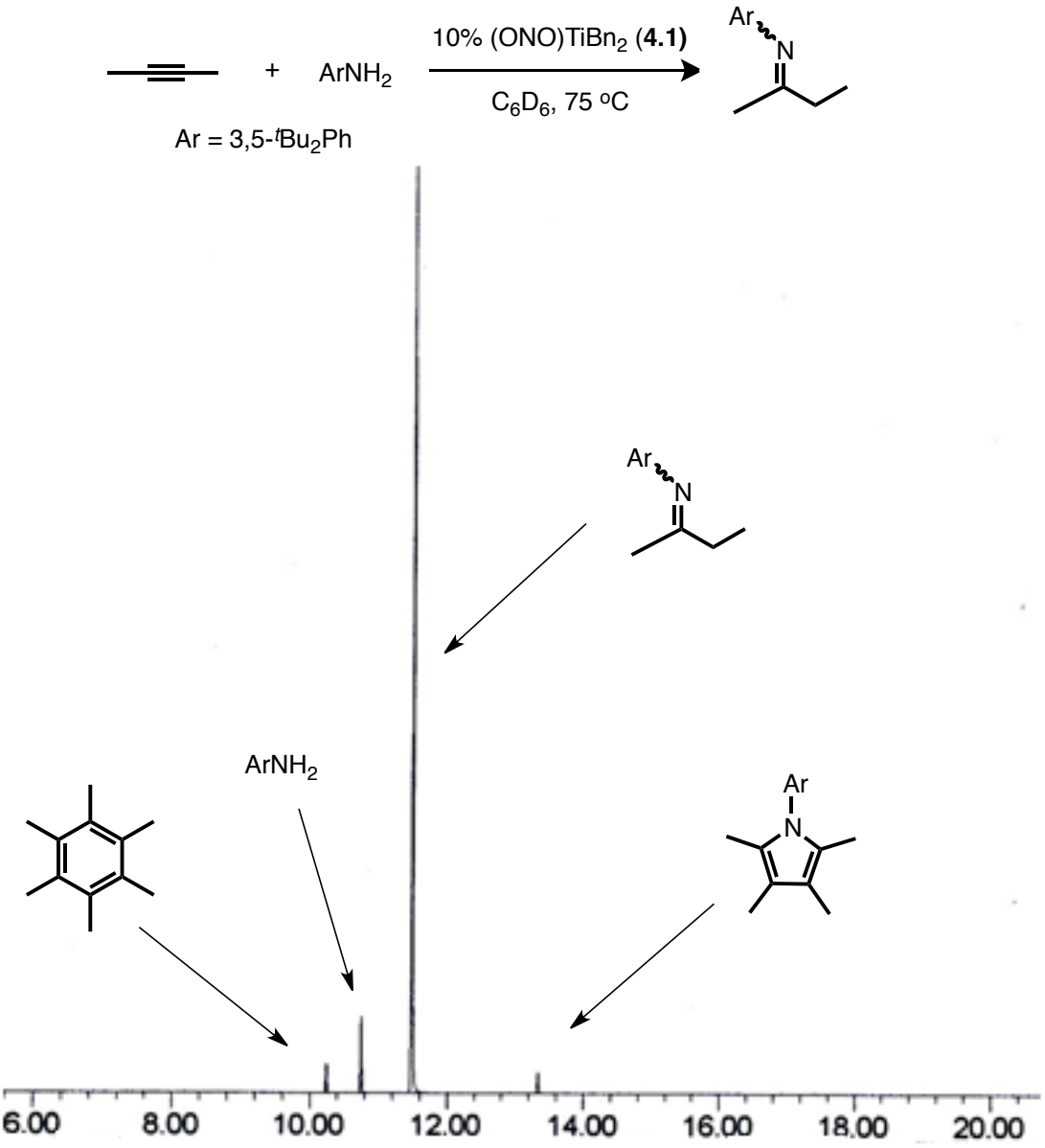

Figure 4.3. GC-MS of the product mixture of the reaction of 2-butyne with 3,5-^{t}Bu$_2$-aniline catalyzed by **4.1**, showing sideproducts resulting from Ti^{II} species.

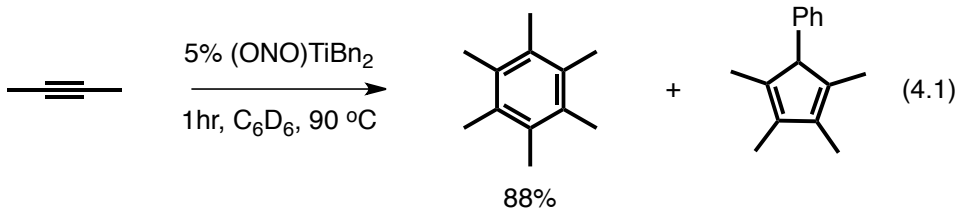

The GC-MS of the alkyne trimerization reaction mixture shows the presence of hexamethylbenzene and also phenyltetramethylcyclopentadiene. This cyclopentadiene product is a result of precatalyst activation. Similar to the mechanism for pyrrole sideproduct formation, the phenyltetramethylcyclopentadiene likely results from double insertion of dimethylacetylene into a titanium benzylidene intermediate (Scheme 4.4). This (ONO)Ti benzylidene complex likely forms from α-H abstraction[9] from (ONO)TiBn$_2$. Since (ONO)TiBn$_2$ is stable at 90 °C over the reaction timescale, this α-H abstraction could be promoted first by alkyne coordination. After benzylidene formation the complex can undergo a [2+2] cycloaddition with dimethylacetylene, leading to a titanacyclobutene. This titanacyclobutene then inserts another equivalent of dimethylacetylene and reductively eliminates the tetramethylcyclopentadiene, generating an (ONO)Ti^{II} species capable of alkyne trimerization.

Scheme 4.4

Mechanism for Ti^{II} formation

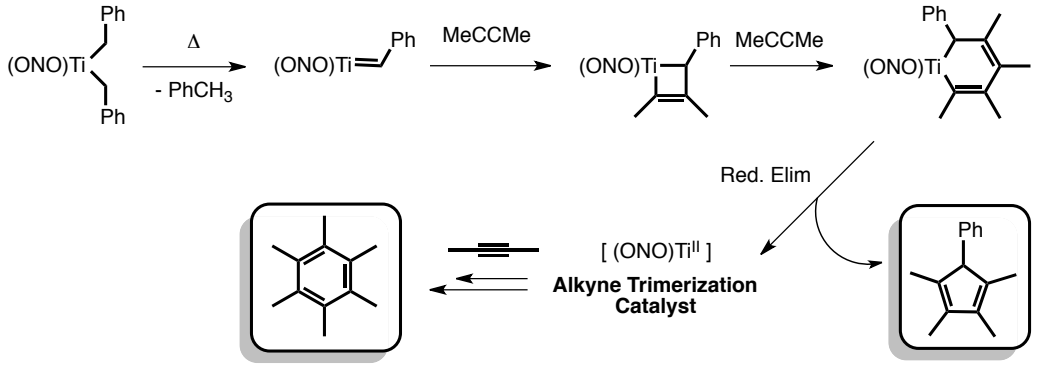

(ONO)Ti^{II} ethylene adduct

Since the (ONO)Ti^{II} species in the alkyne trimerization catalysis is apparently somewhat persistent, we sought to trap an (ONO)Ti^{II} complex with a π-acceptor ligand. When (ONO)Ti($HNMe_2$)Cl_2 (**4.5**) was treated with 1% Na/Hg under an atmosphere of ethylene, Ti^{II}-ethylene adduct (ONO)Ti($HNMe_2$)(C_2H_4) (**4.7**) is generated in moderate yield. X-ray quality crystals of **4.7** were grown from a concentrated pentane solution cooled to -30 °C (Figure 4.4). **4.7** is a rare example[10] of a crystallographically characterized Ti-ethylene adduct. Based on the C29-C30 bond length of 1.4216(1) Å, **4.7** is best described as a Ti^{IV} titanocyclopropane.

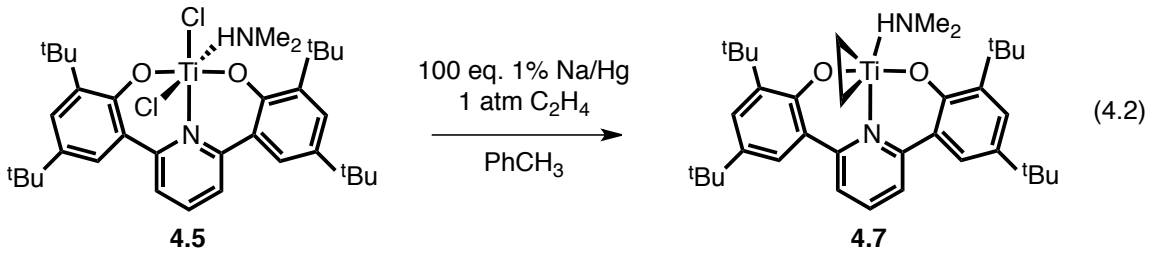

(4.2)

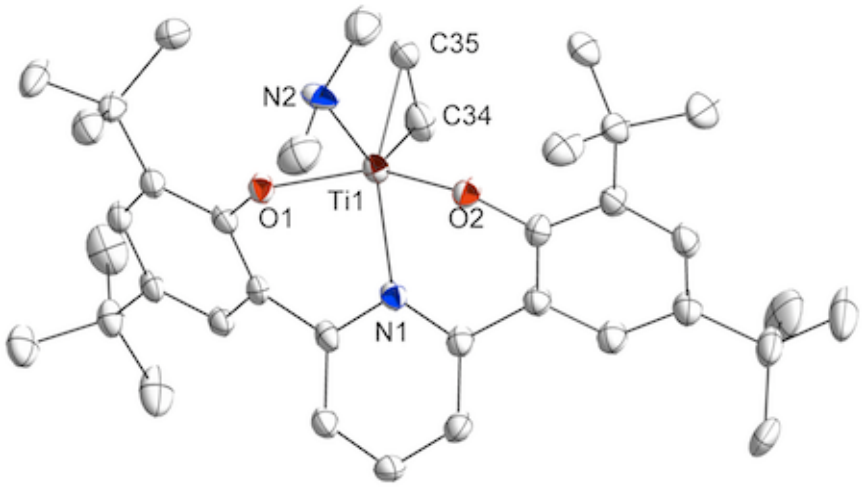

Figure 4.4. 50% Thermal ellipsoid drawing of **4.7**. Selected bond lengths (Å): Ti–N1 2.2314(2); Ti–N2 2.2766(2); Ti–O1 1.8994(2); Ti–O2 1.8929(2); Ti–C34 2.1080(2); Ti–C35 2.1414(3); C34–C35 1.4216(1). H atoms removed, solvent removed, and ligand ^{t}Bu groups trimmed for clarity.

The bound $HNMe_2$ unit remains intact upon reduction from **4.5** to **4.7**. Considering the relative acidity of metal-bound secondary amines, it is of note that the bound $HNMe_2$ does not protonate either the transient $(ONO)Ti^{II}(HNMe_2)$ intermediate to generate $(ONO)TiH(NMe_2)$ or the metallocyclopropane to generate the ethyl-amide complex $(ONO)Ti(NMe_2)(C_2H_5)$. This unusual stability could be a result of the ONO aryl framework stabilizing the Ti^{II} fragment or some other kinetic barrier to reaction.

CONCLUSIONS

Bis(phenolate) titanium complexes have been shown to be highly active catalysts for the intermolecular hydroamination of internal alkynes by arylamines. Unlike many other catalytic systems, sterically unencumbered arylamines are particularly good substrates, while bulky *ortho*-substituted amines are unreactive. Under conditions of excess alkyne, Ti^{II} species are generated *via* the reductive elimination of pyrroles, which can cyclotrimerize dimethylacetylene. Active (ONO)Ti^{II} species can also be generated in the absence of amine through a benzylidene intermediate, allowing for cyclotrimerization without an added reductant. Finally, an (ONO)Ti^{II} complex has been trapped by ethylene, giving a rare example of a crystallographically-characterized Ti-ethylene adduct.

EXPERIMENTAL SECTION

General Considerations and Instrumentation. All air- and moisture-sensitive compounds were manipulated using standard high vacuum and Schlenk techniques or manipulated in a glovebox under a nitrogen atmosphere. Solvents for air- and moisture-sensitive reactions were dried over sodium benzophenone ketyl and stored over titanocene where compatible or dried by the method of Grubbs.[11] Liquid amines and alkynes were degassed and passed through a column of activated alumina or distilled from CaH_2 prior to use. $TiBn_4$,[12] $TiCl_2(NMe_2)_2$,[13] $TiCl_2(HNMe_2)_2(NPh)$,[14] $TiCl_2(py)_2(N^tBu)$,[14] $(ONO)H_2$,[3c] and $(ONO)TiBn_2$[3c] were prepared following literature procedure. Benzene-d_6 was purchased from Cambridge Isotopes and sequentially dried over sodium benzophenone ketyl and titanocene. ^1H and ^{13}C spectra were recorded on Varian Mercury 300 or Varian INOVA 500 spectrometers and chemical shifts are reported with respect to residual protio-solvent impurity for ^1H (s, 7.16 ppm for C_6D_5H; t, 5.32 ppm for $CDHCl_2$) and solvent carbons for ^{13}C (t, 128.39 for C_6H_6; p, 53.84 for CD_2Cl_2). Reproducible elemental analyses were not obtained because of persistent solvents of crystallization.

X-ray Crystal Data: General Procedure. Crystals were removed quickly from a scintillation vial to a microscope slide coated with Paratone N oil. Samples were selected and mounted on a glass fiber with Paratone N oil. Data collection was carried out on a Bruker KAPPA APEX II diffractometer with a 0.71073 Å MoKα source. The structures were solved by direct methods. All non-hydrogen atoms were refined anisotropically. Details regarding refined data and cell parameters are available in Table 4.2 and 4.3.

Synthesis of (ONO)Ti(NMe$_2$)$_2$ (4.2). (ONO)H$_2$ (274 mg, 0.564 mmol, 1 equiv) and KBn (147 mg, 1.127 mmol, 2 equiv) were mixed in 10 mL C_6H_6. The mixture was stirred for 1 hour to generate a yellow solution of (ONO)K$_2$, and then a 5 mL C_6H_6 solution of TiCl$_2$(NMe$_2$)$_2$ (117 mg, .564 mmol, 1 equiv) was added dropwise. The reaction was stirred overnight, filtered to remove KCl, and C_6H_6 was then lyophilized off. The resultant orange powder was washed with a small amount of cold pentane to remove any remaining free ligand. Yielded 326 mg (91%) of **4.2** as a light orange powder. X-ray quality crystals of **4.2** were grown from a saturated solution of **4.2** in 50:50 pentane:ether cooled to -30 °C. ^{1}H NMR (300 MHz, C_6D_6) δ, ppm: 1.41 (*s*, 18 H, C(C*H*$_3$)$_3$); 1.76 (*s*, 18 H, C(C*H*$_3$)$_3$); 3.03 (*s*, 12 H, N(C*H*$_3$)$_2$); 7.07 (*t*, *J* = 7.9 Hz, 1 H, 4-NC$_5$H$_2$-*H*); 7.26 (*d*, *J* = 7.8 Hz, 2 H, 3,5-NC$_5$H-*H*$_2$); 7.50 (*d*, *J* = 2.5 Hz, 2 H, aryl-*H*); 7.76 (*d*, *J* = 2.5 Hz, 2 H, aryl-*H*). ^{1}H NMR (500 MHz, CD_2Cl_2) δ, ppm: 1.37 (*s*, 18 H, C(C*H*$_3$)$_3$); 1.51 (*s*, 18 H, C(C*H*$_3$)$_3$); 2.94 (*s*, 12 H, N(C*H*$_3$)$_2$); 7.43 (*d*, *J* = 2.4 Hz, 2 H, aryl-*H*); 7.48 (*d*, *J* = 2.4 Hz, 2 H, aryl-*H*); 7.57 (*d*, ^{3}*J* = 7.9 Hz, 2 H, 3,5-NC$_5$H-*H*$_2$); 7.86 (*t*, *J* = 8.1 Hz, 1 H, 4-NC$_5$H$_2$-*H*). ^{13}C NMR (125 MHz, CD_2Cl_2) δ, ppm: 30.0, 32.0, 34.9, 35.8, 44.9 (alkyl); 122.8, 124.7, 126.4, 126.5, 138.5, 138.7, 141.5, 157.2, 157.7 (aryl).

Synthesis of (ONO)Ti(HNMe$_2$)(NPh) (4.3). (ONO)H$_2$ (243 mg, 0.5 mmol, 1 equiv) and KBn (130 mg, 1.0 mmol, 2 equiv) were mixed in 10 mL C_6H_6. The mixture was stirred for 1 hour to generate a yellow solution of (ONO)K$_2$, and then a 5 mL C_6H_6 solution of (HNMe$_2$)$_2$TiCl$_2$(NPh) (150 mg, 0.5 mmol, 1 equiv) was added dropwise. The reaction was stirred overnight and then filtered to remove KCl. C_6H_6 was then lyophilized off, and the resultant orange solid washed with 5 mL pentane to remove any remaining free ligand.

Yielded 301 mg (90%) of **4.3** as a yellow powder. ^{1}H NMR (300 MHz, C_6D_6) δ, ppm: 1.44 (*s*, 18 H, C(C*H*$_3$)$_3$); 1.82 (*s*, 18 H, C(C*H*$_3$)$_3$); 2.54 (*d*, *J* = 6.3 Hz, 6 H, NH(C*H*$_3$)$_2$); 3.69–3.86 (*br m*, 1 H, N*H*(CH$_3$)$_2$); 6.25 (*d*, *J* = 7.9 Hz, 2 H, 2,6-C$_6$H$_3$-*H*$_2$); 6.45 (*d*, *J* = 7.6 Hz, 1 H, 2,6-C$_6$H$_4$-*H*); 6.73 (*t*, *J* = 7.7 Hz, 2 H, 3,5-C$_6$H$_3$-*H*$_2$); 7.05 (*t*, *J* = 8.0 Hz, 1 H, 4-NC$_5$H$_2$-*H*); 7.32 (*d*, *J* = 8.0 Hz, 2 H, 4-NC$_5$H-*H*$_2$); 7.44 (*d*, *J* = 2.4 Hz, 2 H, aryl-*H*); 7.82 (*d*, *J* = 2.4 Hz, 2 H, aryl-*H*). ^{1}H NMR (300 MHz, CD_2Cl_2) δ, ppm: 1.39 (*s*, 18 H, C(C*H*$_3$)$_3$); 1.65 (*s*, 18 H, C(C*H*$_3$)$_3$); 2.94 (*d*, *J* = 6.4 Hz, 6 H, NH(C*H*$_3$)$_2$); 3.79–3.94 (*br m*, 1 H, N*H*(CH$_3$)$_2$); 5.82 (*d*, *J* = 8.1 Hz, 2 H, 2,6-C$_6$H$_3$-*H*$_2$); 6.41 (*t*, *J* = 8.1 Hz, 1 H, 4-C$_6$H$_4$-*H*); 6.61 (*t*, *J* = 8.3 Hz, 2 H, 3,5-C$_6$H$_3$-*H*$_2$); 7.41 (*d*, *J* = 2.3 Hz, 2 H, aryl-*H*); 7.55 (*d*, *J* = 2.3 Hz, 2 H, aryl-*H*); 7.70 (*d*, *J* = 8.3 Hz, 2 H, 3,5-NC$_5$H-*H*$_2$); 7.98 (*t*, *J* = 8.3 Hz, 1 H, 4-NC$_5$H$_2$-*H*). ^{13}C NMR (125 MHz, CD_2Cl_2) δ, ppm: 30.4, 32.0, 34.8, 35.9, 40.6 (alkyl); 119.8, 123.1, 124.0, 126.1, 126.8, 127.2, 127.9, 137.0, 139.6, 140.9, 158.8, 159.5, 169.7 (aryl).

Synthesis of (ONO)Ti(py)(N^{t}Bu) (4.4). (ONO)H$_2$ (154 mg, 0.316 mmol, 1 equiv) and KBn (82.5 mg, 0..634 mmol, 2 equiv) were mixed in 10 mL C_6H_6. The mixture was stirred for 1 hour to generate a yellow solution of (ONO)K$_2$, and then a 5 mL C_6H_6 solution of (py)$_2$TiCl$_2$(N^{t}Bu) (110.3 mg, .316 mmol, 1 equiv) was added dropwise. The reaction was stirred overnight and then filtered to remove KCl. C_6H_6 was then lyophilized off, and the resultant yellow solid washed with 5 mL pentane to remove any remaining free ligand. Yielded 195 mg (90%) of **4.4** as a yellow powder. X-ray quality crystals were grown from a saturated pentane solution of **4.4** cooled to -30 ℃.

Synthesis of (ONO)TiCl$_2$(HNMe$_2$) (4.5). (ONO)H$_2$ (194.5 mg, 0.400 mmol, 1 equiv) and TiCl$_2$(NMe$_2$)$_2$ (83 mg, 0.400 mmol, 1 equiv) were mixed in 6 mL C_6H_6. A dark

orange solid immediately precipitated. This dark orange/brown solid was isolated and washed with 5 mL of pentane, yielding a mixture of **4.5** and the base-free (ONO)$TiCl_2$ that was carried on for subsequent reductions.

Synthesis of (ONO)Ti(py)Cl_2 (4.6). (ONO)H_2 (194.5 mg, 0.400 mmol, 1 equiv) and $TiCl_2(NMe_2)_2$ (83 mg, 0.400 mmol, 1 equiv) were mixed in 6 mL C_6H_6. A dark orange solid immediately precipitated. After 15 minutes, 1 mL pyridine was added, which dissolved the precipitate to give a dark red solution. The solution was stirred for 1 hour, then filtered and the benzene was lyophilized off. The orange/red powder was isolated and washed with 10 mL pentane, yielding **5** as an orange/red solid (232 mg, 85%). X-ray quality crystals were grown from slow evaporation of a concentrated solution of **4.6** in benzene. ^{1}H NMR (300 MHz, C_6D_6) δ, ppm: 1.32 (*s*, 18 H, C(CH_3)$_3$); 2.01 (*s*, 18 H, C(CH_3)$_3$); 6.09 (*br s* C_5H_5N); 6.86 (*t*, *J* = 7.9 Hz, 1 H, *p*-NC_5H_2-*H*); 7.02 (*br s* C_5H_5N); 7.30 (*d*, *J* = 7.9 Hz, 2 H, 4-NC_5H-H_2); 7.32 (*d*, *J* = 2.3 Hz, 2 H, aryl-*H*); 7.79 (*d*, *J* = 2.3 Hz, 2 H, aryl-*H*). 8.42 (*br s*, C_5H_5N).

Synthesis of (ONO)Ti($HNMe_2$)(C_2H_4) (4.7). In an inert atmosphere glovebox, 15.8 mg **4.5** (0.024 mmol, 1 equiv) was dissolved in 3 mL toluene and placed in a 50 mL flask fitted with a Kontes valve. 200 equiv of 1% Na/Hg was added to the flask, and the flask was then evacuated on a high vacuum line. 1 atm of ethylene was introduced into the flask, and the reaction was stirred overnight under a constant 1 atm of ethylene. Over the course of the reaction, the color changed from red to green and finally to a green/brown color. The reaction mixture was decanted away from the mercury, filtered to

remove NaCl, and solvent removed *in vacuo.* The product was extracted into 1 mL of pentane and red X-ray quality crystals were obtained after cooling the solution to -30 °C.

Typical Hydroamination Setup. 250 μL of a 2 M C_6D_6 solution of alkyne was added to a J-Young NMR tube, followed by 250 μL of a 2 M C_6D_6 solution of amine, and finally 250 μL of a 1 M C_6D_6 solution of catalyst. The solution was spiked with $SiMe_4$ as an internal standard. The tube was sealed and inverted to mix the three solutions, and an ^1H NMR spectrum was taken. The reaction was then heated to 90 °C in an oil bath for the desired amount of time. After the reaction was complete, the products were analyzed by ^1H NMR, and then the reaction mixture was passed through a plug of silica gel before GC-MS analysis.

Typical Cyclotrimerization Setup. 250 μL of a 2 M C_6D_6 solution of alkyne was added to a J-Young NMR tube, followed by 250 μL of C_6D_6, and finally 250 μL of a 1 M C_6D_6 solution of catalyst. The solution was spiked with $SiMe_4$ as an internal standard. The tube was sealed and inverted to mix the three solutions, and an ^1H NMR spectrum was taken. The reaction was then heated to 90 °C in an oil bath for the desired amount of time. After the reaction was complete, the products were analyzed by ^1H NMR, and then the reaction mixture was passed through a plug of silica gel before GC-MS analysis.

Table 4.2. Crystal and refinement data for complexes **4.2**, and **4.4**.

	4.2	**4.4**
CCDC Number	754732	847140
Empirical formula	$C_{37}H_{55}N_3O_2Ti \cdot C_5H_{12}$	$C_{42}H_{57}N_3O_2Ti \cdot 0.49(C_5H_{12}) \cdot 0.51(C_7H_8)$
Formula weight	693.89	765.95
T (K)	100(2)	100(2)
a, Å	13.9103(6)	14.6930(8)
b, Å	10.2228(4)	14.9636(8)
c, Å	28.5988(12)	20.1744(12)
a, deg		
b, deg	90.995(3)	92.699(3)
g, deg		
Volume, Å^3	4066.2(3)	4430.6(4)
Z	4	4
Crystal system	Monoclinic	Monoclinic
Space group	P $2_1/n$	P $2_1/c$
d_{calc}, g/cm^3	1.133	1.148
q range, deg	1.62 to 29.10	1.70 to 30.51
μ, mm^{-1}	0.247	0.233
Abs. Correction	None	None
GOF	1.764	1.945
R_1 ,[a]	R1 = 0.0650,	R1 = 0.0584,
wR_2 [b] [I>2s(I)]	*w*R2 = 0.0942	*w*R2 = 0.0723

[a] $R_1 = \Sigma||F_o| - |F_c||/\Sigma|F_o|$. [b] $wR_2 = [\Sigma[w(F_o^2-F_c^2)^2]/\Sigma[w(F_o^2)^2]]^{1/2}$.

Table 4.3. Crystal and refinement data for complexes **4.6**, and **4.7**.

	4.6	**4.7**
CCDC Number	856446	822994
Empirical formula	$2(C_{38}H_{48}N_2O_2Cl_2Ti) \cdot 5(C_6H_6)$	$C_{37}H_{53}N_2O_2Ti \cdot 0.5(C_5H_{12})$
Formula weight	878.85	641.79
T (K)	100(2)	100(2)
a, Å	11.8721(6)	17.7536(5)
b, Å	28.5845(14)	10.5239(3)
c, Å	29.6698(15)	20.7880(6)
a, deg		
b, deg	100.018(3)	104.343(2)
g, deg		
Volume, Å^3	9915.2(9)	3762.91(19)
Z	8	4
Crystal system	Monoclinic	Monoclinic
Space group	P $2_1/c$	P $2_1/n$
d_{calc}, g/cm^3	1.177	1.133
q range, deg	1.59 to 35.13	2.02 to 29.99
μ, mm^{-1}	0.320	0.261
Abs. Correction	None	None
GOF	1.877	2.095
R_1 ,[a]	R1 = 0.0415,	R1 = 0.0612,
wR_2 [b] [I>2s(I)]	*w*R2 = 0.0625	*w*R2 = 0.0614

[a] $R_1 = \Sigma||F_o| - |F_c||/\Sigma|F_o|$. [b] $wR_2 = [\Sigma[w(F_o^2-F_c^2)^2]/\Sigma[w(F_o^2)^2]^{1/2}$.

REFERENCES

1. For a comprehensive review, see (a) Muller, T. E.; Hultzsch, K. C.; Yus, M.; Foubelo, F.; and Tada, M. *Chem. Rev.* **2008**, *108*, 3795. (b) Pohlki, F.; Doye, S. *Chem. Soc. Rev.* **2003**, *32*, 104. (c) Muller, T. E.; Beller, M. *Chem. Rev.* **1998**, *98*, 675. Lanthanides: (d) Hong, S.; Marks, T. J. *Acc. Chem. Res.* **2004**, *37*, 673. Calcium: (e) Crimmin, M. R.; Casely, I. J.; Hill, M. S. *J. Am. Chem. Soc.* **2005**, *127*, 2042.
2. (a) Ward, B. D.; Maisse-Francois, A.; Gade, L. H.; Mountford, P. *Chem. Commun.* **2004**, 704. (b) Sweeney, Z. K.; Salsman, J. L.; Andersen, R. A.; Bergman, R. G. *Angew. Chem. Int. Ed.* **2000**, *39*, 2339. (c) Michael, F. E.; Duncan, A. P.; Sweeney, Z. K.; Bergman, R. G. *J. Am. Chem. Soc*. **2003**, *125*, 7184. (d) Michael, F. E.; Duncan, A. P.; Sweeney, Z. K.; Bergman, R. G. *J. Am. Chem. Soc.* **2005**, *127*, 1752. (e) Walsh, P. J.; Baranger, A. M.; Bergman, R. G. *J. Am. Chem. Soc.* **1992**, *114*, 1708. (f) Baranger, A. M.; Walsh, P. J.; Bergman, R. G. *J. Am. Chem. Soc.* **1993**, *115*, 2753. (g) Pohlki, F.; Doye, S. *Angew. Chem. Int. Ed.* **2001**, *40*, 2305. (h) Johnson, J. S.; Bergman, R. G. *J. Am. Chem. Soc.* **2001**, *123*, 2923.
3. (a) Agapie, T.; Bercaw, J. E. *Organometallics* **2007**, *26*, 2957. (b) Agapie, T.; Day. M. W.; Bercaw, J. E. *Organometallics* **2008**, *27*, 6123. (c) Agapie, T.; Henling, L. M.; DiPasquale, A. G.; Rheingold, A. L.; Bercaw, J. E. *Organometallics* **2008**, *27*, 6245. (d) Tonks, I. A.; Henling, L. M.; Day, M. W.; Bercaw, J. E. *Inorg. Chem.* **2009**, *48*, 5096. (e) Golisz, S. R.; Bercaw, J. E. *Macromolecules* **2009**, *42*, 8751.
4. (a) Chan, M. C. W.; Tam, K. H.; Zhu, N. Y.; Chiu, P.; Matsui, S. *Organometallics* **2006**, *25*, 785. (b) Chan, M. C. W.; Tam, K. H.; Pui, Y. L.; Zhu, N. Y. *J. Chem. Soc. Dalton Trans.* **2002**, 3085. (c) Tam, K. H. Chan, M. C. W.; Kaneyoshi, H.; Makio, H.; Zhu, N. Y. *Organometallics* **2009**, *28*, 5877.
5. (A) Khedkar, V.; Tillack, A.; Beller, M. *Org. Lett*. **2003**, *5*, 4767. (b) Tillack, A.; Khedkar, V.; Jiao, H.; Beller, M. *Eur. J. Org. Chem.* **2005**, 5001.
6. Haak, E.; Bytschkov, I.; Doye, S. *Angew. Chem. Int. Ed.* **1999**, *38*, 3389.
7. Heutling, A.; Doye, S. *J. Org. Chem.* **2002**, *67*, 1961.
8. (a) Ojima, I.; Tzamarioudaki, M.; Li, Z.; Donovan, R. J. *Chem. Rev.* **1996**, *96*, 635. (b) Schore, N. E. *Chem. Rev.* **1998**, *88*, 1081. (c) Ozerov, O. V.; Patrick, B. O.; Ladipo, F. T. *J. Am. Chem. Soc.* **2000**, *122*, 6423. And references therein.
9. Golisz, S. A.; Labinger, J. A.; Bercaw, J. E. *Organometallics* **2010**, *29*, 5026.

10. **4.7** is the 2nd crystallographically characterized Ti–C_2H_4 adduct. Cohen, S. A.; Auburn, P. A.; Bercaw, J. E. *J. Am. Chem. Soc.* **1983**, *105*, 1136.
11. Pangborn, A. B.; Giardello, M. A.; Grubbs, R. H.; Rosen, R. K.; Timmers, F. J. *Organometallics* **1996**, *15*, 1518.
12. Hamaed, A.; Trudeau, M.; Antonelli, D. M. *J. Am. Chem. Soc.* **2008**, *130*, 6992.
13. Benzing, E.; Kornicker, W. *Chem. Ber.* **1961**, *94*, 2263.
14. Adams, N.; Bigmore, H. R.; Blundell, T. L.; Boyd, C. L.; Dubberley, S. R.; Sealey, A. J.; Cowley, A. R.; Skinner, M. E. G.; Mountford, P. *Inorg. Chem.* **2005**, *44*, 2882.

CHAPTER 5

$(dme)MCl_3(NNPh_2)$ (dme = dimethoxyethane; M = Nb, Ta): A Versatile Synthon for $[Ta{=}NNPh_2]$ Hydrazido(2-) Complexes

Published in part as:
Tonks, I. A.; Bercaw, J. E. *Inorg. Chem.* **2010**, *49*, 4648.

ABSTRACT

Complexes (dme)$TaCl_3(NNPh_2)$ (**5.1**) and (dme)$NbCl_3(NNPh_2)$ (**5.2**) (dme = 1,2-dimethoxyethane) were synthesized from MCl_5 and diphenylhydrazine *via* a Lewis acid assisted dehydrohalogenation reaction. Monomeric **5.1** has been characterized by X-ray, IR, UV-Vis, ^1H NMR, and ^{13}C NMR spectroscopy and contains a κ^1-bound hydrazido(2-) moiety. Unlike the corresponding imido derivatives, **5.1** is dark blue due to an LMCT that has been lowered in energy as a result of an N_α-N_β antibonding interaction that raises the HOMO. Reaction of **5.1** with a variety of neutral, mono- and dianionic ligands generates the corresponding ligated complexes retaining the κ^1-bound [Ta-$NNPh_2$] moiety.

INTRODUCTION

A longstanding goal in chemistry is the activation and subsequent functionalization of molecular dinitrogen.[1] One of the proposed intermediates along a Chatt-type[2] cycle of N_2 reduction is an end-on (κ^1-) bound hydrazide(2-) moiety ($M{=}NNH_2$). Accordingly, significant research into possible models for these intermediates based on group 5 - 8 metals has been undertaken.[3] In addition to efforts towards the synthesis of ammonia from dinitrogen, recent work towards the synthesis of other nitrogen-containing products from [$M{=}NNR_2$] moieties has proven to be an active area of investigation. Following Bergman's first report,[4] the groups of Mountford,[5] Odom,[6] and Gade[7] have been exploring the reactivity of group 4 hydrazides and have made significant advances in the implementation of these complexes in catalytic nitrene transfer[8] and hydrohydrazination reactions. Additionally, Fryzuk and coworkers have reported an interesting dinuclear tantalum complex with a bridging, side-on, end-on bound N_2 ligand that could be also considered a formal hydrazido moiety. This complex is particularly susceptible to N-N bond cleavage and further functionalization to afford silylamines.[9]

While there exist examples of end-on (κ^1-) hydrazide(2-) vanadium complexes,[3a,10] few complexes of the heavier congeners Nb[11] and Ta[12] have been synthesized and characterized. In fact, only two related complexes containing [$Ta{=}NNR_2$] have been reported: [$Ta(NNR_2)Cl_2(NH_2NR_2)(TMEDA)$]Cl (R = Me, 1,5-$(CH_2)_5$).[12] The utilization of these complexes to prepare other related hydrazido complexes appears limited—all attempts to replace the chloride ligands with amides or alkoxides through salt metathesis reactions have failed. The methodology used to prepare [$V{=}NNR_2$] complexes,

aminolysis of vanadium oxo[10c] or phenoxide[10b] ligands, is not viable for niobium or tantalum due to their increased oxophilicity. Additionally, this methodology typically requires installing the ancillary ligand scaffold before the [M=NNR_2] moiety. With this in mind, we sought to develop a simple synthetic entry point into niobium and tantalum terminal [M=NNR_2] complexes and investigate their reactivity relative to analogous tantalum imido complexes and also to group 4 [M=NNR_2] moieties. Herein we report the synthesis of a versatile group 5 end-on (κ^1-) hydrazido synthon, (dme)M($NNPh_2$)Cl_3 (dme = $CH_3OCH_2CH_2OCH_3$; M = Nb, Ta), along with initial results for the tantalum complex demonstrating that dme and chloride may be cleanly displaced by a variety of chelating ligands.

Results and Discussion

Following a procedure similar to those utilized by Williams to prepare group 5 [Ta=NR] imido complexes,[13] $TaCl_5$ and $NbCl_5$ were treated with diphenylhydrazine and dimethoxyethane (dme) in the presence of pyridine and $ZnCl_2$ to generate (dme)$TaCl_3(NNPh_2)$ (**5.1**) and (dme)$NbCl_3(NNPh_2)$ (**5.2**), respectively, through a Lewis acid assisted dehydrohalogenation reaction (eq 5.1).[14] The dme ligand in **5.1** and **5.2** exhibits two signals in the ^1H and ^{13}C NMR spectra for the methoxy protons, as well as two signals for the methylene protons, indicating a *cis*, *mer* geometry as indicated in equation 5.1. Unfortunately, similar reactions with tantalum involving Me_2NNH_2, $MePhNNH_2$, or N-aminopiperidine yield intractable mixtures of products, possibly a result of the increased basicity of the β-nitrogen (N_β) lone pair and/or the better bridging ability of these less bulky hydrazines. Reactions of niobium with alkylhydrazines were successful; these will be discussed in Chapter 6.

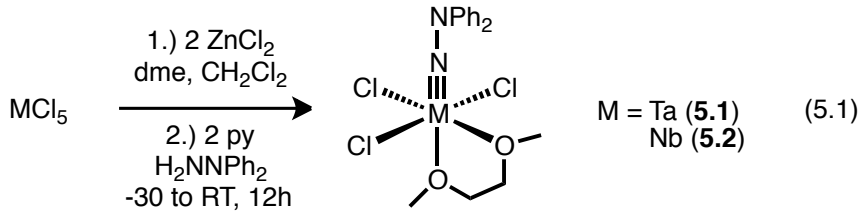

(5.1)

5.1 was crystallized by vapor diffusion of pentane into a concentrated 1,2-dichloroethane solution of **5.1** to give large, blue needles. The X-ray structure of **5.1** (Figure 5.1) confirms that the complex is monomeric containing an end-on, κ^1-bound diphenylhydrazido(2-) ligand. In agreement with NMR data, the ligands are arranged in a *cis,mer* fashion, with one of the dme oxygens *trans* to a chloride and the other *trans* to

the hydrazide ligand. The Ta–N1 bond distance in **5.1** is 1.773(1) Å which indicates a Ta–N LX_2 triple bond, as does the nearly linear Ta–N1–N2 bond angle (173.65(8)°). The N1–N2 distance of 1.347(1) is slightly shorter than that of free diphenylhydrazine, which would be expected on the basis of reduced N_α–N_β lone pair repulsion resulting from N_α lone pair donation to the metal center.

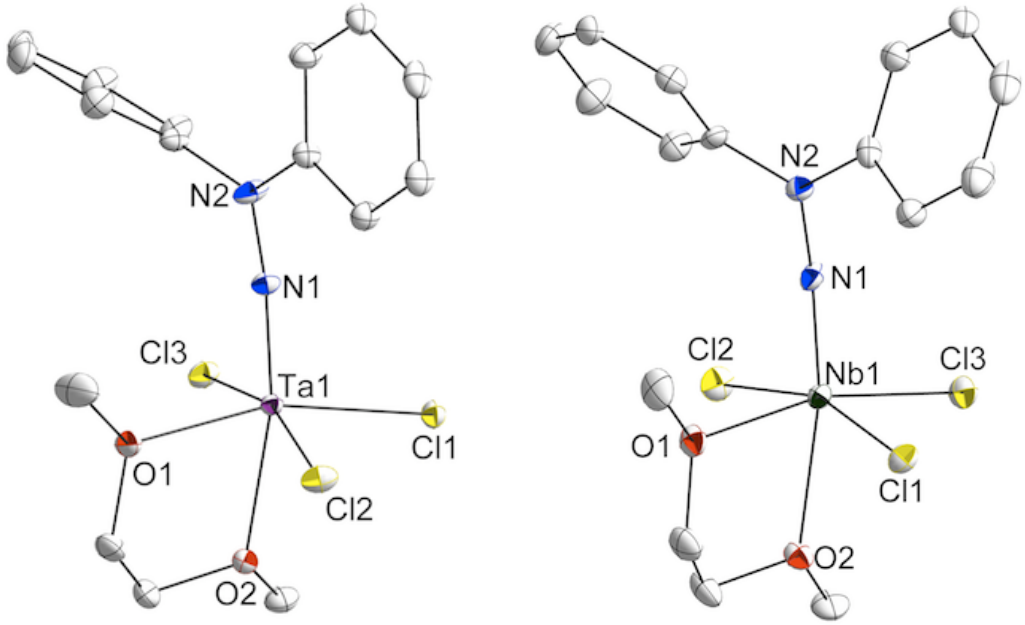

Figure 5.1. Thermal ellipsoid drawings of **5.1** (left) and **5.2** (right). Selected bond lengths (Å) and angles (°): **5.1**: Ta1–N1 1.773(1); Ta1–O1 2.1638(7); Ta1–O2 2.2953(9); N1–N2 1.347(1); Ta1–N1–N2 173.65(8). **5.2**: Nb1–N1 1.765(2); Nb1–O1 2.191(2); Nb1–O2 2.300(2); N1–N2 1.345(3); Nb1–N1–N2 176.1(2). H atoms removed for clarity.

In some $MNNR_2$ complexes the hydrazide unit can be described as a formally neutral diazene L-type ligand,[15] but the short Ta–N distance, the only slightly shortened N_α–N_β bond, and nearly linear Ta–N_α–N_β bond angle indicate that the LX_2-type hydrazido(2–) resonance structure is the major contributor in **5.1**.

Scheme 5.1

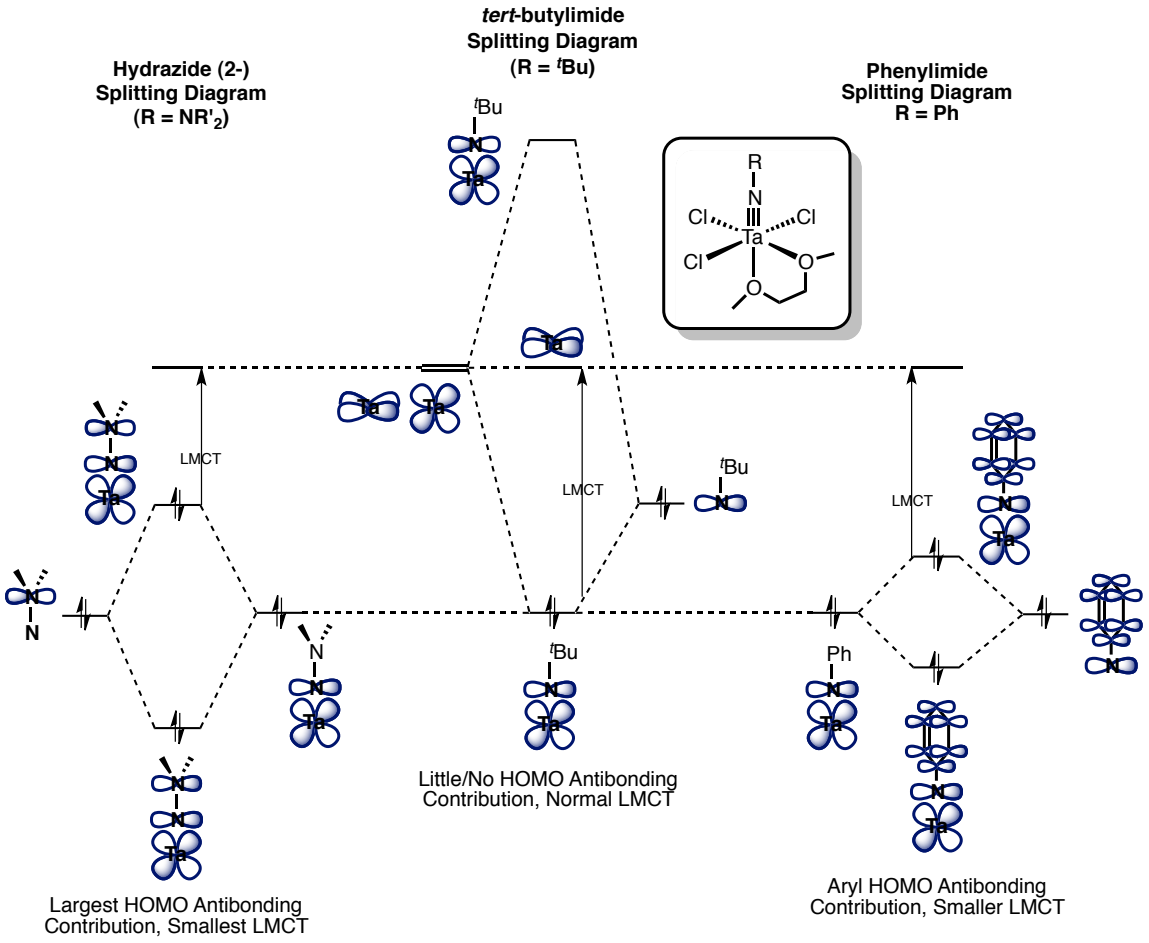

A particularly interesting characteristic of **5.1** is its unique dark blue color. UV-Vis studies of **5.1** show a prominent LMCT band at 583 nm with an extinction coefficient of 400 $M^{-1}cm^{-1}$. In contrast, the corresponding imido complexes (dme)$TaCl_3(N^tBu)$ and (dme)$TaCl_3$(NPh) are colorless (342 nm) and pale yellow (425 nm), respectively.[13] The LMCT in these imido complexes is postulated to arise from a transition from Ta d_{xz}–N_α p_x π bonding orbital (HOMO) to the unoccupied Ta d_{xy} orbital (LUMO).[16] We attribute the large red shift in the LMCT for **5.1** to the interaction of the N_β lone pair

with the Ta d_{xz}–N_α p_x π bonding orbital that serves to destabilize the HOMO via an N_α–N_β antibonding interaction (Scheme 5.1).

A similar phenomenon is observed in (dme)$TaCl_3$(NPh) as a result of an antibonding contribution from the aryl ring, although the effect is smaller (Scheme 5.1).[17] DFT calculations (see experimental section for computational details) of the HOMO–LUMO gap performed on **5.1**, (dme)$TaCl_3$($NCMe_3$) and (dme)$TaCl_3$(NPh) qualitatively agree with this assessment, and the N_α–N_β and N_α–phenyl π antibonding interactions for the HOMOs are clearly evident in **5.1** and (dme)$TaCl_3$(NPh) (Figure 5.2).[18] The calculated HOMO–LUMO gaps for all three compounds were consistently larger than the observed values, so that quantitative comparisons on the lone pair and aryl π effects are not possible. One particularly enticing aspect of this effect is that the addition of the lone pair destabilizes the M=N multiple bond, which could increase the reactivity of hydrazido(2–) complexes toward [2+2] cyclization reactions as compared to the parent imidos. The photophysics of these complexes will be discussed in further detail in Chapter 6.

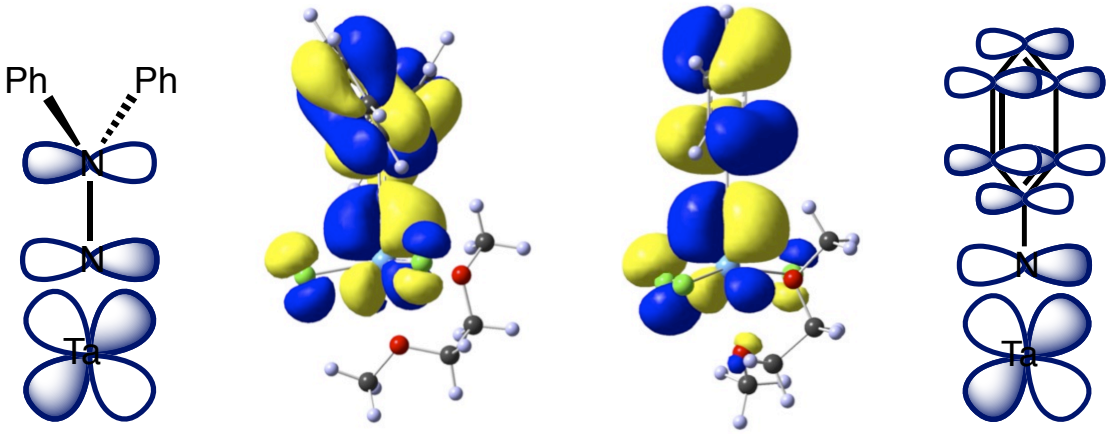

Figure 5.2. Schematic of HOMOs derived from DFT calculations performed on (dme)$TaCl_3$($NNPh_2$) (**5.1**) (left) and (dme)$TaCl_3$(NPh) (right) showing antibonding interactions between the Ta–N π bond and N_β and phenyl substituents, respectively.

L_2 Ligand Substitution

5.1 undergoes ligand substitution with a variety of neutral L-donors to generate new complexes bearing a terminal diphenylhydrazido(2-) moiety (eq 5.2). The dme ligand is readily substituted by nitrogen-based L donors: pyridine, tmeda, and bipyridine will react with **5.1** in benzene to yield $py_2TaCl_3(NNPh_2)$ (**5.3**), $(tmeda)TaCl_3NNPh_2$ (**5.4**) and $(bpy)TaCl_3(NNPh_2)$ (**5.5**), respectively. Adducts **5.3** and **5.4** are stable in solution and were characterized by ^1H and ^{13}C NMR, whereas **5.5** slowly decomposes in solution. Ligand substitution by THF, however, yields the *bis*-THF adduct **5.6** which can be observed by ^1H NMR, but rapidly decomposes to an intractable purple mixture. Similarly, reaction with PPh_3 or chelating phosphines such as *bis*(dimethylphosphino)ethane results in rapid decomposition of the complex. The instability of these complexes is likely a result of weaker monodentate ether or softer phosphine donors.

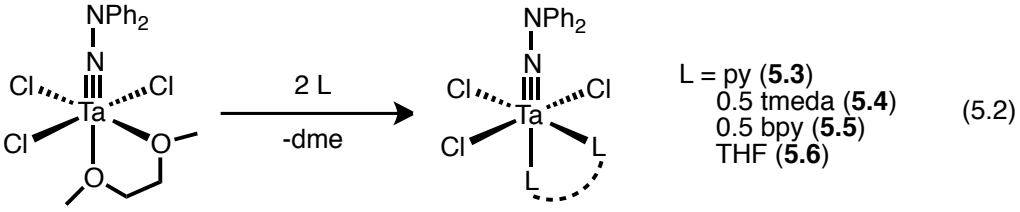

(5.2)

Metallocene Hydrazides

Precursor **5.1** also reacts cleanly with a variety of mono- and dianionic ligands. Treatment of **5.1** with 2 equivalents of NaCp generates the tantalocene product $Cp_2TaCl(NNPh_2)$ (**5.7**) in good yield (eq 5.3). Treatment of **5.1** with only 1 equivalent of NaCp gives 0.5 equiv. **5.7** and 0.5 equiv. of **5.1**, and thus far we have been unable to prepare monocyclopentadienyl complexes of the type $CpTaCl_2(NNR_2)$ *via* **5.1**. Orange

crystals of **5.7** were obtained by layering pentane onto a concentrated toluene solution cooled to -30 °C. The X-ray structure of **5.7** is reported in Figure 5.3.

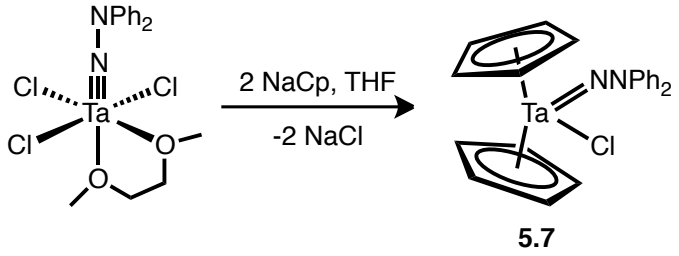

(5.3)

5.7

The bonding in **5.7** is different from all other [Ta=NNR$_2$] complexes reported here. Since the vacant orbital on Ta perpendicular to the tantalocene equatorial plane that is capable of forming a second Ta-N π bond is Ta-Cp antibonding,[19] **5.7** should have a weaker Ta≡N triple bond, approaching more of Ta=N double bond. This intermediate bond order is reflected in the Ta-N bond distance, which at 1.8153(16) Å is longer than all other Ta-N triple bonds that are reported here. Due to the low symmetry of this molecule, it is difficult to determine the occupation of the Ta-Cp antibonding orbital based on Ta-C bond lengths. The Ta-N$_\alpha$-N$_\beta$ bond angle is bent out of the tantalocene wedge to 167.04(1)°, which might also be indicative of some Ta=N character with a stereochemically active N$_\alpha$ lone electron pair as shown in eq 5.3, but this distortion from linearity might be due at least in part to steric interactions between cyclopentadienyl ligands and the large [N$_\beta$Ph$_2$] group (closest non-bonded H-H contacts between the [N$_\beta$Ph$_2$] group and the Cp ring are 2.263 and 2.426 Å). Again, the low symmetry makes distinguishing between electronic and steric effects difficult.

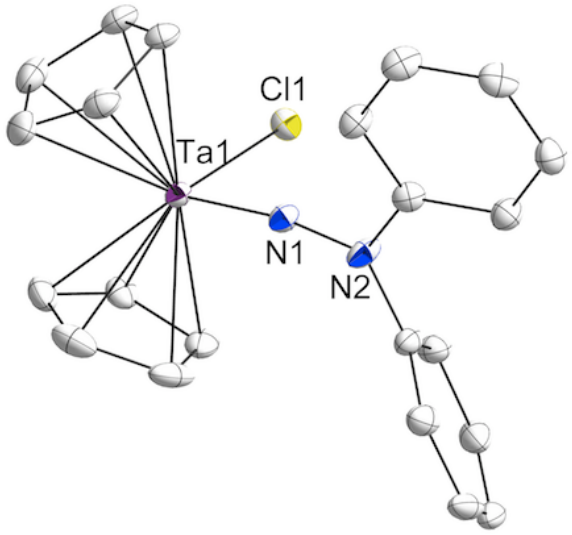

Figure 5.3. Thermal ellipsoid drawing of **5.7**. Selected bond lengths (Å) and angles (°): Ta1–N1 1.8153(16); N1–N2 1.3358(22); Ta1–N1–N2 167.04(1). Summation of angles about N2: 358°. H atoms removed for clarity.

Dianionic Pincer Ligands

Recently, our group has been interested in using aryl-linked *bis*(phenolate) ligand sets as analogs of *bis*(cyclopentadienyl) scaffolds.[20] Hydrazide-containing tantalum *bis*(phenolate) complexes have been synthesized through two methods. First, the salt metathesis reaction of **5.1** with (2,6-(OC_6H_2-^{t}Bu_2)$_2$$C_5H_3N$)$K_2$ in benzene in the presence of excess pyridine led to quantitative formation (NMR) of (ONO)TaCl($NNPh_2$)(py) (**5.8**) (ONO = (2,6-(OC_6H_2-^{t}Bu_2)$_2$$C_5H_3N$)) (eq 5.4). The addition of a sixth ligand (e.g., pyridine) to these reactions is required: attempts to synthesize the related 5-coordinate complexes without an additional L donor always yielded intractable, insoluble product mixtures. Alternately, the complex (ONO)TaCl($NNMe_2$)($HNMe_2$) (**5.9**) could be synthesized through hydrazinolysis of (ONO)Ta(NMe_2)$_2$Cl with H_2NNMe_2 (eq 5.5). Similar hydrazinolysis attempts with H_2NNPh_2 yielded no reaction, likely due to the increased steric bulk of

diphenylhydrazine vs. dimethylhydrazine. We have previously reported that sterically bulky primary amines (e.g., $^{t}BuNH_2$) do not react with $(ONO)Ta(NMe_2)_2Cl$ or $(ONO)TaMe_3$, whereas less bulky amines such as aniline do react to form imides.[20a]

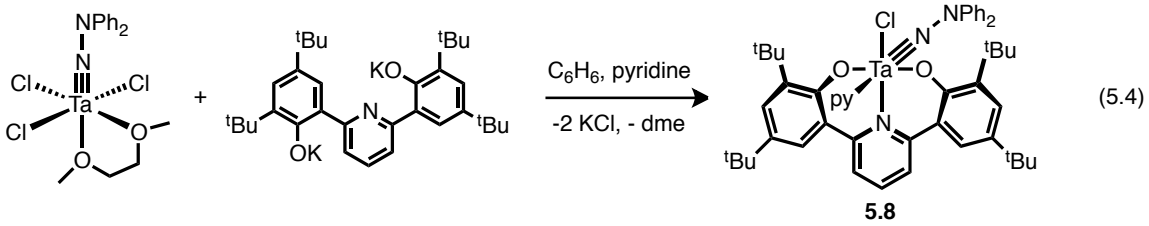

(5.4)

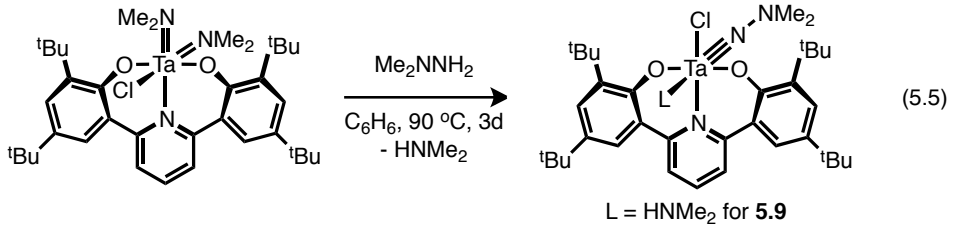

(5.5)

Both **5.8** and **5.9** have been characterized by X-ray diffraction. The former contains a meridionally bound *bis*(phenolate) ligand with the diphenylhydrazide ligand *trans* to an additional molecule of pyridine (Figure 5.4). Similar to complex **5.1**, the hydrazido(2-) ligand forms an LX_2 triple bond with tantalum, evidenced from the Ta-N bond length of 1.7925(8) Å and an essentially linear $Ta-N_\alpha-N_\beta$ angle of 174.62(8)°. The $N_\alpha-N_\beta$ bond distance of 1.355(1) Å is again shorter than free diphenylhydrazine due to reduced $N_\alpha-N_\beta$ lone pair repulsion.

Similar to **5.8**, **5.9** contains a meridionally bound *bis*(phenolate) ligand with the dimethylhydrazido(2-) ligand *trans* to the weakest *trans* influencing ligand $HNMe_2$ (Figure 5.5). The short Ta-N distance of 1.789(1) Å and linear $Ta-N_\alpha-N_\beta$ angle of 175.2(1)° once again indicate a Ta-N triple bond for the $[Ta{\equiv}N-NMe_2]$ moiety. Complex **5.9** is the only Ta dimethylhydrazido(2-) complex that we have fully characterized and provides a

valuable structural contrast to **5.8**, which contains the same basic (ONO)TaLX(NR) framework. For **5.9** the (ONO) ligand is bound in a C_S-symmetric fashion, whereas in **5.8** the ligand geometry is C_2-symmetric.

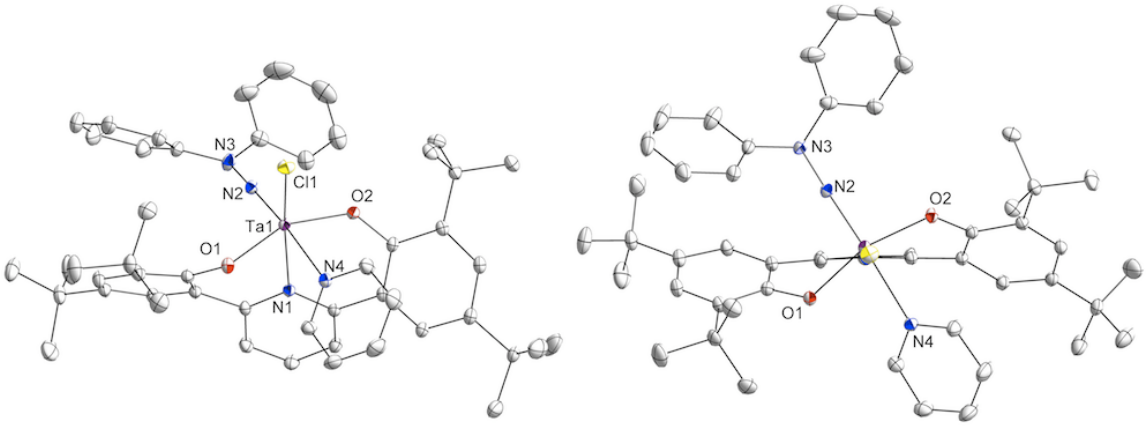

Figure 5.4. Thermal ellipsoid drawing of **5.8**. Side view and view down the Cl-Ta bond showing C_2-symmetric arrangement of the (ONO) ligand. Selected bond lengths (Å) and angles (°): Ta1-O1 1.9762(8); Ta1-O2 1.9856(7); Ta1-N1 2.246(1); Ta1-N2 1.7925(8); Ta1-N4 2.3598(8); N2-N3 1.355(1); Ta1-N2-N3 174.62(8). H atoms removed for clarity.

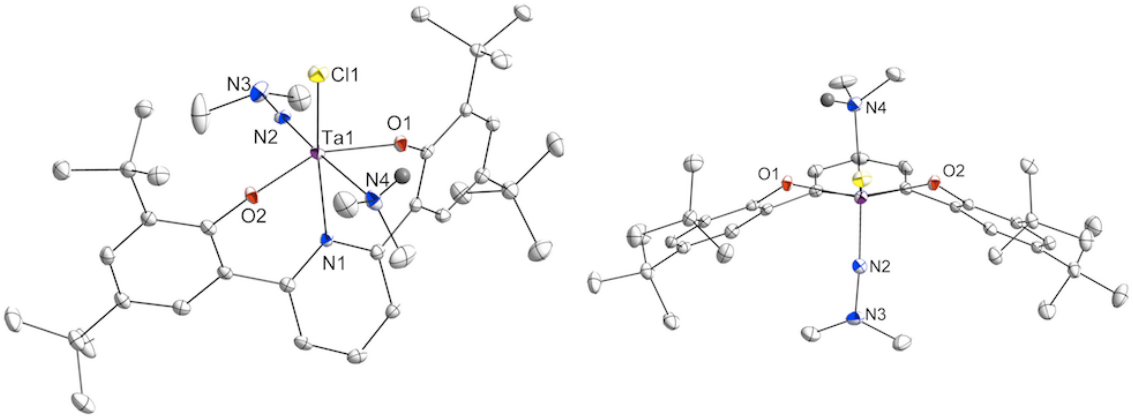

Figure 5.5. Thermal ellipsoid drawing of **5.9**. Side view and view down the Cl-Ta bond showing C_S-symmetric arrangement of the (ONO) ligand. Selected bond lengths (Å) and angles (°): Ta1-O1 1.970(1); Ta1-O2 1.968(1); Ta1-N1 2.303(1); Ta1-N2 1.789(1); Ta1-N4 2.443(1); N2-N3 1.356(2); Ta1-N2-N3 175.2(1). H atoms (except for H on the N4 amine) removed for clarity.

Given the close similarity of the two complexes, we can only suggest that the smaller methyl substituents of the dimethylhydrazido(2-) complex **5.9** are able to accommodate the electronically preferred[20a] C_s-symmetric arrangement of (ONO), as is also found in the corresponding phenyl imido derivative (ONO)Ta($HNMe_2$)Cl(≡NPh).[20a] The structure of **5.8** suggests that the larger N_β-phenyl groups would clash with the bulky *tert*-butyl groups on the *bis*(phenolate) ligand such that the (ONO) ligand to twists to accommodate the less sterically hindered C_2-symmetric (ONO) geometry for the diphenylhydrazido complex. The geometry about N_β also generates greater steric crowding for the diphenylhydrazido (2-) complex **5.8**: while the Ta-N_α and N_α-N_β bonding metrics are roughly the same in **5.8** and **5.9**, the geometry about N_β is different in the two complexes. In **5.8** (as in **5.1**, and other diphenylhydrazido complexes), N_β is almost planar with bond angles of approximately 117° for N_α-N_β-C_{ipso} and 123° for C_{ipso}-N_β-C_{ipso}. In contrast, **5.9** N_β is pyramidal with all angles near 111°. This geometry change could also influence the overall ligand geometry.

Mountford,[5b,c,e] Odom,[6] and Gade[7] have utilized tridentate, dianionic *bis*(amido)amine/pyridine ligand sets to explore the structure and reactivity of group 4 hydrazido(2-) complexes. These compounds can act as catalysts for hydrohydrazination reactions or as catalysts for a unique alkyne *bis*-amination reaction. We sought to make analogous cationic group 5 complexes, envisioning that the increased Lewis acidity of a cationic Ta center would promote reactivity.

Reaction of **5.1** with $MeN[(CH_2)_2NTMS)]_2Li_2$ in benzene produces the *bis*(amide)amine complex, (C_2-N_2N^{Me})TaCl($NNPh_2$) (**5.10**), in high yield (eq 5.6). The ^1H

NMR spectrum for **5.10** shows that the (C_2-N_2N^{Me}) ligand is bound *fac* to Ta, as 4 nonequivalent protons for the methylenes of the backbone of the ligand are observed as multiplets. Similar reaction of **5.1** with the propylene backbone ligand, $MeN[(CH_2)_3NTMS)]_2Li_2$, also produces the desired complex (C_3-N_2N^{Me})TaCl($NNPh_2$) (**5.11**), albeit in lower yield (eq 5.6). The methylene backbone protons for **5.11** are much broader than in **5.10**, suggesting that the structure is fluxional at room temperature. Despite the ill-defined methylenes, **5.11** can be easily identified in the ^{1}H NMR from the characteristic $NNPh_2$ resonances, the N-Me resonance, and the slightly broadened $SiMe_3$ resonance.

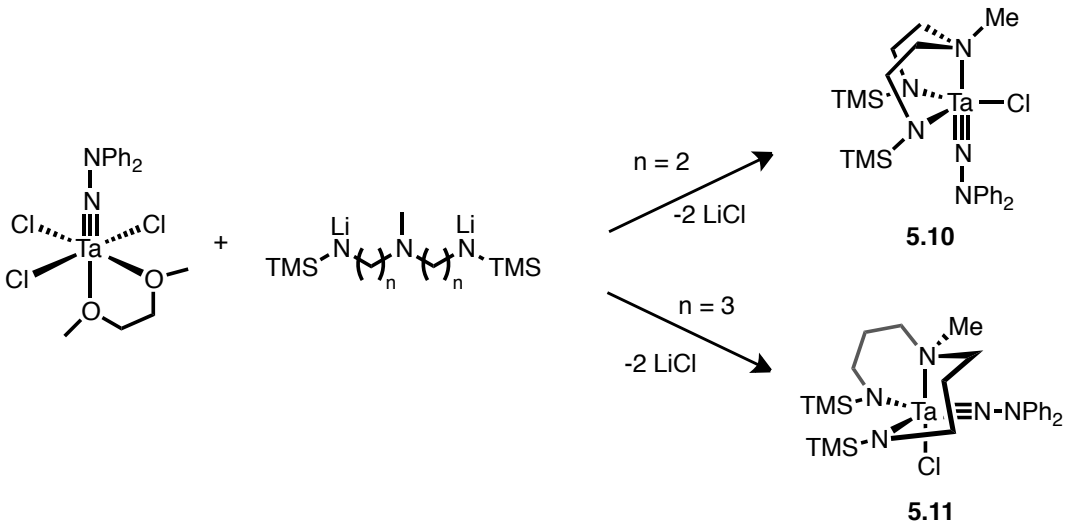

(5.6)

Large orange crystals of **5.10** were grown by slow diffusion of a concentrated hexane solution of **5.10** into TMS_2O. Complex **5.10** is monomeric, 5-coordinate trigonal bipyramidal with the (C_2-N_2N^{Me}) ligand bound in *fac* manner as predicted by ^{1}H NMR (Figure 5.6). The diphenyhydrazido ligand, which is *trans* to the tertiary amine of the (C_2-N_2N^{Me}) ligand, has a Ta-N bond length of 1.7988(1) Å and a Ta-N_α-N_β bond angle of

177.4(1)°, consistent with the metrics of an LX_2 Ta–N triple bond, as is the case for the other hydrazido complexes reported here.

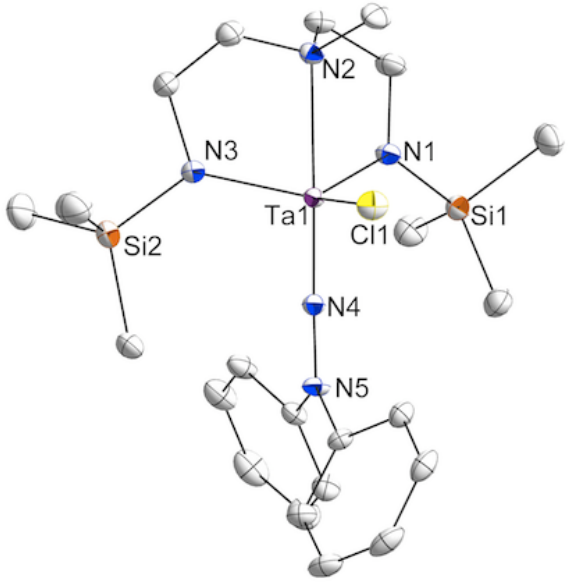

Figure 5.6. Thermal ellipsoid drawing of **5.10**. Selected bond lengths (Å) and angles (°): Ta1–N1 1.7988(1); Ta1–N3 2.0197(1); Ta1–N4 2.3815(1); Ta1–N5 2.0113(1); N1–N2 1.363(1); Ta1–N1–N2 177.42. H atoms removed for clarity.

Perhaps the most notable feature of **5.10** is the position of the hydrazido ligand relative to the (C_2–N_2N^{Me}) ligand. In the Mountford[5b,e] group 4 analogues, the diphenylhydrazido ligand is located in the equatorial plane of the trigonal bipyramid, whereas in **5.10** it lies in an axial position. From an orbital overlap perspective, the *trans* isomer observed in **5.10** would seem to be favored, because the hydrazide and the two amides would then not compete for the same metal d π orbitals. Additionally, the strong *trans* influencing imido should prefer to be opposite the very weakly *trans* influencing tertiary amine. Because all of Mountford's imido and hydrazido complexes have a *cis* conformation, this structure might well require further investigation.

5.11 was crystallized by diffusion of pentane into a concentrated solution of **5.11** in CH_2Cl_2. **5.11** is a C_1-symmetric molecule with a *fac*-coordinated (C_3-N_2N^{Me}) ligand that resembles a *cis*-fused decalin bicyclic ring structure (Figure 5.7). Unlike **5.10** and similar to the complexes observed by Mountford and Gade, **5.11** contains a diphenylhydrazido ligand roughly *cis* to the amine in the (C_3-N_2N^{Me}) ligand. The Ta-N distance of 1.791(1) Å is consistent with a triple bond, although the Ta-N_α-N_β bond angle (163.75(9)°) is significantly bent compared to other Ta-$NNPh_2$ complexes. This bending could be cause by steric repulsion from one of the $SiMe_3$ groups also located in the equatorial plane.

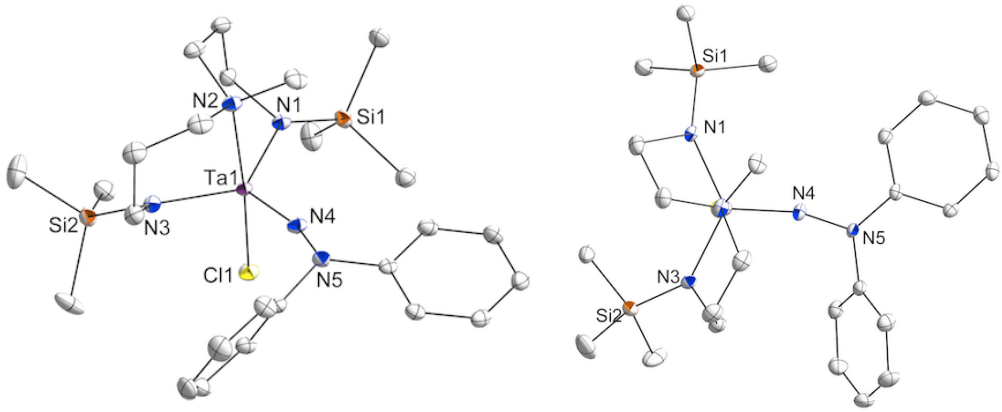

Figure 5.7. Thermal ellipsoid drawing of **5.11**. Side view and top-down view showing *cis*-fused decalin-type metallacycle structure. Selected bond lengths (Å) and angles (°): Ta1-N1 2.004(1); Ta1-N2 2.328(1); Ta1-N3 2.006(1); Ta1-N4 1.791(1); N4-N5 1.374(2); Ta1-N4-N5 163.75(9). H atoms removed for clarity.

When complex **5.10** was treated with $Na^+[BArF_{24}]^-$ ($[BArF_{24}]^-$ = $[B(3,5\text{-}(CF_3)_2C_6H_3)_4]^-$) in CH_2Cl_2 in the presence of excess pyridine, the cationic chloride-abstracted product $[(C_2\text{-}N_2N^{Me})Ta(NNPh_2)(py)][BArF_{24}]$ (**5.12**) was generated with concomitant precipitation of NaCl (eq 5.7). Without the presence of pyridine, or in the

presence of a weaker ligand such as 2,6-lutidine, PPh_3, or perfluoropyridine, reaction with $NaBArF_{24}$ led to fast decomposition after chloride abstraction. Complex **5.12** has been identified by ^1H NMR and ^{13}C NMR and is consistent with the coordination of one molecule of pyridine to a cationic $(C_2\text{-}N_2N^{Me})Ta(NNPh_2)$ fragment with $[BArF_{24}]^-$ as the counteranion.

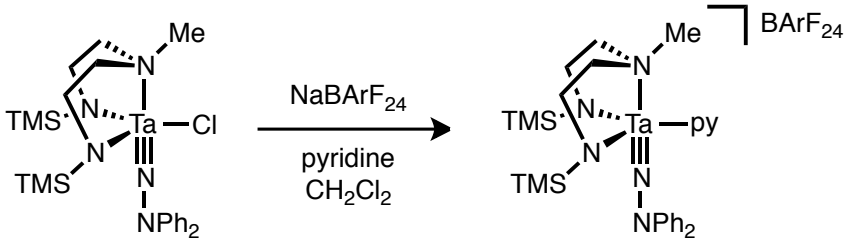

5.10 **5.12** (5.7)

Attempts to carry out pyridine substitution reactions with a variety of ligands (e.g., 4-*tert*-butyl pyridine, PPh_3, THF), as well as attempted and [2+2] reactions with terminal and internal alkynes resulted in no reaction. The inertness of **5.12** was unexpected, particularly considering that it is isoelectronic with analogous neutral, group 4 imido complexes. Attempts to crystallize **5.12** have instead yielded the *bis*(pyridine) adduct, $[(C_2\text{-}N_2N^{Me})Ta(NNPh_2)(py)_2][BArF_{24}]$ (**5.13**), along with significant amounts of intractable noncrystalline solids (eq. 5.8). Addition of 1 equivalent of pyridine in the reaction of **5.10** with $NaBArF_{24}$ yields 100% conversion to **5.12** (^1H NMR), so we are confident that **5.12** is the major product upon chloride abstraction rather than the crystallographically observed **5.13**. Additionally, elemental analysis of **5.12** is consistent with a *mono*(pyridine) rather than a *bis*(pyridine) adduct. Similar reaction with 4-^{t}Bu-pyridine gives an adduct with a 9:18 integration ratio of ^{t}Bu:$SiMe_3$ peaks in the ^1H NMR, consistent with a product analogous to **5.12**. As a result of this evidence, **5.13** is rather a decomposition product of **5.12**.

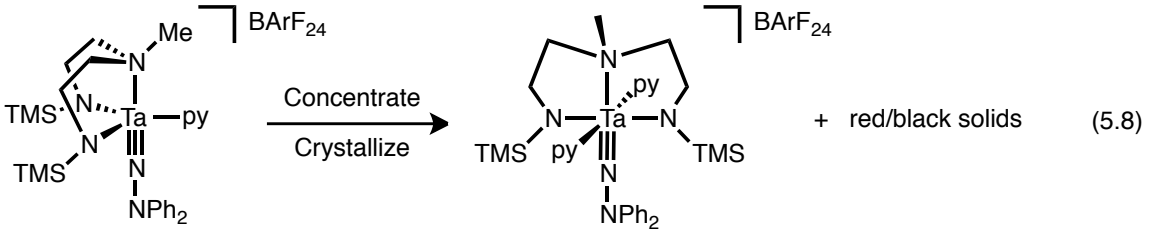

5.11 **5.13**

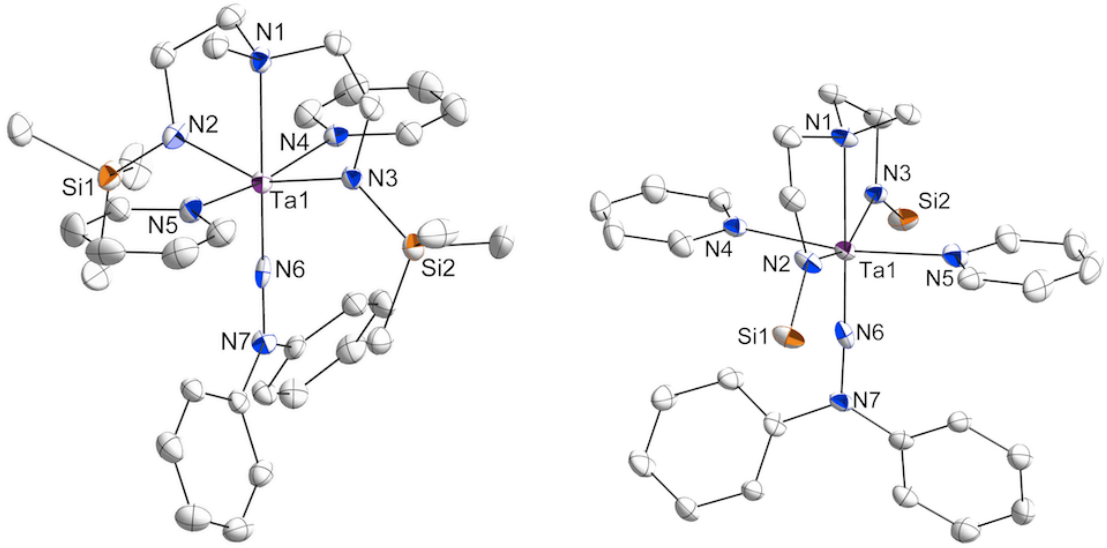

Figure 5.8. Thermal ellipsoid drawing of **5.13**. Right view has TMS groups trimmed for clarity. Selected bond lengths (Å) and angles (°): Ta1–N1 2.379(3); Ta1–N2 2.055(3); Ta1–N3 2.047(3); Ta1–N4 2.314(4); Ta1–N5 2.280(4); Ta1–N6 1.762(3); N6–N7 1.402(4); Ta1–N6–N7 177.6(3). H atoms and $BArF_{24}$ counteranion removed for clarity.

Complex **5.13** contains a meridionally-bound (C_2–N_2N^{Me}) ligand with the diphenylhydrazido moiety *trans* to the amine of the (C_2–N_2N^{Me}) ligand and the two coordinated pyridine molecules mutually *trans* (Figure 5.8). The Ta–N LX_2 triple bond distance is 1.762(3), slightly shorter than in **5.10** as would be expected for a tantalum cation, and the Ta–N_α–N_β bond angle is 177.6(3)°.

In light of the inertness of **5.11**, coordinatively unsaturated species were synthesized in the hope that a vacant coordination site would permit addition reactions of

simple L type donors or [2+2] reactivity with unsaturated substrates. Previously, Bergman showed that 5-coordinate β-di(iminate) (BDI) Nb imido complexes were capable of undergoing associative reactions, and that 4-coordinate (BDI)Nb diimidos could undergo [2+2] cyclization.[21] As a result, analogous (BDI)Nb and Ta hydrazidos were synthesized and their reactivity explored.

Coordinatively Unsaturated (nacnac) Hydrazides

(BDI)$TaCl_2(NNPh_2)$ (**5.14**) and (BDI)$NbCl_2(NNPh_2)$ (**5.15**) ((BDI) = *N,N'*-(pentane-2,4-diylidenato)bis(diisopropylaniline)) were synthesized *via* salt metathesis of **5.1** or **5.2** with (BDI)Li(THF) in Et_2O (eq. 5.9). The complexes appear to be C_S-symmetric in solution by ^1H NMR: the backbone methyl peaks on the BDI ligand are chemically equivalent, and four types of *iso*propyl methyl peaks are observed. This indicates that the top and bottom (as drawn in eq. 5.9) of the BDI aryl groups are inequivalent, but the left and right BDI aryl groups are equivalent.

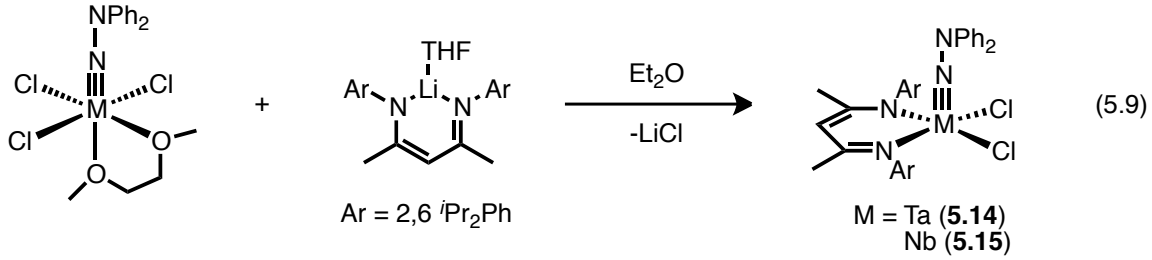

(5.9)

Large dark green crystals of **5.14** and small dark red crystals of **5.15** were grown by layering pentane on a saturated solution of the compound in Et_2O and cooling to -30 °C. The X-ray structures of **5.14** and **5.15** confirm the C_S-symmetric solution structure of the complexes (Figure 5.9). Structurally, **5.14** and **5.15** are very similar. Both are roughly C_S-symmetric with a mirror plane bisecting the Cl-M-Cl angle and passing through the

M–N–N hydrazide vector. There is a slight asymmetry in the binding of the BDI ligand, as one of the imine N–M bond distances is approximately 0.1 Å longer than the other. The geometry of the metal centers is distorted square pyramidal, the $^{i}Pr_2Ar$ groups lie perpendicular to the metal square plane, and a vacant site is located *trans* to the strong hydrazide ligand. The M–N distances and linear M–N–N angles for the hydrazide ligand are typical for those reported earlier for M–N triple bonds.

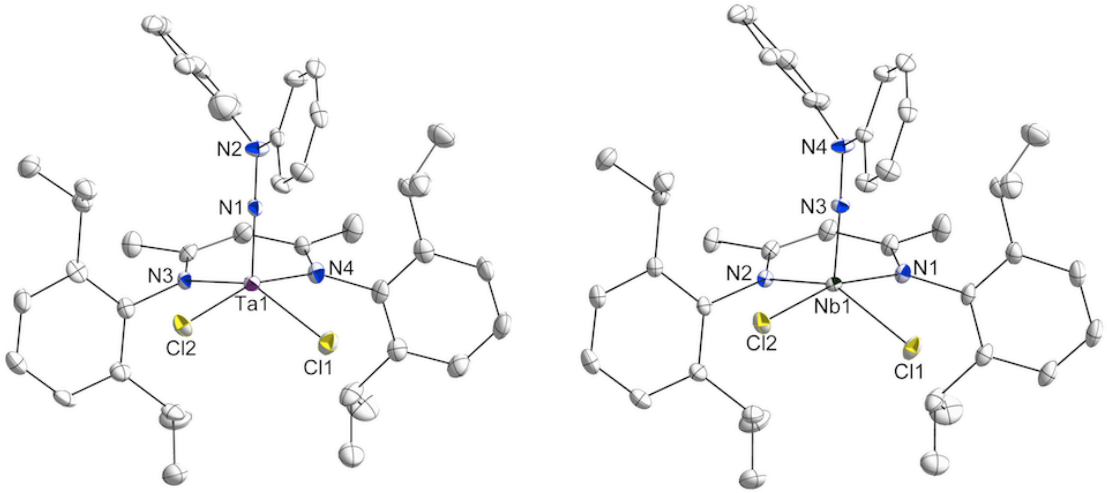

Figure 5.9. Thermal ellipsoid drawing of **5.14** (left) and **5.15** (right). Selected bond lengths (Å) and angles (°): Complex **5.14**: Ta1–N1 1.759(1); Ta1–N3 2.114(1); Ta1–N4 2.2133(5); N1–N2 1.3572(3); Ta1–N1–N2 179.8(1). Complex **5.15** Nb1–N3 1.7620(1); Nb1–N1 2.2456(2); Nb1–N2 2.1254(2); N3–N4 1.3306(1); Nb1–N3–N4 177.8(1). H atoms removed for clarity.

Treatment of **5.14** with excess pyridine generated an asymmetric pyridine adduct, **5.16** (eq. 5.10). In **5.16** the methyl groups on the BDI backbone are inequivalent, indicating that the mirror plane symmetry of the molecule has been broken (Figure 5.10). Although not characterized in the solid state, **5.16** likely contains the hydrazido moiety and pyridine in the equatorial plane with the BDI ligand, with the two chlorides in axial

positions.[21] Pyridine addition is reversible, and repeated washing and removal of solvent *in vacuo* regenerates **5.14**.

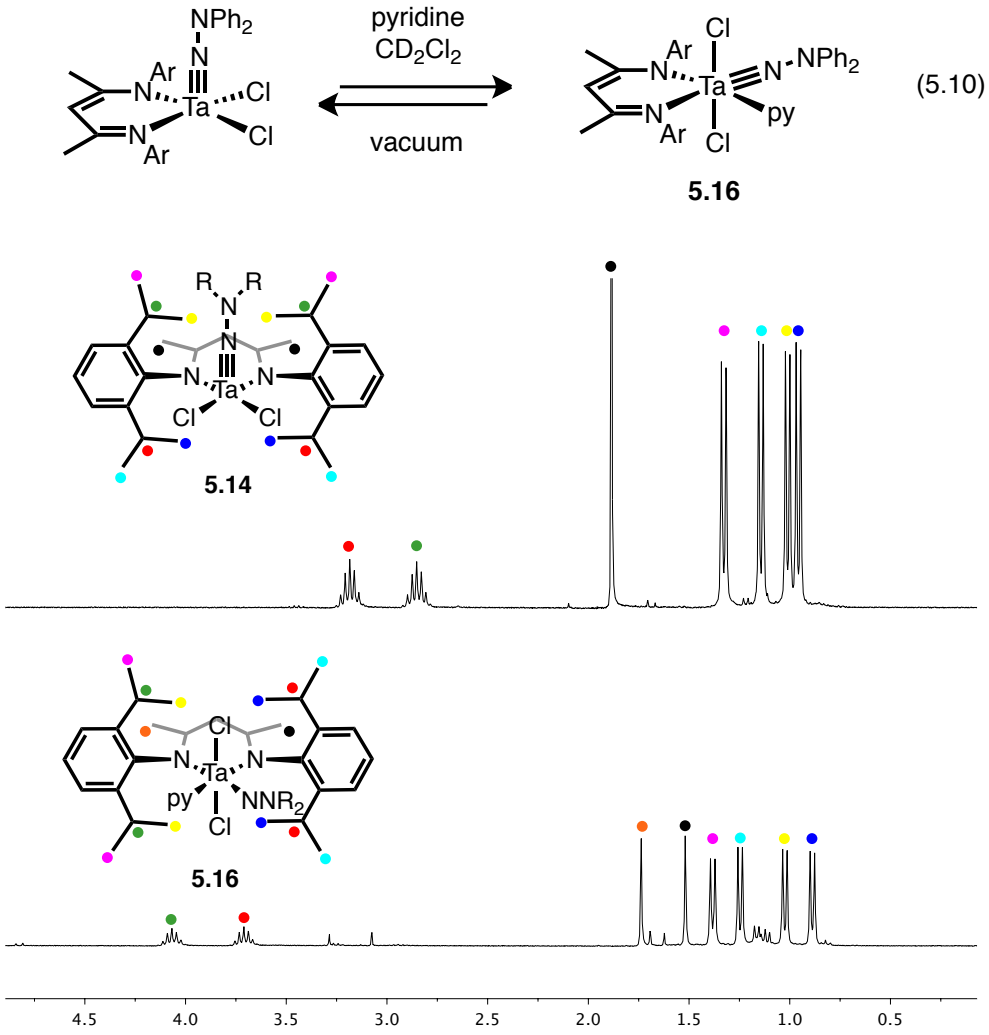

Figure 5.10. ^{1}H NMR spectra of the alkyl regions of **5.14** (top) and **5.16** (bottom).

A similar 6-coordinate complex, (BDI)$NbCl_2(NNMe_2)$(THF) (**5.17**), was independently synthesized from (BDI)Li(THF) and (dme)$NbCl_3(NNMe_2)$ (Ch. 6, **6.2h**) (eq. 5.11). **5.17** was analyzed by X-ray diffractometry, and confirms the equatorial arrangement of **5.16** (Figure 5.11). In this complex, the BDI ligand, THF, and

dimethylhydrazide ligands make up the equatorial plane, with the chlorides in axial positions. Unlike **5.14** and **5.15**, **5.17** has a largely asymmetric binding of the BDI ligand—the imide nitrogen *trans* to the hydrazide ligand is elongated by 0.25 Å compared to the imide *trans* to THF. In general, the Nb complexes **5.15** and **5.17** appear to be more structurally flexible than the Ta congeners: at room temperature, the ^{1}H NMR of **5.15** and **5.17** are much broader than the related **5.14** and **5.16**.

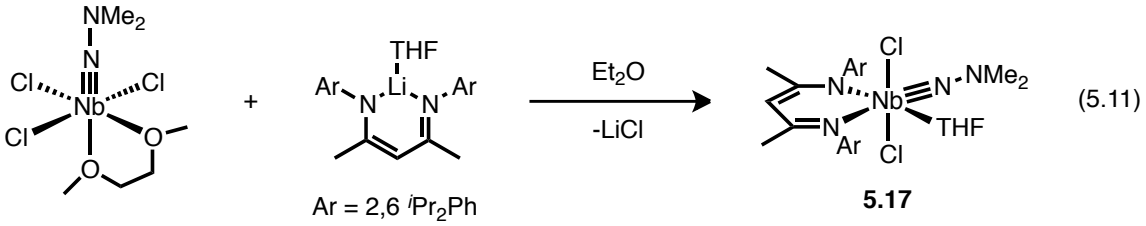

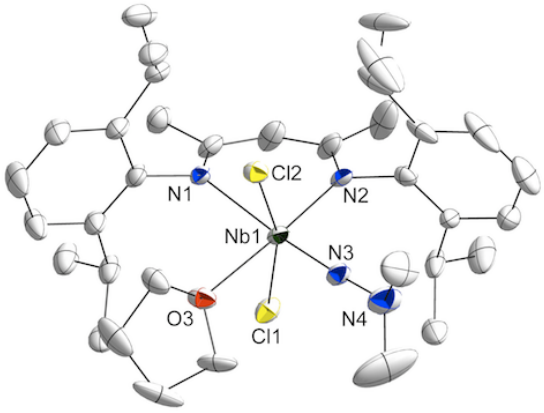

Figure 5.11. Thermal ellipsoid drawing of **5.17.** Selected bond lengths (Å) and angles (°): Nb1–O3 2.3190(4); Nb1–N1 2.3715(2); Nb1–N2 2.1222(3); Nb1–N3 1.7690(2); N3–N4 1.3353(1); Nb1–N3–N4 176.2(1). H atoms removed for clarity.

Unfortunately, **5.14** is also unreactive with internal alkynes and CO_2. However, the open coordination site on the complex is a promising entry point into further chemistry,

and the chloride ligands are easily replaced as well (either with MeMgBr or $TMSN_3$). As a result, the (BDI)-class hydrazides may yet reveal novel reactivity.

N_3N Complexes

Finally, $(N_3N)Ta(NNPh_2)$ (**5.18**) and $(N_3N)Nb(NNR_2)$ (R = Ph_2 **5.19**; R = Me_2 = **5.20**) (N_3N = *tris*(*N*-methylamido-ethyl)amine) were synthesized *via* salt metathesis of **5.1**, **5.2**, or **6.2h** with $(N_3N)Li_3$ in Et_2O (eq. 5.12).

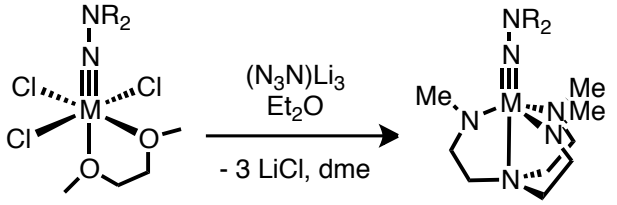

5.1, **5.2**, or **6.2i**

M = Ta, R = Ph **5.18**
M = Nb, R = Ph **5.19**
M = Nb, R = Me **5.20**

(*5.12*)

Complexes **5.18**-**5.20** are isoelectronic to $(TREN)MoNNH_2^+$, which is an intermediate along the (TREN)Mo-catalyzed N_2 reduction cycle.[3b] As such, we sought to study the redox capabilities of these complexes. **5.18** and **5.20** showed two irreversible oxidation waves by cyclic voltammetry (Table 5.1). By contrast, the related imido complex $(N_3N)NbN(^tBu)$ shows only a single irreversible oxidation wave. All three complexes have their first oxidation wave near 0.0 V (*vs.* Fc/Fc^+), and as a result we assign the first oxidation to an oxidation of a nonbonding combination of the triamido lone pairs. The second oxidation at approx. 0.7 V is attributed to oxidation on the hydrazido ligand.

Table 5.1. CV oxidations of **5.18**, **5.20**, and $(N_3N)Nb(N^tBu)$ in MeCN/TBACl vs. Fc/Fc^+.

	Wave 1 (V)	Wave 2 (V)
$(N_3N)Ta(NNPh_2)$ (**5.18**)	-0.14	0.72
$(N_3N)Nb(NNMe_2)$ (**5.20**)	0.03	0.74
$(N_3N)Nb(N^tBu)$	0.10	-

Unfortunately, chemical oxidation of **5.18** and **5.20** with H^+ and Me^+ sources yielded product mixtures. As a result, bulkier ligand derivatives are being explored in analogy to the (TREN)Mo catalysts.

CONCLUSIONS

The complexes (dme)$MCl_3(NNPh_2)$ (M = Ta, **5.1**; Nb, **5.2**) have been prepared from MCl_5 and diphenylhydrazine *via* a Lewis acid assisted dehydrohalogenation reaction. Complex **5.1** is blue whereas related imidos are colorless or yellow. This color arises from an LMCT from a Ta-hydrazide π-bonding HOMO that is destabilized due to an antibonding interaction with the lone pair of the hydrazido N_β. Complex **5.1** has been shown to be a versatile synthon for installing a [$Ta{=}NNPh_2$] moiety into a variety of inorganic or organometallic coordination complexes with other neutral, mono- or dianionic ligand sets. The bonding metrics of all of the reported [$Ta{=}NNR_2$] complexes are consistent with LX_2-type Ta-N triple bonds based on short Ta-N distances and mostly linear Ta-N_α-N_β bond angles. In an attempt to generate cationic Ta analogues of reported group 4 hydrazido complexes, a chloride abstraction for **5.10** was performed with $Na^+[BArF_{24}]^-$ to yield a pyridine adduct, cation, **5.12**, which is surprisingly inert to ligand substitution and [2+2] reactions with alkynes. We are currently further exploring the reactivity of the tantalum-hydrazido moiety as it relates to the analogous tantalum-imido complexes.

EXPERIMENTAL SECTION

General Considerations and Instrumentation. All air- and moisture-sensitive compounds were manipulated using standard high vacuum and Schlenk techniques or manipulated in a glovebox under a nitrogen atmosphere. Solvents for air- and moisture-sensitive reactions were dried over sodium benzophenone ketyl and stored over titanocene where compatible or dried by the method of Grubbs.[22] Pyridine was dried over sodium and distilled prior to use. $TaCl_5$ was purchased from Strem Chemicals and sublimed prior to use. Diphenylhydrazine and dimethylhydrazine were purchased from TCI, distilled from CaH_2 and degassed prior to use. $Na^+[BArF_{24}]^-$,[23] NaCp,[24] (BDI)Li(THF)[25], and (2,6-$(OC_6H_2$-^{t}Bu$_2)_2C_5H_3N)K_2$[20d] were prepared following literature procedures. Benzene-d_6 was purchased from Cambridge Isotopes and dried over sodium benzophenone ketyl, while methylene chloride-d_2, also purchased from Cambridge Isotopes, was dried over CaH_2 and filtered through a plug of activated alumina. All other materials were used as received. ^{1}H, and ^{13}C spectra were recorded on Varian Mercury 300 or Varian INOVA 500 spectrometers and chemical shifts are reported with respect to residual protio-solvent impurity for ^{1}H (s, 7.16ppm for C_6D_5H; t, 5.32 ppm for $CDHCl_2$) and solvent carbons for ^{13}C (t, 128.39 for C_6H_6; p, 54.00 for CD_2Cl_2).

Computational Details. Density functional calculations were carried out using Gaussian 03 Revision D.01.[26] Calculations were performed using the nonlocal exchange correction by Becke[27,28] and nonlocal correlation corrections by Perdew,[29] as implemented using the b3lyp[30,31] keyword in Gaussian. The following basis sets were used: LANL2DZ[32-34] for Ta atoms and 6-31G** basis set for all other atoms. Pseudopotentials

were utilized for Ta atoms using the LANL2DZ ECP. All optimized structures were verified using frequency calculations and did not contain any imaginary frequencies. Iso-surface plots were made using the Gaussian 03 Revision D.01 program.[26]

X-ray Crystal Data: General Procedure. Crystals were removed quickly from a scintillation vial to a microscope slide coated with Paratone N oil. Samples were selected and mounted on a glass fiber with Paratone N oil. Data collection was carried out on a Bruker KAPPA APEX II diffractometer with a 0.71073 Å MoKα source. The structures were solved by direct methods. All non-hydrogen atoms were refined anisotropically. Some details regarding refined data and cell parameters are available in Tables 5.2, 5.3, 5.4 and 5.5.

Synthesis of (κ^2-$CH_3O(CH_2)_2OCH_3$)$TaCl_3(NNPh_2)$ (5.1). $TaCl_5$ (500 mg, 1.4 mmol) and $ZnCl_2$ (380 mg, 2.8 mmol) were mixed in 10 mL CH_2Cl_2 in an inert atmosphere glovebox. Dimethoxyethane (.25 mL) was added to the reaction mixture and the reaction stirred for 15 minutes, yielding a dark solution with a white precipitate. The reaction was cooled to -30 °C and 1,1-diphenylhydrazine (230 μL, 258 mg, 1.4 mmol) and pyridine (226 μL, 221 mg, 2.8 mmol) in 5 mL CH_2Cl_2 was slowly added to the reaction mixture. The initially orange solution slowly turned deep blue and was left to stir overnight. The reaction was then filtered to remove pyridinium-zinc chloride salts. CH_2Cl_2 was removed *in vacuo* and the resulting blue solid was washed with pentane and then was dissolved into 20 mL benzene, filtered, and lyophilized to yield 700 mg **5.1** as a blue powder (90%). Further purification was achieved by crystallization through vapor diffusion of pentane into a concentrated dichloroethane solution of **5.1**, yielding **5.1** as blue/royal blue

dichroic needles. ^{1}H NMR (300 MHz, CD_2Cl_2) δ, ppm: 3.985 (s, 3H, OC*H*$_3$); 4.023 (s, 3H, OC*H*$_3$); 4.136 (m, 2H, OC*H*$_2$); 4.152 (m, 2H, OC*H*$_2$); 7.05 (m, 2H, aryl); 7.425 (m, 8H, aryl). ^{13}C NMR (125 MHz, CD_2Cl_2) δ, ppm: 63.71, 70.91, 72.31, 76.45 ($CH_3OCH_2CH_2OCH_3$); 105.33, 120.86, 125.05, 129.35 (aryl). Calcd for $C_{16}H_{20}Cl_3N_2O_2Ta$: C 34.34, H 3.60, N 5.01; Found: C 34.57, H 3.66, N 4.99 %.

Synthesis of (κ^2-$CH_3O(CH_2)_2OCH_3$)$NbCl_3(NNPh_2)$ (5.2). $NbCl_5$ (160 mg, 0.6 mmol) and $ZnCl_2$ (162 mg, 1.2 mmol) were mixed in 10 mL CH_2Cl_2 in an inert atmosphere glovebox. Dimethoxyethane (.2 mL) was added to the reaction mixture and stirred for 15 minutes, yielding a dark solution with a yellowish precipitate. The reaction was cooled to -30 °C and 1,1-diphenylhydrazine (110 mg, 0.6 mmol) and pyridine (94 mg, 96 μL, 1.2 mmol) in 2 mL CH_2Cl_2 were slowly added to the reaction mixture. The mixture turned dark blue/green, and was left to stir overnight, during which period it turned dark green with a white precipitate. The reaction was then filtered and CH_2Cl_2 removed *in vacuo*. The resulting green residue was washed with pentane, then dissolved into 10 mL benzene, filtered, and then lyophilized to yield **5.2** as 220 mg (78%) of a dull green powder. ^{1}H NMR (300 MHz, CD_2Cl_2) δ, ppm: 3.840 (s, 3H, OC*H*$_3$); 3.944 (s, 3H, OC*H*$_3$); 4.089 (s, 4H, OC*H*$_2$); 7.166 (m, 2H, aryl); 7.454 (m, 8H, aryl). ^{13}C NMR (125 MHz, CD_2Cl_2) δ, ppm: 63.22, 69.68, 72.08, 76.01 ($CH_3OCH_2CH_2OCH_3$); 120.90, 126.10, 129.70, 143.03 (aryl).

Synthesis of $(py)_2TaCl_3(NNPh_2)$ (5.3). 5.1 (72 mg, .13 mmol) was dissolved in 1 mL neat pyridine and stirred overnight. The reaction quickly turned very dark green/blue. After 16 hours, the reaction was filtered and solvent removed *in vacuo* to give **5.3** quantitatively as a dark teal solid. ^{1}H NMR (500 MHz, CD_2Cl_2) δ, ppm: 7.02 (m, 2H,

aryl); 7.35 (m, 8H, aryl); 7.48 (m, 6H, pyridyl); 7.86 (t, 1H, pyridyl); 7.95 (t, 1H, pyridyl); 8.64 (d, 2H, pyridyl); 9.07 (d, 2H, pyridyl). ^{13}C NMR (125 MHz, CD_2Cl_2) δ, ppm: 121.09, 124.87, 125.17, 125.46, 129.23, 139.85, 140.58, 143.17, 152.42, 152.75 (aryl).

Synthesis of (tmeda)$TaCl_3(NNPh_2)$ (5.4). 5.1 (60 mg, .1 mmol) was dissolved in 1 mL neat TMEDA. The reaction turned dark blue and was stirred overnight. The reaction mixture was filtered and solvent removed *in vacuo* to give **5.4** as a dark blue solid (52 mg, 90%). ^{1}H NMR (500 MHz, CD_2Cl_2) δ, ppm: 2.571 (s, 12H, N(C*H*$_3$)$_2$); 2.705 (s, 4H, NC*H*$_2$); 6.604 (m, 2H, aryl); 7.254 (m, 8H, aryl). ^{13}C NMR (125 MHz, CD_2Cl_2) δ, ppm: 48.08 (N*C*H$_3$); 57.37 (N*C*H$_2$); 118.14, 121.27, 124.88, 143.78 (aryl).

Synthesis of (bpy)$TaCl_3(NNPh_2)$ (5.5). 5.1 (28 mg, .05 mmol) in 2 mL C_6H_6 was added to solid 2,2'-bipyridine (78 mg, .5 mmol) and stirred overnight. The reaction slowly turned green. After 16 hours, the reaction was filtered, solvent removed *in vacuo,* and the remaining green residue was washed successively with 3 5 mL portions of pentane to give **5.5** as a green solid. ^{1}H NMR (300 MHz, CD_2Cl_2) δ, ppm: 7.04 (t, 2H, aryl); 7.39 (m, 4H, aryl); 7.50 (t, 1H, bpy); 7.58 (d, 4H, aryl); 7.90 (t, 1H, bpy); 8.23 (m, 2H, bpy); 8.31 (m, 2H, bpy); 9.08 (d, 1H, bpy); 9.69 (d, 1H, bpy).

Synthesis of (THF)$_2TaCl_3(NNPh_2)$ (5.6). 5.1 (20 mg, .036 mmol) was dissolved in 2 mL THF and stirred for 20 minutes. The reaction mixture turned from blue to purple, and solvent was removed *in vacuo* to yield **5.6** and some decomposition products. **5.6** is not stable in solution, which precludes its pure isolation, but can quickly be characterized by ^{1}H NMR. ^{1}H NMR (300 MHz, CD_2Cl_2) δ, ppm: 1.95 (br, 8H, C*H*$_2$CH$_2$O); 4.20 (br, 8H, CH$_2$C*H*$_2$O); 7.02 (m, 2H, aryl); 7.39 (m, 8H, aryl).

Synthesis of $Cp_2TaCl(NNPh_2)$ (5.7). Solid **5.1** (91 mg, .163 mmol) and NaCp (28.4 mg, .326 mmol) were placed in a 50 mL round bottom flask fitted with a needle valve and evacuated on a high vacuum line. 20 mL THF was distilled onto the mixture at −78 °C, then the reaction mixture was warmed to room temperature and stirred overnight. Afterwards, the reaction mixture was filtered, solvent removed *in vacuo*, and the resulting red residue was extracted into 20 mL toluene. Removal of the toluene *in vacuo* yielded 60 mg (70% yield) of **5.7** as an orange/red solid. Further purification could be obtained by layering pentane onto a concentrated, −30 °C solution of **5.7** in toluene which gave high yields of orange, X-ray quality crystals of **5.7** upon cooling the system to −30 °C. ^{1}H NMR (300 MHz, CD_2Cl_2) δ, ppm: 5.990 (s, 10H, C_5H_5); 7.064 (m, 2H, aryl); 7.356 (m, 8H, aryl). ^{13}C NMR (125 MHz, C_6D_6) δ, ppm: 110.09 (C_5H_5); 121.47, 124.36, 129.67, 145.46 (aryl).

Synthesis of $(2,6\text{-}(OC_6H_2\text{-}^tBu_2)_2C_5H_3N)TaCl(NNPh_2)(py)$ (5.8). $(ONO)H_2$ (194.5 mg, .4 mmol) was deprotonated with KBn (104.2 mg, .8 mmol) in 10 mL C_6H_6 over the course of two hours in an inert atmosphere glovebox. After two hours, $(dme)TaCl_3(NNPh_2)$ (244 mg, .4 mmol) and pyridine (31.6 mg, .4 mmol) in 10 mL C_6H_6 was added to the reaction mixture. The reaction was stirred for 24 hours, filtered, and solvent removed *in vacuo*. The resulting orange residue was washed with pentane, yielding **5.8** as 350 mg (91%) of a yellow/orange solid. Yellow/orange crystals suitable for X-ray diffraction were obtained through pentane vapor diffusion into a concentrated CH_2Cl_2 solution. ^{1}H NMR (300 MHz, CD_2Cl_2) δ, ppm: 1.28 (s, 18H, $C(CH_3)_3$); 1.42 (s, 18H, $C(CH_3)_3$); 6.87 (m, 8H, aryl); 7.03 (m, 4H, aryl); 7.20 (s, 2H, aryl); 7.38 (s, 2H, aryl); 7.49 (t, 1H,

pyridyl); 7.69 (d, 2H, pyridyl); 7.91 (t, 1H, pyridyl); 8.30 (d, 2H, pyridyl). ^{13}C NMR (125 MHz, C_6D_6) δ, ppm: 30.40 (C(*C*H$_3$)$_3$); 31.91 (C(*C*H$_3$)$_3$); 34.66 (*C*(*C*H$_3$)$_3$); 35.58 (*C*(*C*H$_3$)$_3$); 120.12, 122.96, 123.69, 124.10, 124.63, 125.80, 126.79, 128.85, 136.85, 138.53, 138.86, 141.39, 145.21, 150.53, 155.55, 159.17 (aryl).

Synthesis of (2,6-(OC$_6$H$_2$-^{t}Bu$_2$)$_2$C$_5$H$_3$N)TaCl(NNMe$_2$)(HNMe$_2$) (5.9). A 10 mL glass tube fitted with a teflon needle valve was charged with (ONO)Ta(NMe$_2$)$_2$Cl (106 mg, .135 mmol), H$_2$NNMe$_2$ (8.08 mg, 10.2 μL, .135 mmol), a stirbar and 5 mL C_6H_6 in an inert atmosphere glovebox. The vessel was sealed and placed in an oilbath preheated to 90 °C and left to stir for three days, where it turned orange/red. After three days, the solvent and HNMe$_2$ were removed *in vacuo* and the yellow-orange residue was washed with 20 mL hexanes to yield 50 mg **5.9** as a yellow-orange powder (43%). ^{1}H NMR (300 MHz, CD_2Cl_2) δ, ppm: 1.344 (s, 18H, C(C*H*$_3$)$_3$); 1.489 (s, 18H, C(C*H*$_3$)$_3$); 1.905 (br s, 6H, HN(C*H*$_3$)$_2$); 2.082 (s, 6H, NN(C*H*$_3$)$_2$); 2.433 (m, 1H, *H*NMe$_2$); 7.358 (d, 2H, aryl); 7.497 (d, 2H, aryl); 7.758 (d, 2H, pyridyl); 8.009 (t, 1H, pyridyl). ^{13}C NMR (125 MHz, C_6D_6) δ, ppm: 30.48 (C(*C*H$_3$)$_3$); 31.94 (C(*C*H$_3$)$_3$); 34.84 (*C*Me$_3$); 35.66 (*C*Me$_3$); 38.57 (HN(*C*H$_3$)$_2$); 47.97 (NN(*C*H$_3$)$_2$); 124.33, 124.91, 126.42, 127.02, 128.85, 137.41, 141.95, 157.94, 158.92 (aryl).

Synthesis of (κ^3-MeN[(CH$_2$)$_2$NTMS)]$_2$)TaCl(NNPh$_2$) (5.10). MeN[(CH$_2$)$_2$NTMS)]$_2$Li$_2$ (418 mg, 1.53 mmol) and (dme)TaCl$_3$(NNPh$_2$) (856 mg, 1.53 mmol) were mixed in 20 mL C_6H_6 in an inert atmosphere glovebox. The reaction quickly turned from dark blue to deep orange, and was left to stir overnight. The reaction was filtered and the benzene lyophilized off, and the orange residue was extracted into 60 mL

pentane. The pentane was removed *in vacuo* to yield 720 mg (71%) of **5.10** as a sticky orange solid. Crystals suitable for X-ray diffraction were grown from vapor diffusion out of a concentrated hexanes solution into TMS_2O. ^1H NMR (500 MHz, CD_2Cl_2) δ, ppm: 0.03 (s, 18H, $NSi(CH_3)_3$); 2.76 (s, 3H, NCH_3); 2.79 (m, 2H $-CHHCH_2-$); 3.15 (m, 2H $-CHHCH_2-$); 3.83 (m, 2H, $-CH_2CHH-$); 3.91 (m, 2H, $-CH_2CHH-$); 6.90 (t, 2H, aryl); 7.26 (m, 4H, aryl); 7.45 (d, 4H, aryl). ^{13}CNMR (125MHz, C_6D_6) δ, ppm: 1.834 ($Si(CH_3)_3$); 45.87 (NCH_3); 49.59 (NCH_2CH_2); 57.54 (NCH_2CH_2); 119.83, 122.19, 128.84, 144.10 Calcd for $C_{23}H_{39}ClN_5Si_2Ta$: C 41.97, H 5.97, N 10.64; Found: C 42.49, H 6.43, N 9.99 %.

Synthesis of (κ^3-MeN[$(CH_2)_3$NTMS)]$_2$)TaCl(NNPh$_2$) (5.11). $MeN[(CH_2)_3NTMS)]_2Li_2$ (94.3 mg, .313 mmol) and $(dme)TaCl_3(NNPh_2)$ (175 mg, .313 mmol) were mixed in 10 mL C_6H_6 in an inert atmosphere glovebox. The reaction quickly turned from dark blue to deep orange/red, and was left to stir overnight. The reaction was filtered and solvent removed *in vacuo*, and the resulting orange residue was washed with pentane. **5.11** was crystallized by vapor diffusion of pentane into a concentrated solution of **5.11** in CH_2Cl_2, yielding 40% as orange/red crystals. ^1H NMR (300 MHz, CD_2Cl_2) δ, ppm: 0.172 (br s, 18H, $NSi(CH_3)_3$); 1.654 (br m, 4H, $-CH_2CH_2CH_2-$); 2.853 (s, 3H, NCH_3); 3.446 (br m, 8H, $-CH_2CH_2CH_2-$); 6.962 (m, 2H, aryl); 7.315 (m, 8H, aryl). ^{13}C NMR (125 MHz, C_6D_6) δ, ppm: 1.07 ($Si(CH_3)_3$); 27.85 ($-CH_2-$); 53.18 (NCH_3); 120.70, 123.37, 129.27, 146.29 (aryl). Calcd for $C_{25}H_{43}ClN_5Si_2Ta$: C 43.76, H 6.32, N 10.21; Found: C 42.50, H 6.49, N 9.99 %.

Synthesis of [(κ^3-MeN[$(CH_2)_2$NTMS)]$_2$)Ta(py)(NNPh$_2$)][B(3,5-$(CF_3)_2C_6H_3)_4$] (5.12). 5.10 (160 mg, .243 mmol) and pyridine (19.2 mg, 19.6 µL, .243 mmol) were

premixed in an inert atmosphere glovebox in 4 mL CH_2Cl_2. The solution of **5.10** and pyridine was then added to solid $Na^+[BArF_{24}]^-$ (215.5 mg, .243 mmol). The reaction mixture quickly turned from yellow to orange as the $Na^+[BArF_{24}]^-$ went into solution. The reaction mixture was stirred for 30 minutes then the solvent was removed *in vacuo*. The dark orange residue was washed with pentane, yielding 346 mg **5.12** (91%) as a dark orange/red solid. ^{1}H NMR (500 MHz, CD_2Cl_2) δ, ppm: .207 (s, 18H, Si(C*H*$_3$)$_3$); 2.035 (s, 3H, NC*H*$_3$); 2.712 (m, 4H, NC*H*$_2$CH$_2$); 4.124 (m, 2H, NC*H*$_2$CH$_2$); 4.256 (m, 2H, NC*H*HCH$_2$); 6.281 (d, 4H, *o*-C_6H_5); 6.801 (t, 2H, *p*-C_6H_5); 6.871 (m, 4H *m*-C_6H_5); 7.570 (s, 4H, *p*-$C_6H_3(CF_3)_2$); 7.738 (s, 8H, *o*-$C_6H_3(CF_3)_2$); 8.205 (t, 1H, pyridyl); 8.831 (d, 2H, pyridyl); 8.950 (br, 2H, pyridyl). ^{13}C NMR (125 MHz, C_6D_6) δ, ppm: Calcd for $C_{60}H_{56}BF_{24}N_6Si_2Ta$: C 46.05, H 3.61, N 5.37; Found: C 46.22, H 3.56, N 5.44%.

Synthesis of (BDI)TaCl$_2$(NNPh$_2$) (5.14). A slurry of (BDI)Li(THF) (366.4 mg, .738 mmol) and (dme)$TaCl_3$(NNPh$_2$) (413 mg, .738 mmol) in 20 mL Et_2O was stirred overnight. The reaction slowly turned from colorless with a blue solid to green with a white precipitate. After 12 hours, the reaction was filtered and Et_2O removed *in vacuo*; the resultant green residue was extracted into minimal Et_2O and filtered again to remove residual LiCl. The solution was then layered with an equal volume of pentane and cooled to −30 °C, which overnight yielded 180 mg (29%) of dark green block crystals of **5.14**. The yield could be increased by further crystallization of the supernatant. ^{1}H NMR (300 MHz, CD_2Cl_2) δ, ppm: 0.94 (d, 6H, ArCH(C*H*$_3$)(CH$_3$)); 1.00 (d, 6H, ArCH(C*H*$_3$)(CH$_3$)); 1.13 (d, 6H, ArCH(C*H*$_3$)(CH$_3$)); 1.32 (d, 6H, ArCH(C*H*$_3$)(CH$_3$)); 1.87 (s, 6H, C*H*$_3$); 2.84 (sept, 2H, ArC*H*(CH$_3$)(CH$_3$)); 3.17 (sept, 2H, ArC*H*(CH$_3$)(CH$_3$)); 6.95-7.50 (m, 16H, aryl).

Synthesis of (BDI)$NbCl_2(NNPh_2)$ (5.15). The same procedure was utilized as in **5.14**, starting from (dme)$NbCl_2(NNPh_2)$ yielded **5.15** as small red block crystals. ^{1}H NMR (300 MHz, C_6D_6) δ, ppm: 0.96 (br d, 6H, ArCH(C*H*$_3$)(CH_3)); 1.05 (br d, 6H, ArCH(C*H*$_3$)(CH_3)); 1.18 (br d, 6H, ArCH(C*H*$_3$)(CH_3)); 1.37 (br d, 6H, ArCH(C*H*$_3$)(CH_3)); 1.57 (br s, 6H, C*H*$_3$); 2.98 (br m, 2H, ArC*H*(CH_3)(CH_3)); 3.21 (br m, 2H, ArC*H*(CH_3)(CH_3)); 6.95–7.50 (m, 16H, aryl).

Synthesis of (BDI)$TaCl_2(NNPh_2)$(py) (5.16). In an NMR tube, 20 mg **5.14** was dissolved in .7 mL CD_2Cl_2 and 50 µL pyridine was added. The solution quickly turned from dark green to olive green. ^{1}H NMR (300 MHz, CD_2Cl_2) δ, ppm: 1.01 (d, 6H, ArCH(C*H*$_3$)(CH_3)); 1.15 (d, 6H, ArCH(C*H*$_3$)(CH_3)); 1.37 (d, 6H, ArCH(C*H*$_3$)(CH_3)); 1.51 (d, 6H, ArCH(C*H*$_3$)(CH_3)); 1.65 (s, 3H, C*H*$_3$); 1.86 (s, 3H, C*H*$_3$); 3.84 (sept, 2H, ArC*H*(CH_3)(CH_3)); 4.19 (sept, 2H, ArC*H*(CH_3)(CH_3)); 6.95–7.50 (m, aryl).

Synthesis of (BDI)$NbCl_2(NNMe_2)$(THF) (5.17). The same procedure was utilized as in **5.14**, starting from (dme)$NbCl_2(NNMe_2)$ yielded **5.17** as orange crystals.

Synthesis of (N_3N)Ta($NNPh_2$) (5.18). (dme)$TaCl_3(NNPh_2)$ (331 mg, .59 mmol) and (N_3N)Li_3 (121.9 mg, .59 mmol) were slurried in 20 mL Et_2O and stirred overnight. The reaction slowly turned green with a white precipitate. After 12 hours, the reaction was filtered through celite and Et_2O was removed *in vacuo* yielding **5.18** as a green solid. ^{1}H NMR (300 MHz, CD_2Cl_2) δ, ppm: 2.99 (*t*, 6H, C*H*$_2$); 3.36 (*s*, 9H, NC*H*$_3$); 3.40 (*t*, 6H, C*H*$_2$); 6.98 (*m*, 2H, aryl); 7.36 (*m*, 8H, aryl).

Synthesis of (N_3N)Nb($NNPh_2$) (5.19). A similar procedure to **5.18** was utilized, starting from (dme)$NbCl_3(NNPh_2)$ and yielding **5.19** as a green solid. ^{1}H NMR

(300 MHz, CD_2Cl_2) δ, ppm: 3.00 (*t*, 6H, C*H*$_2$); 3.33 (*t* + *s*, 6H + 9H, C*H*$_2$ + NC*H*$_3$); 7.06 (*m*, 2H, aryl); 7.40 (*m*, 8H, aryl).

Synthesis of (N_3N)Nb($NNMe_2$) (5.20). A similar procedure to **5.18** was utilized, starting from (dme)$NbCl_3$($NNMe_2$) and yielding **5.20** as a green solid. ^{1}H NMR (300 MHz, CD_2Cl_2) δ, ppm: 2.77 (*s*, 6H, N(C*H*$_3$)$_2$); 2.89 (*t*, 6H, C*H*$_2$); 3.21 (*t*, 6H, C*H*$_2$); 3.44 (*s*, 9H, NC*H*$_3$).

Table 5.2. Crystal and refinement data for complexes **5.1**, **5.2**, and **5.7**.

	5.1	**5.2**	**5.7**
CCDC Number	719414	853697	767430
Empirical formula	$C_{16}H_{20}N_2O_2Cl_3Ta$	$C_{16}H_{20}Cl_3N_2O_2Nb$	$C_{22}H_{20}N_2ClTa$
Formula weight	559.64	471.60	528.80
T (K)	100(2)	100(2)	100(2)
a, Å	13.4839(6)	10.9592(4)	19.1261(8)
b, Å	10.2768(4)	14.1496(5)	10.2503(4)
c, Å	14.8254(7)	12.5713(4)	19.2383(8)
α, deg			
β, deg	108.079(2)	91.137(2)°	100.720(2)
γ, deg			
Volume, Å^3	1952.95(15)	1949.03(12)	3705.8(3)
Z	4	4	8
Crystal system	Monoclinic	Monoclinic	Monoclinic
Space group	$P2_1/c$	$P\,n$	$P2_1/n$
d_{calc}, g/cm^3	1.903	1.607	1.896
θ range, deg	1.59 to 52.22	2.17 to 36.16	2.26 to 40.86
μ, mm^{-1}	6.049	1.039	6.084
Abs. Correction	Semi Emp.	None	Semi Emp.
GOF	1.388	1.369	1.495
R_1 ,[a] wR_2 [b] [I>2σ(I)]	0.0285, 0.0362	0.0290, 0.0421	0.0271, 0.0400

[a] $R_1 = \Sigma||F_o| - |F_c||/\Sigma|F_o|$. [b] $wR_2 = [\Sigma[w(F_o^2-F_c^2)^2]/\Sigma[w(F_o^2)^2]]^{1/2}$.

Table 5.3. Crystal and refinement data for complexes **5.8**, **5.9** and **5.10**.

	5.8	**5.9**	**5.10**
CCDC Number	719322	695847	752439
Empirical formula	$C_{50}H_{58}N_4O_2ClTa$	$C_{37}H_{56}N_4O_2ClTa$	$C_{23}H_{39}N_5Si_2ClTa$
Formula weight	963.40	805.26	658.17
T (K)	100(2)	100(2)	100(2)
a, Å	15.6102(8)	34.7022(12)	13.1052(6)
b, Å	20.2128(10)	9.2582(3)	12.9574(6)
c, Å	15.7963(8)	23.1835(9)	16.9529(8)
α, deg			
β, deg	113.066(3)		90.622(3)
γ, deg			
Volume, Å^3	4585.7(4)	7448.4(5)	2878.6(2)
Z	4	8	4
Crystal system	Monoclinic	Orthorhombic	Monoclinic
Space group	$P2_1/c$	P*bcn*	$P2_1/n$
d_{calc}, g/cm^3	1.395	1.436	1.519
θ range, deg	1.73 to 40.11	1.76 to 36.42	1.95 to 43.76
μ, mm^{-1}	2.498	3.059	4.014
Abs. Correction	Semi Emp.	None	Semi Emp.
GOF	1.718	1.939	2.205
R_1 ,[a] wR_2 [b] [I>2σ(I)]	0.0250, 0.0380	0.0401, 0.0439	0.0285, 0.0506

[a] $R_1 = \Sigma||F_o| - |F_c||/\Sigma|F_o|$. [b] $wR_2 = [\Sigma[w(F_o^2-F_c^2)^2]/\Sigma[w(F_o^2)^2]]^{1/2}$.

Table 5.4. Crystal and refinement data for complexes **5.11**, **5.13** and **5.14**.

	5.11	**5.13**	**5.14**
CCDC Number	719036	739782	856242
Empirical formula	$C_{25}H_{43}N_5Si_2ClTa$	$[C_{33}H_{49}N_7Si_2Ta]^+$ $[C_{32}H_{12}BF_{24}]^-$	$C_{41}H_{51}N_4Cl_2Ta$
Formula weight	686.22	1644.15	851.71
T (K)	98(2)	100(2)	100(2)
a, Å	8.1959(4)	22.0650(16)	12.0036(3)
b, Å	10.4496(5)	13.9417(10)	20.3429(6)
c, Å	34.5115(14)	24.4542(16)	16.0909(4)
α, deg			
β, deg	94.059(2)	114.312(4)	99.712(2)
γ, deg			
Volume, Å^3	2948.3(2)	6855.6(8)	3872.89(18)
Z	4	4	4
Crystal system	Monoclinic	Monoclinic	Monoclinic
Space group	$P2_1/n$	$P2_1/n$	$P2_1/n$
d_{calc}, g/cm^3	1.546	1.593	1.461
θ range, deg	2.04 to 38.82	1.62 to 27.70	1.63 to 27.57
μ, mm^{-1}	3.922	1.750	3.009
Abs. Correction	Semi Emp.	Semi Emp.	Semi Emp.
GOF	1.754	1.652	1.689
R_1 ,[a] wR_2 [b] [I>2σ(I)]	0.0235, 0.0341	0.0387, 0.0666	0.0363, 0.0517

[a] $R_1 = \Sigma||F_o| - |F_c||/\Sigma|F_o|$. [b] $wR_2 = [\Sigma[w(F_o^2-F_c^2)^2]/\Sigma[w(F_o^2)^2]]^{1/2}$.

Table 5.5. Crystal and refinement data for complexes **5.15** and **5.17**.

	5.15	**5.17**
CCDC Number	855002	855261
Empirical formula	$C_{41}H_{51}N_4Cl_2Nb$	$C_{35}H_{55}N_4OCl_2Nb$
Formula weight	763.67	711.64
T (K)	100(2)	100(2)
a, Å	11.9696(5)	20.2667(18)
b, Å	20.2795(9)	15.2998(13)
c, Å	16.1021(7)	23.718(2)
α, deg		
β, deg	99.827(2)	
γ, deg		
Volume, Å^3	3851.2(3)	7354.4(11)
Z	4	10
Crystal system	Monoclinic	Orthorhombic
Space group	P $2_1/n$	P *bca*
d_{calc}, g/cm^3	1.317	1.285
θ range, deg	1.97 to 46.95	2.01 to 31.38
μ, mm^{-1}	0.485	0.504
Abs. Correction	None	None
GOF	1.687	2.739
R_1 ,[a] wR_2 [b] [I>2σ(I)]	0.0278, 0.0452	0.0570, 0.0789

[a] $R_1 = \Sigma||F_o| - |F_c||/\Sigma|F_o|$. [b] $wR_2 = [\Sigma[w(F_o^2-F_c^2)^2]/\Sigma[w(F_o^2)^2]]^{1/2}$.

REFERENCES

1. (a) Fryzuk, M. D.; Johnson, S. A. *Coord. Chem. Rev.* **2000**, *200*, 379. (b) MacKay, B. A.; Fryzuk, M. D. *Chem. Rev,* **2004**, *104*, 385.
2. Chatt, J.; Dilworth, J. R.; Richards, R. L. *Chem. Rev.* **1978**, *78*, 589.
3. For representative examples, see: (a) Banerjee, S.; Odom, A. L. *Dalton Trans.* **2008**, 2005. (b) Yandulov, D. V.; Schrock, R. R. *Science* **2003**, *301*, 76. (c) Schrock, R. R.; Glassman, T. E.; Vale, M. G.; Kol, M. *J. Am. Chem. Soc.* **1993**, *115*, 1760. (d) Dilworth, J. P.; Jobanputra, P.; Parrott, S. J.; Thompson, R. M.; Povey, D. C.; Zubieta, J. A. *Polyhedron* **1992**, *11*, 147. (e) Huynh, M. H. V.; Lee, D. G.; White, P. S.; Meyer, T. J. *Inorg. Chem.* **2001**, *40*, 3842. (f) Huynh, M. H. V.; El-Samanody, E. S.; Demadis, K. D.; White, P. S.; Meyer, T. J. *Inorg. Chem.* **2000**, *39*, 3075. (g) Coia, G M.; Devenney, M.; White, P. S.; Meyer, T. J. *Inorg. Chem.* **1997**, *36*, 2341.
4. Walsh, P. J.; Carney, M. J.; Bergman, R. G. *J. Am. Chem. Soc.* **1991**, *113*, 6343.
5. (a) Parsons, T. B.; Hazari, N.; Cowley, A. R.; Green, J. C.; Mountford, P. *Inorg. Chem.* **2005**, *44*, 8442. (b) Selby, J. D.; Manley, C. D.; Feliz, M.; Schwarz, A. D.; Clot, E.; Mountford, P. *J. Chem. Soc., Chem. Commun.* **2007**, 4937. (c) Selby, J. D.; Schulten, C.; Schwarz, A. D.; Stasch, A.; Clot, E.; Jones, C.; Mountford, P. *J. Chem. Soc., Chem. Commun.* **2008**, 5101. (d) Clulow, A. J.; Selby, J. D.; Cushion, M. G.; Schwarz, A. D.; Mountford, P. *Inorg. Chem.* **2008**, *47*, 12049. (e) Selby, J. D.; Manley, C. D.; Schwarz, A. D.; Clot, E.; Mountford, P. *Organometallics* **2008**, *27*, 6479.
6. (a) Li, Y.; Shi, Y.; Odom, A. L. *J. Am. Chem. Soc.* **2004**, *126*, 1794. (b) Patel, S.; Li, Y.; Odom, A. L. *Inorg. Chem.* **2007**, *46*, 6373.
7. (a) Herrmann, H.; Fillol, J. L.; Wadepohl, H.; Gade, L. H. *Angew. Chem. Int. Ed. Eng.* **2007**, *46*, 8426. (b) Herrmann, H.; Fillol, J. L.;Gehrmann, T.; Enders, M.; Wadepohl, H.; Gade, L. H. *Chem. Eur. J.* **2008**, *14*, 8131. (c) Herrmann, H.; Wadepohl, H.; Gade, L. H. *J. Chem. Soc., Dalton Trans.* **2008**, 2111. (d) Herrman, H.; Gehrmann, T.; Wadepohl, H.; Gade, L. H. *J. Chem. Soc., Dalton Trans.* **2008**, 6231. (e) Weitershaus, K.; Wadepohl, H.; Gade, L. H. *Organometallics*, **2009**, *28*, 3381. (f) Weitershaus, K.; Fillol, J. L.; Wadepohl, H.; Gade, L. H. *Organometallics*, **2009**, *28*, 4747.
8. Mindiola, D. J. *Angew. Chem. Int. Ed. Eng.* **2008**, *47*, 2.

9. (a) Fryzuk, M. D. *Acc. Chem. Res.* **2009**, *42*, 127. (b) Shaver, M. P.; Fryzuk, M. D. *J. Am. Chem. Soc*. **2005**, *127*, 500. (c) MacKay, B. A.; Munha, R. F.; Fryzuk, M. D. *J. Am. Chem. Soc.* **2006**, *128*, 9472.
10. (a) Davies, S. C.; Hughes, D. L.; Janas, Z.; Jerzykiewicz, L.; Richards, R. L.; Sanders, J. R.; Sobota, P. *Chem. Commun.* **1997**, 1261. (b) Henderson, R. A.; Janas, Z.; Jerzykiewicz, L. B.; Richards, R. L.; Sobota, P. *Inorg. Chim. Acta* **1999**, *285*, 178. (c) Davies, S. C.; Hughes, D. L.; Janas, Z.; Jerzykiewicz, L.; Richards, R. L.; Sanders, J. R.; Silverston, J. E.; Sobota, P. *Inorg Chem.* **2000**, *39*, 3485. (d) Davies, S. C.; Hughes, D. L.; Konkol, M.; Richards, R. L.; Sanders, J. R.; Sobota, P. *J. Chem. Soc., Dalton Trans.* **2002**, 2811.
11. Green, M. L. H.; James, J. T.; Saunders, J. F.; Souter, J. *J. Chem. Soc. Dalton Trans.*, **1997**, 1281.
12. Sebe, E.; Heeg, M. J.; Winter, C. H. *Polyhedron*, **2006**, *25*, 2109.
13. Korolev, A. V.; Rheingold, A. L.; Williams, D. S. *Inorg. Chem.* **1997**, *36*, 2647.
14. In all of the schemes in this section, Imido ligands (LX_2) will be drawn as triple bonds since these representations most accurately describe the bonding within these systems (as evidenced by simple electron counting and DFT calculations), despite this notation not being the normal convention.
15. Danopoulos, A. A.; Hay-Motherwell, R. S.; Wilkinson, G.; Sweet, T. K. N.; Hursthouse, M. B. *Polyhedron*, **1997**, *16*, 1081.
16. Williams, D. S.; Thompson, D. W.; Korolev, A. V.; *J. Am. Chem. Soc.* **1996**, *118*, 6526.
17. Williams, D. S.; Korolev, A. V. *Inorg. Chem.* **1998**, *37*, 3809.
18. One reviewer pointed out that in the $NNPh_2$ case, in addition to the lone pair effect, delocalization into the aryl rings may play an important role in the HOMO. Our DFT calculations show that there appears to be contribution from the aryl π system. This is further supported by some related tungsten complexes, where the diphenylhydrazidos have a very low energy LMCT when compared to the dialkylhydrazidos; see Koller, J.; Ajmera, H. M.; Abboud, K. A.; Anderson, T. J.; McElwee-White, L. *Inorg. Chem.* **2008**, *47*, 4457. We are currently investigating this effect as it relates to other heteroatom substituted imido derivatives.
19. Parkin, G.; van Asselt, A.; Leahy, D. J.; Whinnery, L.; Hua, N. G.; Quan, R. W.; Henling, L. M.; Schaefer, W. P.; Santarsiero, B. D.; Bercaw, J. E. *Inorg. Chem.* **1992**, *31*, 82.

20. (a) Tonks, I. A.; Henling, L. M.; Day, M. W.; Bercaw, J. E. *Inorg. Chem.* **2009**, *48*, 5096. (b) Agapie, T.; Bercaw, J. E. *Organometallics* **2007**, *26*, 2957–2959. (c) Agapie, T.; Day, M. W.; Bercaw, J. E. *Organometallics* **2008**, *27*, 6123–6142. (d) Agapie, T.; Henling, L. H.; DiPasquale, A. G.; Rheingold, A. L.; Bercaw, J. E. *Organometallics* **2008**, *27*, 6245–6246. (e) Golisz, S. R.; Bercaw, J. E. *Macromolecules* **2009**, *42*, 8751.
21. Tomson, N. C.; Arnold, J.; Bergman, R. G. *Organometallics* **2010**, *29*, 2926.
22. Pangborn, A. B.; Giardello, M. A.; Grubbs, R. H.; Rosen, R. K.; Timmers, F. J. *Organometallics*, **1996**, *15*, 1518.
23. Brookhart, M.; Grant, B.; Volpe Jr., A. F.; *Organometallics*, **1992**, *11*, 3920.
24. Panda, T. K.; Gamer, M. T.; Roesky, P. W. *Organometallics*, **2003**, *22*, 877–878.
25. Budzelaar, P. H. M.; van Oort, A. B.; Orpen, A. G. *Eur. J. Inorg. Chem.* **1998**, 1485.
26. Frisch, M. J.; Trucks, G. W.; Schlegel, H. B.; Scuseria, G. E.; Robb, M. A.; Cheeseman, J. R.; Montgomery, Jr., J. A.; Vreven, T.; Kudin, K. N.; Burant, J. C.; Millam, J. M.; Iyengar, S. S.; Tomasi, J.; Barone, V.; Mennucci, B.; Cossi, M.; Scalmani, G.; Rega, N.; Petersson, G. A.; Nakatsuji, H.; Hada, M.; Ehara, M.; Toyota, K.; Fukuda, R.; Hasegawa, J.; Ishida, M.; Nakajima, T.; Honda, Y.; Kitao, O.; Nakai, H.; Klene, M.; Li, X.; Knox, J. E.; Hratchian, H. P.; Cross, J. B.; Bakken, V.; Adamo, C.; Jaramillo, J.; Gomperts, R.; Stratmann, R. E.; Yazyev, O.; Austin, A. J.; Cammi, R.; Pomelli, C.; Ochterski, J. W.; Ayala, P. Y.; Morokuma, K.; Voth, G. A.; Salvador, P.; Dannenberg, J. J.; Zakrzewski, V. G.; Dapprich, S.; Daniels, A. D.; Strain, M. C.; Farkas, O.; Malick, D. K.; Rabuck, A. D.; Raghavachari, K.; Foresman, J. B.; Ortiz, J. V.; Cui, Q.; Baboul, A. G.; Clifford, S.; Cioslowski, J.; Stefanov, B. B.; Liu, G.; Liashenko, A.; Piskorz, P.; Komaromi, I.; Martin, R. L.; Fox, D. J.; Keith, T.; Al-Laham, M. A.; Peng, C. Y.; Nanayakkara, A.; Challacombe, M.; Gill, P. M. W.; Johnson, B.; Chen, W.; Wong, M. W.; Gonzalez, C.; Pople, J. A.; *Gaussian 03*, revision C.02,Gaussian, Inc., Wallingford CT, 2004.
27. Becke, A. D. *Phys. Rev. A: At., Mol., Opt. Phys.* **1988**, *38*, 3098–3100.
28. Becke, A. D. *J. Chem. Phys.* **1988**, *88*, 1053–1062.
29. Perdew, J. P. *Phys. Rev. B* **1986**, *33*, 8800–8802.
30. C. Lee, W. Yang, and R. G. Parr, *Phys. Rev. B* **37**, 785 (1988).
31. B. Miehlich, A. Savin, H. Stoll, and H. Preuss, *Chem. Phys. Lett.* **157**, 200 (1989).
32. Hay, P. J.; Wadt, W. R. *J. Chem. Phys.* **1985**, *82*, 270–283.

33. Wadt, W. R.; Hay, P. J. *J. Chem. Phys.* **1985**, *82*, 284–298.
34. Hay, P. J.; Wadt, W. R. *J. Chem. Phys.* **1985**, *82*, 299–310.

CHAPTER 6

β-Substituent Effects on the Ground State and Charge Transfer Bands of Group 5 and 6 Terminal Hydrazido(2-) Complexes

ABSTRACT

A series of colorful terminal hydrazide complexes of the type (dme)$MCl_3(NNR_2)$ (dme = 1,2-dimethoxyethane; M = Nb, Ta; R = alkyl or aryl) or (MeCN)$WCl_4(NNR_2)$ have been synthesized. Perturbing the electronic environment of the β-nitrogen significantly impacts the lowest-energy charge transition in these complexes. This effect is caused by an antibonding interaction between the N_β lone pair and the $M{=}N_\alpha$ π bond. In the group 5 cases, increasing the energy of N_β decreases the LMCT of the complex. An exception is for the electron-rich Nb alkylhydrazides, which pyramidalize N_β in order to reduce the overlap between the $Nb{=}N_\alpha$ π bond and the N_β lone pair. In the W cases increasing the energy of N_β eventually leads to reduction from a formally W^{VI} with a hydrazide(2-) ligand to a W^{IV} supported by a diazenido(0) ligand. The photophysics of these complexes highlight the importance of the difference in reduction potential between metal centers, and could lead to differences in ligand- and/or metal-based redox chemistry in early transition metal hydrazidos, especially in the context of N_2 fixation.

INTRODUCTION

End-on (κ^1-) bound hydrazide(2-) complexes of early transition metals have been identified as important intermediates in an increasingly diverse range of stoichiometric and catalytic processes. For example, one of the proposed intermediates along a Chatt-type[1] cycle of N_2 reduction is a κ^1-bound hydrazide(2-) moiety ($M{=}NNH_2$), and accordingly significant research into possible models for these intermediates based on a large range of transition metals, most notably Mo and W, has been undertaken.[2] Additionally, group 4 hydrazide(2-) complexes have been utilized for the catalytic diamination and hydrohydrazination of alkynes with 1,1-disubstituted hydrazines.[3-7]

While the chemistry of hydrazides of groups 4 and 6 has been well-studied, there has been a paucity of reports on similar group 5 complexes, in particular the heavier congeners Nb[8] and Ta.[9] In Chapter 5, we reported on the synthesis of $(dme)MCl_3(NNPh_2)$ (dme = 1,2-dimethoxyethane; M = Nb, Ta) and its use as a synthon for more elaborately-ligated $M{=}NNR_2$ complexes.[10] One notable feature of $(dme)TaCl_3(NNPh_2)$ is its blue color (λ_{max} = 585 nm), which we postulated arises from a π^* interaction between an $M{=}N_\alpha$ π bond and N_β lone pair that destabilizes the HOMO and lowers the LMCT energy (Scheme 6.1). Herein we report on our continued investigation of the photophysics of complexes of the type $(dme)MCl_3(NNR_2)$, and compare the structure-electronics relationship with a similar series of W complexes, $(MeCN)WCl_4(NNR_2)$.

Scheme 6.1

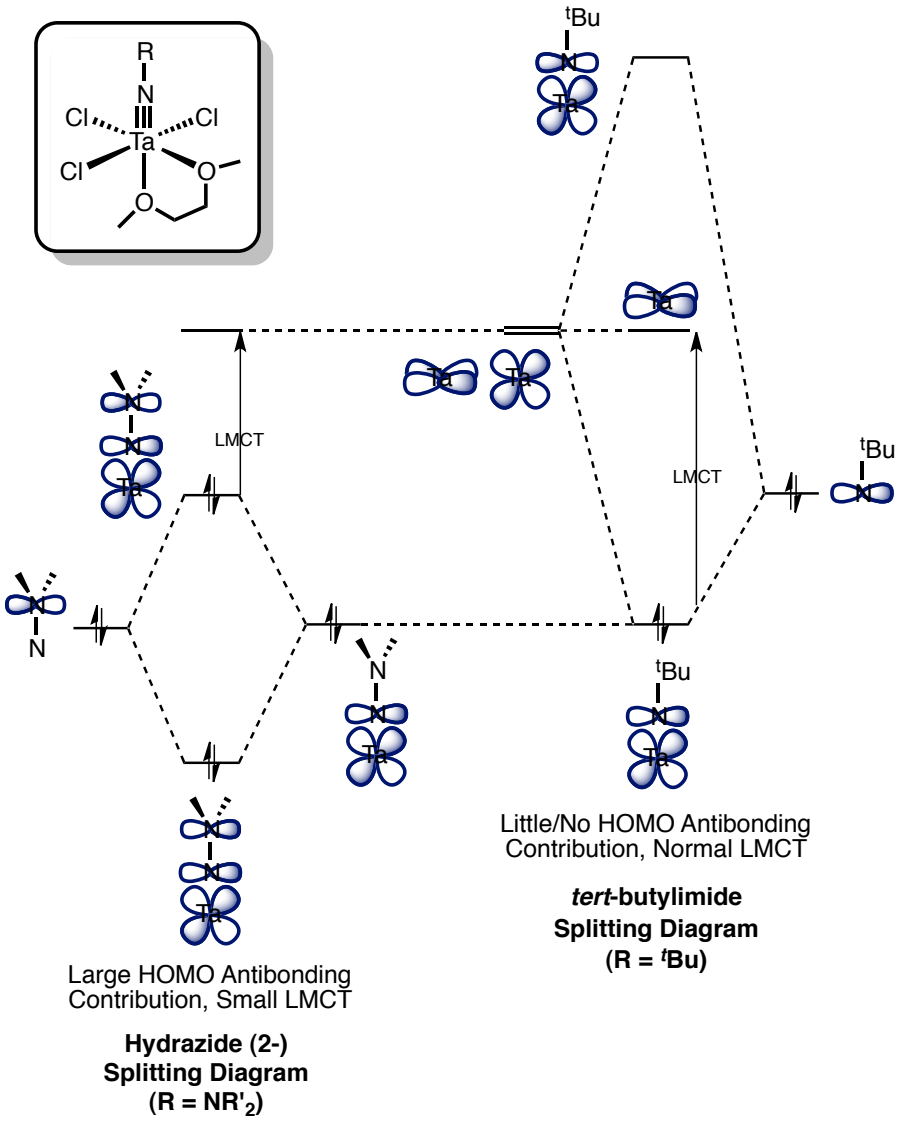
R
N
Cl
Cl
Ta
Cl
O
O
tBu
N
Ta
LMCT
LMCT
tBu
N
N
tBu
N
Ta
Little/No HOMO Antibonding
Contribution, Normal LMCT
tert-butylimide
Splitting Diagram
(R = tBu)
Large HOMO Antibonding
Contribution, Small LMCT
Hydrazide (2-)
Splitting Diagram
(R = NR'2)

Results and Discussion

The resonance Raman spectrum of (dme)$TaCl_3(NNPh_2)$ (**6.1d**) excited into the 585 nm band (Figure 6.1) shows enhancement of the Ta–N, N–N, and aryl stretches. This enhancement confirms our assignment of this low energy band as a charge transfer between Ta and the hydrazido ligand. Significantly, the Raman spectrum also indicates that there is contribution of the aryl system in the HOMO, which led us to further investigate the effect of substituted arylhydrazides on the charge transfer. We hypothesized that by tuning the electronics of N_β it would be possible to change the formal donor ability of the [NNR_2] moiety from a dianionic hydrazido(2–) ligand to a neutral diazenido(0) ligand, thereby accessing a new, 2-electron "redox noninnocent" manifold.

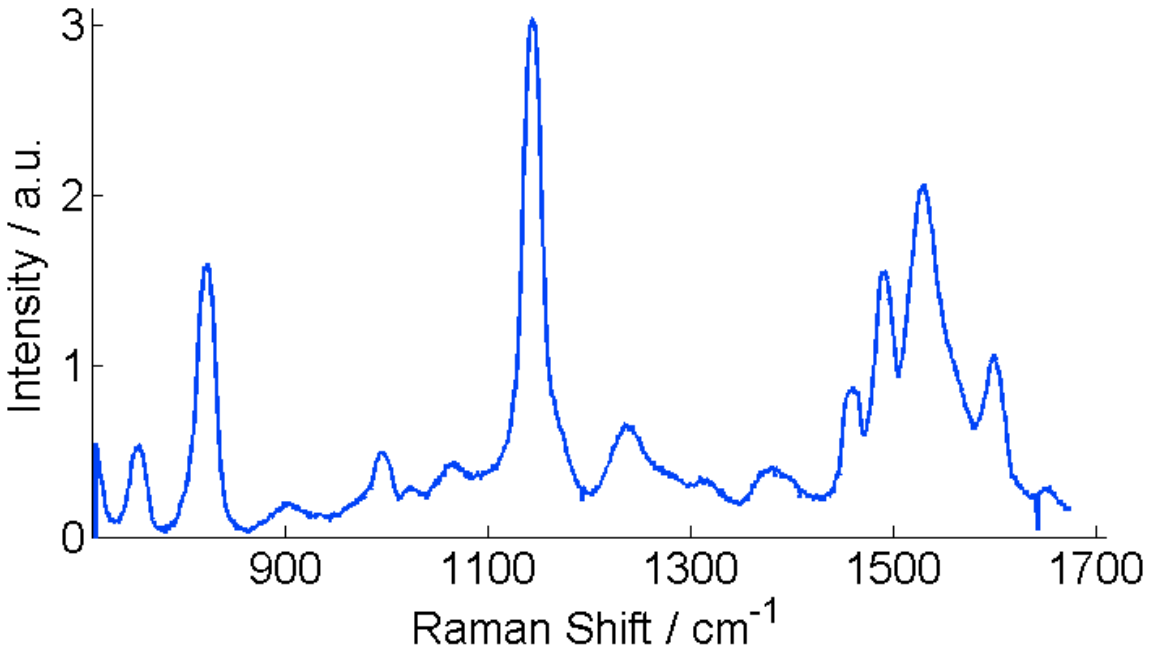

Figure 6.1. Resonance Raman spectrum of (dme)$TaCl_3(NNPh_2)$ (**6.1d**) excited into LMCT showing N–N (865 cm^{-1}), Ta–N (1175 cm^{-1}) and aryl (1500–1650 cm^{-1}) stretches.

(dme)$MCl_3(NNR_2)$ (**6.1a-f** for Ta; **6.2a-i** for Nb, R = alkyl or aryl) were synthesized from MCl_5 and the corresponding 1,1-disubstituted hydrazine *via* the previously reported Lewis acid-assisted dehydrohalogenation pathway (eq 6.1).[10,11] While the Nb alkylhydrazide reactions (**6.2g-i**) proceed cleanly in good yield, we have been unable to synthesize any Ta alkylhydrazides *via* this route. (MeCN)$WCl_4(NNR_2)$ complexes (**6.3a-i**) were synthesized by reacting WCl_6 with the corresponding 1,1-disubstituted hydrazine and MeCN in CH_2Cl_2 (eq 6.2).[12] All of the metallations proceeded in good to excellent yield for synthetically useful purities. However, obtaining spectroscopically pure material proved much more difficult and lower yielding, as the impurities of the reactions tend to be highly colored with extinction coefficients orders of magnitude larger than the desired metal hydrazide (2-) complexes. For **6.2e,f** and **6.3b,c,f,g**, spectroscopically pure material was not reproducibly obtained, and they are presented here only for their synthesis and structural data.

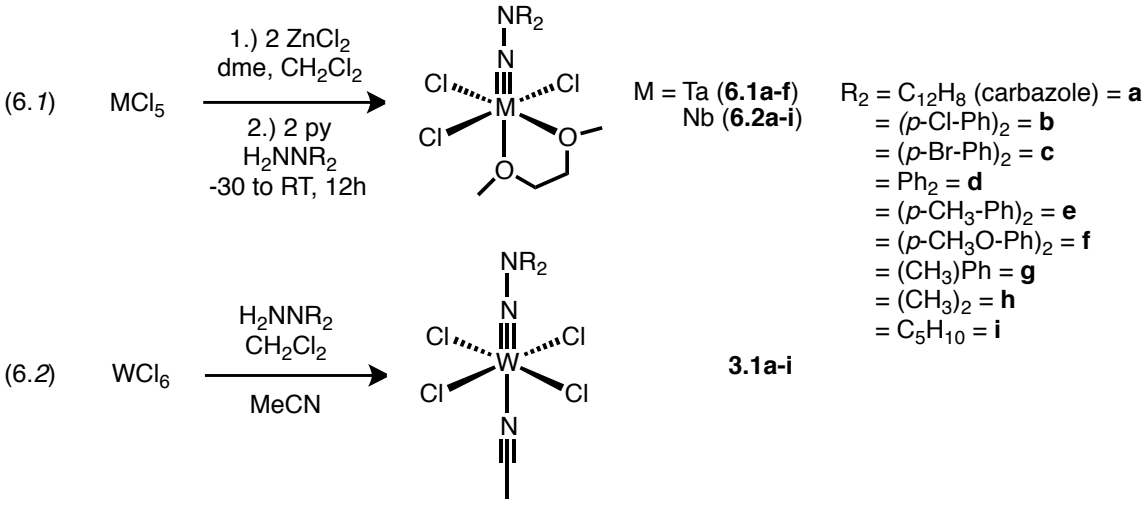

The absorption spectra of **6.1a-f**, **6.2a-d,g-i**, and **6.3a,d,e,h,i** in $C_2H_4Cl_2$ were collected and their lowest-energy absorptions were studied. Unlike the related imido

complexes, the **6.1** and **6.2** series do not exhibit any measurable fluorescence.[13] In addition to the low energy $M{=}NNR_2$ charge transfer, there are higher energy bands associated with the M-Cl LMCT which will not be discussed here. In most cases, the lowest-energy band was well resolved from the other peaks and exhibited nearly Gaussian shape. The absorption spectra are presented in Figures 6.2-6.4. λ_{max} and ϵ values for all compounds are reported in Table 6.1. The Ta absorbances had λ_{max} values between 15300-18900 cm^{-1} and ϵ values between 100-250 M^{-1} cm^{-1}. The Nb congeners give lower-energy λ_{max} values between 13800-16500 cm^{-1} with smaller ϵ values ranging from 17-66 M^{-1} cm^{-1}. The W complex absorbances ranged from 15800-23200 cm^{-1} with larger ϵ values from 330-570 M^{-1} cm^{-1}, however the W alkylhydrazides were not well resolved from higher energy absorptions and appeared as shoulders to the much more intense W-Cl LMCT peak.

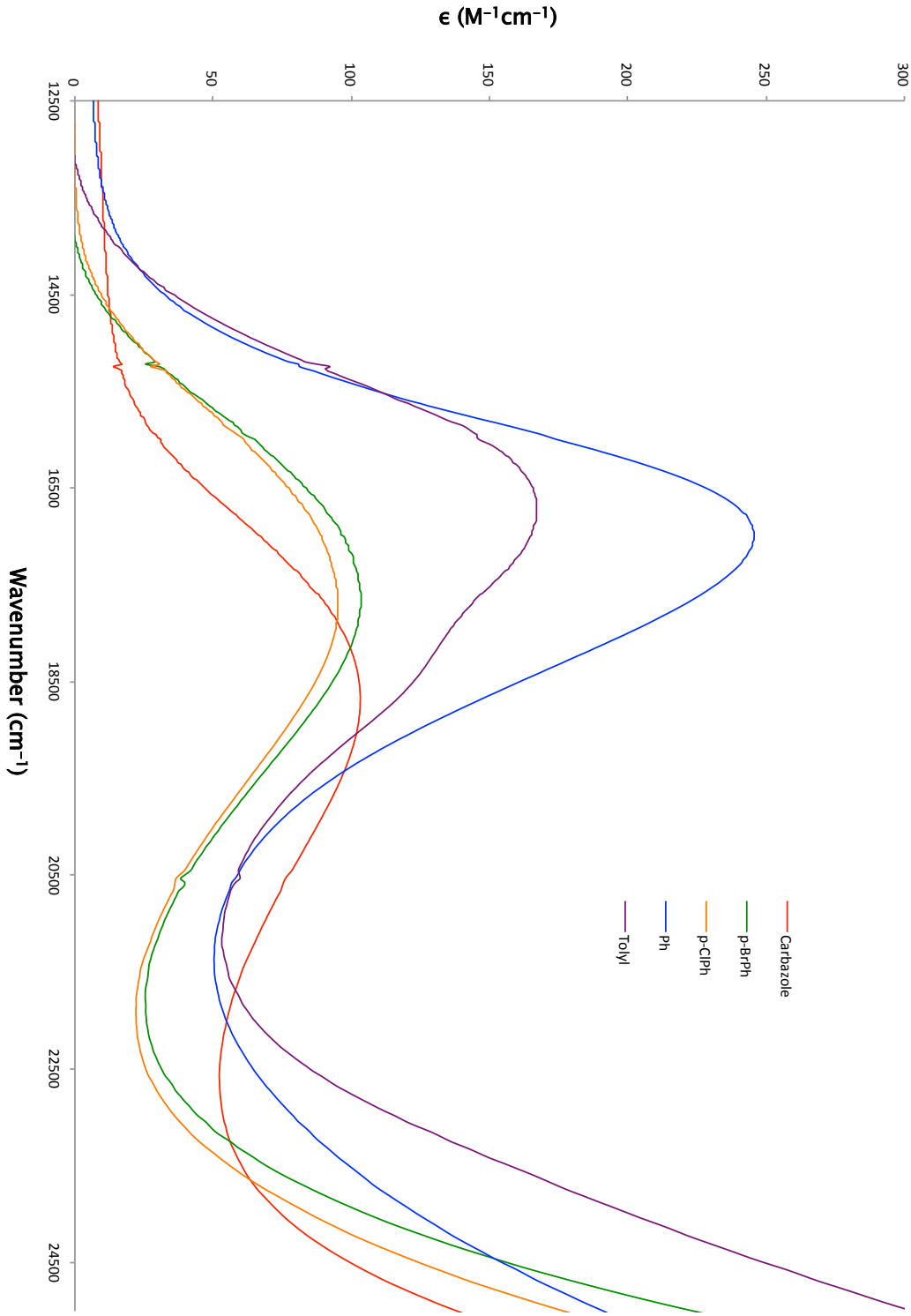

Figure 6.2. Absorption spectra of **6.1a–e** measured in $C_2H_4Cl_2$.

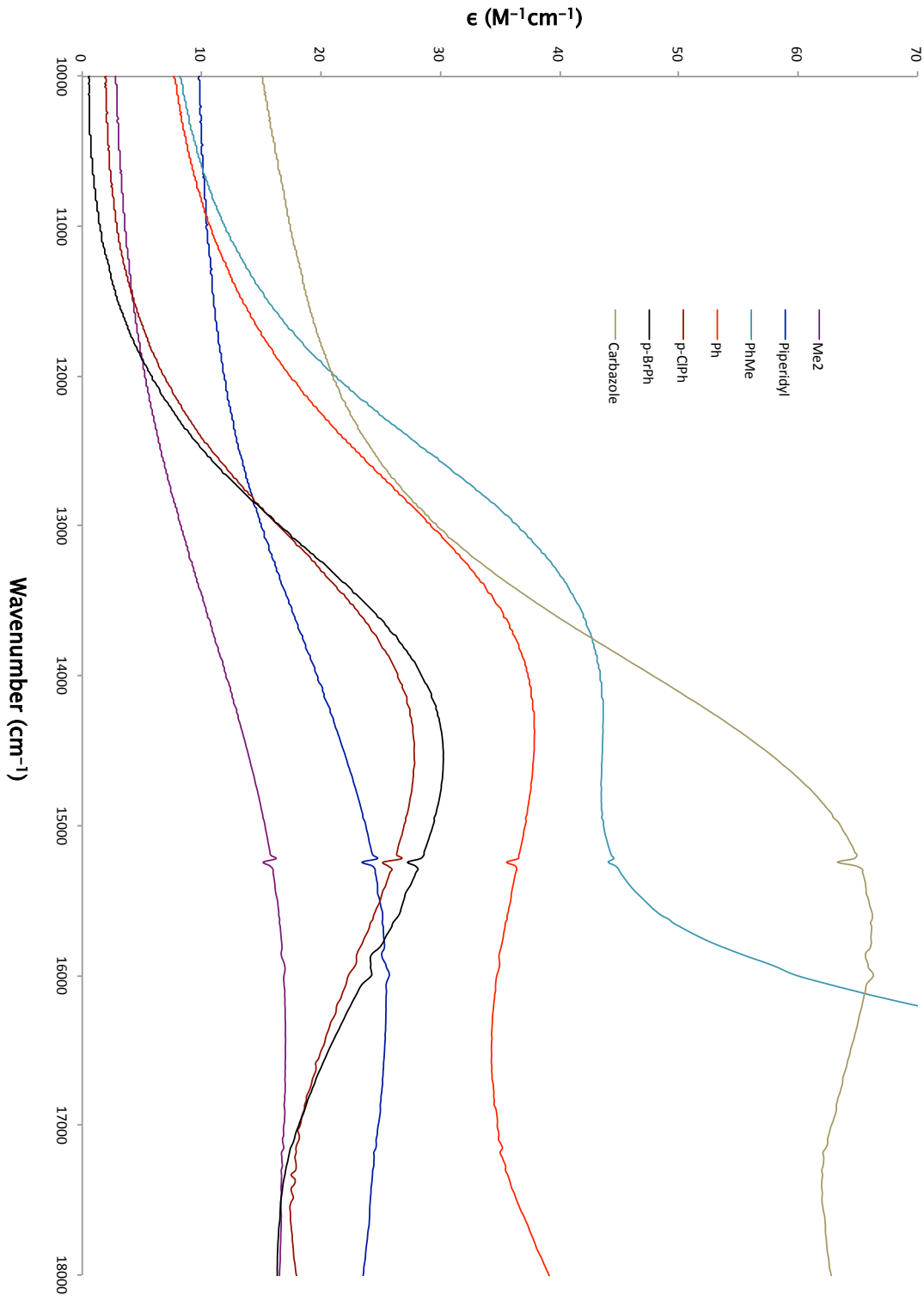

Figure 6.3. Absorption spectra of **6.2a–d,g–l** measured in $C_2H_4Cl_2$.

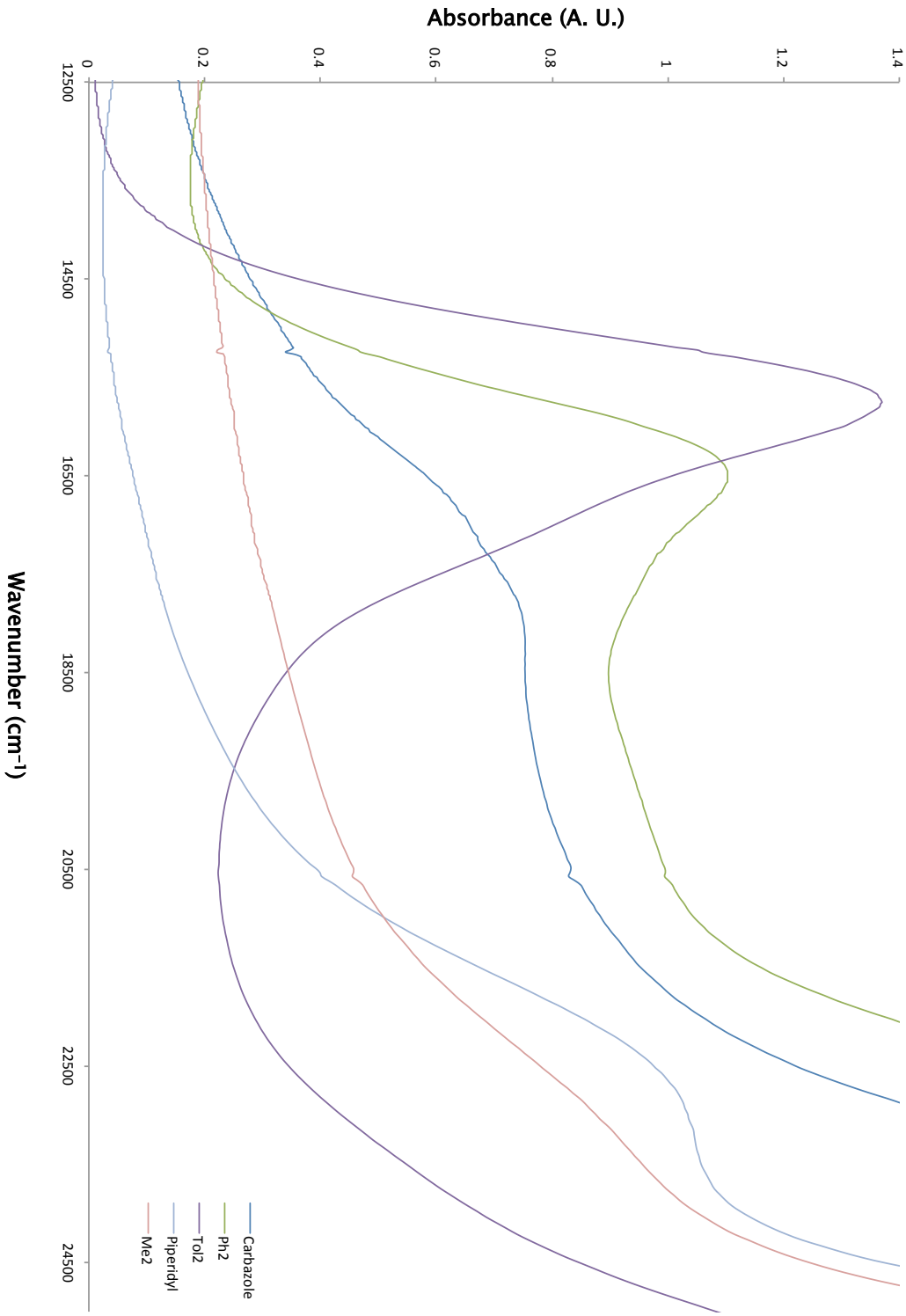

Figure 6.4 Absorption spectra of **6.3a,d,e,h,l** measured in $C_2H_4Cl_2$.

Table 6.1. Lowest energy charge transitions in (dme)$MCl_3(NNR_2)$ and (MeCN)$WCl_4(NNR_2)$. Complexes are ordered by increasing electron density of N_β within each metal series.

M	R_2	σ_{para}	λ_{max} (cm^{-1})	ϵ ($M^{-1}cm^{-1}$)
Ta	$C_{12}H_8$ (**6.1a**)	–	18650	103
	(*p*–ClPh)$_2$ (**6.1b**)	0.24	17670	93
	(*p*–BrPh)$_2$ (**6.1c**)	0.26	17640	103
	Ph_2 (**6.1d**)	0.00	17100	245
	(*p*–CH_3Ph)$_2$ (**6.1e**)	–0.14	16690	167
Nb	$C_{12}H_8$ (**6.2a**)	–	15700	66
	(*p*–ClPh)$_2$ (**6.2b**)	0.24	14580	28
	(*p*–BrPh)$_2$ (**6.2c**)	0.26	14560	30
	Ph_2 (**6.2d**)	0.00	14370	38
	(CH_3)(Ph) (**6.2g**)	–	13790	44
	(CH_3)$_2$ (**6.2h**)	–	16420	17
	C_5H_{10} (**6.2i**)	–	16260	25
W	$C_{12}H_8$ (**6.3a**)	–	17860	350
	Ph_2 (**6.3d**)	0.00	16501	370
	(*p*–CH_3Ph)$_2$ (**6.3e**)	–0.14	15750	570
	(CH_3)$_2$ (**6.3h**)	–	23260 (*sh*)	400
	C_5H_{10} (**6.3i**)	–	22990 (*sh*)	330
–	(dme)$TaCl_3$(NOMe) (**6.4**)	–	23750	–
–	(dme)$NbCl_3$(NOMe) (**6.5**)	–	21300	–

The magnitude of the ϵ values for these complexes also reinforces our assignment of the lowest-energy band to the ligand–metal charge transfer since alternatives such as allowed π/π^* transitions would be expected to have significantly larger ϵ. Also, since the fully conjugated **6.2a** has a higher-energy λ_{max} than the other diaryls, a solely ligand π–based transition can be ruled out as an increase in conjugation should correlate to a decrease in λ_{max} for a π/π^* transition.

In each metal series, the energy of the charge transfer in the arylhydrazide complexes decreased dramatically with an increase in electron density around N_β, as correlated to the Hammett parameter σ_{para}. This bathochromic shift shows that increasing the N_β lone pair energy increases the $M{=}N_\alpha$ π bond and N_β lone pair antibonding interaction in the HOMO, thus raising its energy and shrinking the HOMO–LUMO gap (Scheme 6.2). It should be noted that this is not strictly an inductive effect of N_β, as the more inductively-withdrawing alkoxyimidos (dme)MCl_3(NOMe) (M = Ta, **6.4**, M = Nb **6.5**) have higher-energy LMCTs (M = Ta, 23,750 cm^{-1}; M = Nb, 21,300 cm^{-1}) than the hydrazido complexes.

Scheme 6.2

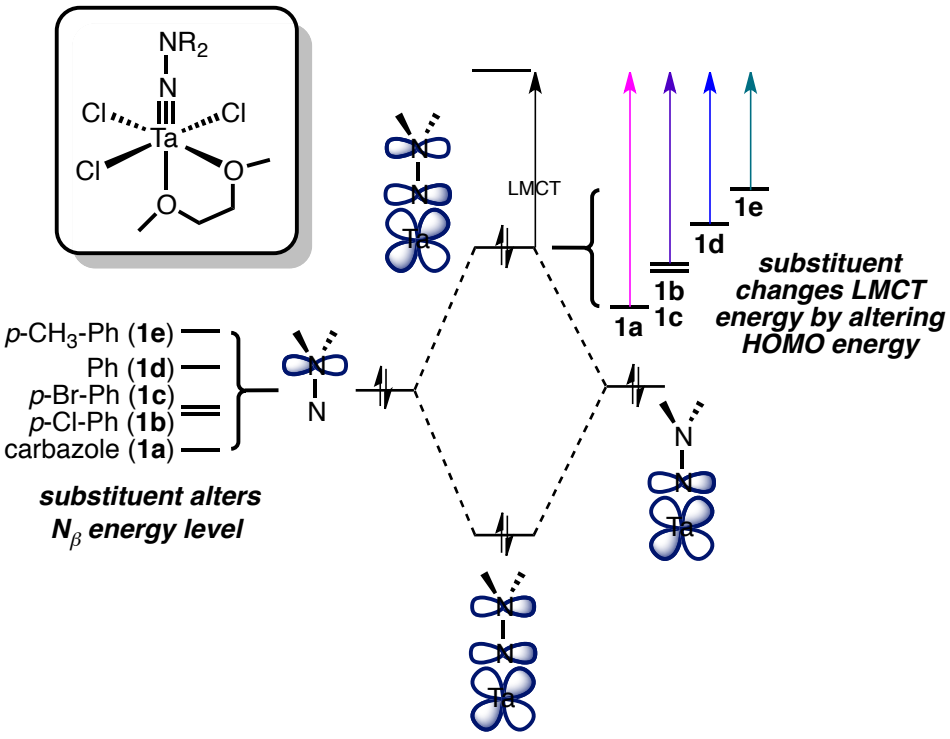

This trend is similar to the "aryl effect" which has been observed in related (dme)MCl_3(NR) (R = alkyl, aryl) imido complexes, in which small aryl– $M{=}N_\alpha$ π antibonding

interactions decreased the LMCT energy of the arylimidos relative to the alkylimidos.[14] However, the observed antibonding effect is much more dramatic in the hydrazido complexes than the arylimidos.

Based on the observations for the arylhydrazides, one would expect the alkyhydrazide complexes (**6.2h, 6.2i, 6.3h, 6.3i**), which are significantly more electron-rich, to display much lower energy LMCTs than the arylhydrazides. However, both the Nb and W alkylhydrazides exhibited much *higher* energy absorptions when compared to the arylhydrazides.

The origin of the alkylhydrazide energy discrepancy can be ascertained by examining the crystal structures of the series. X-ray quality crystals of **6.1a**, **6.1c**, **6.1d**, **6.1e**, and **6.2a-i** were obtained by slow diffusion of pentane into saturated solutions of the metal hydrazide(2-) complex in $C_2H_4Cl_2$. **6.3i** was crystallized from a saturated solution of **6.3i** in 2:1 pentane:toluene cooled to -30 °C. Table 6.2 shows the M-N and N-N bond distances, and the sum of all angles around N_β for all crystallized hydrazido complexes, as well as some crystallized imido and alkoxyimido complexes. The M-N bond distances are typical for triple bonds and the N-N distances are shorter than that of free diphenylhydrazine (1.418 Å). In general, the W N-N bond distances are shorter than in either the Nb or Ta cases and have a larger variance, but these differences are still relatively small. The sum of the angles about N_β indicates that N_β is planarized in all examples except for alkylhydrazides **6.2h** and **6.2i**, which are pyramidalized (Figure 6.5).

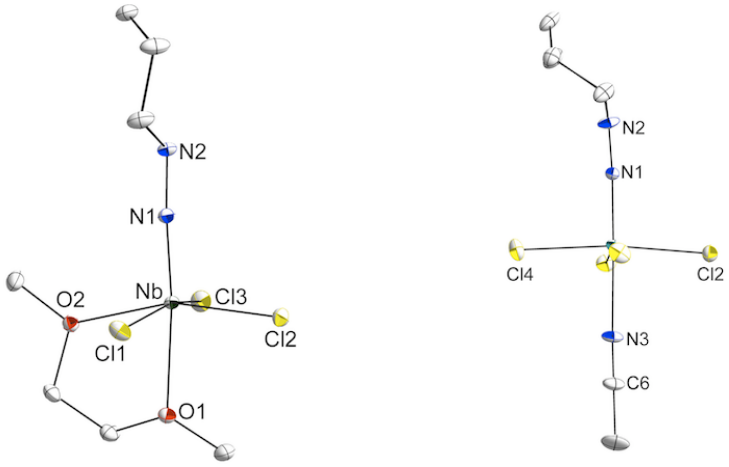

Figure 6.5. Thermal ellipsoid drawings of (dme)$NbCl_3(NNC_5H_{10})$ (**6.2i**, left) and (MeCN)$WCl_4(NNC_5H_{10})$ (**6.3i**, right). Note the different geometries of N_2. Selected bond distances and angles are listed in Table 6.2.

Table 6.2. Bond distances and sum of angles about N_β in (dme)$MCl_3(NNR_2)$ and (MeCN)$WCl_4(NNR_2)$.

M	R_2	M–N (Å)	N–N (Å)	Σ (°$_{N\beta}$)
Ta	$C_{12}H_8$ (**6.1a**)	1.7605(1)	1.3609(1)	359.0
	(*p*–BrPh)$_2$ (**6.1c**)	1.760	1.3608	358.7
	Ph_2 (**6.1d**)[a]	1.773(1)	1.347(1)	359.7
	(*p*–CH_3Ph)$_2$ (**6.1e**)	1.7739(3)	1.3400(2)	358.8
Nb	$C_{12}H_8$ (**6.2a**)	1.7742(1)	1.3282(1)	359.9
	(*p*–ClPh)$_2$ (**6.2b**)	1.7661(1)	1.3335(1)	359.1
	(*p*–BrPh)$_2$ (**6.2c**)	1.7719(1)	1.3374(1)	360.0
	Ph_2 (**6.2d**)[a]	1.7654(1)	1.3447(1)	359.9
	(*p*–CH_3Ph)$_2$ (**6.2e**)	1.7684(1)	1.3305(1)	359.6
	(*p*–CH_3OPh)$_2$ (**6.2f**)	1.7701(1)	1.3362(1)	359.5
	(CH_3)(Ph) (**6.2g**)	1.7726(1)	1.3242(1)	360.0
	(CH_3)$_2$ (**6.2h**)	1.7601(1)	1.3508(1)	342.1
	C_5H_{10} (**6.2i**)	1.7597(1)	1.3392(1)	341.1
W	Ph_2 (**6.3d**)[b]	1.742(4)	1.312(5)	359.3
	(CH_3)$_2$ (**6.3h**)[b]	1.769(5)	1.271(8)	360.0
	C_5H_{10} (**6.3i**)	1.7633(1)	1.2556(1)	359.8
–	(dme)$TaCl_3$(NOMe) (**6.4**)[c]	1.7572(1)	1.3481(1) (N–O)	–
–	(dme)$NbCl_3$(NOMe) (**6.5**)	1.7568(1)	1.3286(1) (N–O)	–

[a]Taken from ref. 10. [b]Taken from ref. 12. [c]Taken from ref. 16.

The bond length data presents no trend with the electron richness of the hydrazido ligand. As a result, no conclusions about either the electronic structure or the donor ability of the hydrazido ligand can be made by examining bond lengths. However, the geometry of N_β gives insight into the nature of the energy discrepancy of the LMCT in the alkylhydrazide complexes (Figure 6.5). In the case of all of the diarylhydrazidos, N_β is planarized due to steric and electronic factors. However, the Nb dialkylhydrazides (**6.2h**, **6.2i**) are pyramidalized at N_β, and as a result the overlap between $Nb{=}N_\alpha$ π and N_β is reduced. Consequently, the HOMO energy is not raised as high in energy as predicted based on the diarylhydrazide trend (Scheme 6.3). Odom has observed a similar trend for LLCTs in titanium hydrazido complexes.[5b]

Scheme 6.3

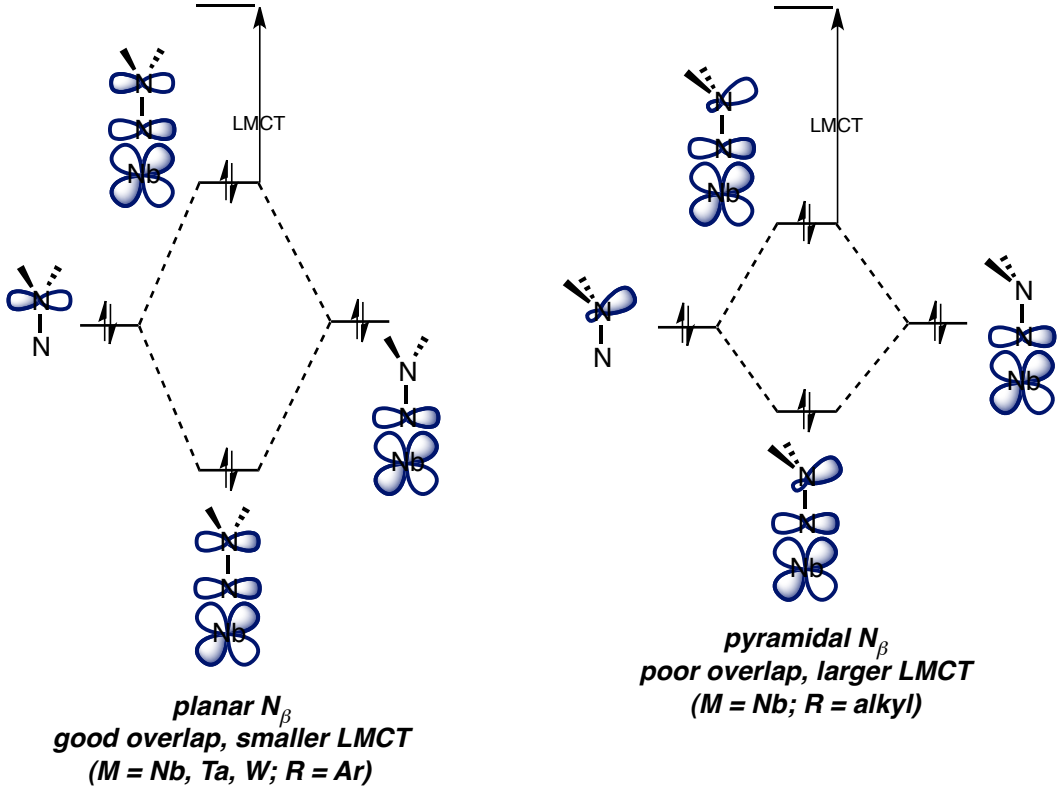

planar N_β
good overlap, smaller LMCT
(M = Nb, Ta, W; R = Ar)

pyramidal N_β
poor overlap, larger LMCT
(M = Nb; R = alkyl)

Conversely, the W dialkylhydrazides (**6.3h**, **6.3i**) remain planarized in the solid state, yet still do not display low energy charge transfers that would be in line with the aryl hydrazide trend. Since a planarized dialkylhydrazide should have a very low energy λ_{max} value based on the aryl trend, we speculate that the W^{VI} dialkylhydrazidos are, in fact, formally diazenido(0) ligands with a reduced W^{IV} center. In this case, the $W{=}N_{\alpha}$ π and N_{β} lone pair antibonding interaction is so strong that the molecular orbital is *higher* in energy than metal-based orbitals, resulting in a formal reduction of W by the hydrazide (Figure 6.6), and thus, the observed charge transition is an MLCT rather than an LMCT. EHMO and *ab initio* calculations on Mo and other hydrazide complexes also provide evidence for at least partial reduction of the metal center.[15]

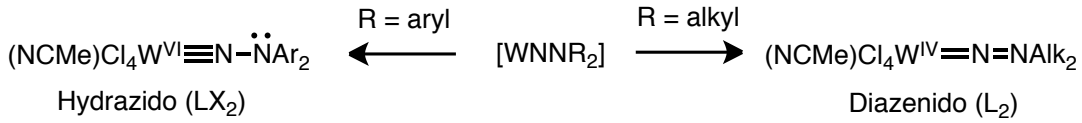

Figure 6.6. Tungsten NNR_2 units exhibit different formal donor ability when R is changed from aryl to alkyl.

In an attempt to access the same hydrazide-diazenido resonance form interchange with the niobium complexes, the more Lewis acidic $(dme)NbBr_3(NNMe_2)$ (**6.6**) and $(dme)NbI_3(NNMe_2)$ (**6.7**) were synthesized in an analogous fashion to **6.2** starting from $NbBr_5$ or NbI_5. In order to limit halide exchange with $ZnCl_2$, $ZnBr_2$ and ZnI_2 were utilized in the Lewis acid-assisted dehydrohalogenation reaction instead. Unlike the previous studies where the HOMO energy was altered, in these complexes the LUMO should be lowered in energy relative to the HOMO. Indeed, this is the case as the observed

charge transfer energies for **6.6** (14790 cm^{-1}) and **6.7** (14045 cm^{-1}, est.) are lower than the chloride analogue, **6.2h** (16420 cm^{-1}). However, **6.6** and **6.7** are still dominated by the hydrazido resonance form, as the crystal structures reveal that N_β remains pyramidalized (Table 6.3).

Table 6.3. Spectroscopic and bond length data for the $Nb(NNMe_2)$ halide series.

	λ_{max} (cm^{-1})	M–N (Å)	N–N (Å)	Σ (°$_{N\beta}$)
(dme)$NbCl_3(NNMe_2)$ **6.2h**	16420	1.7601(1)	1.3508(1)	342.1
(dme)$NbBr_3(NNMe_2)$ **6.6**	14790	1.761(2)	1.327(1)	346.5
(dme)$NbI_3(NNMe_2)$ **6.7**	14045 (*sh*)	1.7621(1)	1.3381(1)	343.5

CONCLUSIONS

In summary, the examination of the spectroscopic and structural properties of these complexes highlights an important difference between the group 5 and group 6 terminal hydrazido moieties. In the case of group 6 terminal hydrazides, the formally reduced metal-diazenido resonance form can be accessed to stabilize electron rich hydrazides (such as $-NNMe_2$), whereas the group 5 (and group 4) metals apparently resist reduction. Since Chatt-type N_2 reduction cycles with group 6 complexes rely heavily on the plasticity of the metal formal oxidation state, these results indicate that intermediates along analogous group 5 (and also likely group 4) N_2 reduction cycles may be less likely to invoke reduction at the metal center for stabilization.[1,2b]

EXPERIMENTAL SECTION

General Considerations and Instrumentation. All air- and moisture-sensitive compounds were manipulated using standard high vacuum and Schlenk techniques or manipulated in a glovebox under a nitrogen atmosphere. Solvents for air- and moisture-sensitive reactions were dried over sodium benzophenone ketyl and stored over titanocene where compatible or dried by the method of Grubbs.[17] Benzene-d_6 was purchased from Cambridge Isotopes and dried over sodium benzophenone ketyl. CD_2Cl_2 was degassed, distilled from CaH_2 and run through a plug of activated alumina prior to use. Liquid 1,1-disubstituted hydrazines were degassed and passed through a plug of activated alumina prior to use. ^1H and ^{13}C spectra were recorded on Varian Mercury 300 or Varian INOVA 500 spectrometers and chemical shifts are reported with respect to residual protio-solvent impurity for ^1H (*s*, 7.16 ppm for C_6D_5H; *t*, 5.32 ppm for $CDHCl_2$) and solvent carbons for ^{13}C (*t*, 128.39 for C_6H_6; *p*, 53.84 for CD_2Cl_2).

Resonance Raman Spectroscopy. The resonance Raman samples were prepared by loading solutions into capillaries in an inert atmosphere glovebox and then flame sealing the capillaries. Excitation was performed at 514 nm using an argon ion laser operating at 10 mw at the sample. A lens collected the light that scattered at 90° and focused it through a low-pass filter and into the entrance slit of a SPEX 750M monochromator. The dispersed light was detected by a LN/CCD array (5 cm^{-1} resolution), and the spectra recorded using Winspec (Princeton Instruments) software. Conversion from pixels to wavenumbers was done by obtaining the spectrum of cyclohexane and deriving the linear plot of pixels versus wavenumber for known vibrations. All spectra

were recorded in $C_2H_4Cl_2$, and in some instances, solvent subtraction or baseline correction was performed.

X-ray Crystal Data: General Procedure. Crystals were removed quickly from a scintillation vial to a microscope slide coated with Paratone N oil. Samples were selected and mounted on a glass fiber with Paratone N oil. Data collection was carried out on a Bruker KAPPA APEX II or a Bruker SMART 1000 diffractometer with a 0.71073 Å MoKα source. The structures were solved by direct methods. All non-hydrogen atoms were refined anisotropically. Details regarding refined data and cell parameters are available in Tables 6.3-6.7.

General Diarylhydrazine Synthesis. All of the hydrazines were synthesized from their respective diarylamines *via* the following procedure: Diarylamine (0.01-0.03 mol, 1 equiv) was dissolved in 100 mL EtOH and cooled to 0 °C in an ice bath. 20 mL concentrated HCl was added, and the mixture was vigorously stirred for 5 minutes. $NaNO_2$ (1.1 equiv) in 20 mL H_2O was added dropwise to the reaction over the course of 5 minutes, which immediately yielded an off-white precipitate of the nitrosamine. The reaction was stirred at 0 °C for 1 hour, and then the nitrosamine was collected by filtration and used without further purification.

The nitrosamine was dried *in vacuo*, then dissolved in 150 mL dry Et_2O in a glovebox. $LiAlH_4$ (1.2 equiv) dissolved in 40 mL Et_2O was then added dropwise over the course of 1 hour to the stirring nitrosamine solution. The reaction bubbled vigorously, indicating release of H_2. After addition was complete and bubbling had subsided, the reaction was stirred for another 2 hours. Next, the reaction was removed from the

glovebox and 200 mL of benchtop Et_2O was added, followed by the careful addition of 200 mL of a saturated sodium potassium tartrate solution. The resultant mixture was then extracted 3x with 200 mL Et_2O. 200 mL of HCl-acidified Et_2O was then added to the combined organics, resulting in the precipitation of the white hydrazine hydrochloride salt that was collected by filtration. The HCl salt was then deprotonated using aqueous NaOH and extracted into 500 mL Et_2O. The organics were dried using $MgSO_4$, then solvent removed *in vacuo* to yield the hydrazine as an off-white powder. Note: these hydrazines are somewhat air-sensitive and turn red/purple upon prolonged air exposure. They should be stored under an inert atmosphere.

Synthesis of N-aminocarbazole. Yielded 2.0 g (0.0108 mol, 28.6% yield) of the hydrazine, starting from 6.326 g (0.038 mol) carbazole. ^{1}H NMR (500 MHz, CD_2Cl_2) δ, ppm: 4.67 (*s*, 2H, N*H*$_2$); 7.24 (*t*, 2H, aryl); 7.49 (*t*, 2H, aryl); 7.57 (*d*, 2H, aryl); 8.07 (*d*, 2H, aryl). ^{13}C NMR (125 MHz, CD_2Cl_2) δ, ppm: 119.0, 119.5, 119.9, 120.1, 120.7, 141.4 (aryl).

Synthesis of (p-Cl-C_6H_4)$_2$NNH$_2$. Yielded 3.51 g (0.0139 mol, 54.2% yield) of the hydrazine, starting from 6.084 g (0.0256 mol) (p-Cl-Ph)$_2$NH. ^{1}H NMR (500 MHz, CD_2Cl_2) δ, ppm: 4.17 (*s*, 2H, N*H*$_2$); 7.15 (*m*, 4H, aryl); 7.24 (*m*, 4H, aryl). ^{13}C NMR (125 MHz, CD_2Cl_2) δ, ppm: 120.7, 121.3, 127.1, 129.1, 129.6, 147.8 (aryl).

Synthesis of (p-Br-C_6H_4)$_2$NNH$_2$. Yielded 5.27 g (0.0163 mol, 44% yield) of the hydrazine, starting from 12.111 g (0.037 mol) (p-Br-Ph)$_2$NH. ^{1}H NMR (500 MHz, CD_2Cl_2) δ, ppm: 4.17 (*s*, 2H, N*H*$_2$); 7.10 (*m*, 4H, aryl); 7.38 (*m*, 4H, aryl). ^{13}C NMR (125 MHz, CD_2Cl_2) δ, ppm: 114.5, 121.1, 121.7, 132.0, 132.5, 148.1 (aryl).

Synthesis of (p-CH_3-C_6H_4)$_2$$NNH_2$. Yielded 3.27 g (0.0154 mol, 52% yield) of the hydrazine, starting from 5.84 g (0.0296 mol) (p-CH_3-Ph)$_2$NH. ^{1}H NMR (500 MHz, CD_2Cl_2) δ, ppm: 2.33 (*s*, 6H, C*H*$_3$); 4.10 (*s*, 2H, N*H*$_2$); 7.10 (*m*, 8H, aryl). ^{13}C NMR (125 MHz, CD_2Cl_2) δ, ppm: 20.8 (*C*H$_3$); 119.5, 120.1, 129.6, 130.1, 131.6, 147.9 (aryl).

Synthesis of (p-CH_3O-C_6H_4)$_2$$NNH_2$. Yielded 1.20 g (0.0049 mol, 51.7% yield) of the hydrazine, starting from 2.176 g (0.0095 mol) (p-CH_3O-Ph)$_2$NH. ^{1}H NMR (500 MHz, CD_2Cl_2) δ, ppm: 3.77 (s, 6H, OC*H*$_3$); 4.05 (br s, 2H, N*H*$_2$); 6.82 (m, 4H, aryl); 7.06 (m, 4H, aryl). ^{13}C NMR (125 MHz, CD_2Cl_2) δ, ppm: 55.4 (O*C*H$_3$); 114.4, 121.3, 144.4, 155.0 (aryl).

General Synthesis of (dme)MCl_3(NNR_2) (6.1, 6.2; M = Ta, Nb). $NbCl_5$ (1 g, 3.7 mmol, 1 equiv) and $ZnCl_2$ (1.009 g, 7.4 mmol, 2 equiv) were added in 15 mL CH_2Cl_2 in an inert atmosphere glovebox. The suspension was stirred vigorously as 1 mL dimethoxyethane was slowly added, then left to stir for an additional hour. Next, the appropriate 1,1-disubstituted hydrazine (3.7 mmol, 1 equiv) and pyridine (600 µL, 585 mg, 7.4 mmol, 2 equiv) in 1 mL CH_2Cl_2 was added dropwise to the suspension of Nb and Zn over the course of 10 minutes. An immediate color change to green was observed. The reactions were left to stir overnight, yielding green solutions with white precipitate ($ZnCl_3$pyH). The solutions were filtered and CH_2Cl_2 removed *in vacuo*. The product was then extracted into 60 mL C_6H_6 and filtered again to remove residual salts. 100 mL pentane was added to the C_6H_6 solution and stirred vigorously, resulting in the hydrazide precipitating out as green microcrystals which were isolated *via* filtration and washed with 20 mL pentane. In some cases, brown or purple material oiled out or crystallized out upon addition of pentane to the benzene solutions prior to the product precipitating out. In

these cases, the solutions were decanted and the supernatant cooled to -30 °C, yielding the desired product as green crystals. X-ray quality crystals were obtained from slow diffusion of pentane into a saturated solution of the product in $C_2H_4Cl_2$, or by cooling the pentane/benzene supernatant to 30 °C. An identical procedure was utilized for (dme)$TaCl_3(NNR_2)$, beginning with 1 g (2.8 mmol) $TaCl_5$.

Synthesis of (dme)$TaCl_3$(Ncarbazole) (6.1a). Yielded 800 mg (%). ^{1}H NMR (500 MHz, CD_2Cl_2) δ, ppm: 4.11 (*s*, 3H, C*H*$_3$O); 4.16 (*s*, 3H, C*H*$_3$O); 4.26 (*m*, 2H, OC*H*$_2$); 4.29 (*m*, 2H, OC*H*$_2$); 7.22 (*t*, 2H, aryl); 7.55 (*t*, 2H, aryl); 8.03 (*d*, 2H, aryl); 8.22 (*d*, 2H, aryl). ^{13}C NMR (125 MHz, CD_2Cl_2) δ, ppm: 64.2 (O*C*H$_2$); 71.0 (O*C*H$_2$); 72.5 (O*C*H$_3$); 76.5 (O*C*H$_3$); 111.6, 120.1, 120.3, 112.3, 126.8, 139.5 (aryl). Calcd for $C_{16}H_{18}Cl_3N_2O_2Ta$ C 34.46 H 2.53 N 5.02; Found C 39.39, H 3.62, N 5.09%.

Synthesis of (dme)$TaCl_3$(NN(*p*-Cl-Ph)$_2$) (6.1b). Yielded 1.41 g (80%). ^{1}H NMR (500 MHz, CD_2Cl_2) δ, ppm: 3.97 (*s*, 3H, C*H*$_3$O); 4.04 (*s*, 3H, C*H*$_3$O); 4.14 (*m*, 2H, OC*H*$_2$); 4.17 (*m*, 2H, OC*H*$_2$); 7.37 (*m*, 4H, aryl); 7.41 (*m*, 4H, aryl). ^{13}C NMR (125 MHz, CD_2Cl_2) δ, ppm: 63.8 (O*C*H$_2$); 70.7 (O*C*H$_2$); 72.3 (O*C*H$_3$); 76.4 (O*C*H$_3$); 121.5, 121.7, 122.1, 122.3, 128.9, 129.1, 129.5, 129.8, 130.0, 141.6 (aryl).

Synthesis of (dme)$TaCl_3$(NN(*p*-Br-Ph)$_2$) (6.1c). Yielded 1.10 g (54.8%). ^{1}H NMR (500 MHz, CD_2Cl_2) δ, ppm: 3.97 (*s*, 3H, C*H*$_3$O); 4.04 (*s*, 3H, C*H*$_3$O); 4.14 (*m*, 2H, OC*H*$_2$); 4.17 (*m*, 2H, OC*H*$_2$); 7.36 (*m*, 4H, aryl); 7.51 (*m*, 4H, aryl). ^{13}C NMR (125 MHz, CD_2Cl_2) δ, ppm: 63.8 (O*C*H$_2$); 70.9 (O*C*H$_2$); 72.3 (O*C*H$_3$); 76.4 (O*C*H$_3$); 117.7, 121.8, 122.0, 122.5, 122.7, 131.9, 132.1, 132.4, 132.7, 142.0 (aryl). Calcd for $C_{16}H_{18}Br_2Cl_3N_2O_2Ta$: C 26.79, H 2.53, N 3.90; Found C 27.32, H 2.55, N 3.79%.

Synthesis of (dme)$TaCl_3(NNPh_2)$ (6.1d). Yielded 1.32 g (84.3%). Spectral data same as previously reported. See ref. 10.

Synthesis of (dme)$NbCl_3$(Ncarbazole) (6.2a). Yielded 410 mg (23.6%). ^{1}H NMR (500 MHz, CD_2Cl_2) δ, ppm: 4.00 (*s*, 3H, C*H*$_3$O); 4.10 (*s*, 3H, C*H*$_3$O); 4.23 (*s*, 4H, OC*H*$_2$); 7.31 (*t*, 2H, aryl); 7.56 (*t*, 2H, aryl); 7.99 (*d*, 2H, aryl); 8.36 (*d*, 2H, aryl). ^{13}C NMR (125 MHz, CD_2Cl_2) δ, ppm: 63.2 (O*C*H$_2$); 69.4 (O*C*H$_2$); 71.9 (O*C*H$_3$); 75.7 (O*C*H$_3$); 111.8, 112.0, 120.0, 122.6, 127.0, 139.1 (aryl). Calcd for $C_{16}H_{18}Cl_3N_2NbO_2$: C 40.92, H 3.86, N 5.97; Found: C 40.81, H 3.83, N 6.05%.

Synthesis of (dme)$NbCl_3$(NN(*p*-Cl-Ph)$_2$) (6.2b). Yielded 850 mg (42.5%). ^{1}H NMR (500 MHz, CD_2Cl_2) δ, ppm: 3.83 (*s*, 3H, C*H*$_3$O); 3.96 (*s*, 3H, C*H*$_3$O); 4.10 (*s*, 4H, OC*H*$_2$); 7.40 (*m*, 4H, aryl); 7.47 (*m*, 4H, aryl). ^{13}C NMR (125 MHz, CD_2Cl_2) δ, ppm: 62.8 (O*C*H$_2$); 69.2 (O*C*H$_2$); 71.6 (O*C*H$_3$); 75.6 (O*C*H$_3$); 121.1, 121.5, 122.0, 128.9, 129.2, 129.8, 130.8, 140.0 (aryl). Calcd for $C_{16}H_{18}Cl_5N_2NbO_2$: C 35.55, H 3.36, N 5.18; Found C 35.81, H 3.59, N 5.14%.

Synthesis of (dme)$NbCl_3$(NN(*p*-Br-Ph)$_2$) (6.2c). Yielded 525 mg (22.5%). ^{1}H NMR (500 MHz, CD_2Cl_2) δ, ppm: 3.83 (*s*, 3H, C*H*$_3$O); 3.96 (*s*, 3H, C*H*$_3$O); 4.11 (*s*, 4H, OC*H*$_2$); 7.41 (*m*, 4H, aryl); 7.55 (*m*, 4H, aryl). ^{13}C NMR (125 MHz, CD_2Cl_2) δ, ppm: 62.8 (O*C*H$_2$); 69.2 (O*C*H$_2$); 71.6 (O*C*H$_3$); 75.5 (O*C*H$_3$); 118.5, 121.5, 121.8, 122.3, 131.9, 132.4, 140.4 (aryl). Calcd for $C_{16}H_{18}Br_2Cl_3N_2NbO_2$: C 30.53, H 2.88, N 4.45; Found C 31.76, H 2.88, N 4.54%.

Synthesis of (dme)$NbCl_3(NNPh_2)$ (6.2d). Yielded 1 g (57.3%). Spectral data same as previously reported. See ref. 10.

Synthesis of (dme)$NbCl_3$(NN(*p*-CH_3-Ph)$_2$) (6.2e). Yielded 100 mg (5.4%). ^{1}H NMR (500 MHz, CD_2Cl_2) δ, ppm: 2.39 (*s*, 6H, $C_6H_4CH_3$); 3.85 (*s*, 3H, CH_3O); 3.93 (*s*, 3H, CH_3O); 4.08 (*s*, 4H, OCH_2); 7.22 (*m*, 4H, aryl); 7.35 (*m*, 4H, aryl). ^{13}C NMR (125 MHz, CD_2Cl_2) δ, ppm: 20.6 (CH_3); 62.6 (OCH_2); 69.1 (OCH_2); 71.5 (OCH_3); 75.4 (OCH_3); 120.0, 129.3, 135.3, 139.2 (aryl). Calcd for $C_{18}H_{24}Cl_3N_2NbO_2$: C 43.27, H 4.84, N 5.61; Found C 43.59, H 4.76, N 5.68%.

Synthesis of (dme)$NbCl_3$(NN(*p*-CH_3O-Ph)$_2$) (6.2f). Yielded 120 mg (6.1%). ^{1}H NMR (500 MHz, CD_2Cl_2) δ, ppm: 3.81 (*s*, 6H, $C_6H_4OCH_3$); 3.85 (*s*, 3H, CH_3O); 3.92 (*s*, 3H, CH_3O); 4.08 (*m*, 4H, OCH_2); 6.95 (*m*, 4H, aryl); 7.37 (*m*, 4H, aryl).

Synthesis of (dme)$NbCl_3$(NNPhMe) (6.2g). Yielded 111 mg (7.3%). ^{1}H NMR (500 MHz, CD_2Cl_2) δ, ppm: 3.88 (*s*, 3H, NCH_3); 3.95 (*s*, 3H, CH_3O); 4.03 (*s*, 3H, CH_3O); 4.11 (*m*, 2H, OCH_2); 4.17 (*m*, 2H, OCH_2); 6.92 (*t*, 1H, aryl); 7.30 (*d*, 2H, aryl); 7.37 (*t*, 2H, aryl). ^{13}C NMR (125 MHz, CD_2Cl_2) δ, ppm: 62.5 (OCH_2); 69.2 (OCH_2); 71.5 (OCH_3); 75.5 (OCH_3); 112.4, 122.7, 128.4, 143.8 (aryl). Calcd for $C_{11}H_{18}Cl_3N_2NbO_2$: C 32.26, H 4.43, N 6.84; Found C 32.07, H 4.36, N 6.72%.

Synthesis of (dme)$NbCl_3$($NNMe_2$) (6.2h). Yielded 732 mg (56.9%). ^{1}H NMR (500 MHz, CD_2Cl_2) δ, ppm: 3.14 (*s*, 6H, $N(CH_3)_2$); 3.86 (*s*, 3H, CH_3O); 4.03 (*m*, 2H, OCH_2); 4.10 (*m*, 2H, OCH_2); 4.10 (*s*, 3H, CH_3O). ^{13}C NMR (125 MHz, CD_2Cl_2) δ, ppm: 43.6 ($N(CH_3)_2$); 62.1 (OCH_2); 69.1 (OCH_2); 71.3 (OCH_3); 75.4 (OCH_3).

Synthesis of (dme)$NbCl_3$(Npiperidyl) (6.2i). Yielded 150 mg (10.5%). ^{1}H NMR (500 MHz, CD_2Cl_2) δ, ppm: 1.47 (*m*, 2H, $N(CH_2)_4CH_2$) 1.66 (*m*, 4H, $N(CH_2)_2(CH_2)_2CH_2$); 3.14 (*s*, 6H, $N(CH_3)_2$); 3.49 (*m*, 4H, $N(CH_2)_2(CH_2)_3$); 3.86 (*s*, 3H, CH_3O); 4.02 (*m*, 2H, OCH_2); 4.09

(*m*, 2H, OC*H*$_2$); 4.09 (*s*, 3H, C*H*$_3$O). ^{13}C NMR (125 MHz, CD_2Cl_2) δ, ppm: 23.8 (*C*H$_2$); 25.3 (*C*H$_2$); 54.6 (*C*H$_2$); 62.5 (O*C*H$_2$); 69.2 (O*C*H$_2$); 71.6 (O*C*H$_3$); 75.7 (O*C*H$_3$). Calcd for $C_9H_{20}Cl_3N_2NbO_2$: C 27.89, H 5.20, N 7.23; Found C 27.79, H 4.99, N 7.22%.

General Synthesis of (MeCN)WCl$_4$(NNR$_2$) (6.3). A modified literature procedure was used. WCl_6 (1 g, 2.52 mmol, 1 equiv) was slurried in 15 mL CH_2Cl_2 in an inert atmosphere glovebox. The appropriate 1,1-disubstituted hydrazine (2.52 mmol, 1 equiv) dissolved in 2 mL CH_2Cl_2 was added dropwise to the slurried WCl_6 over the course of 10 minutes. The reaction was left to stir for 1 hour, then 1 mL MeCN was added. The reaction was stirred for 1 hour and then filtered. The dark filtrate was then added to 150 mL of vigorously stirred pentane, which resulted in the precipitation of the desired product as an orange or purple microcrystalline material. The product was collected *via* filtration and washed with 20 mL pentane.

Synthesis of (CH$_3$CN)WCl$_4$(Ncarbazole) (6.3a). Yielded (%). ^{1}H NMR (500 MHz, CD_2Cl_2) δ, ppm: 2.63 (*s,* 3H, C*H*$_3$CN); 7.07 (*t*, 2H, aryl); 7.68 (*t*, 2H, aryl); 7.92 (*d*, 2H, aryl); 8.10 (*d*, 2H, aryl). ^{13}C NMR (125 MHz, CD_2Cl_2) δ, ppm: 4.4 (*C*H$_3$CN); 121.6 (CH$_3$*C*N); 115.8, 119.8, 123.8, 126.5, 129.0, 134.2 (aryl). Calcd for $C_{14}H_{11}Cl_4N_3W$: C 30.75, H 2.03, N 7.68; Found C 28.98, H 2.29, N 7.27%.

Synthesis of (CH$_3$CN)WCl$_4$(NN(*p*-Cl-Ph)$_2$) (6.3b). Yielded 1.15 g (73.9%). ^{1}H NMR (500 MHz, CD_2Cl_2) δ, ppm: 2.56 (*s,* 3H, C*H*$_3$CN); 7.21 (*m*, 4H, aryl); 7.67 (*m*, 4H, aryl). ^{13}C NMR (125 MHz, CD_2Cl_2) δ, ppm: 4.4 (*C*H$_3$CN); 121.3 (CH$_3$*C*N); 126.2, 126.7, 128.8, 129.0, 129.1, 129.4, 129.5, 131.5, 136.9 (aryl.)

Synthesis of $(CH_3CN)WCl_4(NN(p\text{-}Br\text{-}Ph)_2)$ (6.3c). Yielded 1.40 g (79.2%). ^1H NMR (500 MHz, CD_2Cl_2) δ, ppm: 2.55 (*s,* 3H, C*H*$_3$CN); 7.15 (*m*, 4H, aryl); 7.82 (*m*, 4H, aryl). ^{13}C NMR (125 MHz, CD_2Cl_2) δ, ppm: 4.4 (*C*H$_3$CN); 120.9 (CH$_3$*C*N); 124.5, 125.6, 126.0, 126.5, 131.5, 131.7, 131.8, 131.9, 132.1 (aryl.)

Synthesis of $(CH_3CN)WCl_4(NNPh_2)$ (6.3d). See ref. 12.

Synthesis of $(CH_3CN)WCl_4(NN(p\text{-}CH_3\text{-}Ph)_2)$ (6.3e). Yielded 1.05 g (72.2%).

Synthesis of $(CH_3CN)WCl_4(NNMe_2)$ (6.3h). See ref. 12.

Synthesis of $(CH_3CN)WCl_4$(Npiperidyl) (6.3i). See ref. 12. X-ray quality crystals of **6.3i** were obtained from a saturated solution of **6.3i** in 2:1 pentane:toluene cooled to -30 °C.

Synthesis of $(dme)TaCl_3(NOMe)$ (6.4). See ref. 16.

Synthesis of $(dme)NbCl_3(NOMe)$ (6.5). A similar preparation to **6.4** was utilized, starting with $NbCl_5$. X-ray quality crystals of **6.5** were grown from a vapor diffusion of pentane into a saturated solution of **6.5**. ^1H NMR (300 MHz, CD_2Cl_2) δ, ppm: 3.98 (*s*, 3H, C*H*$_3$O); 4.02 (*s*, 3H, C*H*$_3$O); 4.10 (*m*, 4H, OC*H*$_2$); 4.25 (*s*, 3H, C*H*$_3$ON).

Synthesis of $(dme)NbBr_3(NNMe_2)$ (6.6). A similar preparation to **6.2h** was utilized, starting from $NbBr_5$ and $ZnBr_2$ instead of $NbCl_5$ and $ZnCl_2$. X-ray quality crystals were grown from a vapor diffusion of pentane into a saturated solution of **6.6** in $C_2H_4Cl_2$. ^1H NMR (300 MHz, CD_2Cl_2) δ, ppm: 3.32 (*s*, 6H, N(C*H*$_3$)$_2$); 4.03 (*s*, 3H, C*H*$_3$O); 4.05 (*s*, 3H, C*H*$_3$O); 4.15 (*m*, 4H, OC*H*$_2$).

Synthesis of $(dme)NbI_3(NNMe_2)$ (6.7). A similar preparation to **6.2h** was utilized, starting from NbI_5 and ZnI_2 instead of $NbCl_5$ and $ZnCl_2$. X-ray quality crystals

were grown from a vapor diffusion of pentane into a saturated solution of **6.7** in $C_2H_4Cl_2$. ^1H NMR (300 MHz, CD_2Cl_2) δ, ppm: 3.66 (*s*, 6H, $N(CH_3)_2$); 3.84 (*s*, 3H, CH_3O); 4.17 (*m*, 2H, OCH_2); 4.37 (*s*, 3H, CH_3O); 4.39 (*m*, 2H, OCH_2).

Table 6.4. Crystal and refinement data for complexes **6.1a**, **6.1c**, and **6.1e**.

	6.1a	**6.1c**	**6.1e**
CCDC Number	855853	856712	854441
Empirical formula	$C_{16}H_{18}N_2O_2Cl_3Ta \cdot C_6H_6$	$C_{16}H_{16}N_2O_2Br_2Cl_3Ta$	$C_{18}H_{24}Cl_3N_2O_2Ta$
Formula weight	635.73	717.43	587.69
T (K)	100(2)	100(2)	100(2)
a, Å	10.9765(4)	7.2890(3)	7.3415(4)
b, Å	14.9892(6)	13.3859(5)	9.2663(5)
c, Å	15.2682(6)	10.9809(4)	9.2663(5)
α, deg			78.390(3)
β, deg	110.395(2)	90.292(1)	84.353(3)
γ, deg			84.864(2)
Volume, Å^3	2354.58(16)	1071.39(7)	1075.72(10)
Z	4	2	2
Crystal system	Monoclinic	Monoclinic	Triclinic
Space group	$P2_1/c$	$P2_1$	P-1
d_{calc}, g/cm^3	1.793	2.218	1.814
θ range, deg	1.97 to 43.56	1.85 to 30.53	2.25 to 51.69
μ, mm^{-1}	5.030	11.000	5.496
Abs. Correction	Semi-Empirical	Semi-Empirical	Semi-Empirical
GOF	1.892	1.455	1.218
R_1 ,[a]	R1 = 0.0253,	R1 = 0.0196,	R1 = 0.0237,
wR_2 [b] [I>2σ(I)]	*w*R2 = 0.0359	*w*R2 = 0.0380	*w*R2 = 0.0343

[a] $R_1 = \Sigma||F_o| - |F_c||/\Sigma|F_o|$. [b] $wR_2 = [\Sigma[w(F_o^2-F_c^2)^2]/\Sigma[w(F_o^2)^2]]^{1/2}$.

Table 6.5. Crystal and refinement data for complexes **6.2a**, **6.2b**, and **6.2c**.

	6.2a	**6.2b**	**6.2c**
CCDC Number	85445	855001	856445
Empirical formula	$C_{16}H_{18}Cl_3N_2NbO_2$	$C_{16}H_{18}N_2O_2Cl_5Nb$	$C_{16}H_{18}Br_2Cl_3N_2NbO_2$
Formula weight	469.58	540.48	629.40
T (K)	100(2)	100(2)	100(2)
a, Å	19.4748(9)	7.3791(4)	8.8532(4)
b, Å	9.6654(4)	8.9250(4)	26.6360(13)
c, Å	19.3262(9)	16.3801(8)	9.4480(5)
α, deg		80.331(2)	
β, deg	93.727(2)	84.651(2)	99.838(2)
γ, deg		85.152(2)	
Volume, Å^3	3630.1(3)	1056.20(9)	2195.21(19)
Z	8	2	4
Crystal system	Monoclinic	Triclinic	Monoclinic
Space group	C 2/*c*	P–1	$P2_1/n$
d_{calc}, g/cm^3	1.718	1.699	1.904
θ range, deg	2.10 to 55.67	2.32 to 40.82	2.32 to 45.45
μ, mm^{-1}	1.116	1.216	4.567
Abs. Correction	None	None	None
GOF	2.165	2.169	1.445
R_1 ,[a]	R1 = 0.0263,	R1 = 0.0203,	R1 = 0.0247,
wR_2 [b] [I>2σ(I)]	*w*R2 = 0.0445	*w*R2 = 0.0515	*w*R2 = 0.0401

[a] $R_1 = \Sigma||F_o| - |F_c||/\Sigma|F_o|$. [b] $wR_2 = [\Sigma[w(F_o^2-F_c^2)^2]/\Sigma[w(F_o^2)^2]]^{1/2}$.

Table 6.6. Crystal and refinement data for complexes **6.2e**, **6.2f**, and **6.2g**.

	6.2e	**6.2f**	**6.2g**
CCDC Number	855000	856713	855003
Empirical formula	$C_{18}H_{24}N_2O_2Cl_3Nb$	$C_{18}H_{24}N_2O_4Cl_3Nb \cdot 0.5(C_7H_8)$	$C_{11}H_{18}N_2O_2Cl_3Nb$
Formula weight	499.65	577.72	409.53
T (K)	100(2)	100(2)	100(2)
a, Å	7.3620(4)	7.4401(3)	7.6003(4)
b, Å	9.2470(5)	10.5793(5)	10.5217(6)
c, Å	16.2248(10)	16.3555(7)	11.2752(6)
α, deg	78.177(3)	97.7650(10)°	64.736(2)
β, deg	85.220(3)	95.120(2)°	79.530(2)
γ, deg	84.498(3)	99.874(2)°	83.340(2)
Volume, Å^3	1073.81(11)	1248.30(9)	801.09(8)
Z	2	2	2
Crystal system	Triclinic	Triclinic	Triclinic
Space group	P–1	P–1	P–1
d_{calc}, g/cm^3	1.545	1.537	1.698
θ range, deg	2.26 to 44.88	1.26 to 30.57	2.02 to 51.72
μ, mm^{-1}	0.948	0.830	1.250
Abs. Correction	None	Semi Empirical	None
GOF	2.163	2.445	2.009
R_1 ,[a]	R1 = 0.0237,	R1 = 0.0332,	R1 = 0.0223,
wR_2 [b] [I>2σ(I)]	*w*R2 = 0.0556	*w*R2 = 0.0624	*w*R2 = 0.0476

[a] $R_1 = \Sigma||F_o| - |F_c||/\Sigma|F_o|$. [b] $wR_2 = [\Sigma[w(F_o^2-F_c^2)^2]/\Sigma[w(F_o^2)^2]]^{1/2}$.

Table 6.7. Crystal and refinement data for complexes **6.2h**, **6.2i**, and **6.3i**.

	6.2h	**6.2i**	**6.3i**
CCDC Number	855020	855260	855852
Empirical formula	$C_6H_{16}N_2O_2Cl_3Nb$	$C_9H_{20}N_2O_2Cl_3Nb$	$C_7H_{13}N_3Cl_4W$
Formula weight	347.47	387.53	464.85
T (K)	100(2)	100(2)	100(2)
a, Å	20.6913(14)	6.8865(3)	9.6582(4)
b, Å	12.5611(8)	12.1853(5)	14.7762(7)
c, Å	15.4117(10)	18.5285(8)	9.7818(4)
α, deg			
β, deg	90.294(4)		92.958(2)
γ, deg			
Volume, Å^3	4005.5(5)	1554.80(11)	1394.12(10)
Z	12	4	4
Crystal system	Monoclinic	Orthorhombic	Monoclinic
Space group	$P2_1/c$	$P2_12_12_1$	$P2_1/n$
d_{calc}, g/cm^3	1.729	1.656	2.215
θ range, deg	1.90 to 44.67	2.00 to 47.65	2.50 to 53.16
μ, mm^{-1}	1.482	1.282	9.026
Abs. Correction	None	None	Semi Empirical
GOF	1.516	1.310	1.462
R_1 ,[a]	R1 = 0.0287,	R1 = 0.0313,	R1 = 0.0210,
wR_2 [b] [I>2σ(I)]	*w*R2 = 0.0408	*w*R2 = 0.0417	*w*R2 = 0.0323

[a] $R_1 = \Sigma||F_o| - |F_c||/\Sigma|F_o|$. [b] $wR_2 = [\Sigma[w(F_o^2-F_c^2)^2]/\Sigma[w(F_o^2)^2]]^{1/2}$.

Table 6.8. Crystal and refinement data for complexes **6.4**, **6.5**, and **6.6**.

	6.4	**6.5**	**6.6**
CCDC Number	853141	854222	855855
Empirical formula	$C_5H_{13}NO_3Cl_3Ta$	$C_5H_{13}NO_3Cl_3Nb$	$C_6H_{16}N_2O_2Br_3Nb$
Formula weight	422.46	334.42	480.85
T (K)	100(2)	100(2)	100(2)
a, Å	14.4450(8)	14.3723(6)	14.9534(4)
b, Å	6.9104(4)	6.9176(3)	7.1414(2)
c, Å	11.9863(7)	12.0742(5)	26.5581(6)
α, deg			
β, deg			
γ, deg			
Volume, Å^3	1196.48(12)	1200.44(9)	2836.09(13)
Z	4	4	8
Crystal system	Orthorhombic	Orthorhombic	Orthorhombic
Space group	P $na2_1$	P $na2_1$	P $na2_1$
d_{calc}, g/cm^3	2.345	1.850	2.252
θ range, deg	3.27 to 43.34	2.83 to 53.14	1.53 to 27.48
μ, mm^{-1}	9.834	1.648	9.284
Abs. Correction	Semi-empirical	Semi-empirical	Semi Empirical
GOF	1.129	1.557	1.279
R_1 ,[a]	R1 = 0.0231,	R1 = 0.0247,	R1 = 0.0218,
wR_2 [b] [I>2σ(I)]	*w*R2 = 0.0274	*w*R2 = 0.0363	*w*R2 = 0.0331

[a] $R_1 = \Sigma||F_o| - |F_c||/\Sigma|F_o|$. [b] $wR_2 = [\Sigma[w(F_o^2-F_c^2)^2]/\Sigma[w(F_o^2)^2]]^{1/2}$.

Table 6.9. Crystal and refinement data for complex **6.7**.

	6.7
CCDC Number	856043
Empirical formula	$C_6H_{16}N_2O_2I_3Nb$
Formula weight	621.82
T (K)	100(2)
a, Å	15.2855(9)
b, Å	7.3944(4)
c, Å	27.2523(15)
α, deg	
β, deg	
γ, deg	
Volume, Å^3	3080.2(3)
Z	8
Crystal system	Orthorhombic
Space group	P $na2_1$
d_{calc}, g/cm^3	2.682
θ range, deg	2.67 to 30.58
μ, mm^{-1}	6.780
Abs. Correction	Semi Empirical
GOF	2.184
R_1 ,[a]	R1 = 0.0505,
wR_2 [b] [I>2σ(I)]	*w*R2 = 0.1033

[a] $R_1 = \Sigma||F_o| - |F_c||/\Sigma|F_o|$. [b] $wR_2 = [\Sigma[w(F_o^2-F_c^2)^2]/\Sigma[w(F_o^2)^2]]^{1/2}$.

REFERENCES

1. Chatt, J.; Dilworth, J. R.; Richards, R. L. *Chem. Rev.* **1978**, *78*, 589.
2. For representative examples, see: (a) Banerjee, S.; Odom, A. L. *Dalton Trans.* **2008**, 2005. (b) Yandulov, D. V.; Schrock, R. R. *Science* **2003**, *301*, 76. (c) Schrock, R. R.; Glassman, T. E.; Vale, M. G.; Kol, M. *J. Am. Chem. Soc.* **1993**, *115*, 1760. (d) Dilworth, J. P.; Jobanputra, P.; Parrott, S. J.; Thompson, R. M.; Povey, D. C.; Zubieta, J. A. *Polyhedron* **1992**, *11*, 147. (e) Huynh, M. H. V.; Lee, D. G.; White, P. S.; Meyer, T. J. *Inorg. Chem.* **2001**, *40*, 3842. (f) Huynh, M. H. V.; El-Samanody, E. S.; Demadis, K. D.; White, P. S.; Meyer, T. J. *Inorg. Chem.* **2000**, *39*, 3075. (g) Coia, G. M.; Devenney, M.; White, P. S.; Meyer, T. J. *Inorg. Chem.* **1997**, *36*, 2341.
3. Walsh, P. J.; Carney, M. J.; Bergman, R. G. *J. Am. Chem. Soc.* **1991**, *113*, 6343.
4. (a) Parsons, T. B.; Hazari, N.; Cowley, A. R.; Green, J. C.; Mountford, P. *Inorg. Chem.* **2005**, *44*, 8442. (b) Selby, J. D.; Manley, C. D.; Feliz, M.; Schwarz, A. D.; Clot, E.; Mountford, P. *J. Chem. Soc., Chem. Commun.* **2007**, 4937. (c) Selby, J. D.; Schulten, C.; Schwarz, A. D.; Stasch, A.; Clot, E.; Jones, C.; Mountford, P. *J. Chem. Soc., Chem. Commun.* **2008**, 5101. (d) Clulow, A. J.; Selby, J. D.; Cushion, M. G.; Schwarz, A. D.; Mountford, P. *Inorg. Chem.* **2008**, *47*, 12049. (e) Selby, J. D.; Manley, C. D.; Schwarz, A. D.; Clot, E.; Mountford, P. *Organometallics* **2008**, *27*, 6479.
5. (a) Li, Y.; Shi, Y.; Odom, A. L. *J. Am. Chem. Soc.* **2004**, *126*, 1794. (b) Patel, S.; Li, Y.; Odom, A. L. *Inorg. Chem.* **2007**, *46*, 6373.
6. (a) Herrmann, H.; Fillol, J. L.; Wadepohl, H.; Gade, L. H. *Angew. Chem. Int. Ed. Eng.* **2007**, *46*, 8426. (b) Herrmann, H.; Fillol, J. L.;Gehrmann, T.; Enders, M.; Wadepohl, H.; Gade, L. H. *Chem. Eur. J.* **2008**, *14*, 8131. (c) Herrmann, H.; Wadepohl, H.; Gade, L. H. *J. Chem. Soc., Dalton Trans.* **2008**, 2111. (d) Herrman, H.; Gehrmann, T.; Wadepohl, H.; Gade, L. H. *J. Chem. Soc., Dalton Trans.* **2008**, 6231. (e) Weitershaus, K.; Wadepohl, H.; Gade, L. H. *Organometallics*, **2009**, *28*, 3381. (f) Weitershaus, K.; Fillol, J. L.; Wadepohl, H.; Gade, L. H. *Organometallics*, **2009**, *28*, 4747.
7. Mindiola, D. J. Angew. Chem. Int. Ed. Eng. **2008**, 47, 2.
8. Green, M. L. H.; James, J. T.; Saunders, J. F.; Souter, J. *J. Chem. Soc. Dalton Trans.*, **1997**, 1281.

9. Sebe, E.; Heeg, M. J.; Winter, C. H. *Polyhedron*, **2006**, *25*, 2109.
10. Tonks, I. A.; Bercaw, J. E. *Inorg. Chem.* **2010**, *49*, 4648.
11. Korolev, A. V.; Rheingold, A. L.; Williams, D. S. *Inorg. Chem.* **1997**, *36*, 2647.
12. Koller, J.; Ajmera, H. M.; Abboud, K. A.; Anderson, T. J.; McElwee-White, L. *Inorg. Chem.* **2008**, *47*, 4457.
13. Williams, D. S.; Thompson, D. W.; Korolev, A. V. *J. Am. Chem. Soc.* **1996**, *118*, 6526.
14. Williams, D. S.; Korolev, A. V. *Inorg. Chem.* **1998**, *37*, 3809.
15. Kahlal, S.; Saillard, J.-Y.; Hamon, J.-R.; Manzur, C.; Carrillo, D. *Dalton Trans.* **1998**, 1229.
16. Haug, K.; Hiller, W.; Strahle, J. *Z. Anorg. Allg. Chem.* **1986**, *533*, 49.
17. Pangborn, A. B.; Giardello, M. A.; Grubbs, R. H.; Rosen, R. K.; Timmers, F. J. *Organometallics*, **1996**, *15*, 1518.

CHAPTER 7

Kinetics and Mechanism of Indene C–H Activation by $[(COD)IrOH]_2$

ABSTRACT

The hydroxy-bridged dimer $[(COD)IrOH]_2$ (COD = 1,5-cyclooctadiene) (**7.1**) cleanly C-H activates indene and cyclopentadiene to form (COD)Ir(η^3-indenyl) (**7.2**) and (COD)Ir(η^5-C_5H_5) (**7.3**), respectively. The kinetics of the formation of **7.2** has been investigated, and the mechanism involves coordination of indene to the dimeric **7.1** followed by rate determining C-H activation from the dimer-indene unit. This is similar to the rhodium analog, $[(COD)RhOH]_2$, but different from group 10 hydroxy dimers, which must dissociate to monomeric solvento species prior to substrate coordination. Additionally, the crystal structure of $[(COD)Ir]_5(\mu_4\text{-O})(\mu_3\text{-O})(\mu_2\text{-OH})$ (**7.4**), a dehydration product of **7.1**, is presented.

INTRODUCTION

The selective functionalization of C–H bonds could have a significant impact on areas such as commodity chemical development, pharmaceuticals, and fuels.[1] Many transition-metal complexes capable of C–H activation are unstable or unreactive in the presence of water, which represents a significant obstacle since water is a potential byproduct of oxidative C–H functionalizations utilizing O_2. Additionally, many model systems for electrophilic C–H activation require making a new C–H bond as the desired C–H bond is broken. In order to overcome these barriers, several groups have studied C–H bond activation utilizing metal alkyoxy and hydroxy complexes in the presence of alcohols and water.[2–4]

Recently, our group has found that the air- and water-stable hydroxy-bridged dimers $[(diimine)M_2(\mu_2\text{-}OH)]_2^{2+}$ and the *bis*(aquo) dications $[(diimine)M(OH_2)]^{2+}$ (M = Pd, Pt) are capable of reacting with a variety of C–H bonds.[5] Mechanistic studies showed that the Pd dimers can dissociate to (diimine)PdOH(solv) monomers in the presence of weakly coordinating solvents and then react directly with indene, whereas the Pt dimers required acid assistance to generate the $(diimine)Pt(OH_2)_2$ dication before reaction with indene. In both cases, displacement of the coordinated solvent ligand by indene was rate limiting, and as a result we explored the neutral dimer $[(COD)RhOH]_2$ (COD = 1,5-cyclooctaidene) anticipating that solvent displacement from a neutral (COD)RhOH(solv) species would be faster than the cationic group 10 analogues.[6] However, $[(COD)RhOH]_2$ instead reacted directly from the dimer and the rate limiting step was found to be C–H activation rather

than ligand displacement. As a result of the mechanistic change, the Rh dimer reacted with indene slightly slower than the group 10 dimers. Thus, we have turned our attention to the Ir congener, $[(COD)IrOH]_2$, anticipating that it may C–H activate more rapidly than $[(COD)RhOH]_2$.

RESULTS AND DISCUSSION

[(COD)IrOH]$_2$ (**7.1**) reacts with 2 equivalents of indene to generate the η^3-indenyl species, **7.2**, quantitatively as determined by ^{1}H NMR spectroscopy (eq. 7.1). **7.1** is only slightly soluble in neat CD_2Cl_2, so solvent mixtures of d_3-TFE (TFE = 1,1,1-trifluroethanol) and CD_2Cl_2 were utilized in the studies below.

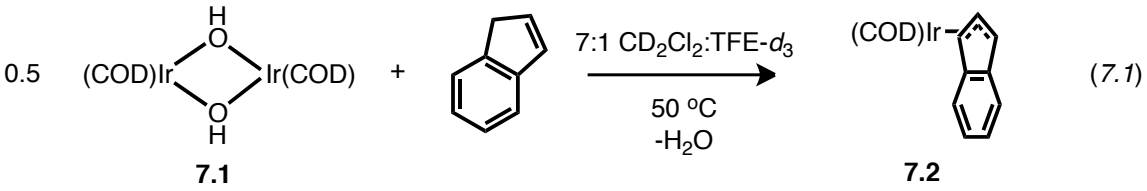

7.1 **7.2** (*7.1*)

Kinetics of Indene C-H Activation with [(COD)]IrOH]$_2$

The kinetics of the reaction were followed using the conditions shown in eq. 7.1, with varying quantities of [Indene] and [TFE]. No intermediates were observed by ^{1}H NMR. The log plots with varying [Indene] are shown in Figure 7.1 along with the accompanying graph of k_{obs} *vs.* [Indene]. The reaction was found to be first order with respect to indene and first order with respect to [(COD)IrOH]$_2$. There appears to be a slight dependence on [TFE], although it is not first order (*vide infra*). The kinetic isotope effect (KIE) for the reaction was determined by measuring the rate of parallel reactions of **7.1** with indene and 1,1,3-trideuteroindene, and was found to be k_H/k_D = 3.1(1), consistent with rate-determining C-H activation.

An Eyring analysis of reactions carried out at different temperatures gave the following activation parameters: $\Delta H^{\ddagger}$ = 87.4(2) kJ mol^{-1} and $\Delta S^{\ddagger}$ = -53.0(2) J mol^{-1} K^{-1} (Figure 7.2). The large negative entropic parameter is consistent with a transition state

where indene has associated to the IrOH dimer but C–H activation/H_2O release has not yet occurred.

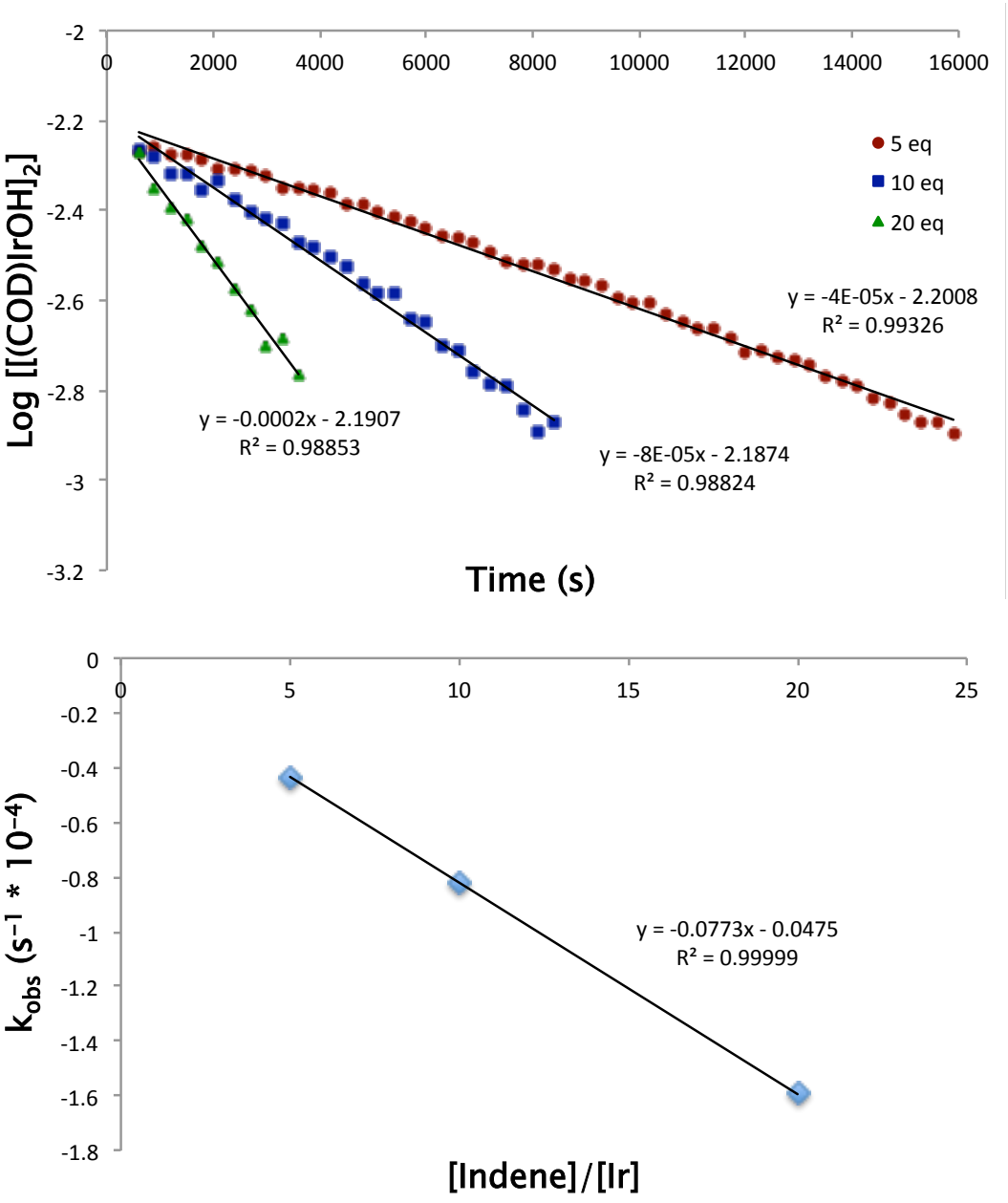

Figure 7.1. Log plot analysis of the reaction of **7.1** with indene at varying concentrations of indene. Log plots remain linear up to about 3 half lives of the reaction, confirming 1st order behavior for $[(COD)IrOH]_2$.

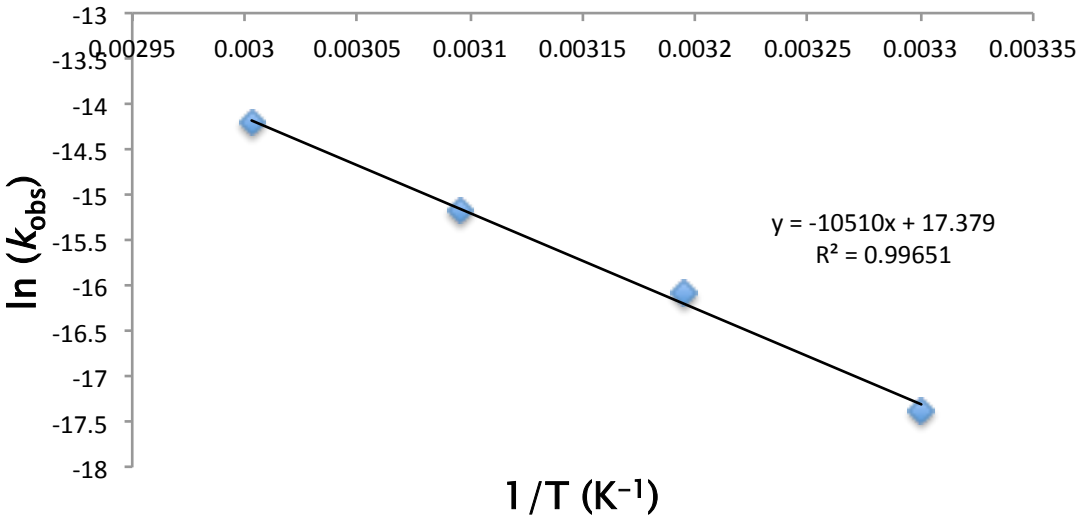

Figure 7.2. Eyring analysis of the reaction of **7.1** with indene.

The kinetic and Eyring data are most consistent with a mechanism similar to the $[(COD)RhOH]_2$ C–H activation mechanism, outlined in Scheme 7.1. In this mechanism, **7.1** and indene are in preequilibrium with the indene adduct **A**, with the equilibrium strongly favoring **7.1** since no intermediates are observed by ^1H NMR. The C–H activation must occur through a dimeric Ir species since the kinetics show a first order dependence on dimer, whereas a half order dependence would be expected if the dimer dissociated prior to C–H activation. **A** then intramolecularly C–H activates indene in the rate determining step to generate one equivalent of **7.2** and one equivalent of (COD)Ir(OH)(solv) **C**. This step is likely rate determining due to the large negative entropy of activation and large KIE. Since there is a dependence on [TFE], there may be competitive precoordination of TFE to generate **B**, which can C–H activate in a similar manner to generate **7.2** and **C**. Alternately, the rate dependence on [TFE] could be a result of a change in solvent polarity, since TFE comprises greater than 10% of the

solvent by volume. From here, **C** undergoes fast reaction with another equivalent of indene to generate a second equivalent of **7.2**.

Scheme 7.1

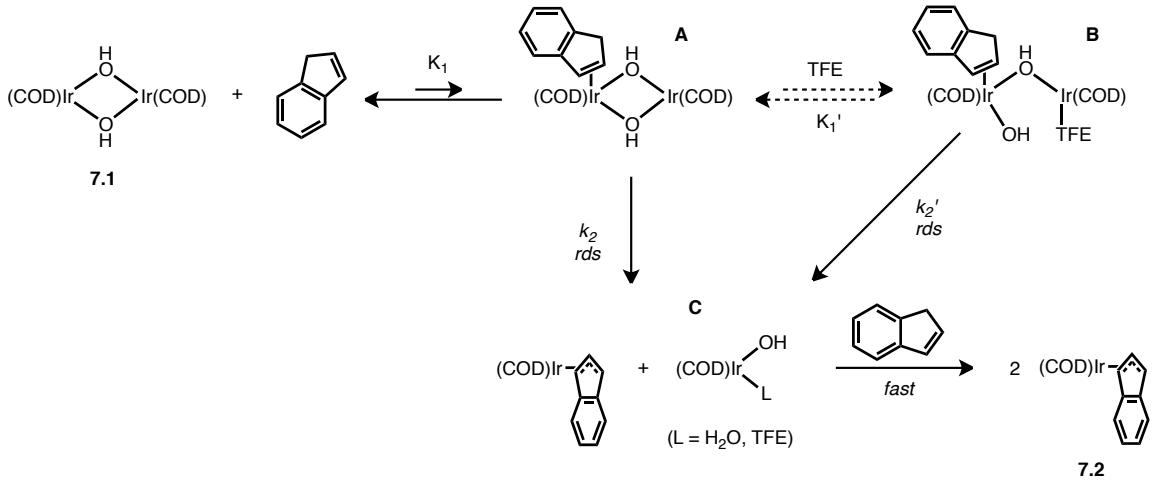

When compared to indene C–H activation with $[(COD)RhOH]_2$, the rate of the reaction with **7.1** is roughly the same order of magnitude and proceeds through a similar mechanism. The enthalpy of activation is larger for the Ir case (87.4(2) *vs.* 69.4(2) kJ mol^{-1} for Rh). One possible explanation for the differences in activation enthalpy could be a result of the differences in M–OH bond strength. For example, if the transition state of C–H activation involved significant M–OH bond breakage (such as an intramolecular electrophilic substitution[2] or σ–bond metathesis[3]), breakage of the stronger Ir–OH bond would lead to a larger enthalpy of activation than the corresponding Rh analog. Moreover, since the oxidation of Ir^{I} to Ir^{III} should be more facile than for Rh, a smaller enthalpy of activation would be expected for Ir if the transition state involved oxidative addition to the metal center. As a result, the activation parameters and kinetics of the Ir and Rh systems lead us to rule out a formal

oxidative addition of the indene C–H bond to the metal center, and instead favor direct attack of the C–H bond by the Ir–OH bond (Scheme 7.2).

Scheme 7.2

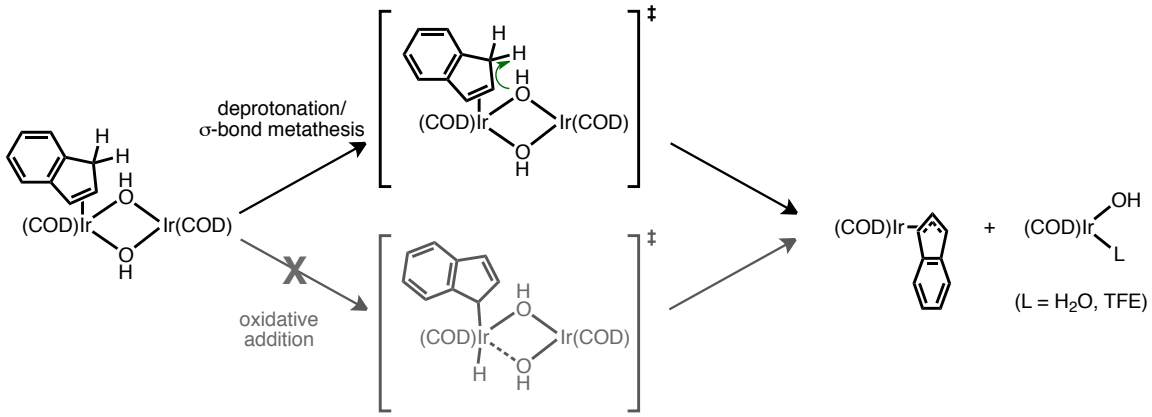

Unfortunately, **7.1** does not react with the C–H bonds of cyclopentene, cyclohexene, or other more challenging substrates. However, **7.1** does rapidly C–H activate cyclopentadiene to generate (COD)Ir(η^5-C_5H_5) (**7.3**) (eq 7.2).

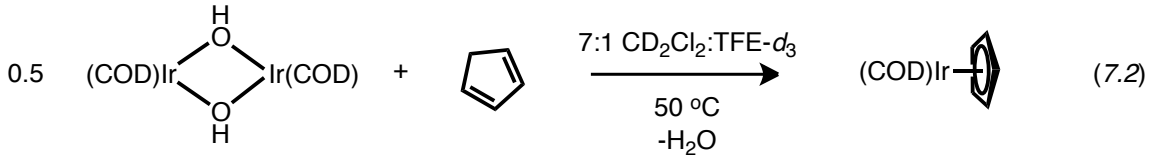

7.1 **7.3** (*7.2*)

Spontaneous Dehydration of [(COD)IrOH]₂

Interestingly, **7.1** is not stable in dry dichloromethane. When yellow **7.1** was dissolved in dichloromethane dried over CaH_2 or passed through an activated alumina column, the solution turned orange over the course of a few hours, and after standing overnight the solution yielded small, dark red crystals. X-ray diffraction analysis of the red crystalline material revealed it to be a dehydrogenation product of **7.1**, [(COD)Ir]$_5$(μ_4-O)(μ_3-O)(μ_2-OH) (**7.4**) (eq. 7.3, Figure 7.3). Using wet solvent shuts down the reaction, so

the reaction appears to be driven by the expulsion of H_2O from **7.1** and the insolubility of the product. Unfortunately, the reaction does not appear to be reversible as the addition of H_2O to the mixture does not regenerate **7.1**.

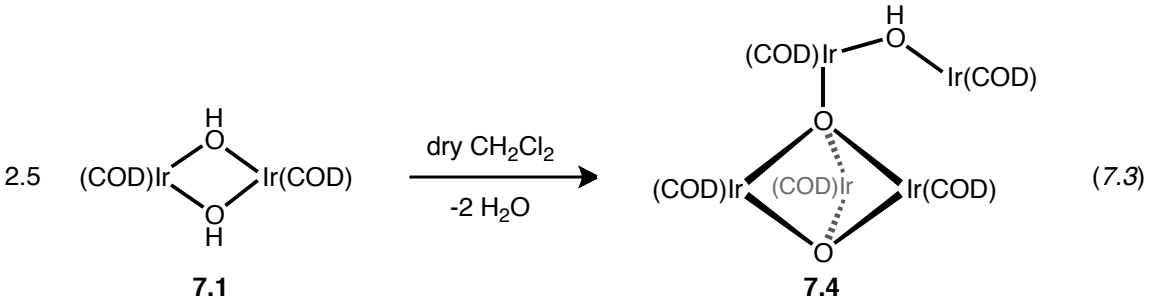

7.1 **7.4** (*7.3*)

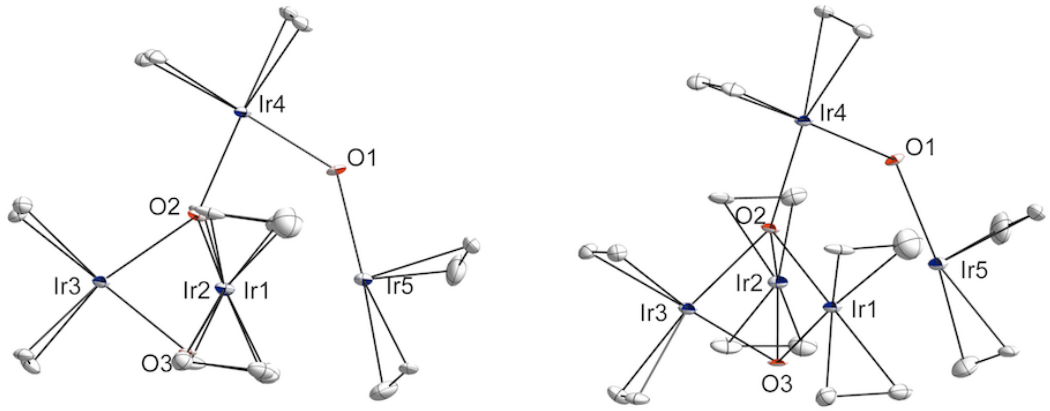

Figure 7.3. Thermal ellipsoid drawings of **7.4**. Selected bond distances (Å): Ir1–O2 2.102(1); Ir2–O2 2.0885(1); Ir3–O2 2.1409(1); Ir4–O2 2.0827(1); Ir1–O3 2.0225(1); Ir2–O3 2.0467(1); Ir3–O3 2.0536(1); Ir4–O1 2.0361(1); Ir5–O1 2.0906(1). Intermetallic distances (Å): Ir1–Ir2 3.0443(1); Ir1–Ir3 2.7610(1); Ir1–Ir5 2.8632(2); Ir2–Ir3 2.7292(2); Ir2–Ir5 3.0890(2). H atoms and methylene groups of the COD ligands have been removed for clarity.

7.4 consists of a trinuclear Ir_3 core capped by two oxo ligands, similar to an Ir^{II} trinuclear complex observed by Cotton, $[(COD)Ir]_3(\mu_3\text{-}O)_2(\mu_2\text{-}I)$, which was prepared by Ag^+ abstraction of an iodide ligand from $[(COD)IrI]_2I_2$.[7] The intermetallic distances in **7.4** range from 2.73–3.09 Å, indicating that there could be some degree of Ir–Ir bonding

within the molecule. The pendent [(COD)IrOH] unit is necessary to electronically satisfy the Ir_4O_2 core, since the 3-coordinate bridging oxygen is incapable of donating electron density to the 4th dangling Ir because of geometric constraints.

7.4 likely forms from the dehydration of **7.1** to form a bridging Ir oxo complex, (COD)IrOIr(COD), which then dimerizes to form a tetranuclear Ir_4O_2 core. The product then crystallizes out of solution by reaction with an additional half equivalent of **7.1**. While the mechanism is purely speculative, the net result of the reaction is the spontaneous intramolecular deprotonation of a hydroxyl group to generate a bridging Ir^{I} oxo species. This transformation is unprecedented on Ir^{I}, and complex **7.4** represents the first crystallographically characterized example of a formally Ir^{I} species containing bridging oxo ligands. This type of elementary reaction is garnering increased attention in late transition metal complexes, as hydroxyl deprotonation is an important step along catalytic water oxidation cycles.[8] A number of research groups have been investigating Ir^{III} complexes as water oxidation, but little work has gone into Ir^{I} complexes.[9] As a result, complexes similar to **7.4** could represent an entrypoint into potential Ir^{I} -catalyzed water oxidation cycles instead of the more precedented Ir^{III} systems.

CONCLUSIONS

7.1 C–H activates indene or cyclopentadiene to generate 2 equivalents of COD)Ir(η^3–indenyl) (**7.2**) or (COD)Ir(η^5–C_5H_5) (**7.3**). The kinetic and isotope labeling studies of the reaction reveal that **7.1** reacts directly from the dimeric species and that C–H activation is rate limiting. This reactivity is similar to the rhodium analog, $[(COD)RhOH]_2$. Comparison of the activation parameters of **7.1**– and $[(COD)RhOH]_2$–promoted C–H activation shows that **7.1** has a higher enthalpy of activation than $[(COD)RhOH]_2$, which indicates that the mechanism of C–H activation is likely an intramolecular deprotonation/σ–bond metathesis rather than oxidative addition of the C–H bond to the metal center to generate Ir^{III}. It was also noted that **7.1** spontaneously dehydrates in dry solvents to generate a bridging oxo complex, **7.4**, which is an elementary step along a water oxidation catalytic cycle.

EXPERIMENTAL SECTION

General Considerations and Instrumentation. All manipulations were carried out in a glovebox under a nitrogen atmosphere. $[(COD)IrOH]_2$[11] and 1,1,3-trideuteroindene[12] were prepared according to literature procedure. Indene and dicyclopentadiene were reagent grade commercial samples purchased from Sigma-Aldrich. Dicyclopentadiene was freshly cracked to cyclopentadiene prior to use. CD_2Cl_2 and trifluoroethanol-d_3 were purchased from Cambridge Isotopes and degassed prior to use. For some experiments, CH_2Cl_2 was dried *via* the method of Grubbs.[12] ^1H NMR spectra were recorded using a Varian INOVA 500 MHz spectrometer.

X-ray Crystal Data: General Procedure. Crystals were removed quickly from a scintillation vial to a microscope slide coated with Paratone N oil. Samples were selected and mounted on a glass fiber with Paratone N oil. Data collection was carried out on a Bruker KAPPA APEX II diffractometer with a 0.71073 Å MoKα source. The structures were solved by direct methods. All non-hydrogen atoms were refined anisotropically. Details regarding refined data and cell parameters are available in Table 7.1.

Synthesis of (COD)Ir(η^3-indenyl) (7.2). 5.0 mg **7.1** (0.0079 mmol, 1 equiv) was dissolved in 0.65 mL CD_2Cl_2 and 0.10 mL TFE-d_3 in a J-Young NMR tube. 36.9 µL of indene (.315 mmol, 40 equiv) was added to the solution, and the tube sealed and heated to 50 °C. The reaction was followed by NMR, with complete conversion occurring after 4 hours. The identity of the product was confirmed by comparing the ^1H NMR spectrum to an authentic sample of **7.2** purchased from Strem.

Synthesis of (COD)Ir(η^5-C_5H_5) (7.3). A similar preparation to **7.2** was used, substituting freshly cracked cyclopentadiene for indene. The reaction was followed by ^{1}H NMR and was complete within 30 minutes. The identity of **7.3** was confirmed by comparing the ^{1}H NMR spectrum to a sample prepared *via* salt metathesis of **7.1** with NaCp following literature procedure.[13]

Synthesis of [(COD)Ir]$_5$(μ_4-O)(μ_3-O)(μ_2-OH) (7.4). 10 mg (0.016 mmol) **7.1** was suspended in 2 mL dry, degassed CH_2Cl_2 in a J-Young NMR tube. The tube was sealed and the suspension was refluxed in an oil bath for 1 hour to give an orange solution with a small amount of **7.1** undissolved at the bottom. The solution was cooled to room temperature and left to stand overnight, during which time small red crystals of **7.4** formed. After 12 hours, near quantitative formation of **7.4** occurred. **7.4** was identified *via* X-ray crystallography since it was insoluble in all solvents tested. The formation of **7.4** could also be achieved without heating the suspension, but the general insolubility of **7.1** resulted in this method being slower and lower yielding.

Standard Reaction Protocol for Kinetics Experiments. 0.75 mL of a 6.5:1 CD_2Cl_2:TFE-d_3 stock solution containing 0.001M **7.1** (5 mg, 0.0079 mmol) and 5 µL TMS_2O (as a standard) was syringed into a J-Young NMR tube inside of a glovebox. The sample was cooled to 0 °C and the desired amount of a 1.575 M stock solution of indene in CD_2Cl_2 was added to the reaction (50 µL, 100 µL, or 200 µL) *via* syringe. An additional amount of CD_2Cl_2 was added to reactions that contained less than 200 µL of the indene stock solution to give all reactions a total volume of 0.95 mL. The reactions were then inserted into the preheated NMR probe and the temperature was allowed to equilibrate for

5 minutes before locking and shimming the instrument. An additional 5 minutes were utilized for locking and shimming before finally starting data collection 10 minutes after initial sample insertion. Single spectra were collected every 5 minutes until the starting material was completely consumed. The spectra were processed using the MestReNova software package and the starting material and product peaks were integrated against the internal TMS_2O standard. The two peaks used for all kinetic determinations were the vinylic COD peak in **7.1** (Figure 7.4, 3.68 ppm) and the 2-position of the η^3-indenyl in **7.2** (Figure 7.4, 6.04 ppm). In all cases, disappearance of the starting material was directly correlated to appearance of product. Several of the reactions were run in duplicate or triplicate to confirm reproducibility. The KIE experiments were carried out in a similar manner, utilizing 1,1,3-trideuteroindene in place of normal indene.

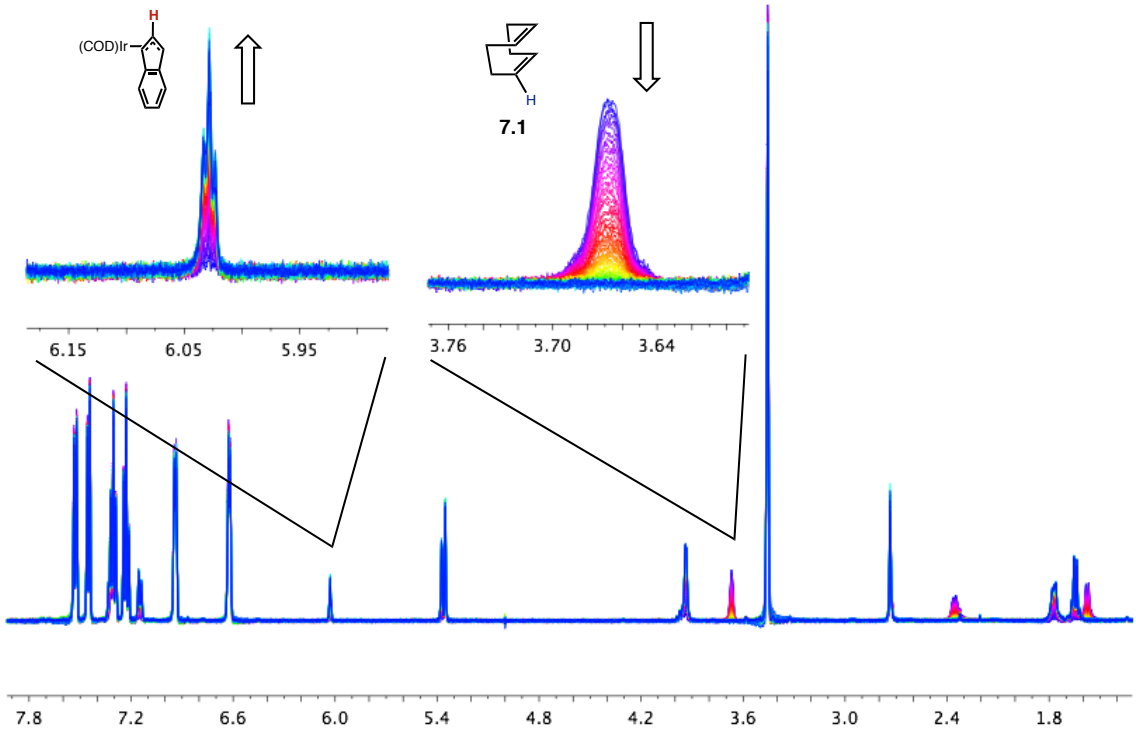

Figure 7.4. Example spectral array for a kinetic run of **7.3** with 10 equivalents of indene at 50 °C. The peaks that were integrated were the vinylic COD protons on the starting material **7.1** and the 2-H position on the product **7.2**.

Table 7.1. Crystal and refinement data for complex **7.4**.

	7.4
CCDC Number	885854
Empirical formula	$C_{40}H_{60}O_3Ir_5 \cdot CH_2Cl_2$
Formula weight	1635.93
T (K)	100(2)
a, Å	10.3282(4)
b, Å	22.4057(9)
c, Å	17.2239(7)
α, deg	
β, deg	92.280(2)
γ, deg	
Volume, Å^3	3982.6(3)
Z	4
Crystal system	Monoclinic
Space group	$P2_1/n$
d_{calc}, g/cm^3	2.726
θ range, deg	2.17 to 32.63
μ, mm^{-1}	16.819
Abs. Correction	Semi Empirical
GOF	1.436
R_1 ,[a]	R1 = 0.0236,
wR_2 [b] [I>2σ(I)]	*w*R2 = 0.0381

[a] $R_1 = \Sigma||F_o| - |F_c||/\Sigma|F_o|$. [b] $wR_2 = [\Sigma[w(F_o^2-F_c^2)^2]/\Sigma[w(F_o^2)^2]]^{1/2}$.

REFERENCES

1. (a) Crabtree, R. H. *Dalton Trans.* **2001**, *17*, 2437. (b) Labinger, J. A.; Bercaw, J. E. *Nature* **2002**, *417*, 507. (c) Fekl, U.; Goldberg, K. I. *Adv. Inorg. Chem.* **2003**, *54*, 259. (d) Vedernikov, A. N. *Curr. Org. Chem.* **2007**, *11*, 1401.
2. (a) Tenn, W. J.; Young, K. J. H.; Bhalla, G.; Oxgaard, J.; Goddard, W. A.; Periana, R. A. *J. Am. Chem. Soc*. **2005**, *127*, 14172. (b) Tenn, W. J.; Young, G. J.; Oxgaard, J.; Nielson, R. J.; Goddard, W. A.; Periana, R. A. *Organometallics* **2006**, *25*, 5173. (c) Oxgaard, J.; Tenn, W. J.; Nielson, R. J.; Periana, R. A.; Goddard, W. A. Organometallics 2007, 26, 1565.
3. (a) Feng, Y.; Lail, M.; Barakat, K. A.; Cundari, T. R.; Gunnoe, T. B.; Petersen, J. L. *J. Am. Chem. Soc.* **2005**, *127*, 14174. (b) Feng, Y.; Lail, M.; Foley, N. A.; Gunnoe, T. B.; Barakat, K. A.; Cundari, T. R.; Petersen, J. L. *J. Am. Chem. Soc*. **2006**, *128*, 7982. (c) Cundari, T. R.; Grimes, T. V.; Gunnoe, T. B. *J. Am. Chem. Soc*. **2007**, *129*, 13172.
4. (a) Kloek, S. M.; Heinekey, D. M.; Goldberg, K. I. *Angew. Chem., Int. Ed*. **2007**, 46. (b) Hanson, S. K.; Heinekey, D. M.; Goldberg, K. I. *Organometallics* **2008**, *27*, 1454.
5. (a) Williams, T. J.; Caffyn, A. J. M.; Hazari, N.; Oblad, P. F.; Labinger, J. A.; Bercaw, J. E. *J. Am. Chem. Soc*. **2008**, *130*, 2418. (b) Bercaw, J. E.; Hazari, N.; Labinger, J. A.; Oblad, P. F. *Angew. Chem., Int. Ed*. **2008**, *47*, 9941. (c) Bercaw, J. E.; Hazari, N.; Labinger, J. A. *J. Org. Chem*. **2008**, *73*, 8654. (d) Oblad, P. F.; Bercaw, J. E.; Hazari, N.; Labinger, J. A. *Organometallics* **2010**, *29*, 789.
6. Bercaw, J. E.; Hazari, N.; Labinger, J. A. *Organometallics* **2009**, *28*, 5489.
7. Cotton, F. A.; Lahuerta, P.; Sanau, M.; Schotzer, W. *J. Am. Chem. Soc.* **1985**, *107*, 8284.
8. (a) Lewis, N. S.; Nocera, D. G. *Proc. Natl. Acad. Sci. U.S.A*. **2006**, *103*, 15729. (b) Sala, X.; Romero, I.; Rodriguez, M.; Escriche, L.; Llobet, A. *Angew. Chem., Int. Ed*. **2009**, *48*, 2842. (c) Brimblecombe, R.; Dismukes, G. C.; Swiegers, G. F.; Spiccia, L. *Dalton Trans*. **2009**, 9374.
9. (a) McDaniel, N. D.; Coughlin, F. J.; Tinker, L. L.; Bernhard, S. *J. Am. Chem. Soc*. **2008**, *130*, 210. (b) Hull, J. F.; Balcells, D.; Blakemore, J. D.; Incarvito, C. D.; Eisenstein, O.; Brudvig, G. W.; Crabtree, R. H. *J. Am. Chem. Soc*. **2009**, *131*, 8730. (c) Blakemore, J. D.; Schley, N. D.; Balcells, D.; Hull, J. F.; Olack, G. W.; Incarvito, C. D.; Eisenstein, O.; Brudvig, G. W.; Crabtree, R. H. *J. Am. Chem. Soc*.

2010, *132*, 16017. (d) Savini, A.; Bellachioma, G.; Ciancaleoni, G.; Zuccaccia, C.; Zuccaccia, D.; Macchioni, A. *Chem. Commun*. **2010**, *46*, 9218. (e) Lalrempuia, R.; McDaniel, N. D.; M€uller-Bunz, H.; Bernhard, S.; Albrecht, M. *Angew. Chem. Int. Ed*. **2010**, *49*, 9765. (f) Hetterscheid, D. G. H.; Reek, J. N. H. *Chem. Commun*. **2011**, *47*, 2712. (g) Brewster, T. P.; Blakemore, J. D.; Schley, N. D.; Incarvito, C. D.; Hazari, N.; Brudvig, G. W.; Crabtree, R. H. *Organometallics* **2011**, *30*, 965. (h) Schley, N. D.; Blakemore, J. D.; Subbaiyan, N. K.; Incarvito, C. D.; D'Souza, F.; Crabtree, R. H.; Brudvig, G. W. *J. Am. Chem. Soc*. **2011**, *133*, 10473. (i) Dzik, W. I.; Calvo, S. E.; Reek, J. N. H.; Lutz, M.; Ciriano, M. A.; Tejel, C.; Hetterscheid, D. G. H.; de Bruin, B. *Organometallics* **2011**, *30*, 372.

10. Green, L. M.; Meek, D. W. *Organometallics* **1989**, *8*, 659.
11. Yasuda, M.; Pak, C.; Sakurai, H. *Bull. Chem. Soc. Jpn.* **1980**, *53*, 502.
12. Pangborn, A. B.; Giardello, M. A.; Grubbs, R. H.; Rosen, R. K.; Timmers, F. J. *Organometallics* **1996**, *15*, 1518.
13. Sowa Jr., J. R.; Angelici, R. J. *J. Am. Chem. Soc.* **1991**, *113*, 2537.

APPENDIX A

Structure and Reactivity of Neutral and Cationic Tantalocene Imido Complexes

ABSTRACT

$Cp_2TaCl(N^tBu)$ (**A.1**) was synthesized *via* salt metathesis of NaCp with $(py)_2TaCl_3(N^tBu)$. Reaction of **A.1** with MeLi yielded $Cp_2TaMe(N^tBu)$ (**A.2**). The cationic complexes $[Cp_2Ta(N^tBu)(py)][BArF_{24}]$ (**A.3**) and $[Cp_2TaMe(HN^tBu)(THF)][BArF_{20}]$ (**A.4**) were synthesized *via* halide abstraction and protonation from **A.1** and **A.2**, respectively. Halide abstraction of **A.1** in the presence of MeCCMe led slowly to the formation of the azametallacycle $[Cp_2Ta(\kappa^2\text{-}2\text{-butenyl-}2\text{-}^i\text{Bu-amide})][BArF_{24}]$ **A.5**. The crystal structures of **A.1** and **A.3** are reported and are compared to **5.7** and other tantalocene imidos.

INTRODUCTION

Over the past 30 years, many neutral tantalum imido complexes have been synthesized, but their reactivity patterns remain ambiguous.[1-4] Typically, group 5 imidos are less reactive than their group 4 counterparts: tantalum imidos have been used as ancillary ligands for polymerization,[5] addition of hydrogen to Ta-alkyls,[6] and isocyanide insertion into Ta-alkyls.[7] However, they have also been observed to be reactive sites, for example in the migratory insertion of isocyanides or CO_2, C-H activation, and [2+2] addition to the Ta-N multiple bond.[8-10] Less is known about the reactivity of cationic tantalum imides, which may be more reactive due to their isoelectronic relationship to neutral group 4 imidos.

The most well-studied example of a cationic Ta imido is Bercaw's $[Cp^*_2Ta(THF)(N^tBu)][BArF_{20}]$, which can add H_2, PhCCH, or the Cp* methyl C-H across the Ta-N multiple bond.[11] These results prompted us to further investigate the reactivity of cationic Cp_2Ta imido compounds, in the hope that successful reactions could then be applied to analogous compounds containing the hydrazido(2-) ligands described in Chapters 5 and 6.

RESULTS AND DISCUSSION

Synthesis and Reactivity of Tantalocene Imidos

$Cp_2TaCl(N^tBu)$ (**A.1**) was synthesized *via* salt metathesis of NaCp with $(py)_2TaCl_3(N^tBu)$. Reaction of **A.1** with MeLi yielded $Cp_2TaMe(N^tBu)$ (**A.2**) (eq. A.1).[3]

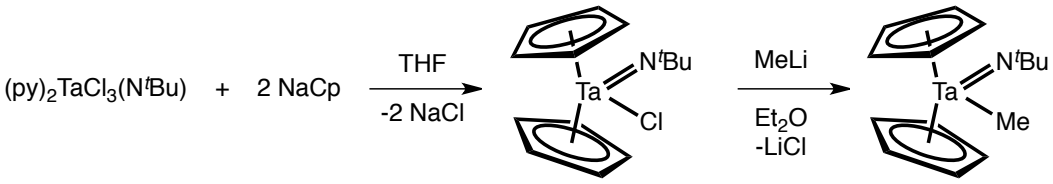

A.1 **A.2** (*A.1*)

Several routes were attempted to make cationic tantalocene complexes. First, chloride abstraction of **A.1** with $Na[BArF_{24}]$ ($BArF_{24}$ = $B(3,5\text{-}(CF_3)_2\text{-}C_6H_3)_4^-$) was attempted. Reacting **A.1** with $Na[BArF_{24}]$ in CD_2Cl_2 resulted in the slow formation of two unidentified Cp_2Ta products over the course of 1 week. However, if the reaction was performed in the presence of pyridine, quantitative conversion to $[Cp_2Ta(N^tBu)(py)][BArF_{24}]$ (**A.3**) was observed overnight (eq. A.2).

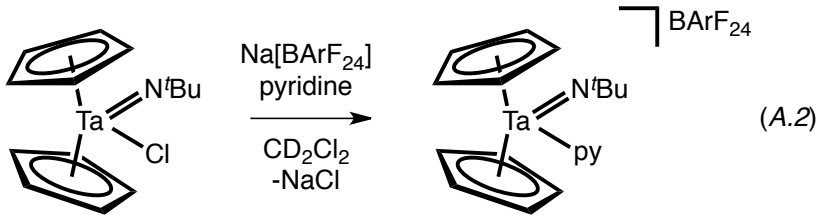

A.1 **A.3** (*A.2*)

Unfortunately, **A.3** does not exhibit any further reactivity with alkynes or H_2. It appears that the Ta–pyridine unit is not substitutionally labile. Since the coordinatively and electronically saturated **A.3** would need to dissociate a ligand in order to open up a reactive site, it appears as if the nonlabile pyridine will prevent any further reactivity.

Attempts to carry out the halide abstraction in THF, hoping to generate a weaker THF adduct, were unsuccessful.

Another route to cationic complexes that was attempted was protonolysis of the Ta–Me bond in **A.2**. However, reaction of **A.2** with $[HMe_2NPh][BArF_{20}]$ ($BArF_{20}$ = $B(C_6F_5)_4^-$) instead protonated the imido group, generating cationic amide **A.4** (eq. A.3). Prolonged heating of **A.4** resulted in no reaction rather than in the formation of the desired imido and CH_4.

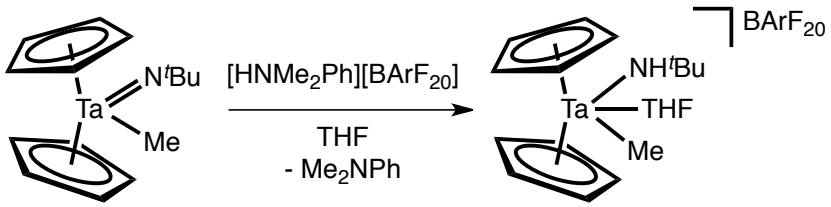

A.2 **A.4** (*A.3*)

While **A.3** is unreactive toward alkynes, reaction of **A.1** with $Na[BArF_{24}]$ in CD_2Cl_2 with excess MeCCMe resulted in the slow formation of the [2+2] addition product, $[Cp_2Ta(\kappa_2\text{-}2\text{-butenyl-}2\text{-}^t\text{Bu-amide})][BArF_{24}]$ (**A.5**) (eq. A.4). Full conversion took over 3 days at room temperature. Presumably, **A.1** reacts with $Na[BArF_{24}]$ to generate the cationic imido $[Cp_2Ta{=}N^tBu]^+$, which then undergoes [2+2] reaction with the alkyne. Unfortunately, reaction with other substituted alkynes was unsuccessful, and the extremely slow rate of reaction indicates that achieving similar reactivity with related hydrazido complexes would be challenging.

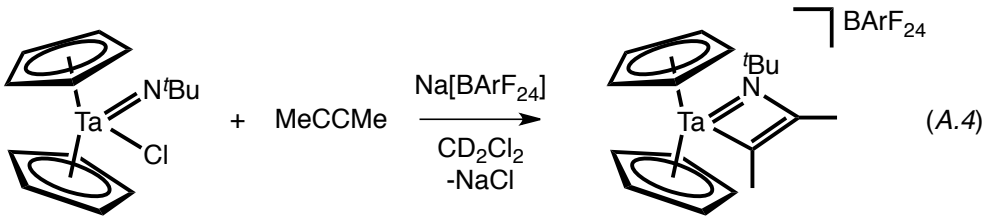

(*A.4*)

A.1 **A.5**

Structure of Tantalocene Imidos

The crystal structures of **A.1** and **A.3** are presented in Figure A.1. Interestingly, despite **A.3** being cationic, the bonding metrics in **A.1** and **A.3** are almost identical: both the Ta–N bond distances (1.78 Å) and Ta–N–C bond angles (174°) are within experimental error of each other. If the imido is treated as an LX_2–type donor in **A.1** and **A.3**, the complexes would be formally 20–electron. As a result, the imido functionality is best considered an X_2 donor with a lone pair mostly localized on N.[12] In this case, one might expect the Ta–N–C angle to be bent to accommodate the lone pair; however, studies have shown that the energy difference between the linear and bent forms is extremely low.[13] One comparison that can be made, though, is to the hydrazido compound $Cp_2TaCl(NNPh_2)$ (**5.7**). In this complex, the Ta–N–N angle is significantly bent (167°, unlike all other Cp_2Ta imidos); rather than an electronic difference (which, as mentioned before seems to be negligible), we believe that this angle difference is likely a result of the extremely large steric profile of the $NNPh_2$ unit, which must bend into the metallocene wedge in order to reduce steric clashing between the NPh_2 unit and the cyclopentadiene ligands.

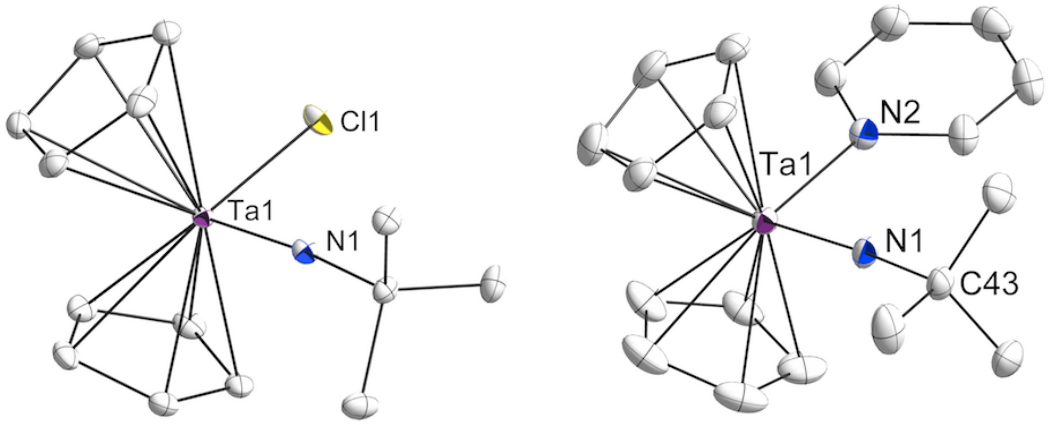

Figure A.1. Thermal ellipsoid drawings of **A.1** (left) and **A.3** (right). Counteranion of **A.3** removed for clarity. Selected bond lengths (Å) and angles (°): **A.1**: Ta1–N1 1.778(1); Ta1–N1–C11 174.5(2). **A.3**: Ta1–N1 1.781(3); Ta1–N1–C43 174.6(2).

EXPERIMENTAL SECTION

General Considerations and Instrumentation. All air- and moisture-sensitive compounds were manipulated using standard high vacuum and Schlenk techniques or manipulated in a glovebox under a nitrogen atmosphere. Solvents for air- and moisture-sensitive reactions were dried over sodium benzophenone ketyl and stored over titanocene where compatible or dried by the method of Grubbs.[14] Pyridine was distilled from sodium prior to use. Benzene-d_6 was dried over sodium benzophenone ketyl. CD_2Cl_2 was degassed and passed through a column of activated alumina prior to use. $(py)_2TaCl_3(N^tBu)$[15] and $Na[BArF_{24}]$[16] were prepared *via* literature procedure. ^1H and ^{19}F spectra were recorded on Varian Mercury 300 and chemical shifts are reported with respect to residual protio-solvent impurity for ^1H (*s*, 7.16 ppm for C_6D_5H; *t,* 5.32 ppm for $CDHCl_2$).

X-ray Crystal Data: General Procedure. Crystals were removed quickly from a scintillation vial to a microscope slide coated with Paratone N oil. Samples were selected and mounted on a glass fiber with Paratone N oil. Data collection was carried out on a Bruker KAPPA APEX II diffractometer with a 0.71073 Å MoKα source. The structures were solved by direct methods. All non-hydrogen atoms were refined anisotropically. Details regarding refined data and cell parameters are available in Table A.1.

Synthesis of $Cp_2TaCl(N^tBu)$ (A.1). $(py)_2TaCl_3(N^tBu)$ (48 mg, .09 mmol) was dissolved in 4 mL THF. This solution was then added to solid NaCp (16 mg, .09 mmol), and the reaction was stirred overnight. The solvent was then removed *in vacuo*, and the product was extracted into hexanes and dried *in vacuo* to yield **A.1** as a yellow/orange

solid. X-ray quality crystals of **A.1** were obtained by slow evaporation of a concentrated CH_2Cl_2 solution of **A.1**. ^{1}H NMR (300 MHz, CD_2Cl_2) δ, ppm: 1.08 (*s*, 9H, C(C*H*$_3$)$_3$); 6.13 (*s*, 10H, C_5H_5).

Synthesis of $Cp_2TaMe(N^tBu)$ (A.2). A.1 (16 mg, .038 mmol) and MeLi (1.1 mg, .05 mmol) were added in 2 mL Et_2O and stirred overnight. The solvent was removed *in vacuo*, and the yellow residue was extracted into pentane and dried to yield **A.2**. ^{1}H NMR (300 MHz, CD_2Cl_2) δ, ppm: 0.58 (*s*, 3H, C*H*$_3$); 0.98 (*s*, 9H, C(C*H*$_3$)$_3$); 5.79 (*s*, 10H, C_5H_5).

Synthesis of $[Cp_2Ta(N^tBu)(py)][BArF_{24}]$ (A.3). A.1 (12.9 mg, .031 mmol) and pyridine (2.5 µL, .031 mmol) were mixed in 1 mL CD_2Cl_2 and added to $Na[BArF_{24}]$ (27.5 mg, .031 mmol). The solution was mixed and placed in an NMR tube, and the reaction progress followed by ^{1}H NMR. After 24 hours, the reaction was complete. X-ray quality crystals were grown from the slow diffusion of pentane into a saturated solution of **A.3** in CD_2Cl_2. ^{1}H NMR (300 MHz, CD_2Cl_2) δ, ppm: 1.23 (*s*, 9H, C(C*H*$_3$)$_3$); 6.22 (*s*, 10H, C_5H_5); 7.57 (*s*, 4H, $C_6H_2(CF_3)_2H$); 7.62 (*t*, 2H, $C_5H_3NH_2$); 7.73 (*s*, 8H, $C_6H_2(CF_3)_2$H); 8.11 (*t*, 1H, C_5H_4NH); 8.70 (*d*, 2H, $C_5H_3NH_2$).

Synthesis of $[Cp_2TaMe(HN^tBu)(THF)][BArF_{20}]$ (A.4). 24.3 mg $[HNMe_2Ph][BArF_{20}]$ (.03 mmol) in 4 mL THF was added to 12 mg (.03 mmol) **A.2**. The reaction mixture turned light yellow and was stirred for 4 hours. The THF was removed *in vacuo*, and the pale yellow residue was washed with pentane to remove the aniline byproduct. ^{1}H NMR (300 MHz, CD_2Cl_2) δ, ppm: 0.70 (*s*, 3H, C*H*$_3$); 1.27 (*s*, 9H, C(C*H*$_3$)$_3$); 1.93 (*t*, 4H, C_4H_8O); 3.75 (*t*, 4H, C_4H_8O); 6.23 (*s*, 10H, C_5H_5); 8.43 (*br s*, 1H, N*H*).

Synthesis of [$Cp_2Ta(\kappa_2$-2-butenyl-2-^{i}Bu-amide)][$BArF_{24}$] (A.5). 12.5 mg **A.1** (.03 mmol) and 26.7 mg Na[$BArF_{24}$] (.03 mmol) were added in a J-Young NMR tube along with 1 mL CD_2Cl_2. 50 µL MeCCMe was added in, and the tube was sealed and mixed (by constant inversion of the tube) for three days. The reaction turned somewhat brown. ^{1}H NMR (300 MHz, CD_2Cl_2) δ, ppm: 1.37 (*s*, 9H, $C(CH_3)_3$); 2.36 (*s*, 3H, alkenyl-CH_3); 2.67 (*s*, 3H, alkenyl-CH_3); 6.53 (*s*, 10H, C_5H_5); 7.57 (*s*, 4H, $C_6H_2(CF_3)_2H$); 7.73 (*s*, 8H, $C_6H_2(CF_3)_2H$).

Table A.1. Crystal and refinement data for complexes **A.1** and **A.3**.

	A.1	**A.3**
CCDC Number	852809	852405
Empirical formula	$C_{14}H_{19}NClTa$	$[C_{19}H_{24}N_2Ta]^+$ $[C_{32}H_{12}BF_{24}]^-$
Formula weight	417.70	1324.58
T (K)	100(2)	100(2)
a, Å	9.5506(7)	12.4012(5)
b, Å	11.8193(8)	12.8565(5)
c, Å	12.6100(9)	18.0207(7)
α, deg		94.926(2)
β, deg	105.592(4)	91.525(2)
γ, deg		118.228(2)
Volume, Å^3	1371.05(17)	2514.69(17)
Z	4	2
Crystal system	Monoclinic	Triclinic
Space group	P $2_1/n$	P–1
d_{calc}, g/cm^3	2.024	1.749
θ range, deg	2.39 to 39.44	1.81 to 39.25
μ, mm^{-1}	8.189	2.314
Abs. Correction	Semi Empirical	Semi Empirical
GOF	1.342	2.437
R_1 ,[a]	R1 = 0.0174,	R1 = 0.0311,
wR_2 [b] [I>2σ(I)]	*w*R2 = 0.0263	*w*R2 = 0.0560

[a] $R_1 = \Sigma||F_o| - |F_c||/\Sigma|F_o|$. [b] $wR_2 = [\Sigma[w(F_o^2-F_c^2)^2]/\Sigma[w(F_o^2)^2]]^{1/2}$.

REFERENCES

1. Wigley, D. E. In *Progress in Inorganic Chemistry*; 1994; Vol. 42, pp 239–482.
2. Pugh, S. M.; Trosch, D. J. M.; Skinner, M. E. G.; Gade, L. H.; Mountford, P. *Organometallics* **2001**, *20*, 3531–3542.
3. Schmidt, S.; Sundermeyer, J. *J. Organomet. Chem.* **1994**, *472*, 127– 138.
4. Gust, K. R.; Heeg, M. J.; Winter, C. H. *Polyhedron* **2001**, *20*, 805– 813.
5. Bolton, P. D.; Mountford, P. *AdV. Synth. Catal.* **2005**, *347*, 355– 366.
6. Gavenonis, J.; Tilley, T. D. *J. Am. Chem. Soc.* **2002**, *124*, 8536– 8537.
7. Burckhardt, U.; Casty, G. L.; Gavenonis, J.; Tilley, T. D. *Organometallics* **2002**, *21*, 3108–3122.
8. Royo, P.; Sanchez-Nieves, J. *J. Organomet. Chem.* **2000**, *597*, 61– 68.
9. Burland, M. C.; Pontz, T. W.; Meyer, T. Y. *Organometallics* **2002**, *21*, 1933–1941.
10. Ong, T. G.; Yap, G. P. A.; Richeson, D. S. *Chem. Commun.* **2003**, 2612–2613.
11. Blake, R. E.; Antonelli, D. M.; Henling, L. M.; Schaefer, W. P.; Hardcastle, K. I.; Bercaw, J. E. *Organometallics* **1998**, *17*, 718–725.
12. Parkin, G.; van Asselt, A.; Leahy, D. J.; Whinnery, L.; Hua, N. G.; Quan, R. W.; Henling, L. M.; Schaefer, W. P.; Santarsiero, B. D.; Bercaw, J. E. *Inorg. Chem.* **1992**, *31*, 82.
13. Jorgenson, K. A. *Inorg. Chem.* **1993**, *32*, 1521.
14. Pangborn, A. B.; Giardello, M. A.; Grubbs, R. H.; Rosen, R. K.; Timmers, F. J. *Organometallics*, **1996**, *15*, 1518.
15. Korolev, A. V.; Rheingold, A. L.; Williams, D. S. *Inorg. Chem.* **1997**, *36*, 2647.
16. Brookhart, M.; Grant, B.; Volpe Jr., A. F. *Organometallics* **1992**, *11*, 3920.

APPENDIX B

Synthesis and Characterization of Neutral and Cationic Pyridine *bis*(phenolate) Tantalum Alkyls

ABSTRACT

A series of pyridine-linked *bis*(phenolate) tantalum alkyl complexes, (^{R}ONO)$TaCl_2R'$ (^{R}ONO = pyridine-2,6-*bis*(4,6-$^{t}Bu_2$-phenolate) **B.1** for R = ^{t}Bu; pyridine-2,6-*bis*(4-Me-6-Adamantyl-phenolate **B.2** for R = Ad; R' = CH_3, $CH_2C(CH_3)_3$, $CH_2Si(CH_3)_3$) were synthesized. These complexes were examined as possible entry points into the synthesis of tantalum alkylidene complexes *via* reduction-induced α-H abstraction pathways. Similarly, (ONO) tantalum dimethyl cations were synthesized, and deprotonations to form alkylidenes were attempted.

INTRODUCTION

Multiply bonded Ta species Ta=X (X = NR, CR_2) are implicated in a variety of catalytic processes such as hydroamination[1] and olefin metathesis[2], and the chemistry of their insertion products has been heavily studied.[3,4] Recently, the Kol,[5] Schrock,[6] and Bercaw[7] groups have all synthesized tantalum alkylidene complexes supported by polydentate, tri- or di-anionic hard ligand sets (Figure B.1). The Schrock [N_3N] alkylidene decomposes rapidly upon thermolysis to a product with cleaved C-N bonds in the backbone of the ligand. In Kol's [N_2O_2] ligand system, the formation of the multiply bonded tantalum species was severely hindered by competitive β-H elimination from the ligand. In stark comparison, the tantalum benzylidene supported by a pyridine-linked *bis*(phenolate) ligand set is thermally stable and suffers from no competitive elimination products, as the ligand lacks sp^3 backbone carbons and β-hydrogens. Herein, some alternative synthetic entrypoints into tantalum alkylidenes are presented in an attempt to advance the reaction chemistry of (ONO)Ta=CR_2-type complexes.

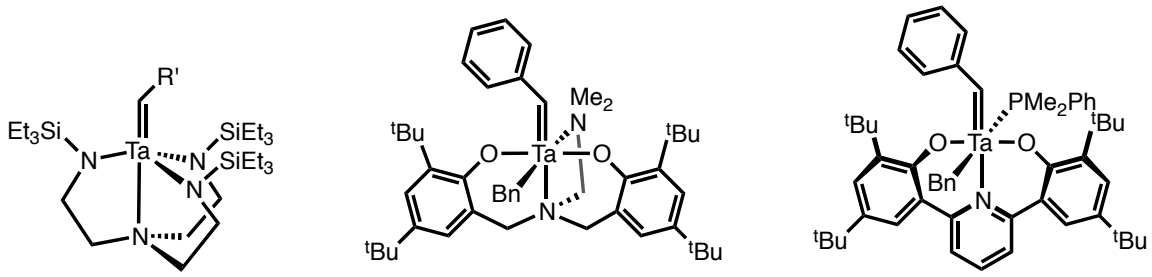

Schrock **Kol** **Bercaw/Agapie**

Figure B.1. Recent tantalum alkylidenes based on polydentate polyanionic ligand sets.

Results and Discussion

Complexes of the type (^{R}ONO)TaCl$_2$R (**B.1a-c**, **B.2a-c**) were generated through protonolysis of the corresponding R_3TaCl_2 with the protonated ligand (^{R}ONO)H$_2$ in good yield (eq. B.1). Complex **B.1a** has been previously reported, but the remaining compounds are unprecedented.

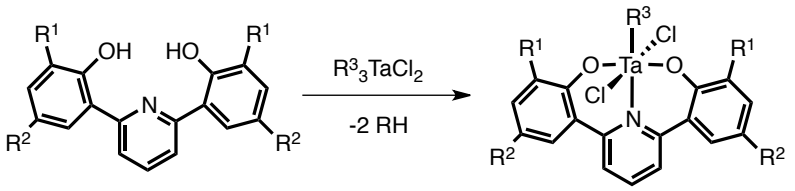

(*B.1*)

It was anticipated that a 2-electron reduction of **B.1** and **B.2** would generate a Ta^{III} species that would spontaneously α-H abstract to generate the corresponding alkylidene hydride, (ONO)Ta^{V}(=CHR)H (eq. B.2).

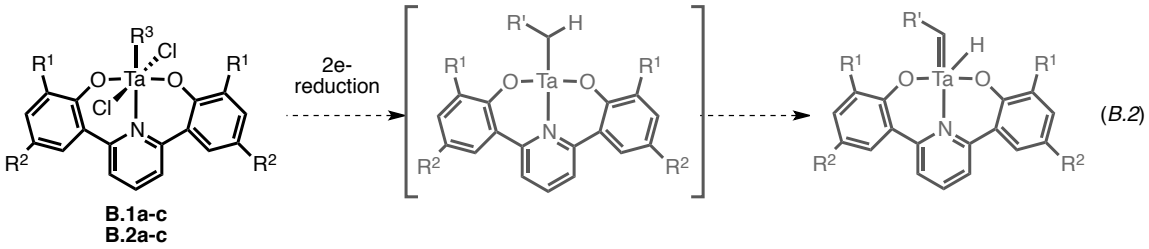

(*B.2*)

These attempted reductions were unsuccessful. The reductants employed were: Na^0, K^0, C_8K, Mg($C_{14}H_{10}$), Na($C_{10}H_8$), and Cp_2Co under a variety of different conditions. Although reaction occurred, the reactions always gave a large mixture of paramagnetic products and were not consistently reproducible. It appears that reduction first occurs on a ligand-based orbital, which is consistent with earlier DFT calculations that show that the LUMO is predominantly ligand based.

Additionally, tantalum dimethyl cations **B.3** and **B.4** were synthesized *via* methide abstraction from (ONO)TaMe$_3$ with [Ph$_3$C]$^+$[B(C$_6$F$_5$)$_4$]$^-$ and B(C$_6$F$_5$)$_3$, respectively (eq. B.3). **B.3** is an insoluble red ionic liquid. **B.4**, on the other hand, is a soluble solid. The ^{19}F spectrum of **B.4** shows a ^{19}F chemical shift difference, $\Delta\delta$, of 2.6 ppm for the *meta* and *para* fluorines in [MeB(C$_6$F$_5$)$_3$]$^-$ which is consistent with a tight ion pair between [(ONO)TaMe$_2$]$^+$ and [MeB(C$_6$F$_5$)$_3$]$^-$.[8] Initial deprotonation attempts of these complexes to generate methylidenes with *n*-BuLi and KBn were unsuccessful. However, it may we worth revisiting related complexes with bulkier alkyl groups, more mild or coordinating bases, or carrying out the reductions in the presence of a coordinating ligand in the hopes of generating a more stable 6-coordinate (ONO)TaR(CHR)L complex.

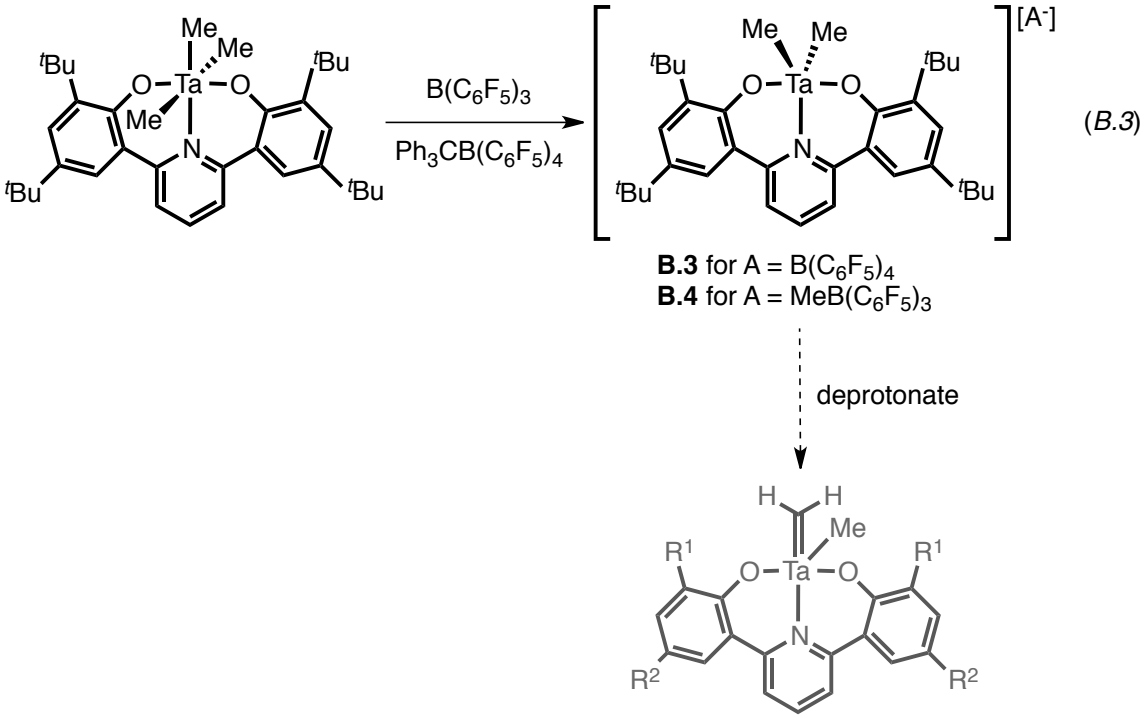

(*B.3*)

EXPERIMENTAL SECTION

General Considerations and Instrumentation. All air- and moisture-sensitive compounds were manipulated using standard high vacuum and Schlenk techniques or manipulated in a glovebox under a nitrogen atmosphere. Solvents for air- and moisture-sensitive reactions were dried over sodium benzophenone ketyl and stored over titanocene where compatible or dried by the method of Grubbs.[9] Benzene-d_6 was purchased from Cambridge Isotopes and dried over sodium benzophenone ketyl. $(ONO)H_2$,[7] $(^{Ad}ONO)H_2$,[10] $(ONO)TaMe_3$[7] and R_3TaCl_2[11] were synthesized *via* literature procedures. $[Ph_3C]^+[B(C_6F_5)_4]^-$ and $B(C_6F_5)_3$ were purchased from Albemarle and used as received. ^1H and ^{19}F spectra were recorded on Varian Mercury 300 and chemical shifts are reported with respect to residual protio-solvent impurity for ^1H (*s*, 7.16 ppm for C_6D_5H).

Synthesis of $(ONO)TaCl_2Me$ (B.1a). A 100 mL bomb fitted with a teflon screwcap valve was charged with Me_3TaCl_2 (700 mg, 2.36 mmol, 1 equiv) and $(ONO)H_2$ (1.15 g, 2.36 mmol, 1 equiv). The flask was evacuated on a high vacuum line, 30 mL C_6H_6 was vacuum transferred on, and the flask warmed to room temperature and stirred for 1 hour. Upon warming, the solution changed from pale yellow to orange and gas formation was evident. After 1 hour, the solvent was removed *in vacuo*, yielding **B.1a** as an orange powder. Recrystallization from petroleum ether at -30 °C gave 1.6 g (90%) of the product as a yellow/orange solid. ^1H NMR (300 MHz, C_6D_6) δ, ppm: 1.308 (*s*, 18H, $C(CH_3)_3$); 1.814 (*s*, 18H, $C(CH_3)_3$); 2.353 (*s*, 3H, Ta-CH_3); 6.922 (*t*, 1H, 4-C_5NH_3); 7.115 (*d*, 2H, 3,5-C_5NH_3); 7.261 (*d*, 2H, aryl-*H*); 7.775 (*d*, 2H, aryl-*H*).

Synthesis of (ONO)$TaCl_2(CH_2TMS)$ (B.1b). A similar procedure to **B.1a** was followed. Starting from 100 mg $(ONO)H_2$ and 105.7 mg $(CH_2TMS)_3TaCl_2$ yielded 160 mg (95%) **B.1b** as a yellow powder. ^1H NMR (300 MHz, C_6D_6) δ, ppm: 0.508 (*s*, 9H, $Si(CH_3)_3$); 1.345 (*s*, 18H, $C(CH_3)_3$); 1.870 (*s*, 18H, $C(CH_3)_3$); 3.208 (*s*, 2H, Ta–CH_2Si); 6.977 (*t*, 1H, 4–C_5NH_3); 7.192 (*d*, 2H, 3,5–C_5NH_3); 7.281 (*d*, 2H, aryl–*H*); 7.805 (*d*, 2H, aryl–*H*).

Synthesis of (ONO)$TaCl_2(CH_2CMe_3)$ (B.1c). A similar procedure to **B.1a** was followed. Starting from 100 mg $(ONO)H_2$ and 95.8 mg Np_3TaCl_2 yielded 138 mg (83%) **B.1c** as a yellow/orange powder. ^1H NMR (300 MHz, C_6D_6) δ, ppm: 1.300 (*s*, 18H, $C(CH_3)_3$); 1.527 (*s*, 9H, $TaCH_2C(CH_3)_3$); 1.852 (*s*, 18H, $C(CH_3)_3$); 3.413 (*s*, 2H, $TaCH_2$); 6.976 (*t*, 1H, 4–C_5NH_3); 7.092 (*d*, 2H, 3,5–C_5NH_3); 7.215 (*d*, 2H, aryl–*H*); 7.772 (*d*, 2H, aryl–*H*).

Synthesis of (^{Ad}ONO)$TaCl_2Me$ (B.2a). A procedure identical to **B.1a** was employed. Starting from $(^{Ad}ONO)H_2$ gave **B.2a** in 62% yield as a yellow/orange solid. ^1H NMR (300 MHz, C_6D_6) δ, ppm: 1.801 (*d*, 6H, adamantyl–*H*); 1.973 (*m*, 6H, adamantyl–*H*); 2.149 (*s*, 6H, adamantyl–*H*); 2.270 (*s*, 6H, adamantyl–*H*); 2.458 (*s*, 3H, Ta–CH_3); 2.495 (*s*, 6H, adamantyl–*H*); 2.575 (*s*, 6H, Ar–CH_3); 6.784 (*s*, 2H, aryl–*H*); 6.931 (*m*, 3H, aryl–*H*); 7.332 (*s*, 2H, aryl–*H*).

Synthesis of (^{Ad}ONO)$TaCl_2(CH_2TMS)$ (B.2b). A procedure identical to **B.1a** was employed. Starting from $(^{Ad}ONO)H_2$ yielded 82% **B.2b.** ^1H NMR (300 MHz, C_6D_6) δ, ppm: 0.545 (*s*, 9H, –$Si(CH_3)_3$); 1.881 (*m*, 12H, adamantyl–*H*); 2.172 (*br s*, 6H, adamantyl–

H); 2.271 (*s*, 6H, Ar-C*H*$_3$); 2.559 (*s*, 12H, adamantyl-*H*); 3.399 (*s*, 2H, C*H*$_2$TMS); 6.770 (*s*, sH, aryl-*H*); 6.951 (*s*, 2H, aryl-*H*); 7.029 (*s*, 1H, aryl-*H*); 7.328 (*s*, 2H, aryl-*H*).

Synthesis of [(ONO)TaMe$_2$]$^+$[B(C$_6$F$_5$)$_4$]$^-$ (B.3). (ONO)TaMe$_3$ (100 mg, .141 mmol, 1 equiv) and [Ph$_3$C]$^+$[B(C$_6$F$_5$)$_3$]$^-$ (129.9 mg, .141 mmol, 1 equiv) were mixed in 10 mL CH_2Cl_2 in an inert atmosphere glovebox. The reaction was stirred for 12 hours, after which the CH_2Cl_2 was removed *in vacuo*. The resulting reddish oil was washed with petroleum ether and pumped dry. ^{19}F NMR (282 MHz, CD_2Cl_2) δ, ppm: -133.3 (*o-F*); -163.9, -167.7 (*m*- and *p*- F).

Synthesis of [(ONO)TaMe$_2$]$^+$[MeB(C$_6$F$_5$)$_3$]$^-$ (B.4). In an inert atmosphere glovebox, (ONO)TaMe$_3$ (9.6 mg, .0135 mmol, 1 equiv) and B(C$_6$F$_5$)$_3$ (7 mg, .0135 mmol, 1 equiv) were added to a J-Young NMR tube with the aid of 1 mL C_6D_6. The reaction mixture was shaken, and after 15 minutes the reaction was complete by NMR. ^{1}H NMR (300 MHz, C_6D_6) δ, ppm: 0.968 (br s, 3H, Ar$_3$BC*H*$_3$); 1.118 (s, 6H, Ta(C*H*$_3$)$_2$); 1.365 (s, 18H, C(C*H*$_3$)$_3$); 1.580 (s, 18H, C(C*H*$_3$)$_3$); 7.418 (t, 1H, 4-C$_5$N*H*$_3$); 7.491 (d, 2H, aryl-*H*); 7.543 (d, 2H, 3,5-C$_5$N*H*$_3$); 7.818 (d, 2H, aryl-*H*). ^{19}F NMR (282 MHz, C_6D_6) δ, ppm: -132 (*o-F*); -164.5, -167 (*m*- and *p-F*).

REFERENCES

1. Anderson, L.L.; Arnold, J.; Bergman, R. G. *Organic Letters* **2004**, *6*, 2519-2522.
2. Rocklage, S. M.; Fellman, J. D.; Rupprecht, A. G.; Schrock, R. R. *J. Am. Chem. Soc.* **1981**, *103*, 1440.
3. Guiducci, A. E.; Boyd, C. L.; Mountford, P. *Organometallics* **2006**, *25*, 1167.
4. Antinolo, A.; Dorado, I.; Eajardo, M.; Garces, A.; Kubicki, M. M.; Lopez-Mardomingo, C.; Otero, A.; Prashar, S. *J. Organomet. Chem.* **2006**, *691*, 1361.
5. Groysman, S.; Goldberg, I.; Kol, M.; Genizi, E.; Goldschmidt, Z. *Organometallics* **2004**, *23*, 1880.
6. Freundlich, J. S.; Schrock, R. R.; Davis, W. M. *Organometallic*s **1996**, *15*, 2777.
7. Agapie, T.; Day, M. W.; Bercaw, J. E. *Organometallics* **2008**, *27*, 6123.
8. Horton, A. D. *Organometallics* **1996**, *15*, 2675.
9. Pangborn, A. B.; Giardello, M. A.; Grubbs, R. H.; Rosen, R. K.; Timmers, F. J. *Organometallics*, **1996**, *15*, 1518.
10. Golisz, S. R.; Bercaw, J. E. *Macromolecules* **2009**, *42*, 8751.
11. Moorhouse, S.; Wilkinson, G. *J. Chem. Soc. Dalton Trans.***1974** 2187.

APPENDIX C

Titanium-Mediated N-N Bond Forming Reactions; $MOCl_4$-Promoted C-H Activation of Aminoisocyanates

ABSTRACT

During attempts to make titanium alkoxyimides, $L_nTi(NOR)$, and high valent terminal molybdenum hydrazides, $L_nMo^{VI}(NNR)$, two new reactions were discovered. First, $TiCl_2(NMe)_2$ mediates the umpolung reaction of H_2NOMe with $HNMe_2$ to form H_2NNMe_2; and second, $MOCl_4$ promotes C-H activation in diarylaminoisocyanates, Ar_2NNCO, to generate heterocycles. The chemistry presented herein is preliminary, but the observed product mixtures indicate the future potential of these two new classes of the reaction.

INTRODUCTION

We desired to synthesize titanium alkoxyimides, $L_nTi(NOR)$, in order to answer some mechanistic questions about titanium catalyzed diamination of alkynes with hydrazines. While there is very little experimental mechanistic insight into the reaction, it is believed that upon reaction of an alkyne with a Ti hydrazide, the β-NR_2 unit migrates to Ti to form an amide and an aziridenene (eq C.1). The amide then nucleophilically attacks the aziridenene to generate the diamine.[1]

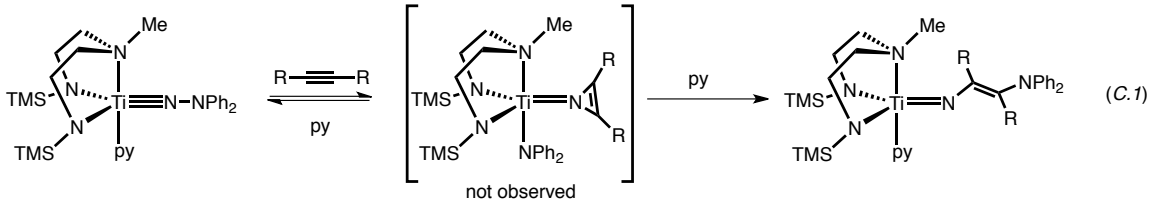

(*C.1*)

We postulated that similar reactivity with a titanium alkoxyimide would lead to stable titanium alkoxide products, which would not reinsert due to the stability of the Ti–O bond. This would allow for more rigorous study of the first step of the reaction, the attack of alkyne on Ti (eq C.2).

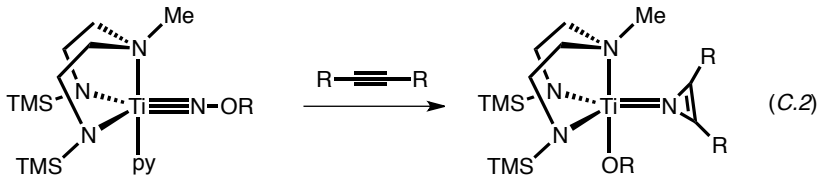

(*C.2*)

During the course of our studies on the photophysics of early metal hydrazides (Chapter 6), we attempted to make analogous molybdenum hydrazides, $(MeCN)MoCl_4(NNR_2)$. Since $MoCl_6$ (and many other Mo^{VI} analogs of common W^{VI} starting materials) is not a stable compound, we sought to start from $MoOCl_4$ instead. There are examples of $WOCl_4$ reacting with isocyanates, RNCO, to generate the corresponding

W=NR imide and CO_2 (eq C.3).[2] We sought to explore similar reactivity with $MoOCl_4$ and aminoisocyanates, R_2NNCO.

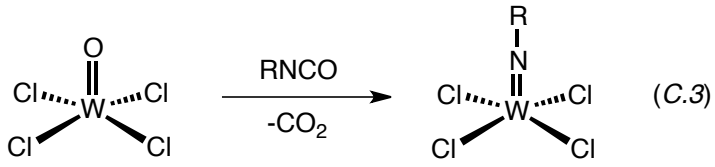

(*C.3*)

RESULTS AND DISCUSSION

Titanium-Mediated N-N Bond Formation

$(HNMe_2)_2Cl_2Ti(NR)$ (R = alkyl, aryl, amino) is a common titanium imido starting material that is synthesized by reaction of $TiCl_2(NMe_2)_2$ with the corresponding amine or hydrazine (eq. C.4).[3] When H_2NOMe is used as the starting amine, however, the corresponding alkoxyimide, $(HNMe_2)_2Cl_2Ti(NOMe)$, is *not* generated. Instead, a bridging tetranuclear dimethylhydrazide(2-) dimer, **C.1**, is formed in less than 50% yield (eq C.5).

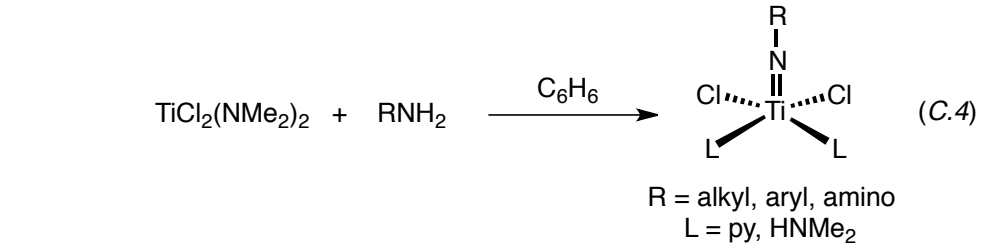

(*C.4*)

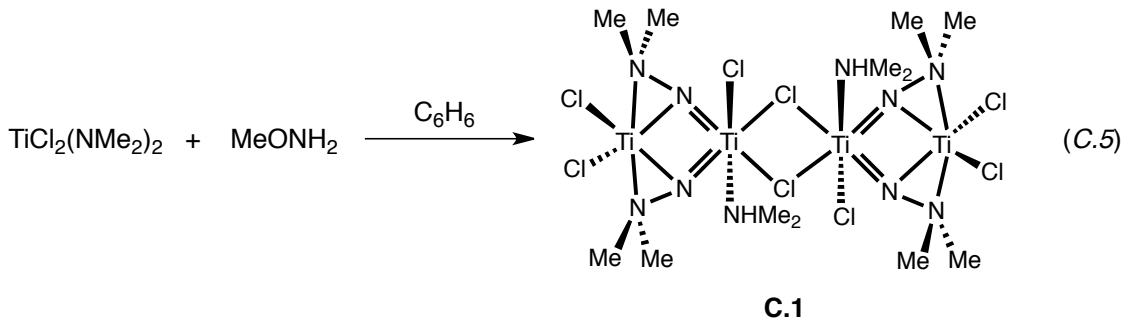

(*C.5*)

C.1

The crystal structure of **C.1** is presented in Figure C.1. **C.1** is a dimer, with the dinuclear monomeric units bridged by two chlorides. The monomeric unit contains two titanium atoms and two bridging hydrazide (2-) ligands. Based on the bond lengths, the bridging hydrazido unit functions as an LX donor to Ti1 (Ti1-N distances 1.8444(6) and 1.8445(5) Å) and as an X donor to Ti2 (Ti2-N distances of 1.9419(6) and 1.9302(6) Å). The Ti2 center has an additional donor interaction with the β-NMe_2 unit. This structure is

similar to one reported by Mountford, which was obtained by reaction of $TiCl_2(NMe_2)_2$ with H_2NNMe_2.[4]

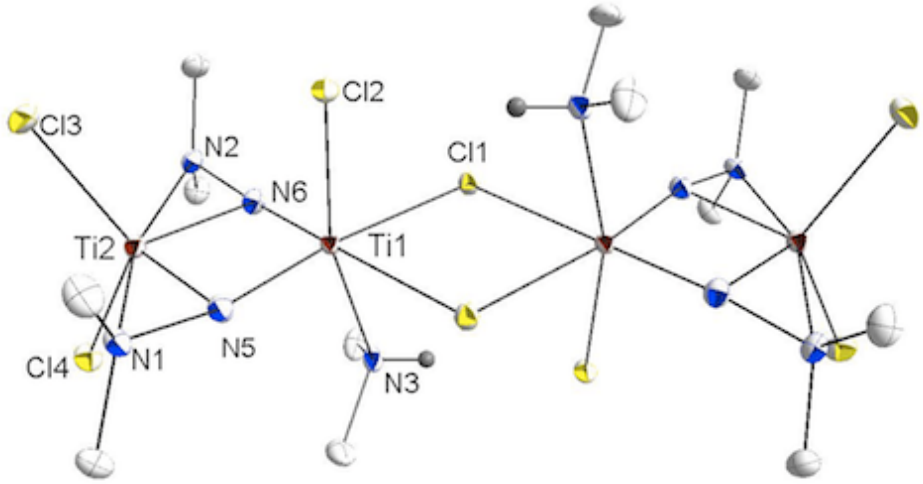

Figure C.1. Thermal ellipsoid drawing of **C.1** dimer. Selected bond lengths (Å): Ti1–Cl1 2.5370(2); Ti1–Cl2 2.3983(3); Ti1–N3 2.2112(8); Ti1–N5 1.8444(6); Ti1–N6 1.8445(5); Ti1–Ti2 2.7338(2); Ti2–Cl3 2.2796(3); Ti2–Cl3 2.2724(3); Ti2–N1 2.1844(6); Ti2–N2 2.2008(6); Ti2–N5 1.9419(6); Ti2–N6 1.9302(6). Solvent removed for clarity.

Presumably, H_2NOMe is reacting with $TiCl_2(NMe_2)_2$ to generate H_2NNMe_2, which then reacts with more $TiCl_2(NMe_2)_2$ to generate **C.1** in a manner similar to Mountford's reaction. The mechanism for the N–N bond forming reaction remains unclear at this point. Free $HNMe_2$ and H_2NOMe do not react, so the transformation appears to be mediated by titanium, and is probably driven by the formation of a strong Ti–O bond. This transformation could occur *via* a number of mechanisms; two limiting cases are presented in Scheme C.1.

For example, $TiCl_2(NMe_2)_2$ could react with H_2NOMe to generate $(HNMe_2)_2Cl_2Ti(NOMe)$, which then acts as a masked "electrophilic nitrene" and is nucleophilically attacked by $HNMe_2$ to generate the N–N bond (pathway A). Alternately,

H_2NOMe could coordinate to Ti *via* oxygen, which would make the –OMe unit a better leaving group. From there, Ti–NMe_2 could nucleophilically attack the nitrogen in H_2NOMe, expelling Ti–OMe and generating the N–N bond (pathway B). Currently, the latter mechanism is favored based on similar reactivity in the titanium-mediated amination of Grignard reagents using primary and secondary amines.[5]

Scheme C.1

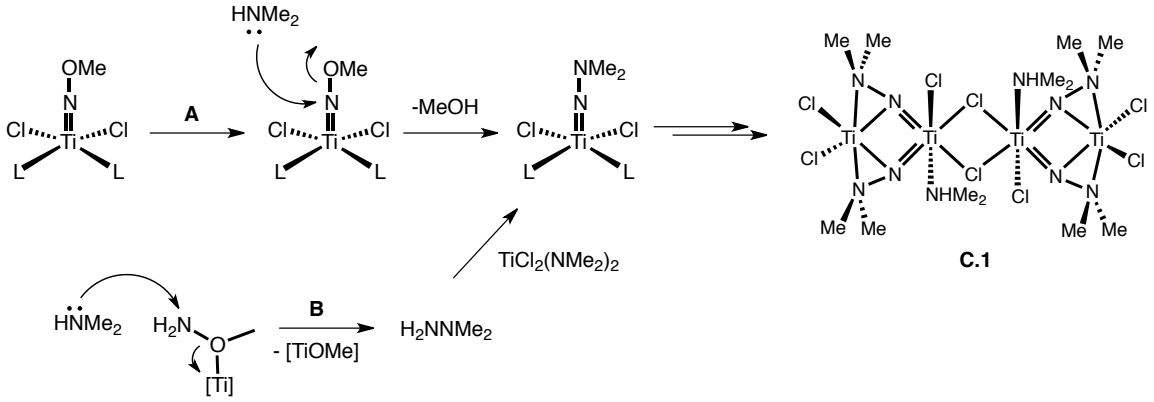

Additionally, there is evidence of Ti–OMe bond formation in other reactions. For example, when the reaction of H_2NOMe with $TiCl_4$ is carried out in the presence of pyridine, the salt $[(py)Cl_4TiOMe]^-[pyH]^+$ (**C.2**) crystallizes out in low yield (eq. C.6, Figure C.2). While such crystal fishing does not indicate the distribution of species in solution, it at least reveals the fate of the –OMe group in the reaction.

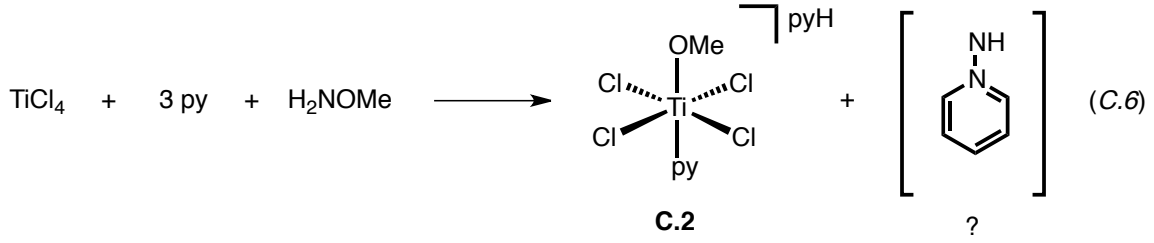

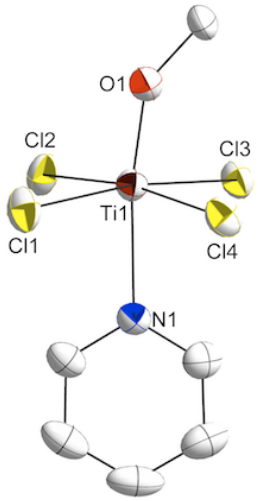

Figure C.2. Thermal ellipsoid drawing of **C.2.** PyH^+ counteraction and solvent removed for clarity. Selected bond lengths (Å) and angles (°): Ti1–Cl1 2.371(1); Ti1–Cl2 2.334(1); Ti1–Cl3 2.354(1); Ti1–Cl4 2.383(1); Ti1–N1 2.289(3); Ti1–O1 1.742(3). Ti1–O1–C 146.2(2).

$MoOCl_4$-promoted C–H Activation of Aminoisocyanates

Reaction of $MoOCl_4$ with Ph_2NNCO did not result in the formation of the expected hydrazide and CO_2, and instead produced a dark solution from which two major products crystallized out (eq C.8). The first product was a cocrystallization of $[MoOCl_4]_2$ with 1-phenyl-indazol-3-one **C.3**, which is the product of *ortho* C–H activation of Ph_2NNCO and C–H addition across the N–C double bond (Figure C.3). The second product is also an indazolone derivative. In **C.4**, the resultant indazolone has further reacted with $MoOCl_4$ and inserted into an equivalent of "Ph_2NCO," which is likely a contaminant from the century-old preparation of Ph_2NNCO (Figure C.3). C–H activations of arene solvents by $MoOCl_4$ and phenylisocyanate have been observed, but this indazolone formation is unprecedented.[6]

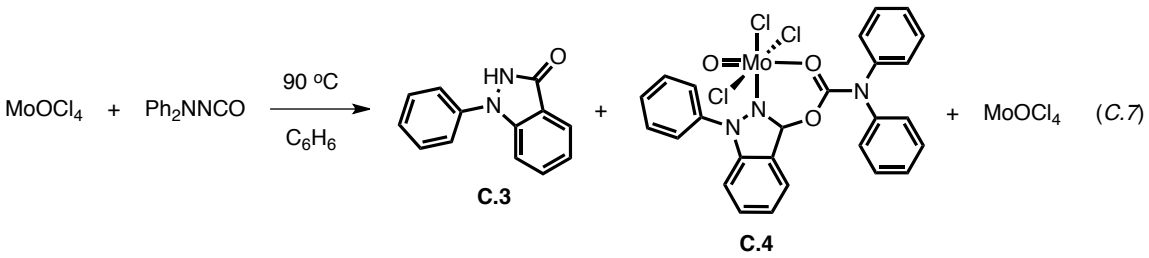

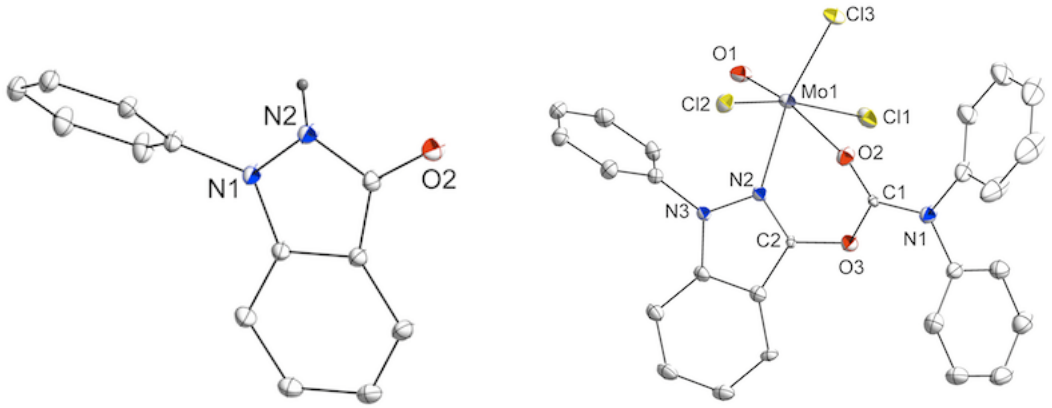

Figure C.3. Thermal ellipsoid drawing of **C.3** (left) and **C.4** (right). Selected bond lengths (Å) and angles (°): **C.3**: N1–N2 1.3670(1); C3–O2 1.3172(1). **C.4**: Mo1–Cl1 2.3929(2); Mo1–Cl2 2.3374(2); Mo1–Cl3 2.3332(2); Mo1–O1 1.6552(1); Mo1–O2 2.2539(1); Mo1–N2 2.2155(1). Solvents and cocrystallized $[MoOCl_4]_2$ in **C.3** removed for clarity.

OUTLOOK

While the development of the two discussed reactions remains limited to date, these two reactions could potentially find use in synthetic methodology. The Ti-catalyzed N-N bond forming reaction could provide a new method for the generation of substituted hydrazines (as compared to the Olin-Raischig Process,[7] which uses NH_2Cl and NH_3) or other N-N containing products. Likewise, the development of aminoisocyanate intramolecular C-H activation could lead to new synthetic methodology for the 1-substituted-3-indazolones.

EXPERIMENTAL SECTION

General Considerations and Instrumentation. All air- and moisture-sensitive compounds were manipulated using standard high vacuum and Schlenk techniques or manipulated in a glovebox under a nitrogen atmosphere. Solvents for air- and moisture-sensitive reactions were dried over sodium benzophenone ketyl and stored over titanocene where compatible or dried by the method of Grubbs.[8] $TiCl_2(NMe_2)_2$,[9] and Ph_2NNCO[10] were prepared *via* literature procedure. Pyridine was distilled from Na^0/Ph_2CO and H_2NOMe was degassed and passed through a plug of activated alumina prior to use.

X-ray Crystal Data: General Procedure. Crystals were removed quickly from a scintillation vial to a microscope slide coated with Paratone N oil. Samples were selected and mounted on a glass fiber with Paratone N oil. Data collection was carried out on a Bruker KAPPA APEX II diffractometer with a 0.71073 Å MoKα source. The structures were solved by direct methods. All non-hydrogen atoms were refined anisotropically. Details regarding refined data and cell parameters are available in Tables C.1 and C.2.

Synthesis of Ti Tetramer (C.1). $TiCl_2(NMe_2)_2$ (96.7 mg, .467 mmol) was dissolved in 20 mL C_6H_6 and H_2NOMe (22 mg, .467 mmol) was syringed in. The solution was stirred overnight, the resultant white precipitate was filtered away, and solvent removed *in vacuo*. X-ray quality crystals were obtained by vapor diffusion of pentane into a saturated solution of **C.1** in C_6H_6 at room temperature.

Synthesis of $[(py)TiCl_4(OMe)]^-[pyH]^+$. A procedure analogous to **C.1** was employed, with 2 equivalents of pyridine added to the reaction mixture.

Synthesis of 1-phenyl-3-indazolone (C.3) and coupled product (C.4). $MoOCl_4$ (128.5 mg, .51 mmol) and Ph_2NNCO (106.4 mg, .51 mmol) were measured into a 25 mL glass tube fitted with a teflon Kontes valve. 3 mL C_6H_6 was added, and the vessel was sealed and heated to 90 °C overnight, giving an orange solution with a large amount of dark precipitate. The reaction was filtered and concentrated. Small orange crystals (**C.3**) and large green blades (**C.4**) grew from the reaction mixture overnight.

Table C.1. Crystal and refinement data for complexes **C.1** and **C.2**.

	C.1	**C.2**
CCDC Number	852406	854070
Empirical formula	$C_{12}H_{36}N_{10}Cl_8Ti_4 \cdot C_6H_6$	$[C_6H_8NOCl_4Ti][C_5H_6N]^+ \cdot 0.5(CH_2Cl_2)$
Formula weight	951.92	420.40
T (K)	100(2)	160(2)
a, Å	7.8813(3)	26.6246(11)
b, Å	11.6942(5)	12.1937(5)
c, Å	11.9887(5)	11.0769(5)
α, deg	87.569(2)	
β, deg	83.250(2)	101.332(2)
γ, deg	74.478(2)	
Volume, Å^3	1057.20(7)	3526.0(3)
Z	1	8
Crystal system	Triclinic	Monoclinic
Space group	P–1	C 2/*c*
d_{calc}, g/cm^3	1.495	1.584
θ range, deg	1.71 to 45.50	1.84 to 26.42
μ, mm^{-1}	1. .264	1.238
Abs. Correction	None	None
GOF	1.299	2.537
R_1 ,[a]	R1 = 0.0287,	R1 = 0.0638,
wR_2 [b] [I>2σ(I)]	*w*R2 = 0.0524	*w*R2 = 0.0863

[a] $R_1 = \Sigma||F_o| - |F_c||/\Sigma|F_o|$. [b] $wR_2 = [\Sigma[w(F_o^2-F_c^2)^2]/\Sigma[w(F_o^2)^2]]^{1/2}$.

Table C.2. Crystal and refinement data for complexes **C.3** and **C.4.**

	C.3	**C.4**
CCDC Number	855663	853662
Empirical formula	$[C_{13}H_{11}N_2O]^+ \cdot 0.5[Cl_8Mo_2O_2]^{-2} \cdot C_6H_6$	$C_{26}H_{19}N_3O_3Cl_3Mo \cdot C_6H_6$
Formula weight	543.09	701.84
T (K)	100(2)	100(2)
a, Å	7.8372(4)	17.6222(7)
b, Å	11.4163(6)	9.1929(3)
c, Å	13.0340(6)	19.5015(7)
α, deg	115.219(2)°	
β, deg	94.648(2)	105.851(2)
γ, deg	90.019(2)	
Volume, Å^3	1050.77(9)	3039.10(19)
Z	2	4
Crystal system	Triclinic	Monoclinic
Space group	P–1	$P2_1/c$
d_{calc}, g/cm^3	1.716	1.534
θ range, deg	1.97 to 55.40	2.17 to 42.27
μ, mm^{-1}	1.151	0.734
Abs. Correction	None	None
GOF	2.441	2.587
R_1 ,[a]	R1 = 0.0285,	R1 = 0.0388,
wR_2 [b] [I>2σ(I)]	*w*R2 = 0.0640	*w*R2 = 0.0658

[a] $R_1 = \Sigma||F_o| - |F_c||/\Sigma|F_o|$. [b] $wR_2 = [\Sigma[w(F_o^2-F_c^2)^2]/\Sigma[w(F_o^2)^2]]^{1/2}$.

REFERENCES

1. Mindiola, D. J. *Angew. Chem. Int. Ed.* **2008**, *47*, 2.
2. Schrock, R. R.; Krause, S. A.; Knoll, K.; Feldman, J.; Murzdezek, J. S.; Yang, D. C. J. *Mol. Catal.* **1988**, *46*, 243.
3. Adams, N.; Bigmore, H. R.; Blundell, T. L.; Boyd, C. L.; Dubberley, S. R.; Sealey, A. J.; Cowley, A. R.; Skinner, M. E. G.; Mountford, P. *Inorg. Chem.* **2005**, *44*, 2882.
4. Parsons, T. B.; Hazari, N.; Cowley, A. R.; Green, J. C.; Mountford, P. *Inorg. Chem.* **2005**, *44*, 8442.
5. Barker, T. J.; Jarvo, E. R. *Angew. Chem. Int. Ed.* **2011**, *50*, 8325.
6. De la mata, F. J.; Ziller, J. W. *J. Organomet. Chem.* **1998**, *564*, 85.
7. Maxwell, G. R. Synthetic Nitrogen Products: A Practical Guide to the Products and Processes. Kluwer Academic: New York, 2004.
8. Pangborn, A. B.; Giardello, M. A.; Grubbs, R. H.; Rosen, R. K.; Timmers, F. J. *Organometallics* **1996**, *15*, 1518.
9. Benzing, E.; Kornicker, W. *Chem. Ber.* **1961**, *94*, 2263.
10. Acree, S. F. *Chem. Ber.* **1903**, *36*, 3148.